NUREG/CR–6107
SAND93–2042

Summary of MELCOR 1.8.2 Calculations for Three LOCA Sequences (AG, S2D, and S3D) at the Surry Plant

Prepared by
L. Kmetyk/SNL
L. Smith/GCI

Sandia National Laboratories
Operated by
Sandia Corporation

Geo-Centers Inc.

Prepared for
U.S. Nuclear Regulatory Commission

AVAILABILITY NOTICE

Availability of Reference Materials Cited in NRC Publications

Most documents cited in NRC publications will be available from one of the following sources:

1. The NRC Public Document Room, 2120 L Street, NW., Lower Level, Washington, DC 20555-0001

2. The Superintendent of Documents, U.S. Government Printing Office, Mail Stop SSOP, Washington, DC 20402-9328

3. The National Technical Information Service, Springfield, VA 22161

Although the listing that follows represents the majority of documents cited in NRC publications, it is not intended to be exhaustive.

Referenced documents available for inspection and copying for a fee from the NRC Public Document Room include NRC correspondence and internal NRC memoranda; NRC bulletins, circulars, information notices, inspection and investigation notices; licensee event reports; vendor reports and correspondence; Commission papers; and applicant and licensee documents and correspondence.

The following documents in the NUREG series are available for purchase from the GPO Sales Program: formal NRC staff and contractor reports, NRC-sponsored conference proceedings, international agreement reports, grant publications, and NRC booklets and brochures. Also available are regulatory guides, NRC regulations in the *Code of Federal Regulations*, and *Nuclear Regulatory Commission Issuances*.

Documents available from the National Technical Information Service include NUREG-series reports and technical reports prepared by other Federal agencies and reports prepared by the Atomic Energy Commission, forerunner agency to the Nuclear Regulatory Commission.

Documents available from public and special technical libraries include all open literature items, such as books, journal articles, and transactions. *Federal Register* notices, Federal and State legislation, and congressional reports can usually be obtained from these libraries.

Documents such as theses, dissertations, foreign reports and translations, and non-NRC conference proceedings are available for purchase from the organization sponsoring the publication cited.

Single copies of NRC draft reports are available free, to the extent of supply, upon written request to the Office of Administration, Distribution and Mail Services Section, U.S. Nuclear Regulatory Commission, Washington, DC 20555-0001.

Copies of industry codes and standards used in a substantive manner in the NRC regulatory process are maintained at the NRC Library, 7920 Norfolk Avenue, Bethesda, Maryland, for use by the public. Codes and standards are usually copyrighted and may be purchased from the originating organization or, if they are American National Standards, from the American National Standards Institute, 1430 Broadway, New York, NY 10018.

DISCLAIMER NOTICE

NUREG/CR-6107
SAND93-2042

Summary of MELCOR 1.8.2 Calculations for Three LOCA Sequences (AG, S2D, and S3D) at the Surry Plant

Manuscript Completed: October 1993
Date Published: March 1994

Prepared by
L. Kmetyk/Sandia National Laboratories
L. Smith/Geo-Centers Inc.

Sandia National Laboratories
Albuquerque, NM 87185

Geo-Centers Inc.
2201 Buena Vista Dr. SE
Albuquerque, NM 87106

Prepared for
Division of Safety Issue Resolution
Office of Nuclear Regulatory Research
U.S. Nuclear Regulatory Commission
Washington, DC 20555-0001
NRC FIN L2486

Abstract

Activities involving regulatory implementation of updated source term information were pursued. These activities include the identification of the source term, the identification of the chemical form of iodine in the source term, and the timing of the source term's entrance into containment. These activities are intended to support a more realistic source term for licensing nuclear power plants than the current TID-14844 source term and current licensing assumptions. MELCOR calculations were performed to support the technical basis for the updated source term.

This report presents the results from three MELCOR calculations of nuclear power plant accident sequences and presents comparisons with Source Term Code Package (STCP) calculations for the same sequences. The three low-pressure sequences were analyzed to identify the materials which enter containment (source terms) and are available for release to the environment , and to obtain timing of sequence events. The source terms include fission products and other materials such as those generated by core-concrete interactions. All three calculations, for both MELCOR and STCP, analyzed the Surry plant, a pressurized water reactor (PWR) with a subatmospheric containment design.

Table of Contents

List of Figures

List of Figures (continued)

List of Figures (continued)

List of Figures (continued)

List of Tables

Acknowledgements

The authors would like to acknowledge a number of individuals who contributed significantly to this report. The MELCOR development team (Sam Thompson, Randy Cole, Russ Smith and Randy Summers) provided substantial assistance with these calculations, including correcting coding errors and identifying input errors. Sam Thompson also provided user-convenient plot programs. Susan Dingman and Tom Brown provided the final, formal technical review, which resulted in a large number of improvements and clarifications to the text.

1 Introduction

1.1 Background and Objectives

Activities involving regulatory implementation of updated source term information were pursued. These activities include the identification of the source term, the identification of the chemical form of iodine in the source term, and the timing of the source term's entrance into containment. These activities are intended to support a more realistic source term for licensing nuclear power plants than the current TID-14844 source term and current licensing assumptions. MELCOR calculations were performed to support the technical bias for the updated source term.

This report summarizes the results from three MELCOR calculations of nuclear power plant accident sequences and TID-14844 presents comparisons with Source Term Code Package (STCP) calculations for the same sequences.[1] The program task was to run the MELCOR program for three low-pressure sequences to identify the materials which enter containment (source terms) and are available for release to the environment, and to obtain timing of sequence events. The source terms include fission products and other materials such as those generated by core-concrete interactions. All three calculations, with both MELCOR and STCP, analyzed loss-of-coolant accidents (LOCAs) in the Surry plant, a pressurized water reactor (PWR) with a subatmospheric containment design.

In the AG sequence, a large break LOCA, both passive and active Emergency Core Cooling System (ECCS) safety systems for protection of the primary system were assumed to be available until containment failure occurred. Containment protective systems available for use included the containment fan coolers and containment sprays. Since the containment recirculation spray system coolers were inoperable, there was no capability for containment heat removal as the accident progressed. For the small break LOCA's, S2D and S3D, the ECCS systems were assumed unavailable, with the exception of the passive accumulators. For those two accident sequences, the containment spray systems were fully operable, including the capability for containment heat removal via the containment spray recirculation system coolers. Since each of the three accident sequences progressed through core melt, core slumping, reactor vessel failure, and ex-vessel core-concrete interaction, they provided a good test of the ability of MELCOR to simulate integrated accidents that progressed to the point of radionuclide release to the containment or environment.

This report is designed to satisfy the documentation requirements of FIN L2486 (Surry MELCOR calculations) performed for the U.S. Nuclear Regulatory Commission (NRC) by Sandia National Laboratories (SNL). The purpose of the report is to compare the results of three STCP analyses of Surry accident sequences carried out by Battelle Memorial Institute (BMI) for the NUREG-1150 program with new analyses of the same accident sequences using MELCOR.

1.2 MELCOR

MELCOR[2] began development in 1982 as a fully integrated, engineering-level computer code that models the progression of severe accidents in light water reactor nuclear power plants. MELCOR is being developed at Sandia National Laboratories for the U.S. Nuclear Regulatory Commission as a second-generation plant risk assessment tool and the successor to the Source Term Code Package.[3] The entire spectrum of severe accident phenomena, including reactor coolant system and containment thermal-hydraulic response, core heatup, degradation and relocation, and fission product release and transport, is treated in MELCOR in a unified framework for both boiling water reactors and pressurized water reactors. MELCOR has been especially designed to facilitate sensitivity and uncertainty analyses. Its current uses include estimation of severe accident source terms and their sensitivities and uncertainties in a variety of applications.

The newest version of MELCOR, MELCOR 1.8.2, was released in May 1993. The Surry analyses documented in this report were carried out with that release version.

(This report assumes a reader having some familiarity with MELCOR terminology and capabilities. For those with little or no previous experience with MELCOR, Ref. 2 is recommended as a good introduction and source of background information.)

1.3 Organization of Report

Section 2 contains a brief description of the Surry PWR with subatmospheric containment design. The AG, S2D, and S3D accident sequences are summarized briefly in Section 3. Section 4 describes the MELCOR model, along with features particular to the given accident sequences being analyzed. Results of the MELCOR

calculations, along with comparisons to the STCP results, are presented in Section 5, for each of the three accident sequences. Section 6 contains a brief summary and conclusions.

2 PWR Subatmospheric Containment Design

The MELCOR analyses described in this volume were based on the Surry Power Station, Unit 1. Operated by the Virginia Electric Power Company, it is located on the James River in southeastern Virginia, about 16 kilometers (10 miles) south of Williamsburg, Virginia. Two units are located on the site, with Unit 2 essentially identical to Unit 1.

2.1 Reactor and Primary System

The nuclear reactor of Surry Unit 1 is a 2441 MWt pressurized water reactor (PWR) designed and built by Westinghouse. The Reactor Coolant System (RCS) is a three loop design, with a reactor coolant pump (RCP) and a U-tube steam generator (SG) in each loop. In addition, Loop C contains the primary system pressurizer. Under normal operating conditions, the RCS operates at ~15.5 MPa (155 bar, 2,250 psia), with a core inlet coolant temperature of 557 K (543°F) and a core exit coolant temperature of 593 K (608°F). The RCS coolant flow rate during normal operation is 12,688 kg/s (27,972 lb/s).

The reactor vessel (see Figure 2.1) contains the core, core barrel, core support structures, and control rod and instrumentation component structures. Water from the SGs is pumped through the cold legs by the RCPs to the reactor vessel (RV) inlet nozzles, transitting the downcomer and RV lower plenum prior to passing through the lower core support plate and entering the core. Moving upward through the core, the coolant flows out the top and exits the RV via the outlet nozzles, flowing through the hot legs into the steam generators again. The reactor core is made up of 32,028 Zircaloy-4 clad fuel rods containing sintered UO_2 distributed in 157 fuel assemblies. The core active height is 3.66 m (12 ft). RCS overpressure control is assured by three safety valves set to open at a nominal pressure of 17.24 MPa (172.4 bar, 2,500 psia). Capacity of each safety valve is 36.3 kg/s (80 lb/s). Two Power Operated Relief Valves (PORVs) are available, set to relieve RCS pressure when it reaches 16.2 MPa (162 bar, 2,350 psia). PORV nominal relief capacity is 22.6 kg/s (49.7 lb/s).

Safety grade emergency systems are designed to protect the RCS in the event of an accident. Should normal feedwater flow be lost, the auxiliary feedwater system (AFWS) is available to provide coolant to the steam generator secondaries. The AFWS has three pumps: two are driven by electric motors; the third is driven by a steam turbine. The AFWS takes suction from the condensate storage tank (CST). The Emergency Core Cooling System is a suite of systems designed to deliver coolant water to the reactor vessel in the event of a LOCA. The ECCS provides makeup water during small break accidents when the RCS remains at a relative high pressure via three High Pressure Injection System (HPIS) pumps. These pumps serve as charging pumps under normal operative conditions. For larger breaks in the RCS, the Low Pressure Injection System (LPIS) is available to provide high volume, low pressure coolant flow to the RCS. Both the HPIS and the LPIS can function in a recirculation mode as well as in an injection mode. In the recirculation mode they take suction from the containment sump. Surry also has three passive accumulators to provide immediate, high flow, low pressure injection to the RV in the case of large breaks in the RCS.

2.2 Containment

The Surry containment, designed and built by Stone and Webster, is a reinforced concrete cylinder with a hemispherical dome. Figure 2.2 shows a cross section of the containment. The cylindrical portion of the containment sits on a basemat that is 3.05 m (10 ft) thick. The wall of the cylinder is about 1.3 m (4.3 ft) thick. The dome thickness is about 0.8 m (2.6 ft). A welded steel liner forms the pressure boundary. Containment volume is 50,971 m^3 (1,800,000 ft^3), and the design pressure is 0.41 MPa (4.1 bar, 45 psig, 59.7 psia). Due to conservatisms in design and construction, most estimates of the failure pressure are between two and three times the design pressure. For the MELCOR analyses, a containment failure pressure of 0.97 MPa (9.7 bar, 126 psig, 140.7 psia) was used, which identical to the mean value used for the calculations done for the Surry plant in support of NUREG-1150[4] and documented in the supporting document.[5]

During normal operation, the interior of the containment is maintained at about 0.07 MPa (0.7 bar, 10 psia). Normal containment cooling is by fan coolers. These are not safety grade, and they will be partially submerged if the containment sump is full of water. Emergency containment heat removal is accomplished by the spray systems. The containment spray injection system (SCIS) has two trains, each with one pump which takes suction from the Refueling Water Storage Tank (RWST). There are two containment spray recirculation systems (CSRS), each with two trains. Each of the six containment spray

trains is independent of the other spray systems, except that each requires electrical power for the pumps. Each containment spray recirculation train includes a heat exchanger that is cooled by the service water system and a pump that takes suction directly from the containment sump. One system has its pumps located inside the containment and the other has its pumps located outside the containment.

There is no connection between the containment sump and the reactor cavity at a low elevation in the Surry containment. Water from a pipe break in containment will flow to the sump. The reactor cavity will remain dry unless the containment sprays operate.

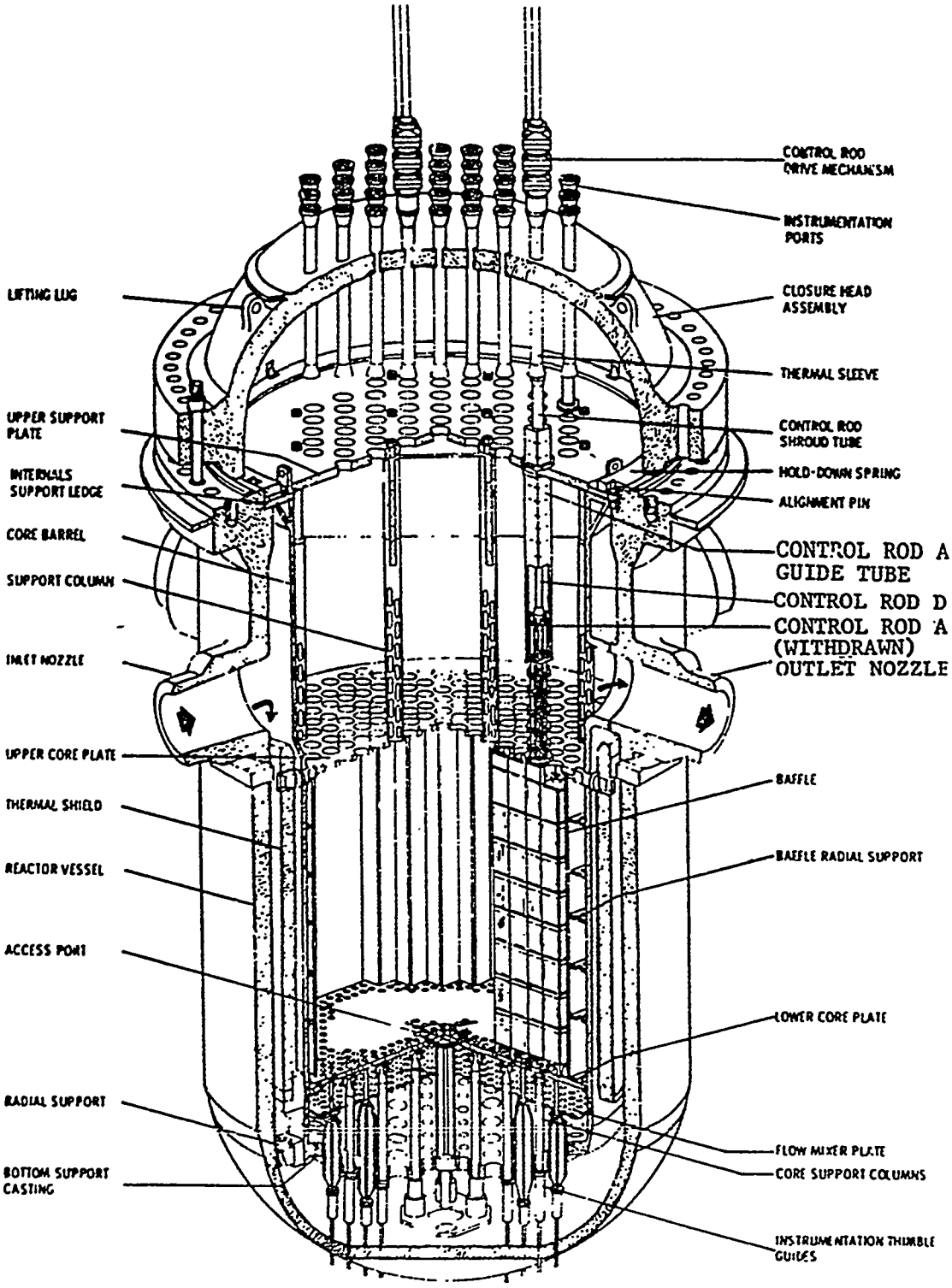

Figure 2.1 Surry Reactor Vessel

PWR

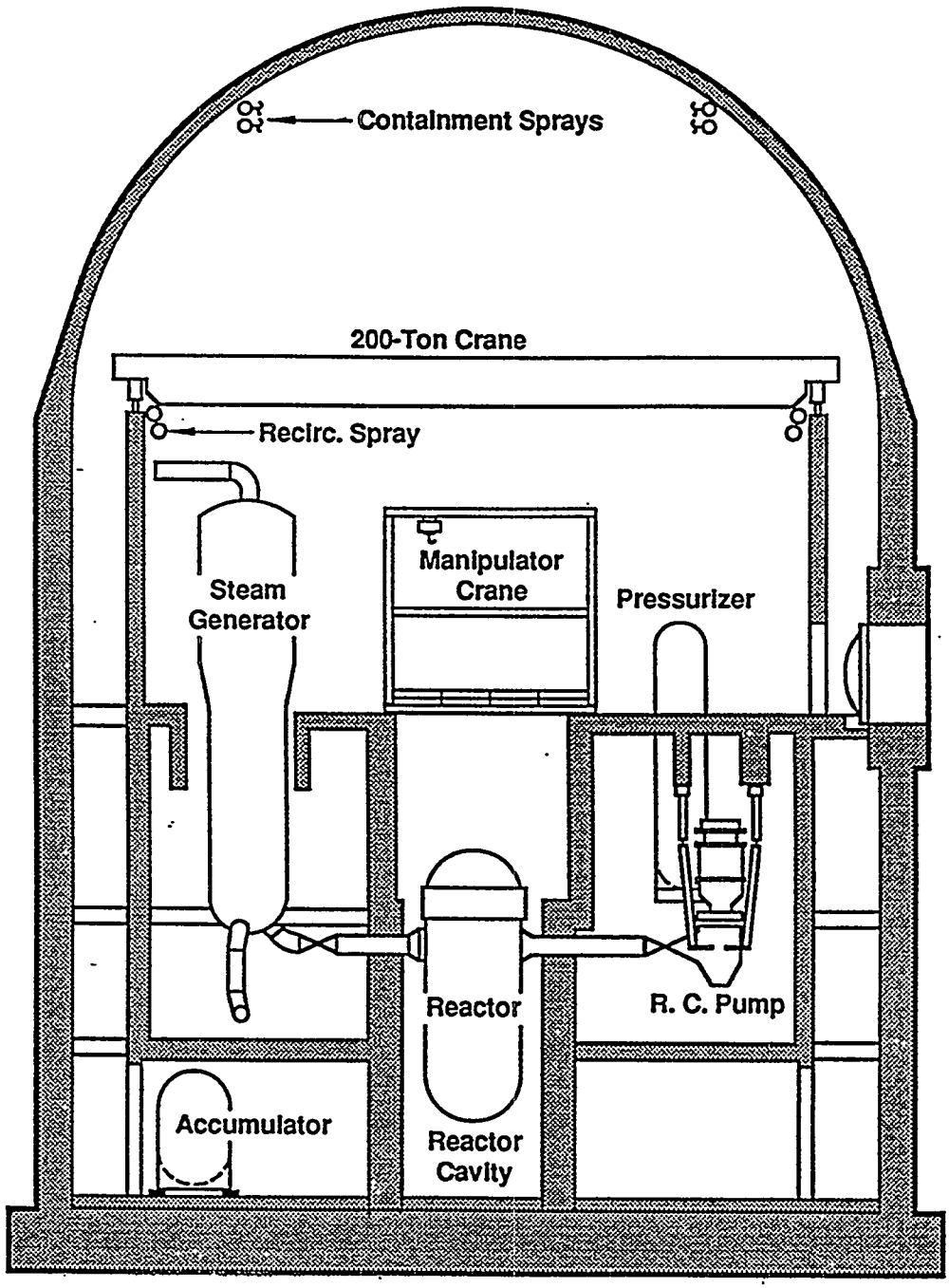

Figure 2.2 Surry Subatmospheric Containment

3 Accident Sequences

The accident sequences analyzed with MELCOR and documented in this report are described using the nomenclature originally defined in the Reactor Safety Study, also referred to as WASH-1400.[6] The AG accident refers to a large break loss of coolant accident, and the S2D and S3D accidents refer to small break LOCA's, as per the WASH-1400 accident naming convention, all initiated when the reactor is at full power. The accident sequences are defined in the following paragraphs.

3.1 AG Large Break LOCA Sequence

The AG accident sequence analyzed with MELCOR was characterized by a 0.74 m (29 in) diameter break in the Loop A hot leg combined with loss of containment heat removal capability, but with all the other safety systems operational. Additionally, the Auxiliary Feedwater System (AFW) remained in operation throughout the accident, and the steam generator secondaries were depressurized to a target pressure of 1.31 MPa (13.1 bar, 190 psia) by the operators, starting at 30 min. At the beginning of the incident, the normal containment cooling system (fan cooling system) was operating but tripped off within a few seconds due to the rise in containment pressure above the 0.172 MPa (1.72 bar, 25 psia) setpoint. The Containment Spray Injection System initiated based on this same 0.172 MPa setpoint, delivering water from the Refueling Water Storage Tank through the spray nozzles located in the containment dome and reducing containment pressure in the process. Concurrently, the passive accumulators and the active ECCS components, the High Pressure Injection System and Low Pressure Injection System, provided cooling water to the core. The combined action of the containment sprays and ECCS led to rapid depletion of the RWST and consequent switchover to recirculation mode. From that point onward, with the Containment Recirculation Spray System (CSRS) coolers inoperable, the containment pressure began to rise slowly toward the containment failure point. Upon containment failure, the ECCS systems ceased operation and boiloff of the remaining inventory commenced, leading to core uncovery, core melting, and vessel breach. When the core exit gas temperature reached 922 K (1,200°F), the operators manually opened the primary system power operated relief valve (PORV), although, by that point, the primary system was already depressurized.

3.2 S2D Small Break LOCA Sequence

This accident sequence was initiated by a 0.05 m (2 in) diameter break in the Loop A hot leg. The AFW system was available indefinitely, but all active ECCS systems, i.e., HPIS and LPIS, were unavailable for injection to the primary system. Primary system passive accumulators were functional. Once they were discharged, boiloff of the primary system inventory progressed through core uncovery, core melting, and vessel breach. Containment Engineered Safety Features (ESF), containment coolers and containment sprays, were available from the start of the accident. The containment coolers were operating at the beginning of the accident, shifting to high capacity when the containment temperature reached 313.7 K (105°F). When containment pressure rose to the 0.172 MPa (1.72 bar, 25 psia) setpoint, the containment coolers shut down, and the containment sprays began injecting water drawn from the RWST. With RWST depletion, the containment spray system shifted to recirculation mode, drawing water from the containment sumps and passing it through the containment spray recirculation coolers prior to spraying it back into the containment atmosphere. Operator depressurization of the steam generator secondaries to a pressure of 1.31 MPa (13.1 bar, 190 psia) began at 30 min, with completion scheduled for 60 min. The primary system was depressurized by the operators when the core exit gas temperature reached 922 K (1,200°F).

3.3 S3D Pump Seal LOCA Sequence

This accident sequence was initiated by a very small break, characterized as a pump seal LOCA, with a total leak rate at normal operating conditions of 2,839 liters per min (750 gpm). For the MELCOR run, all three primary system loops were given breaks sized to produce leakage flows of 946.3 liters per min (250 gpm) at normal system pressure. All other pertinent accident sequence characteristics were identical to those specified for the S2D sequence described in Section 3.2.

4 MELCOR Plant Model

4.1 General Features

Our MELCOR Surry model was developed from a MELCOR input deck originally received from the Idaho National Engineering Laboratory[7-9] (INEL), which in turn was based on a SCDAP/RELAP5 input deck developed by INEL[10] and subsequently modified by a Sandia National Laboratories analyst for use in station blackout sequence calculations.[11,12] For the analyses documented in this report, that deck was modified further, from a single loop to a three loop model. ECCS active and passive systems models were added, along with containment Engineered Safety Features models. Furthermore, models were created to simulate intentional depressurization of the steam generator secondaries and manual depressurization of the primary system when the core exit gas temperature reached a specified value.

4.2 Nodalization

The MELCOR Surry model for these calculations is made up of 33 control volumes (6 for the reactor vessel and internals, 16 for the primary system loops, 4 for the steam generator secondaries, 6 for the containment, and 1 for the environment); 67 flow paths (51 internal to the RCS, 10 internal to the containment, 5 connecting the RCS to containment, and 1 linking the containment to the environment); and 143 heat structures (114 for the RCS and 29 for the containment). Figure 4.2.1 and 4.2.2 give a graphic representation of the basic nodalization used for the primary system and for the containment, respectively, of the Surry plant; note that time-specified control volumes representing SG feedwater and AFW sources and sinks, and the environment outside containment, are not shown in these figures, for simplicity.

All control volumes were specified to use nonequilibrium thermodynamics and were specified to be vertical volumes; all heat structures used the steady-state temperature-gradient self-initialization option. Detailed volume-altitude tables and junction flow segments were used to correctly represent subcomponents in and between the major components modelled.

Nodalization of the reactor core, a separate model from the control volumes listed above, consists of 39 core cells divided into 3 radial rings and 13 axial levels. Axial levels 4 through 13 make up the active core region, while levels 1 through 3 model the lower plenum, including the core support plate in level 3. Figure 4.2.3 illustrates the reactor core nodalization used.

The cavity under the reactor vessel was specified to have an internal depth and radius of 1.00 m and 4.28 m, respectively; the concrete is 1.302 m thick on the sides and 3.04 m thick below the cavity.

The hydrogen combustion model in MELCOR was activated, with all default input settings used. Therefore, the hydrogen and oxygen mole fraction limits for ignition in the absence of igniters were taken as 0.10 and 0.05, respectively, while the combined H_2O and CO_2 mole fraction limit for inerting volumes with excessive diluents was taken as 0.55.

The default classes in the MELCOR RN and DCH packages were used. Table 4.2.1 contains a list of the MELCOR fission product material classes, including the total radioactive mass inventory of each class initially present; a small fraction of these were specified to be in the gap rather than in the fuel. These calculations were done using the CORSOR fission product release model. These analyses also were done specifying two MAEROS components, one for the water (Class 14) and another for all other aerosols and fission product vapors, and the default number (five) of aerosol distribution size bins and size bin diameters.

A large number of control functions (435) were used to track the source term release and subsequent distribution, to determine timing and flow of various AFW, ECCS and spray systems, and to adjust valves and pumps as required. In particular, control functions were used to track the total and radioactive masses of each class (1) released from the intact fuel and/or debris in the vessel (either in the core, the bypass or in the lower plenum), (2) released from the debris in the cavity, (3) remaining in the primary system (i.e., the reactor vessel), (4) in the containment, and (5) in the environment. Those control functions provided time-dependent source term release and distribution data for subsequent postprocessing in a form more convenient for analysis and evaluation.

4.3 Plant Model Features

MELCOR is sufficiently flexible to allow creation of as detailed a model as necessary in order to analyze the accident sequences in a realistic way. The AG accident sequence required the most complicated input deck, since both primary ECCS and containment ESF systems were in operation at some point in the calculation. Sufficient modeling input was included to model properly the High Pressure Injection System (HPIS), the High Pressure

Recirculation System (HPRS), the Low Pressure Injection System (LPIS), and the Low Pressure Recirculation System (LPRS). Detailed modeling of the primary system passive accumulators was included in the station blackout deck. Models were furnished to simulate the Containment Spray Injection System (CSIS) and the Containment Spray Recirculation System (CSRS), including the capability for simultaneous operation. The containment coolers were modeled for both the normal and enhanced operating modes.

Sources and sinks were utilized to model the Auxiliary Feedwater System. Control function logic models were included to model operator depressurization of the steam generator secondaries at a time of choice, and to model operator depressurization of the primary system via the Power Operated Relief Valve (PORV) when the core exit gas temperature reached 922 K (1,200°F). Finally, control function logic was included to allow the operators to shift delivery of ECCS water from the cold legs to the hot legs at the 16 hr mark, as assumed in the AG accident sequence.

Table 4.2.1 MELCOR RN Classes and Initial Inventories

Class Name	Representative	Member Elements	Class Total Radioactive Mass, (Kg)
1. Noble Gases	Xe	He, Ne, Ar, Kr, Xe, Rn, H, N	2.4483E+02
2. Alkali Metals	Cs	Li, Na, K, Rb, Cs, Fr, Cu	1.3645E+02
3. Alkaline Earths	Ba	Be, Mg, Ca, Sr, Ba, Ra, Es, Fm	1.0740E+02
4. Halogens	I	F, Cl, Br, I, At	1.0545E+01
5. Chalcogens	Te	O, S, Se, Te, Po	2.1481E+01
6. Platinoids	Ru	Ru, Rh, Pd, Re, Os, Ir, Pt, Au, Ni	1.5110E+02
7. Early Transition Elements	Mo	V, Cr, Fe, Co, Mn, Nb, Mo, Tc, Ta, W	1.7819E+02
8. Tetravalents	Ce	Ti, Zr, Hf, Ce, Th, Pa, Np, Pu, C	3.1440E+02
9. Trivalents	La	Al, Sc, Y, La, Ac, Pr, Nd, Pm, Sm, Eu, Gd, Tb, Dy, Ho, Er, Tm, Yb, Lu, Am, Cm, Bk, Cf	2.9170E+02
10. Uranium	U	U	6.1025E+04
11. More Volatile Main Group	Cd	Cd, Hg, Zn, As, Sb, Pb, Tl, Bi	7.1350E-01
12. Less Volatile Main Group	Sn	Ga, Ge, In, Sn, Ag	4.0521
13. Boron	B	B, Si, P	0
14. Water	H_2O	H_2O	0
15. Concrete	---	---	0

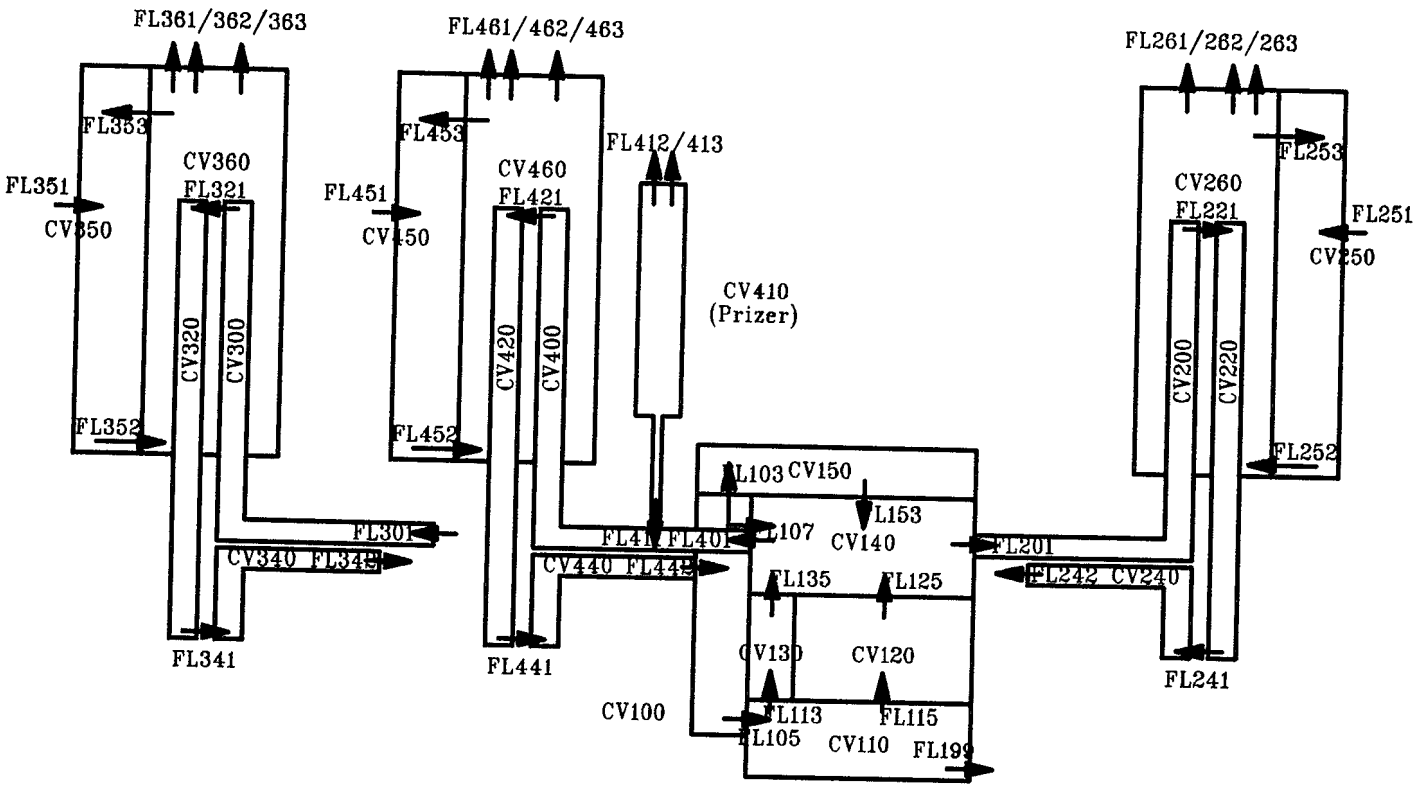

Figure 4.2.1 MELCOR Nodalization for Primary System

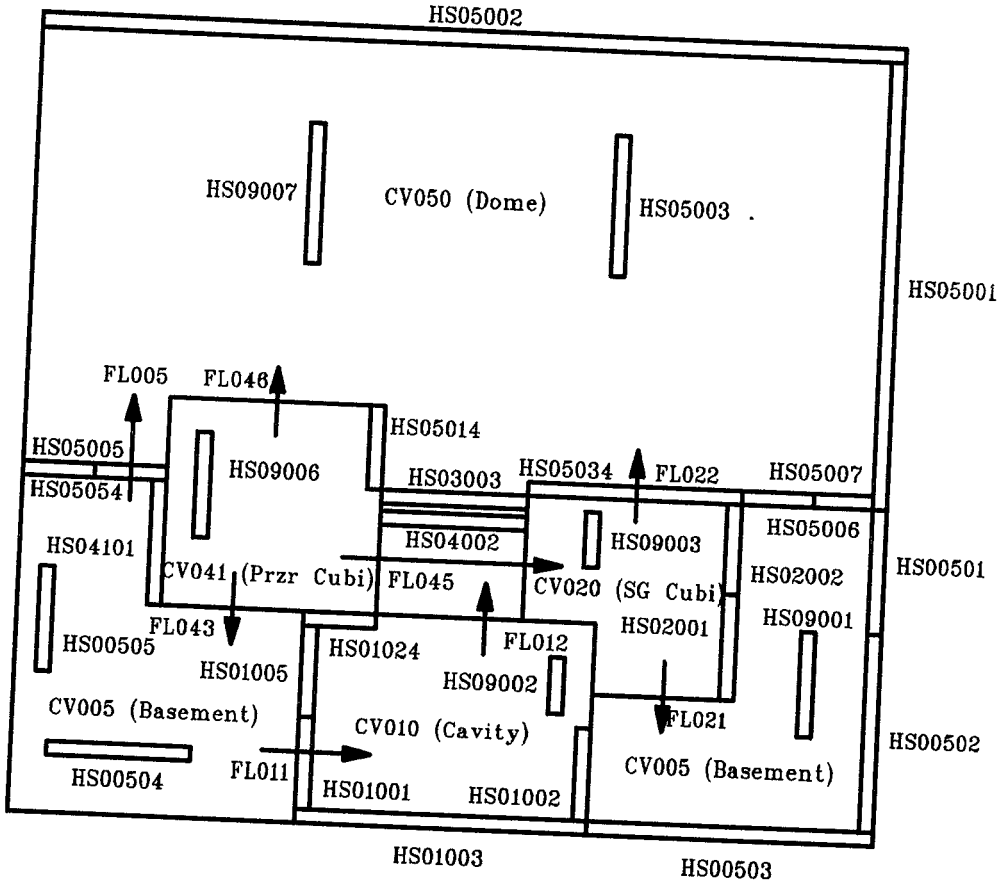

Figure 4.2.2 MELCOR Nodalization for Containment

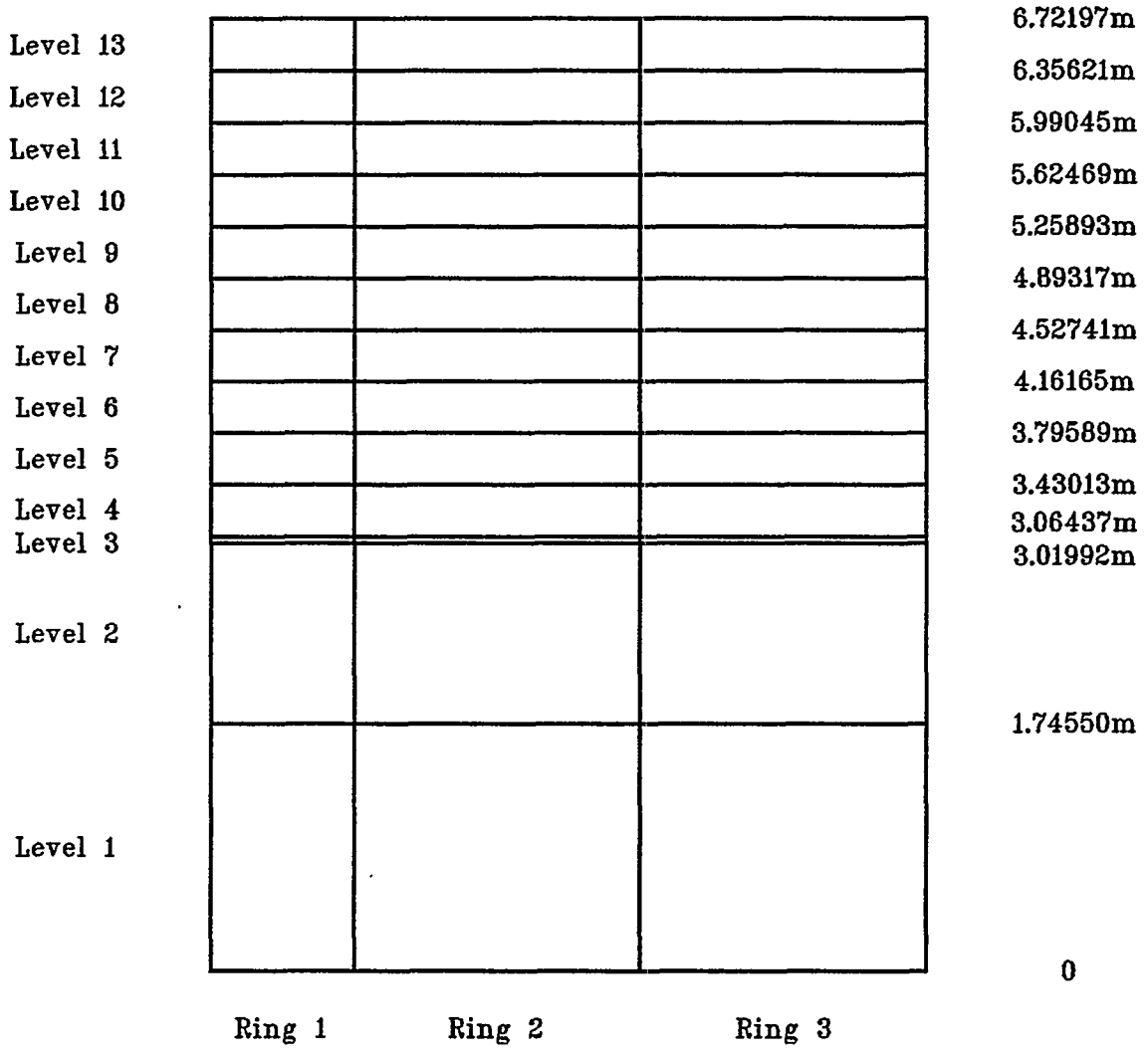

Figure 4.2.3 MELCOR Nodalization for Core

5 Results and Comparisons with STCP

5.1 General Comments Applicable to All Three Accident Simulations

For each of the accident sequences simulated with MELCOR, the fuel release model selected was CORSOR with surface-to-volume ratio correction. Based on the structural response issues expert opinion elicitation used for the NUREG-1150 study,[4] the containment failure pressure was specified at 0.97 MPa (9.7 bars, 140.7 psia). The STCP calculations defined containment failure pressure at 0.93 MPa (9.3 bars, 135 psia). The MELCOR calculations were run on an IBM RISC-6000 Model 550 workstation, with the AG sequence requiring 128,000 seconds of computing time to run through 300,000 seconds of accident time; the S2D sequence used 27,400 seconds to carry the simulation through 50,000 seconds, and the S3D sequence required 93,000 computer seconds to simulate 100,000 seconds.

5.2 AG Sequence

The AG accident sequence analyzed with MELCOR was characterized by a 0.74 m (29 in) diameter break in the Loop A hot leg combined with loss of containment heat removal capability, but with all the other safety systems operational. The main features and assumptions of this sequences are briefly described in Section 3.1.

5.2.1 Key Events

Table 5.2.1 summarizes the AG accident sequence predicted timing of events for both the STCP and MELCOR calculations, starting with accident initiation. Immediately upon rupture of the 0.74 m (29 in) diameter Loop A hot leg pipe, the primary system commenced a rapid blowdown, pressurizing the containment above the 25 psia containment spray initiation setpoint in just a few seconds. Both STCP and MELCOR predicted containment sprays to begin delivery in less than a minute after accident initiation. With the massive blowdown, the containment sumps fill rapidly to a level sufficient to allow the containment recirculation sprays to begin delivery within a few minutes, adding their flow to that already present due to the injection sprays.

While the containment safety systems were delivering water through the spray systems, the active and passive emergency core cooling systems were supplying water to the primary. A rather large difference exists between STCP and MELCOR concerning the time when the passive accumulators were fully discharged. STCP predicted 25.1 min, while MELCOR predicted 1.0 min. MELCOR predicted HPIS and LPIS injection to begin just 0.4 min after accident initiation. Since the primary active ECCS systems, with their high flow rates, initiated early in the accident, the timing of the passive accumulator delivery is not critical to the outcome of the accident progression. With both containment sprays and ECCS operating in the injection mode, the RWST (Refueling Water Storage Tank) was depleted at the 50 minute mark, according to the MELCOR simulation, with the consequent shift from the injection mode to the recirculation mode for the high pressure and low pressure ECCS systems. The MELCOR simulation continued in this mode, with sprays and ECCS systems in operation, up until the 960 min point, when the operators shifted ECCS injection from the loop cold legs to the hot legs, as per emergency procedures. With the containment spray coolers inoperable, there was no way to remove heat from the containment atmosphere, and it continued to pressurize in a linear fashion. STCP predicted containment failure at 3,054.2 min, based on a containment failure pressure of 9.3 bars (~135 psia), while MELCOR predicted the containment to fail at 3,540 min, using 0.97 MPa (9.7 bars, 140.7 psia) as the failure pressure. Both codes assumed ECCS failure within about a minute of containment failure. At that point, there was no further source of water to the primary system, and it entered a boiloff stage.

STCP predicted the start of core uncovery at 3,080.6 min, and MELCOR predicted this to occur at 3,570.2 min. MELCOR modeled the core in 3 radial rings and 10 axial nodes. MELCOR predicted the onset of zircaloy cladding oxidation at 3,619.6 min, with the initial gap release occurring at 3,621.5 min, both in ring 1. MELCOR predicted the start of core melting in the innermost ring at 3,665.0 min. STCP did not differentiate between the different core components and predicted core melt to begin at 3,155.6 min. MELCOR calculated the beginning of core collapse in radial ring 1 at 3,684.3 min, while STCP calculated global core collapse at 3,209.2 min. Since the MELCOR analysis produces a more gradual collapse of the core than STCP, the reactor vessel bottom head did not completely dry out prior to failure. For the STCP run, bottom head dryout was predicted at 3,237.6 min, and bottom head failure at 3,371.6 min. MELCOR calculated failure of the bottom head in the region underneath radial ring 1 at 3,685.4 min. For both the MELCOR and STCP runs, debris ejection began immediately, with the entire mass of molten corium transferred to the cavity in a single time step for the STCP run. The MELCOR calculation took on the order

of 45 min to transfer the core from the vessel to the cavity. For both codes, as soon as molten corium was transferred to the cavity, core concrete attack began, producing aerosols and gases in the process. Neither code predicted deflagrations, as the containment was steam inerted at this point.

5.2.2 Primary System Behavior

Figures 5.2.1 through 5.2.4 show primary system response based on parameters calculated by MELCOR. Figure 5.2.1 shows the pressure response of the upper plenum (CV140), the vessel downcomer region (CV100), and the core (CV120), all virtually identical. Due to the large size of the break in hot leg A, the primary pressure fell very rapidly at the start of the accident, reaching equilibrium with containment at about the 1 minute mark. From that point onward, the primary system pressure tracked containment pressure (presented later in Figure 5.2.7) as it slowly increased to the failure pressure of 0.97 MPa (9.7 bars, 140.7 psia). With containment failure at 3,540 minutes, the primary pressure fell to atmospheric.

Primary temperatures in the reactor vessel downcomer and upper plenum control volumes are given in Figure 5.2.2. As long as the ECCS systems injected into the cold legs, the reactor vessel downcomer volume was a few degrees cooler than the upper plenum volume. At 960 min, when ECCS flow was shifted from cold legs to hot legs, the temperatures in the downcomer and lower plenum volumes became essentially the same. This remained the case until containment failure at 3,540 min, when all ECCS flow was lost to the primary system and boiloff of the remaining coolant inventory began. At that point, the temperature of the upper plenum spiked upward, reflecting the effect of the core uncovery and melting.

Figure 5.2.3 shows the core exit gas temperature as predicted in the upper plenum control volume (CV140), and also the local core fluid temperatures in the uppermost axial level in each radial ring. Steam exited the core at about 400 K (260°F) for the first 960 min. At that juncture, the temperature of the exiting gas jumped because the ECCS flow had been redirected from the loop cold legs to the hot legs. After settling down to about 425 K (305°F) by 1,600 min, the temperature increased slowly to around 450 K (350°F) by the time of containment failure, a reflection of the gradual heatup of the coolant inventory being recycled through the core by the ECCS systems. With ECCS no longer available, the temperature of the gas exiting the core rose to nearly 850 K (1,070°F) at the time of vessel failure.

Figure 5.2.4 is a plot of collapsed and swollen liquid levels in the reactor vessel, in the upper plenum, core and lower plenum. (Dotted lines are provided in the figure indicating the top-of-core/bottom-of-UP elevation at 6.72197 m and the bottom-of-core/top-of-LP elevation at 3.06437 m, for reference.) There was very little level swell predicted anywhere in the vessel except in the core. The core remained fully covered until the 960 min point in the accident, when the ECCS flow is shifted from cold legs to hot legs. At that point, the water level in both the downcomer and the core fell below the top of the active fuel, even though significant liquid still remained in the upper plenum. The collapsed liquid level in the core dropped to about the core midplane, but the significant level swell in the core kept the swollen level near the top of the active fuel, and thus maintained core cooling. Water levels then remained about constant until containment failure at 3,540 min, when ECCS flow was lost. At that point, the water levels in the vessel dropped quickly, with all inventory lost at the point of vessel lower head failure, 3,685.4 min.

Integrated outflows from the primary system through the hot leg break and through the vessel breach are given in Figures 5.2.5 and 5.2.6, respectively; the outflows are subdivided into liquid water, steam and hydrogen flows in both cases. As expected in a large break LOCA sequence, most of the RCS inventory is lost as liquid water out the break. Liquid remaining in the lower plenum at the time of vessel lower head failure is lost out the vessel breach to the cavity.

5.2.3 Core Degradation

Figure 5.2.7 through 5.2.9 show cladding temperatures predicted at different axial levels in the various radial rings during the core damage period. (Recall that MELCOR modelled the core in 3 radial rings and 10 axial levels in the active fuel region.) The behavior in all three rings is very similar, only slightly delayed in time in the outer rings due to lower power densities. MELCOR predicted the start of core heatup in the uppermost axial levels immediately after core uncovery began. Core uncovery and core heatup continued with no major interruption, with cladding oxidation and initial gap release beginning at ~3,620 min. The core heatup and damage was quite rapid -- MELCOR predicted the start of core melting in the innermost ring at 3,665 min and

core collapse and lower head penetration failure about 20 min later.

Figure 5.2.10 shows the total masses of core materials (UO_2, Zircaloy and zirc oxide, stainless steel and steel oxide, and control rod poison) remaining in the vessel during the later portion of the AG transient. Figure 5.2.11 shows the same information, but normalized by the initial masses of each material present. (Note that the fractions of ZrO_2 and steel oxide use the initial masses of zircaloy and stainless steel, respectively, as normalizing masses, because no oxides are present initially.) Debris ejection began immediately after lower head failure, and it took on the order of 45 min to transfer the majority of the core material from the vessel to the cavity. All the UO_2 is transferred to the cavity, as is most of the unoxidized zircaloy and almost all the oxides; however, much of the steel in the core support plate and the lower plenum structure is predicted to remain unmelted and in place even after vessel breach.

The temperature and mass of debris in the lower plenum (i.e., on the lower head) are presented in Figures 5.2.12 and 5.2.13. There is only a brief period of time when a substantial mass of debris is found in the lower plenum, between initial core plate failure and initial lower head penetration failure and ejection to the cavity.

5.2.4 Containment Response

Containment pressure and temperature response are presented in Figure 5.2.14 and Figure 5.2.15 as calculated by MELCOR and with the corresponding STCP result [Ref.1, Vol.3, Figures 4.1 and 4.2] given for comparison. The containment atmosphere pressures and temperatures predicted by both codes behaved in similar ways. The pressures and temperatures rose precipitously in the initial minutes of the accident, in reaction to the rapid initial blowdown of primary system coolant, and then decayed back down to the 0.1 MPa (1 bar, 15 psia) and 330 K (135°F) range, as relatively cold water was injected to the containment volumes by the containment spray injection system and to the primary system via the ECCS injection systems. After the RWST was depleted of cool water, the containment began its slow heatup and repressurization, as energy was released to a containment without capability for heat removal. During this pressurization period, the containment temperature remained at the corresponding saturation temperature. The containment pressurized slightly faster in the STCP analysis which combined with the different failure pressures assumed in the two analyses caused the containment to fail slightly earlier in the STCP calculation than in the MELCOR calculation. With containment failure at 3,054.2 min for the STCP calculation and at 3,540.0 min for the MELCOR calculation, the pressure and temperature within containment fell rapidly. The pressure returned to ambient, while the containment atmosphere temperature stabilized at around 373 K (212°F), saturation temperature at ambient atmospheric pressure.

Figure 5.2.16 shows the mole fractions of steam, nitrogen, oxygen, hydrogen and other noncondensable gases in the cavity control volume (CV010). The results for the cavity control volume atmosphere given in figure is representative of the other containment control volumes, and it shows that prior to failure the containment is steam inerted. After containment failure, practically all of the noncondensible gases are swept out into the environment leaving only steam in the containment atmosphere. No combustible gas deflagrations are predicted, by either the MELCOR or STCP codes.

Figure 5.2.17 shows the total decay heat present during the accident, along with the amount associated with the cavity after reactor vessel bottom head failure. It is apparent that most of the fission products are retained in the cavity, either in the corium or in the cavity water. This is due, in part, to the reactivation of the containment sprays after containment failure.

In the MELCOR calculation being reported here, these sprays were lost at the ~65,000 sec (1,083 min) mark, due to a control function that checks to see if the sump water used as the source of inventory for the containment sprays in recirculation mode is too hot to allow the system to pump it (a way of looking at NPSH difficulties). If that is the case, the sprays fail. What happened in the run is that the sprays failed for this reason, and then, with the containment failure and depressurization of the containment back to ambient atmospheric conditions, the sprays reactivated themselves (not a likely thing to happen) and began spraying water again, just when the inventory of aerosols in the containment atmosphere was richest.

Since the thrust of our work was to estimate the source term to the containment, it may be immaterial whether the radionuclides have been washed out of the atmosphere by the sprays or are located somewhere else. If the inventory split between pools, deposition onto heatsinks, and suspension in the containment atmosphere is deemed critical to the presentation of this report, then the AG

sequence needs to be rerun with containment spray control parameters adjusted to make the sprays behave in whatever manner is deemed most suitable.

The mass of core debris in the cavity, the mass of ablated concrete, the mass of gas produced, and the total mass of debris (including core debris together with ablated and reacted concrete) are presented in Figure 5.2.18. Before about 4,133 min, the debris in the cavity was primarily debris ejected from the vessel; after that time significant core-concrete interaction began and substantial masses of ablated and reacted concrete were added to the total cavity debris.

Figure 5.2.19 shows the mass inventories of the metallic and oxidic debris in the cavity, and Figure 5.2.20 shows the temperature histories of those debris layers. At around 4,133 min, a CORCON layer flip occurred, in which the debris bed switched from an initial configuration with a metallic debris layer above a heavy oxide layer to a later configuration with a light oxide layer above a metallic debris layer. This layer flip occurred when enough concrete had been ablated (with its resultant low-density silicate oxides) to dilute the high-density zirc oxide and steel oxide debris to an average density value less than the metallic debris density.

Figure 5.2.21 shows cavity heat sources due to decay heat and chemical reactions occurring in the corium. It is interesting to note that, for a brief period around the 4,133 min mark, the chemical reaction energy release is roughly 7 times the magnitude of the energy release due to decay heat. This time corresponds to the CORCON layer flip just described.

The CORCON layer inversion resulted in greatly increased heat transfer from the melt to the concrete. The maximum cavity depth and radius are presented in Figure 5.2.22. The relocation of the metallic layer to the bottom of the cavity causes an increase in the rate of ablation vertically downward and halts further radial ablation. The heat generated by chemical reactions within the cavity also increases dramatically at this point, as just noted in Figure 5.2.22.

Figure 5.2.23 gives an accounting of the total mass of non-condensible gases released from the cavity and from the core during core damage and during core-concrete interaction. The majority of non-condensible gas produced is carbon monoxide, and the majority of that production occurs in the cavity during core-concrete interaction.

5.2.5 Fission Product Transport and Release to the Environment

The overall behavior of fission products released from fuel is described in Tables 5.2.2 and 5.2.3 and shown graphically in Figures 5.2.24 through 5.2.47. Tables 5.2.2 and 5.2.3 give the radionuclide fractional distribution at the end of the accident simulation, 3,973.1 min for STCP and 5,000 min for MELCOR. Figures 5.2.24 through 5.2.35 show the mass of radionuclides, by fission product material class, released from the fuel in both the in-vessel and ex-vessel portions of the accident, along with a trace giving the sum of the two, all normalized by the initial inventories of each class. Figures 5.2.36 through 5.2.47 are plots of radionuclide masses released into the primary control volumes, the containment control volumes, the environment, and a sum total of the three, also normalized by the initial inventory present of each class; these latter figures include any radionuclides suspended in the atmosphere and deposited in pools and on structures, but do not include radionuclides still in the fuel debris in the core and/or cavity.

Fuel damage does not occur until after failure of the ECCS systems; and by that point, the containment has failed already. Thus, a path to the environment was available and open when the first gap releases occurred at ~3,620 min. Prior to reactor vessel lower head failure, fission products were transported from the primary system and into the containment via the Loop A 0.74 m (29 in) diameter hot leg break. At lower head penetration failure, molten corium was transferred in stages to the cavity, where further fission product release to the containment occurred.

When comparing environmental releases between the MELCOR and STCP simulations, significant differences exist. As noted above, besides the fact that MELCOR models revolatization of radionuclides from the primary system and STCP does not, it is unclear whether the containment sprays were in operation at the time of reactor vessel lower head failure for the STCP run; for the MELCOR simulation, they were in operation at this time.

The fractional release of radionuclides into the containment and environment combined are roughly the same between the two runs for the release groups identified by the representative elements Xe, and Cs. MELCOR predicts a significantly higher fractional distribution for Ba and marginally higher for I.

MELCOR predicts a higher release for Ru, too; but only trace amounts are being compared. Both codes predict the bulk of the Ru to remain in the core debris in the cavity. Comparisons between the two codes for fractional distribution of Ce and La show some differences between trace amounts in the containment and environment, combined, but both codes show nearly all of the inventory of these radionuclides residing in the fuel debris in the cavity. MELCOR predicted the fractional distribution of Te for the combined containment and environment to be significantly less than was predicted by STCP; the fractional distribution in the RCS was smaller for the MELCOR run, a significantly larger fraction resided in the cavity, the containment inventory was roughly equal to the STCP value, but the fraction released to the environment was much less than for the STCP run.

Figures 5.2.24 and 5.2.25 show that almost all of the Class 1 and Class 2 volatiles are released from the fuel in the MELCOR calculation. About 60% of that release occurs in-vessel, with the remaining ~40% released ex-vessel in the cavity. Note that Figure 5.2.27 shows a very similar release pattern for Class 4 (halogens like iodine, also considered volatiles) in-vessel, but no additional release in the cavity. This is due to a coding problem in MELCOR: the VANESA code, which is used to calculate the ex-vessel release within MELCOR, considers iodine to be released as CsI; since there is no separate CsI class in these MELCOR calculations, MELCOR counts that CsI release to be a Class 2 (Cs) release (incidentally explaining why the total Class 2 release fraction shown in Figure 5.2.25 is greater than 100%, which should be impossible). Based upon physical insight, the Class 4 release should closely resemble the Class 1 and 2 results.

The release behavior predicted by MELCOR can be grouped into several subdivisions. Assuming the correct iodine behavior, ~100% of the Class 1, Class 2 and (corrected) Class 4 radionuclide inventories are released, about 50%/50% in-vessel and ex-vessel. The next major release fractions are of Ba/Sr (~15%) and Te (~25%), both mostly predicted to occur in the cavity. About 6-7% of the Cd and Sn radionuclide inventory is released, and about 3% of the Mo radionuclide inventory. (Note that these amounts consider only the release of radioactive forms of these classes, and not additional releases of nonradioactive aerosols from structural materials.) Finally, a total ≤0.02% of the initial inventory of the refractories (Ru, Ce, La and U) are released.

The release patterns become more varied as the release amount decreases. Most of the Class 9 (La) releases are predicted to occur in the cavity, similar to the behavior of Class 3 (Ba) and Class 5 (Te). All of the Class 8 (Ru) and almost all of the Class 11 (Cd) releases are predicted to occur in-vessel. Class 7 (Mo), Class 8 (Ce), Class 10 (U) and Class 12 (Sn) have most of their releases predicted to occur in-vessel, but a significant, non-zero, fraction of the initial inventory of these classes is released in the cavity.

The released radionuclide distributions are also predicted to fall into a few subdivisions. All of the noble gases (Class 1) and iodine (Class 4) are released to the environment by the end of the MELCOR simulation. Most of the Ba, Te and La (≥90% of the amount released) remain in the containment, with ~5% of the amount released still in the RCS and ~5% lost to the environment. All of the other classes have ~75% of the amount released remaining in the containment, with ~15% of the amount released still in the RCS and ~10% lost to the environment.

The total mass of fission products released from the fuel is shown in Figure 5.2.48. More than half the total release occurs during in-vessel core damage and melt ejection. The in-cavity release primarily occurs before the CORCON layer flip at around 4,133 min, with very little release at later times. Most of the fission products released are found in control volumes, in either atmosphere or pool, and about 50-70% of the fission products in the control volumes are vapors rather than aerosols (mostly because aerosols settle out and deposit onto heat structures more readily). Very few (≤5%) of the fission products are deposited onto heat structures.

5.3 S2D Sequence

This accident sequence was initiated by a 0.05 m (2 in) diameter break in the Loop A hot leg. The main features and assumptions controlling this sequence are described briefly in Section 3.2.

5.3.1 Key Events

Table 5.3.1 provides a summary of the event timing for the S2D accident sequence from both the STCP and MELCOR calculations. The starting point is accident initiation, when a 0.05 m (2 in) diameter Loop A hot leg pipe break occurred, and blowdown of the primary system coolant inventory to the containment began. By 1.0 min in the STCP calculation and 0.3 min in the MELCOR calculation, the containment fan coolers shifted from

normal operation to high capacity operation, when the containment atmosphere temperature rose above 313.7 K (105 °F). According to the accident sequence definition, the operators took action to depressurize the secondary side of the steam generators, beginning at 30 min and scheduled for completion at 60 min. Initial core uncovery occurred in the STCP calculation at 41.3 min and at 35.6 min for MELCOR. For both calculations, initial accumulator delivery commenced after the core had begun to uncover, at 44.0 min for the STCP calculation and 38.8 min for the MELCOR calculation. STCP predicted an uninterrupted delivery of accumulator water to the primary system that continued until depletion at 65.0 min. MELCOR predicted delivery in two stages, with the first finishing at 68.6 min, after having delivered 85 percent of the total accumulator inventory. MELCOR predicted a second accumulator delivery of the remaining inventory between 158.0 min and 158.5 min, after the core had begun to collapse. Both codes predicted initial accumulator delivery beginning just after the start of core uncovery, such that the core was recovered, but then a second core uncovery occurred. Timing for the second uncovery was 114.7 min according to STCP and 101.9 min for MELCOR. The MELCOR core model consisted of 3 radial rings and 10 axial nodes. Because of the recovering of the core with accumulator water, MELCOR predicted gap release in radial rings 1 and 2 prior to the onset of zircaloy oxidation. Radial ring 1 gap release was predicted at 46.5 min, ring 2 gap release at 48.1 min, and cladding oxidation at 61.7 min. MELCOR predicted gap release for radial ring 3 much later, at 135.7 min, due to the cooling effect of the accumulator water addition to the primary system.

A large difference in timing is evident between the two codes for their predictions of when the operators depressurize the primary system via the power operated relief valve, (PORV). For both simulations, depressurization of the primary system was scheduled to commence when the core exit gas temperature reached 922 K (1,200°F). This occurred for the MELCOR run at 49.0 min and at 148.0 min for STCP. The difference is not likely to have affected the final source term release to the containment very much. The nodalization of the core in the MELCOR run, such that the core melts in discrete stages, is the likely reason for the large timing difference between the runs.

MELCOR predicted the onset of core melting in the inside radial ring at 130.0 min, as compared to the STCP value of 161.6 min. Core slump in the MELCOR run occurred at 140.0 min, again in radial ring 1, while STCP predicted core slump at 176.8 min. STCP indicated global core collapse at 180.6 min, while MELCOR predicted collapse of the inner core segment, as modeled by radial ring 1, at 146.7 min.

With the melting and collapse of the core, containment pressure rose to the initiation setpoint for the containment sprays, 0.17 MPa (1.7 bars, 25 psia). Two things happened at that point. The containment coolers tripped off, and the containment spray injection system, drawing water from the Refueling Water Storage Tank (RWST), began operation. STCP predicted the containment sprays to commence injection at 188.0 min, while MELCOR predicted this to occur at 267.0 min. In conjunction with the Injection Spray System, the Recirculation Spray System commenced operation at 282.4 min for the STCP simulation and at 272 min for the MELCOR run. Water circulation through the Recirculation Spray System coolers provided heat removal capability for the containment. While STCP predicted bottom head dryout to occur at 209.2 min, prior to bottom head failure at 314.4 min, the MELCOR run predicted a much earlier localized bottom head failure in ring 1 at 148.3 min, with water still remaining in the lower head at that time. Debris ejection to the cavity began immediately upon lower head failure for the STCP run, with the onset of concrete attack at 315.5 min. For the MELCOR run, debris ejection to the cavity was delayed until 164.4 min, some 16 min after bottom head failure, due to the more gradual collapse of the core and the cooling effect of the water resident in the lower head. MELCOR predicted the onset of concrete attack and a layer inversion in the cavity at 333.3 min. STCP predicted corium layer inversion at 372.5 min.

5.3.2 Primary System Behavior

Compared to the rapid blowdown exhibited during the AG sequence large break LOCA, the primary behavior for the S2D sequence was much more benign in nature. However, with no Emergency Core Cooling Systems (ECCS) injecting makeup water to the primary system, the accident progressed with greater rapidity than did the AG sequence. Figures 5.3.1 through 5.3.4 give primary system response based on the MELCOR calculation.

Figure 5.3.1 shows the primary system pressure during the accident progression for the MELCOR analysis. After accident initiation, the primary pressure fell quite rapidly during the first few minutes from normal system pressure to 6 MPa (60 bar, 870 psia) and then made a rapid reversal, climbing back up to 7.4 MPa (74 bar, 1,075 psia) by the 15 min mark. At that point, the

primary pressure stabilized as decreasing primary inventory was offset by increasingly hot steam exiting the reactor core upper plenum. At 30 minutes, the first of several events occurred that reversed the primary repressurization trend, causing a precipitous drop. The first event was the operator initiated depressurization of the steam generator secondaries, beginning at 30 minutes and concluding at 68.6 minutes. Secondly, as the primary pressure fell below the passive accumulator setpoint, 4.24 MPa (42.4 bars, 615 psia), they began delivery of water to the cold legs. MELCOR predicted initial core uncovery at 35.6 minutes, with accumulator discharge beginning at 38.8 minutes. Thirdly, MELCOR predicted that the core exit gas temperature reached 922 K (1,200°F) at 49 minutes, prompting the operators to depressurize the primary system by opening the PORV valve. By approximately the 70 minute mark, the MELCOR analysis showed the primary pressure reduced to the 1MPa (10 bar, 145 psia) level, where it remained until bottom head failure in ring 1 at 148.3 minutes. At that point, the primary pressure equalized with containment pressure.

The primary system pressure predicted by STCP [Ref. 1, Vol. 6, Figure 4.2.50] is included in Figure 5.3.1 for comparison to the MELCOR calculation. The results are qualitatively very similar for the first ~150 min, with the MELCOR RCS pressure predicted generally slightly lower than the STCP predicted response. The repressurization at 180-220 min in the STCP result has no counterpart in the MELCOR analysis; it corresponds in timing to the period between core collapse (at 180.6 min for STCP) and bottom head dryout (at 209.2 min for STCP), and is likely due to boiling off the remaining lower plenum water inventory. MELCOR fails the lower head very soon after core collapse (148.3 min and 146.7 min, respectively), and thus any water left in the lower plenum simply falls into the cavity; after lower head failure, the MELCOR RCS pressure calculated remains essentially at the containment pressure.

Figure 5.3.2 gives primary temperatures in the reactor vessel downcomer and upper plenum control volumes. One must keep in mind that after the onset of debris ejection at 164.4 min, the downcomer and upper plenum had been drained of water, for all practical purposes. The primary temperatures in the downcomer and upper plenum were in the 550 K (530°F) range until the start of operator initiated depressurization of the steam generator secondaries, when they began a downward trend. An abrupt temperature spike in the upper plenum temperature occurred at 39 min, coincides with the delivery of accumulator water to the core and the resulting rapid production of steam. This temperature spike is quite apparent in Figure 5.3.3, the plot of core exit gas temperature, rising to near 1,040 K (1,412°F) prior to falling back to the 600 K (620°F) range at the end of the initial delivery of accumulator water at 69 min. With the start of the second core uncovery at 102 min, the upper plenum temperature began to oscillate between 475 K (395°F) and 625 K (665°F), while the downcomer temperature remained about 475 K (395°F). As the core began to melt at 130 min and progressed into core slump at 140 min, the primary temperatures began a steady climb to approximately 1,100 K (1,520°F) by the time of core collapse. Quenching of the molten corium in the lower head served to lower the primary temperature somewhat just prior to vessel failure and subsequent debris ejection at 164 min.

Figure 5.3.4 provides a plot of collapsed and swollen water levels in the reactor vessel, in the upper plenum, core and lower plenum. (Dotted lines are provided in the figure indicating the top-of-core/bottom-of-UP elevation at 6.72197 m and the bottom-of-core/top-of-LP elevation at 3.06437 m, for reference.) Since the only source of water to the primary is the accumulators, the collapsed levels track their performance. Reactor vessel water inventory fell from the outset, with initial core uncovery at 35.6 min. The coolant level continued to decrease until the accumulators began delivery at 38.8 min and continued to rise until they ceased delivery at 68.6 min, having successfully recovered the core. From that point onward, the coolant inventory decreased, and the collapsed water level in the reactor vessel fell in a linear fashion. The core uncovered for the second time at 101.9 min and was almost completely voided at the time of vessel failure, 148.3 min. As seen for the AG sequence in Figure 5.2.4, there was very little level swell predicted anywhere in the vessel except in the core. The core collapsed and swollen liquid levels both fell even during those periods when significant liquid still remained in the upper plenum. The significant level swell in the core during these periods helped maintain core cooling.

Integrated outflows from the primary system through the hot leg break and through the vessel breach are given in Figures 5.3.5 and 5.3.6, respectively; the outflows are subdivided into liquid water, steam and hydrogen flows in both cases. Most of the RCS inventory is lost as liquid water out the break. Liquid remaining in the lower plenum at the time of vessel lower head failure is lost out the vessel breach to the cavity. Note that relatively less inventory is lost out the small break and relatively more

out the vessel breach than predicted for the large break LOCA in the AG sequence (Figures 5.2.5 and 5.2.6).

5.3.3 Core Degradation

This core partial uncovery, recovery and final uncovery is also visible in the core temperature response predicted. Figures 5.3.7 through 5.3.9 show cladding temperatures at various levels in the different radial rings during the core damage period. The behavior in all three rings is very similar, only slightly delayed in time in the outer two rings due to lower power densities. MELCOR predicted core heatup in the uppermost axial levels beginning at about 35 min, when the core first uncovers. By about 50 min, the upper half of the core showed elevated clad temperatures. Accumulator injection interrupted core uncovery and heatup, with almost all of the core recovered to saturation temperatures by 70 min. After that time, with the loss of the accumulator water injection, the core began to heat up again and damage was quite rapid -- MELCOR predicted the start of core melting in the innermost ring at 140 min and core collapse and lower head penetration failure about 10 min later.

Figure 5.3.10 shows the total masses of core materials (UO_2, Zircaloy and zirc oxide, steel and steel oxide, and control rod poison) remaining in the vessel during the S2D transient. Figure 5.3.11 shows the same information, but normalized by the initial masses of each material present. (Note that the fractions of ZrO_2 and steel oxide use the initial masses of zircaloy and stainless steel, respectively, as normalizing masses, because no oxides are present initially.) Debris ejection began about 15 min after lower head failure. As in the AG-sequence results shown in Figures 5.2.10 and 5.2.11, all the UO_2 is transferred to the cavity, as is most of the unoxidized zircaloy and the oxides; however, much of the structural steel in the lower plenum and core support plate is predicted to remain unmelted and in place even after vessel breach.

The temperature and mass of debris in the lower plenum (i.e., on the lower head) are presented in Figures 5.3.12 and 5.3.13. There is only a brief period of time when a substantial mass of debris is found in the lower plenum, between initial core plate failure and initial lower head penetration failure and ejection to the cavity. Again, this is quite similar to the corresponding results for the AG sequence given in Figures 5.2.12 and 5.3.13, except in timing.

5.3.4 Containment Response

The containment pressure and temperature response, for both the MELCOR and the STCP calculations, are presented in Figure 5.3.14 and Figure 5.3.15. (The STCP results are taken from Ref. 1, Vol. 6, Figures 4.2.55 and 4.2.56.) Qualitatively, the predictions made by both codes concerning containment pressure and temperature were similar, although the timing of the events varied between the two codes. Pressure and temperature spikes attributable to hydrogen deflagrations for the MELCOR run are the major difference between the two. The STCP analysis did not allow hydrogen burns to occur.

Both codes predicted a relatively rapid rise in containment pressure after accident initiation as blowdown from the primary system entered the containment via the break. With depressurization of the steam generator secondaries commencing at 30 min, the containment pressurization curve began to turn over, almost reaching the 0.172 MPa (1.72 bar, 25 psia) containment spray initiation setpoint in the STCP calculation prior to falling off at the 65 min mark. MELCOR predicted the containment pressure to rise to 0.134 MPa (1.34 bar, 19.4 psia) at 39 min, when the effects of steam generator secondary depressurization and accumulator delivery to the primary helped reduce containment pressure to approximately 0.126 MPa (1.26 bar, 18.3 psia) by 68.6 min, when both initial accumulator water delivery and secondary side depressurization were completed.

The STCP calculation predicted a repressurization of the containment up to the containment spray initiation setpoint of 0.172 MPa (1.72 bar, 25 psia) at 188 min, followed by a steep decline in containment pressure as the containment sprays injected relatively cool water from the RWST until it was depleted at 282 min. At that point, with containment pressure at approximately 0.09 MPa (0.9 bar, 13 psia), the containment recirculation sprays began operation. Their coolers were operable, but were unable to fully counteract the increase in containment pressure that occurred as the core melted, rupturing the reactor vessel lower head, and fell into the cavity at 315 min. By definition, the STCP analysis did not allow the molten corium in the cavity to be quenched. By the end of the run at 915.5 min, the containment pressure had risen, gradually after corium layer inversion had been completed at 372.5 min, to 0.14 MPa (1.4 bar, 20.3 psia), well below containment failure pressure.

The MELCOR analysis predicted a similar type of behavior, with the added spice of hydrogen deflagrations thrown in for good measure. After the end of accumulator delivery to the primary, the containment pressure rose to approximately 0.14 MPa (1.4 bar, 20.3 psia) by the time of debris ejection, 164.4 min. Along with debris ejection, a hydrogen deflagration in the cavity caused a small containment pressure spike up to 0.16 MPa (1.6 bar, 23.2 psia). After decaying, the containment pressure began to rise again, as the corium in the cavity reacted with the concrete, adding noncondensible gases to the containment atmosphere. Containment pressure rose to the 0.172 MPa (1.72 bar, 25 psia) level at 267 min in the MELCOR calculation, and the resulting containment spray injection flow helped to lower containment pressure back down to the 0.09 MPa (0.9 bar, 13 psia) level by 300 min, much the same as had happened with the STCP run. From that point, the MELCOR analysis predicted two distinct sets of hydrogen deflagrations involving numerous containment and primary system volumes, at the 310 min and 332 min marks. The first raised containment pressure by just a few bar, and the second caused a more pronounced spike up to 0.24 MPa (2.4 bar, 34.8 psia), the maximum containment pressure witnessed during the MELCOR analysis. A third series of hydrogen deflagrations occurred between 385 min and 470 min, raising containment pressure to about 0.125 MPa (1.25 bar, 18.1 psia) by the 470 min mark. At the end of the MELCOR simulation, 833.4 min, the containment pressure had risen slightly, to 0.14 MPa (1.40 bar, 20.3 psia), exactly the same as predicted by the STCP analysis.

Little needs to be said concerning the containment atmosphere temperature plot, Figure 5.3.15, except to say that once the containment atmosphere became saturated early in the accident analysis, it remained saturated, and the containment atmosphere temperature reflected that condition. The STCP plot of containment atmosphere temperature is a more benign trace since it does not reflect the spikes caused by hydrogen deflagrations that are present in the MELCOR plot.

Figures 5.3.16 and 5.3.17 show the mole fractions of steam and noncondensables in the cavity and containment dome control volumes, respectively. Since the containment was not steam inerted at the time of lower head failure and debris ejection, hydrogen deflagrations occurred in containment for the MELCOR analysis, initially in the cavity volume. Later deflagrations were distributed throughout the containment volumes. None threatened containment integrity. The STCP analysis did not consider hydrogen deflagrations. Figures 5.3.18 through 5.3.23 provide information concerning decay heat, both total and the portion connected with the cavity, along with characteristics of the debris resident in the cavity after lower head failure. By the end of the MELCOR analysis, the corium debris temperature was approximately 1,650 K (2,510°F) and trending downward slowly.

5.3.5 Fission Product Transport and Release to the Environment

The STCP analysis did not look at source term releases for the S2D accident. The following discussion therefore refers solely to MELCOR source term results. (Recall that, for reference, Table 4.2.1 gives the list of the MELCOR fission product classes and their total radioactive mass inventories.) Table 5.3.2 gives the radionuclide fractional distribution at the end of the MELCOR analysis, 833.4 min. Figures 5.3.25 through 5.3.36 show the radionuclide mass fraction, according to fission product class, released from the fuel in the in-vessel and ex-vessel portions of the accident, accompanied by a trace showing the total of the two. Figures 5.3.37 through 5.3.48 give plots of radionuclide masses in the primary, containment, environment, and a sum total of all three, all as a fraction of the initial class inventory present. Since the containment was not predicted to fail, no releases to the environment occurred.

Significant radionuclide releases from the fuel occurred at the outset of core melt, ~130 min, and continued through the remainder of the in-vessel portion of the accident and on into the ex-vessel segment. Transportation to the containment for the more volatile radionuclide classes was rapid, while the less volatile classes showed significant release from the fuel after it had relocated to the cavity. Generally, for the noble gases, halogens, and main group metals, releases to the containment were finished by 250 min. The other radionuclide groups were slower, completing their releases from the fuel mass to the containment by approximately 330 min. After that point, very little release of radioactive radionuclides to containment occurred.

As discussed in Section 5.2.5 for the AG sequence results, Figures 5.3.25 and 5.3.26 show that almost all of the Class 1 and Class 2 volatiles are released from the fuel in the MELCOR calculation. About 50% of that release occurs in-vessel, with the remaining 50% released ex-vessel in the cavity. Note that Figure 5.3.28 shows a very similar release pattern for Class 4 (I) in-vessel, but no additional release in the cavity. This is because

VANESA, which is used to calculate the ex-vessel release within MELCOR, considers iodine to be released as CsI; since there is no separate CsI class in these MELCOR calculations, MELCOR counts that CsI release to be a Class 2 (Cs) release (also explaining why the total Class 2 release fraction shown in Figure 5.3.26 is greater than 100%). Based upon physical insight, the Class 4 release should closely resemble the Class 1 and 2 results.

The release behavior predicted by MELCOR can be grouped into several subdivisions. Assuming the correct iodine behavior, ~100% of the Class 1, Class 2 and (corrected) Class 4 radionuclide inventories are released, about 50%/50% in-vessel and ex-vessel. The next major release fractions are of Ba and Te (~30%), both mostly predicted to occur in the cavity. About 12-14% of the Cd and Sn radionuclide inventory is released, and ≤3% of the Mo radionuclide inventory. (Note that these amounts consider only the release of radioactive forms of these classes, and not additional releases of nonradioactive aerosols from structural materials.) Finally, a total ≤0.3% of the initial inventory of the refractories (Ru, Ce, La and U) are released. The release patterns are very similar to the release patterns predicted for the AG sequence. Most of the La releases are predicted to occur in the cavity, similar to the behavior of Ba and Te. All of the Ru and almost all of the Cd releases are predicted to occur in-vessel. The remaining classes, Mo, Ce, U and Sn, have most of their releases predicted to occur in-vessel, but a significant fraction occurs in the cavity.

The released radionuclide distributions are also predicted to fall into a few subdivisions. Except for the difference that with no containment failure there is no release to the environment, the distribution patterns predicted by MELCOR for the S2D sequence resemble those obtained for the AG sequence. All of the noble gases (Class 1) and iodine (Class 4) are in the containment by the end of the MELCOR simulation. Most of the Ba, Te and La (≥95% of the amount released) are in the containment, while all of the other classes also have most of their released inventory (~90% of the total released) in the containment.

The total mass of fission products released from the fuel is shown in Figure 5.3.49. About half the total release occurs during in-vessel core damage and melt ejection. The in-cavity release primarily occurs before the CORCON layer flip after 300 min, with very little release at later times. Most of the fission products released are found in control volumes, in either atmosphere or pool, and about 50-70% of the fission products in the control volumes are vapors rather than aerosols (mostly because aerosols settle out and deposit onto heat structures more readily). Relatively few fission products (≤5%) are deposited onto heat structures in this sequence.

5.4 S3D Sequence

This accident sequence was initiated by a very small break, characterized as a pump seal LOCA, with a total leak rate at normal operating conditions of 2,839 liters per min (750 gpm). All other pertinent accident sequence characteristics were identical to those specified for the S2D sequence described in Section 3.2.

5.4.1 Key Events

The summary of event timing for the S3D accident sequence is provided in Table 5.4.1, for both the STCP and the MELCOR calculations. The accident initiating event was a pump seal LOCA with a total leak rate to containment of 2,839 litters per min (750 gpm) at normal primary system operating pressure. For the MELCOR analysis, each primary system loop was provided with a break in the pump suction control volumes (CV220, CV320, and CV420) sufficient to produce a 946 liters per min (250 gpm) leak rate at normal system operating pressure. The STCP analysis utilized a single break sized to allow the total 2,839 liters per min (750 gpm) flow rate. The containment fan coolers shifted from normal operation to high capacity operation when the containment atmosphere temperature rose above 383.7 K (105 °F), at 1 min in the STCP calculation and 0.4 min in the MELCOR calculation. By accident sequence definition, the operators began manual depressurization of the steam generator secondaries at 30 min for both STCP and MELCOR, aiming to reach a target pressure of 1.31 MPa (13.1 bar, 190 psia) by 60 min. The STCP analysis predicted initial accumulator delivery at 40 min, while MELCOR predicted it to occur at 38.8 min. As with the S2D calculation, the MELCOR accumulator flow was divided into two distinct segments, with the initial delivery of 80 percent of the total accumulator inventory accomplished by 113.3 min. The MELCOR calculation predicted a second, and final accumulator discharge from 656 min through 701 min, after the onset of core melt and slumping. The STCP analysis modeled a single delivery of accumulator water that was completed at 80.5 min.

Core uncovery began at 525.4 min for the STCP analysis and at 590.6 min for the MELCOR calculation. The MELCOR nodalization of the core consisted of 3 radial

rings and 10 axial nodes. MELCOR predicted gap release in radial ring 1 at 606.2 min, shortly after the onset of core uncovery. Ring 2 gap release was predicted at 608.6 min, with ring 3 following at 617.3 min. MELCOR predicted cavity debris layer inversion at 900 min.

Since the STCP code predicted a maximum containment pressure of 0.152 MPa (1.52 bar, 22 psia) around the 700 min mark, the containment sprays never reached their actuation setpoint of 0.172 MPa (1.72 bar, 25 psia). On the other hand, MELCOR predicted the containment spray injection system to initiate at 851 min, followed shortly thereafter at 855 min by the containment spray recirculation system. The reason for their operation was a set of hydrogen deflagrations that occurred in the containment volumes, beginning at 849.3 min and continuing for 40 seconds, that drove the containment pressure above the 0.172 MPa (1.72 bar, 25 psia) spray initiation setpoint. The STCP calculation did not allow hydrogen combustion. A second set of two relatively weak hydrogen deflagrations occurred in the pressurizer, at 961.6 min and 990.4 min, after the lower head had failed, barely causing a blip in the containment pressure. The MELCOR calculation predicted depletion of the Refueling Water Storage Tank (RWST) at 944 min, at which point the containment spray injection system ceased operation, leaving the containment spray recirculation system, with its operable coolers, as the sole source of containment heat removal. The STCP calculation was halted at 1,450 min, while the MELCOR run was stopped at 1,667 min.

5.4.2 Primary System Behavior

Because of the relatively small leak rate from the primary system, the S3D accident takes a significant period of time to develop, even though there is no active source of coolant injection. Figure 5.4.1 through 5.4.4 provide information concerning primary system response based on the MELCOR calculation.

Figure 5.4.1 shows the primary system pressure as it fell from normal operating pressure to the 8.0 MPa (80 bar, 1,160 psia) range during the initial stages of the calculation, where it remained until the beginning of operator depressurization of the steam generator secondaries at 30 min. Successful completion of this procedure, along with delivery of water to the primary system from the passive accumulators, helped to reduce the primary system pressure to the 1.6 MPa (16 bar, 230 psia) range by 130 min. The primary pressure remained at that level until the operator manually depressurized the system at 617 min, causing it to fall. By the time of lower head failure at 740 min, the primary pressure had decreased to approximately 0.5 MPa (5 bar, 73 psia). After lower head failure, primary pressure was very close to containment pressure.

The primary system pressure predicted by STCP [taken from Ref. 1, Vol. 6, Figure 4.2.41] is included in Figure 5.4.1 for comparison to the MELCOR calculation. The results from the two codes are qualitatively very similar, with the MELCOR primary system pressure predicted generally slightly lower than the STCP predicted response for the first ~750 min (before vessel breach brings the RCS pressure to the containment pressure). The large pressure spike at 700-750 min in the STCP result has only a tiny counterpart in the MELCOR analysis. This comparison between MELCOR and STCP predictions is very similar to the comparison for the S2D sequence presented in Figure 5.3.1. As with the S2D sequence results, the timing of the pressure spike corresponds to the time between core collapse (at ~710 min for STCP) and bottom head dryout (at ~740 min for STCP), and is likely due to boiling off the remaining lower plenum water inventory. As in the AG sequence, MELCOR predicts the lower head failure very soon after predicting core collapse (739.9 min and 739.0 min, respectively), and thus any water left in the lower plenum simply falls into the cavity; after lower head failure, the MELCOR RCS pressure remains essentially at the containment pressure.

Figure 5.4.2 gives primary temperatures in the reactor vessel downcomer and upper plenum control volumes. Figure 5.4.3 provides a plot of the core exit gas temperature. From these plots it can be seen that the primary temperatures fell from the 575 K (575°F) range in the initial stages of the calculation, to approximately 480 K (404°F) by the end of the manual operation to depressurize the steam generators and the end of the first accumulator inventory delivery. Both downcomer and upper plenum temperatures remained in that range until the beginning of core melting at 625 min, when the upper plenum temperature began to rise precipitously to approximately 1,400 K (2,060°F) by 656 min. At that point, MELCOR predicted the remainder of the accumulators finally depleted, the upper plenum temperature climbed quickly, reaching the 1,050 K (1,430°F) range at the time of bottom head failure, 740 min. After that point, the downcomer and upper plenum have been completely drained of coolant, for all practical purposes.

Figure 5.4.4 gives a plot of the collapsed water levels in the reactor vessel. The levels track the performance of the accumulators, since they are the only source of water to the primary. As can be discerned from the plot, the core remained covered until 591 min, when the upper plenum voided, and the collapsed water level dropped below the top of the core. From that point, the collapsed water level fell off rather rapidly, and the core was completely voided by the time of core collapse and bottom head failure, 739 min.

Figure 5.4.4 is a plot of collapsed and swollen liquid levels in the reactor vessel, in the upper plenum, core and lower plenum. (Dotted lines are provided in the figure indicating the top-of-core/bottom-of-UP elevation at 6.72197 m and the bottom-of-core/top-of-LP elevation at 3.06437 m, for reference.) There was very little level swell predicted anywhere in the vessel except in the core. The core remained fully covered until the 960 min point in the accident, when the ECCS flow is shifted from cold legs to hot legs. At that point, the water level in both the downcomer and the core fell below the top of the active fuel, even though significant liquid still remained in the upper plenum. The collapsed liquid level in the core dropped to about the core midplane, but the significant level swell in the core kept the swollen level near the top of the active fuel, and thus maintained core cooling. Water levels then remained about constant until containment failure at 3,540 min, when ECCS flow was lost. At that point, the water levels in the vessel dropped quickly, with all inventory lost at the point of vessel lower head failure, 3,685.4 min.

Integrated outflows from the primary system through the pump seal leaks and through the vessel breach are given in Figures 5.4.5 and 5.4.6, respectively; the outflows are subdivided into liquid water, steam and hydrogen flows in both cases. Most of the RCS inventory is lost as liquid water out the pump seal leaks until vessel failure occurs; liquid remaining in the lower plenum at the time of vessel lower head failure is lost out the vessel breach to the cavity.

5.4.3 Core Degradation

Figures 5.4.7 through 5.4.9 show cladding temperatures at various levels in the three radial rings during the core damage period. The behavior in all three rings is very similar, only slightly delayed in time in the outer rings due to lower power densities. MELCOR predicted intermittent core heatup in the uppermost axial level beginning at about 200 min. Significant core heatup began after 590 min, when accelerated core uncovery began, and the core damage process was quite rapid -- MELCOR predicted the start of core melting in the innermost ring at 625 min and core collapse and lower head penetration failure about 2 hr later.

Figure 5.4.10 shows the total masses of core materials (UO_2, Zircaloy and zirc oxide, steel and steel oxide, and control rod poison) remaining in the vessel during the S3D transient. Almost all the core material is transferred to the cavity soon after vessel breach. All the UO_2 is transferred to the cavity, as is most of the unoxidized zircaloy, the oxides and the control rod poison; however, much of the structural steel in the lower plenum is predicted to remain unmelted and in place even after vessel breach. Figure 5.4.11 shows the same information, but normalized by the initial masses of each material present. (Note that the fractions of ZrO_2 and steel oxide use the initial masses of zircaloy and stainless steel, respectively, as normalizing masses, because no oxides are present initially.)

The temperature and mass of debris in the lower plenum (i.e., on the lower head) are presented in Figures 5.4.12 and 5.4.13. There is only a brief period of time when a substantial mass of debris is found in the lower plenum, between initial core plate failure and initial lower head penetration failure and ejection to the cavity.

5.4.4 Containment Response

The containment pressure and temperature response, for both the MELCOR and the STCP analyses, are given in Figure 5.4.14 and Figure 5.4.15. (The STCP results were obtained from Figures 4.2.46 and 4.2.47 in Ref.1, Vol. 6.) Although the timing of events varies between the two analyses, the progress of the accident is similar, qualitatively. The major difference between the containment response is driven by the fact that MELCOR allowed hydrogen deflagrations to occur, while STCP did not. Each code predicted a relatively benign rise in containment pressure during the initial minutes of the calculations. The STCP calculation showed a containment pressure rise to just under 0.1 MPa (1 bar, 14 psia) at 55 min, after which it leveled off and fell to the 0.09 MPa (0.9 bar, 13 psia) range. The MELCOR code predicted similar containment response, with an initial pressure rise to 0.08 MPa (0.8 bar, 11.6 psia) and then a general leveling off of the containment pressure as the primary system coolant level slowly fell. Both codes predicted a

pronounced increase in containment pressure after the core uncovered, began to overheat, and the operators manually depressurized the primary system via the PORV. For the STCP analysis, this occurred at 658 min, with the containment pressure rising from 0.09 MPa (0.9 bar, 12.75 psia) to 0.11 MPa (1.1 bar, 16.5 psia) by 687 min, when core melting commenced. At that point in the STCP analysis, the containment pressure spiked upward, reaching 0.15 MPa (1.5 bar, 22 psia) by 717 min, the time of core collapse into the lower head. Containment pressure gradually trailed off afterwards, falling to 0.125 MPa (1.25 bar, 18 psia) by the time of bottom head failure and the commencement of core-concrete interaction, 850 min. Thereafter, with no containment sprays in operation, the containment pressure rose gradually to 0.15 MPa (1.5 bar, 22 psia) by the end of the calculation at 1,450 min.

After the PORV was manually opened at 617 min in the MELCOR analysis, containment pressure rose from 0.085 MPa (0.85 bar, 12.3 psia) to 0.1 MPa (1 bar, 14.8 psia) by the time of core collapse into the lower head, 739 min. From that point, containment pressure increased further to 0.14 MPa (1.4 bar, 20 psia) by 833 min, well after lower head failure and corium transfer to the cavity had occurred. The large hydrogen deflagrations that occurred in the MELCOR calculation at that point caused the containment pressure to spike upward to ~0.39 MPa (3.9 bar, 56.6 psia), after which it decayed rapidly due to the cooling effect of the containment injection spray system that began operation at 851 min. By the time the injection spray system had depleted the RWST at 944 min, the containment pressure had fallen to 0.08 MPa (0.8 bar, 11.6 psia). From that point onward, only the containment recirculation spray system was functioning, and the containment began to repressurize as energy and noncondensible gases were added from the core-concrete interaction. By the end of the MELCOR accident calculation, the containment pressure had climbed back up to 0.115 MPa (1.15 bar, 16.7 psia) and was changing very little.

Figure 5.4.15 gives the containment atmosphere temperature plots. The temperatures reflect a saturated containment atmosphere after the initial stages of the accident. As expected, the MELCOR temperature plot shows a divergence in the temperature of the cavity atmosphere after lower head failure and relocation of the corium to the cavity. The STCP temperature trace is more benign since it does not reflect the effects of the hydrogen deflagrations that are present in the MELCOR plots.

Figures 5.4.16 and 5.4.17 present the mole fractions of steam and noncondensables in the cavity and containment dome control volumes, respectively. For the MELCOR analysis, the containment was not steam inerted at the time of lower head failure and debris ejection, and large hydrogen deflagrations occurred throughout the containment at that point. Containment integrity was not threatened by the pressure rise that resulted. Figures 5.4.18 through 5.4.24 provide information concerning decay heat, both total and the portion connected with the cavity, along with characteristics of the debris resident in the cavity after lower head failure. At the end of the MELCOR analysis, the corium debris temperature was approximately 1,650 K (2,510°F) and showing no signs of changing very much.

5.4.5 Fission Product Transport and Release to the Environment

The STCP analysis did not look at source term releases for the S3D accident. Thus, the following discussion refers solely to MELCOR source term results. For reference, Table 4.2.1 gives the list of the MELCOR fission product classes and their total radioactive mass inventories. Table 5.4.2 gives the radionuclide fractional distribution at the end of the MELCOR analysis, 1,667 min. Figures 5.4.25 through 5.4.36 show the radionuclide mass fraction, according to fission product class, released from the fuel in the in-vessel and ex-vessel portions of the accident, accompanied by a trace showing the total of the two. Figures 5.4.37 through 5.4.48 give plots of radionuclide masses in the primary, containment, environment, and a sum total of all three, all normalized to the initial inventory of each class present in the core. As in the S2D analysis, since the containment was not predicted to fail, no releases to the environment occurred.

Significant radionuclide releases from the fuel occurred at the onset of core melting, ~625 min, and continued through the remainder of the in-vessel portion of the accident and on into the ex-vessel segment. Transportation to the containment for the more volatile radionuclide classes was practically complete by the time of lower head failure at 740 min. Less volatile classes showed significant release from the fuel during both the in-vessel and ex-vessel phases of the calculation. In general, radionuclide releases from the fuel were completed by the 850 min mark, with the exception of Te, which exhibited a prolonged ex-vessel release that lasted until the 1,170 min mark.

Results and Comparisons

The same problem with ex-vessel iodine release identified in the AG and S2D sequences is found in the S3D sequence results. Figures 5.4.25 and 5.4.26 show that almost all of the Class 1 and Class 2 volatiles are released from the fuel in the MELCOR calculation. For the S3D sequence almost all that release occurs in-vessel, with $\leq 5\%$ released ex-vessel in the cavity. Note that Figure 5.4.28 shows a very similar release pattern for I in-vessel, but no additional release in the cavity. As discussed in Sections 5.2.5 and 5.3.5, the "missing" iodine release is found in Figure 5.4.26 in the $>100\%$ release total for Cs. One would expect the Class 4 release to closely resemble the Class 1 and 2 results.

Much larger in-vessel releases are predicted to occur during the S3D sequence than in the AG and S2D sequences. Assuming the correct iodine behavior, $\sim 100\%$ of the Class 1, Class 2 and (corrected) Class 4 radionuclide inventories are released, almost all in-vessel (as in the AG and S2D sequences). The next major release fractions are of Cd and Sn, both with $\sim 75\%$, much greater than found for the AG or S2D sequence, and almost all in-vessel, followed by Te ($\geq 60\%$), about equally in-vessel and in the cavity, and Ba ($\leq 50\%$) and Mo ($\leq 20\%$), both mostly in-vessel. (Note that all these include only the release of radioactive forms of these classes, and not additional nonradioactive aerosols from structural materials.) Finally, a total $\leq 2\%$ of the refractories (Ru, Ce, La and U) are released.

The released radionuclide distributions are also predicted to fall into a few subdivisions, generally different for the S3D sequence than the patterns predicted for the AG and S2D sequences. All of the noble gases and iodine are found in the containment by the end of the MELCOR simulation (as in the S2D simulation). Slightly more than half of the Cs and Ba released remain in the primary system, and most ($\sim 75\%$) of the Ru, Mo, Ce, U, Cd and Sn released remain in the primary system. Te and La are the only classes found mostly ($\sim$60-70%) in containment at the end of the MELCOR calculation.

The total mass of fission products released from the fuel is shown in Figure 5.4.49. Most of the total release occurs during in-vessel core damage and melt ejection. About 60% of the fission products released are found in control volumes, in either atmosphere or pool, and about 70% of the fission products in the control volumes are vapors rather than aerosols (mostly because aerosols settle out and deposit onto heat structures more readily). There is significant ($\sim 40\%$) deposition of fission products onto heat structures soon after release begins. The fractions of fission products in control volumes and on heat structures remains nearly constant through the latter portion of this sequence.

Table 5.2.1 Sequence of Events Predicted during AG Sequence, Compared to STCP

Key Event	Time (min)	
	STCP	MELCOR
Accident initiation	0.0	0.0
Containment injection sprays on	0.7	0.6
Containment recirculation sprays on	6.1	5.1
ECCS injection on, (HPIS/LPIS)		0.4
Accumulators depleted	25.1	1.0
ECCS recirculation on, cold legs	29.0	50.0
RWST depleted	29.0	50.0
ECCS recirculation shift to hot legs		960.0
Containment failure	3,054.2	3,540.0
ECCS off	3,055.2	3,541.7
Core uncovery begins	3,080.6	3,570.2
Begin zircaloy oxidation		3,619.6
Gap release, Ring-1		3,621.5
Gap release, Ring-2		3,626.4
Gap release, Ring-3		3,641.6
Core melt starts	3,155.6	3,665.0
Core slump	3,206.6	3,680.0
Core collapse	3,209.2	3,684.3 (partial) ring-1
Bottom head dryout	3,237.6	
Bottom head failure	3,371.6	3,685.4 (partial) ring-1
Commence debris ejection		3,685.4
Begin concrete attack	3,371.6	3,686.9
End of calculation	3,973.1	5,000.0

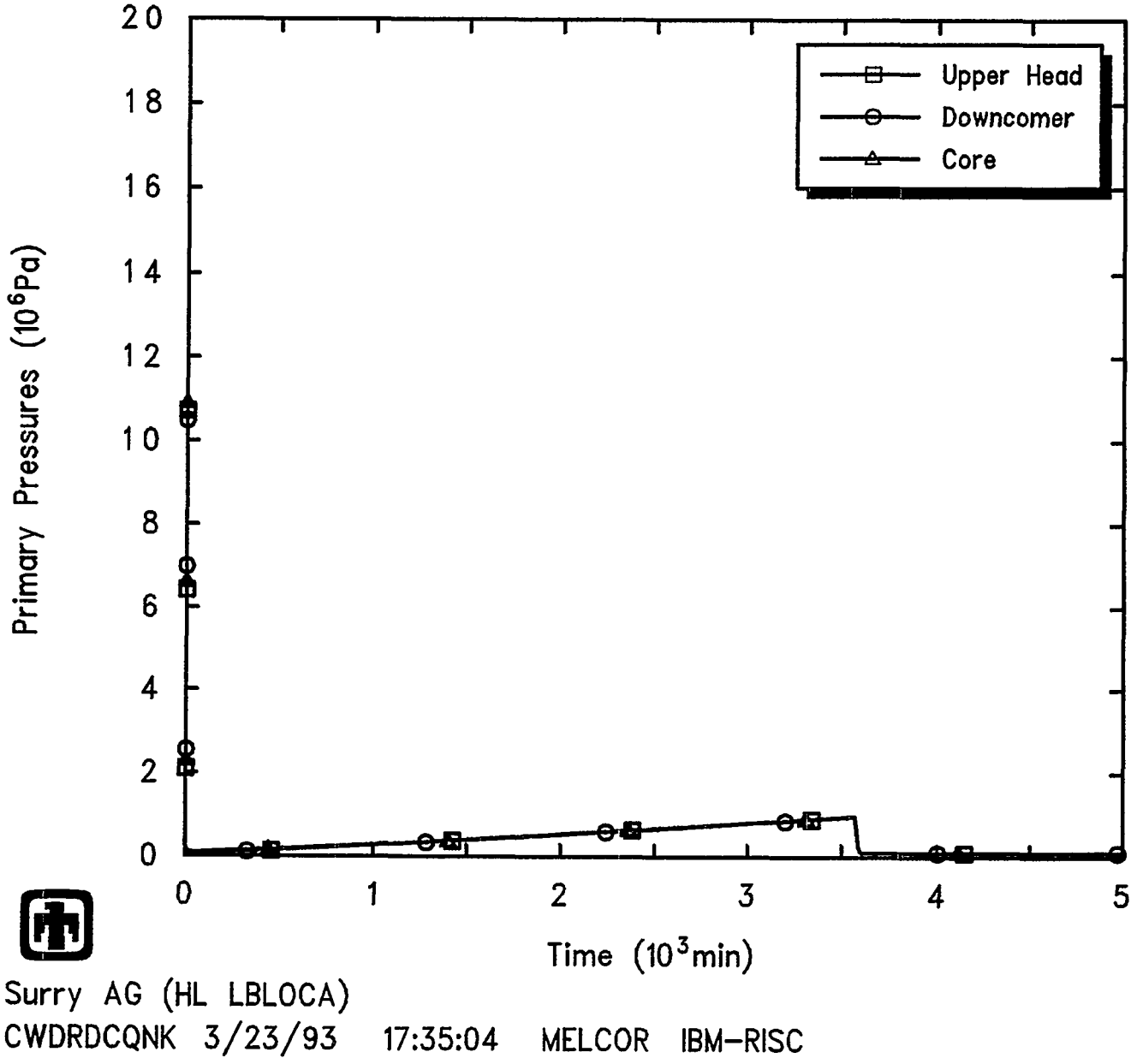

Figure 5.2.1 Primary System Pressures Predicted during AG Sequence

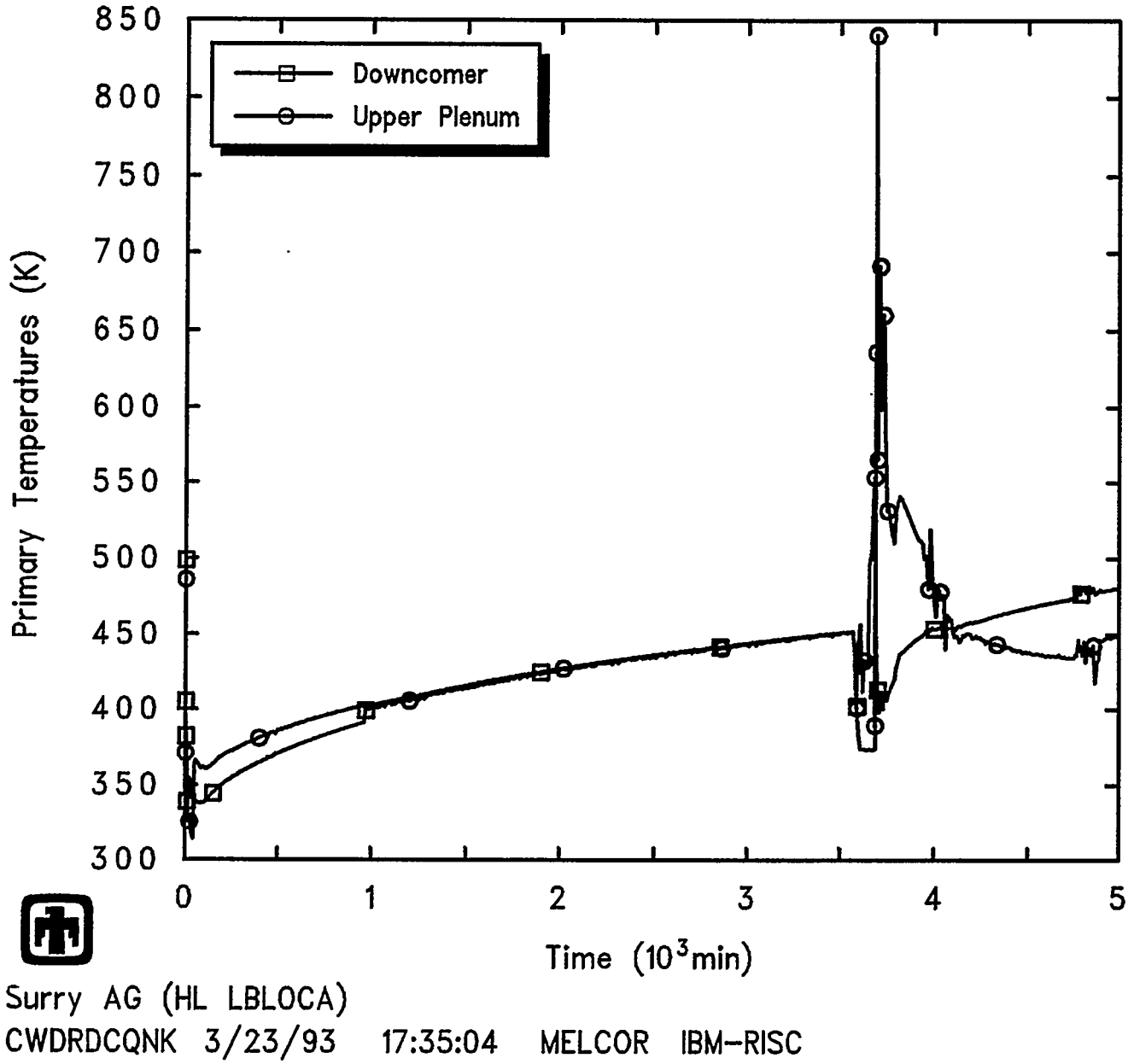

Figure 5.2.2 Primary System Temperatures, in Downcomer and in Upper Plenum, Predicted during AG Sequence

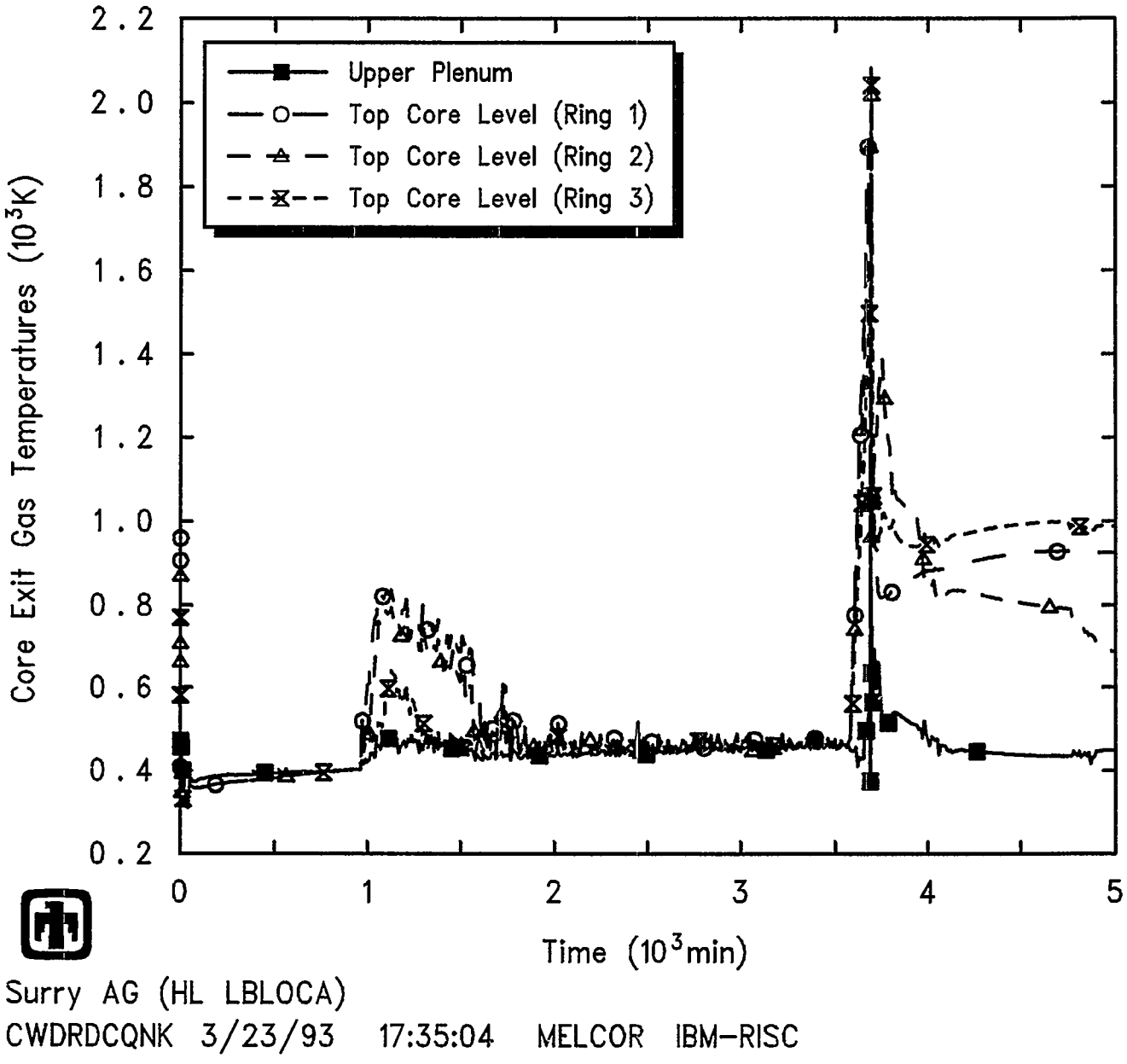

Figure 5.2.3 Core Exit Gas Temperatures, in Upper Plenum and in Uppermost Core Cells, Predicted during AG Sequence

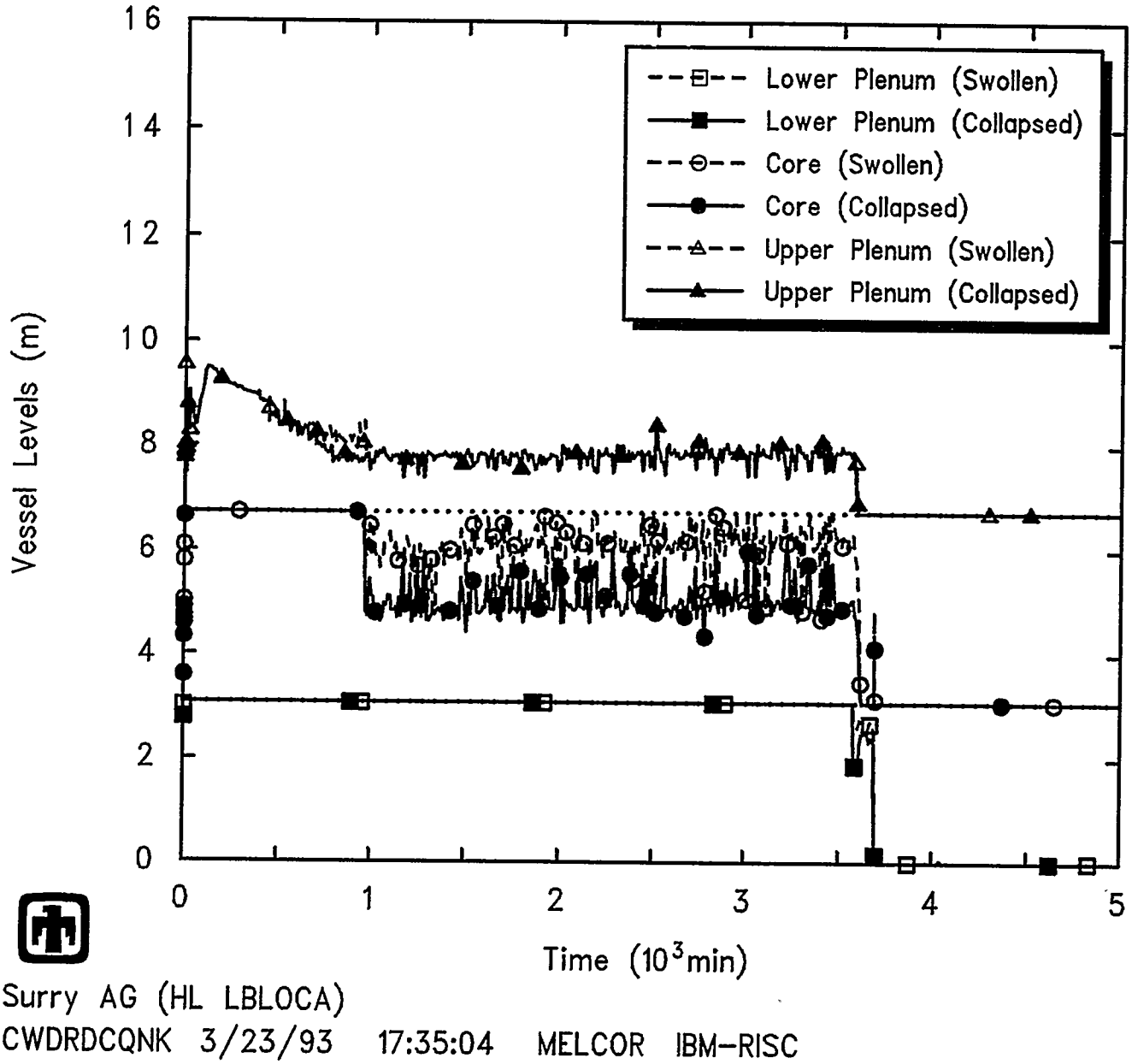

Figure 5.2.4 Reactor Vessel Liquid Levels Predicted during AG Sequence

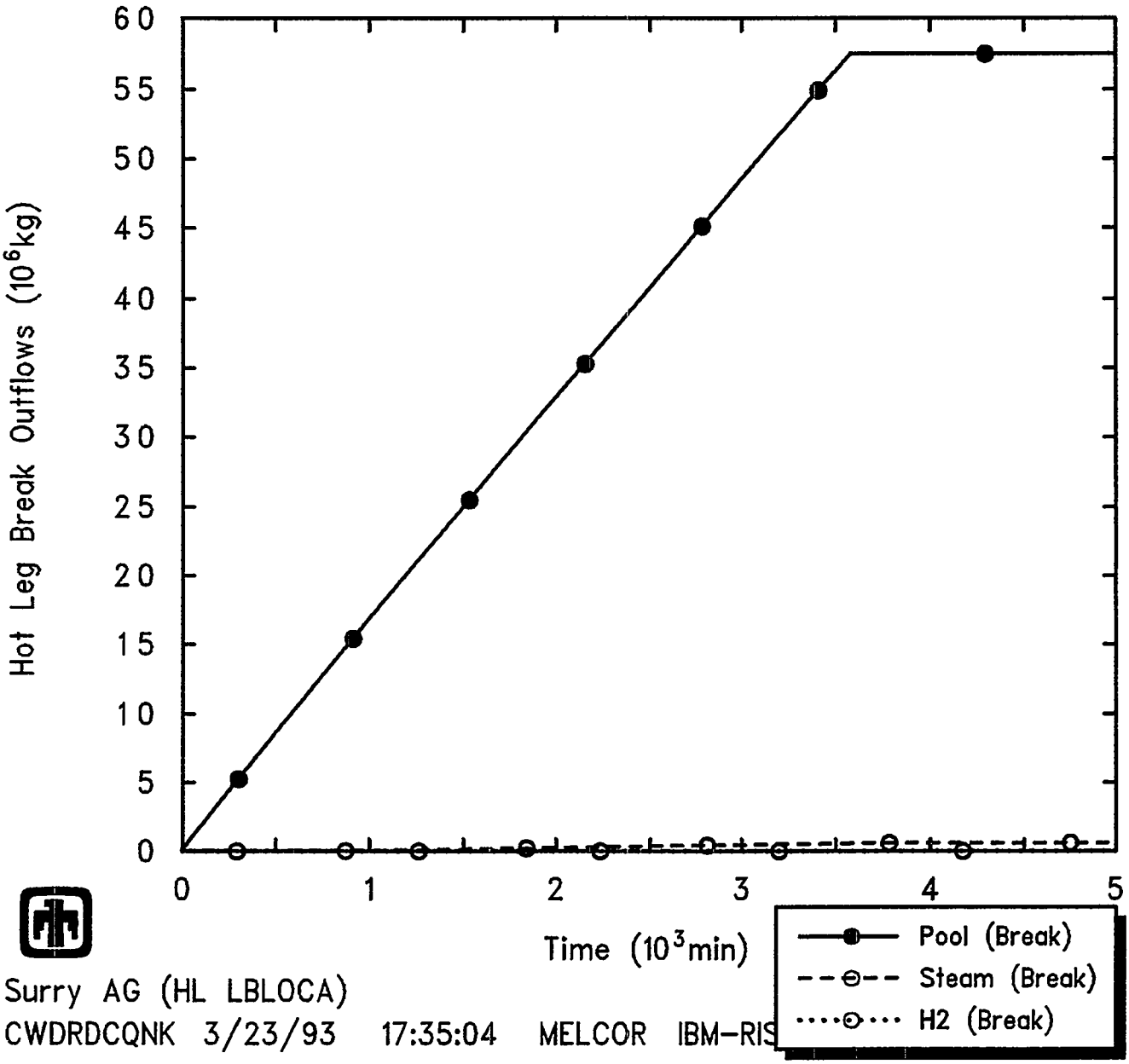

Figure 5.2.5 Integrated Outflows of Liquid, Steam and Hydrogen through the Hot Leg Break Predicted during AG Sequence

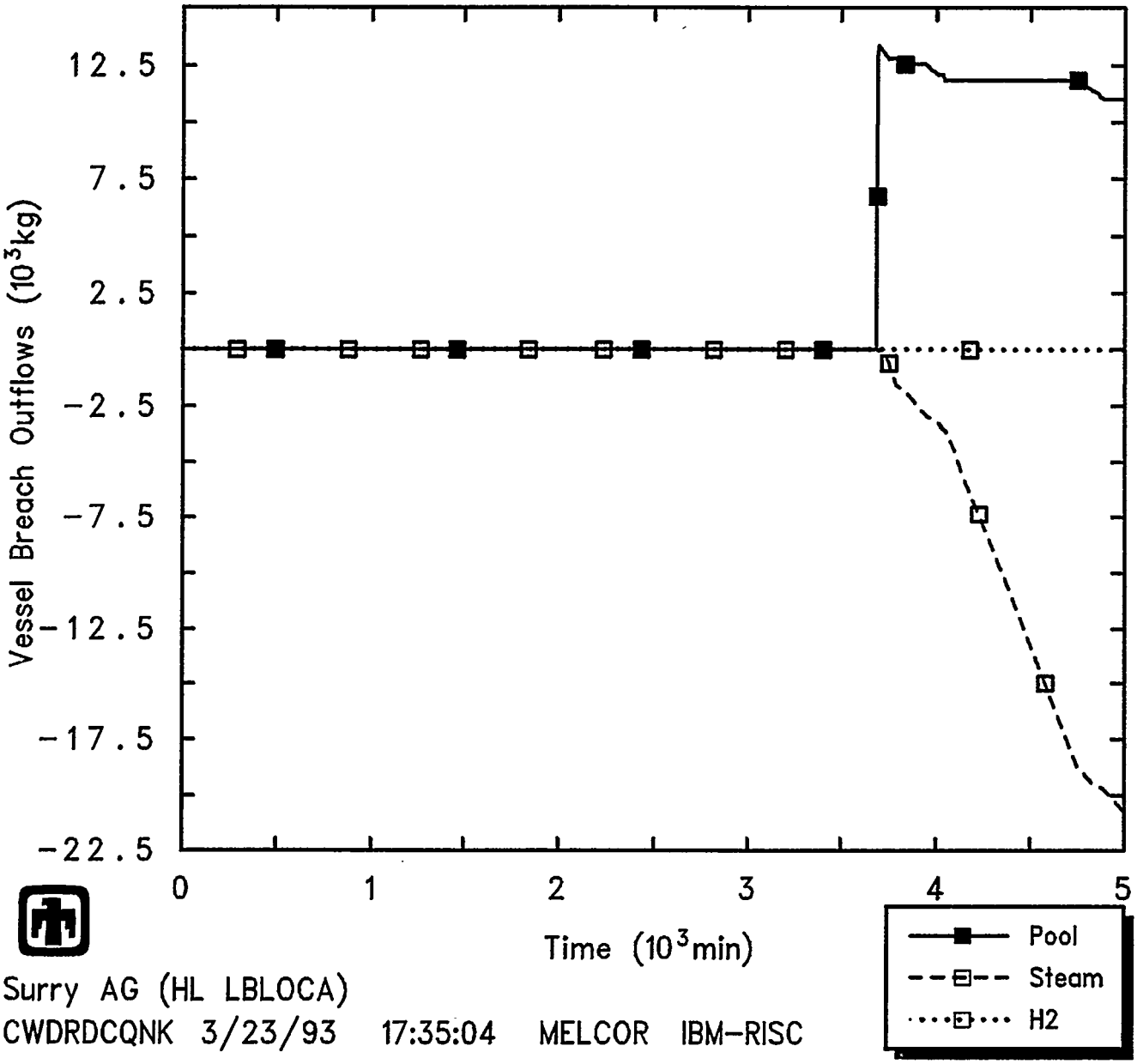

Figure 5.2.6 Integrated Outflows of Liquid, Steam and Hydrogen through the Vessel Breach Predicted during AG Sequence

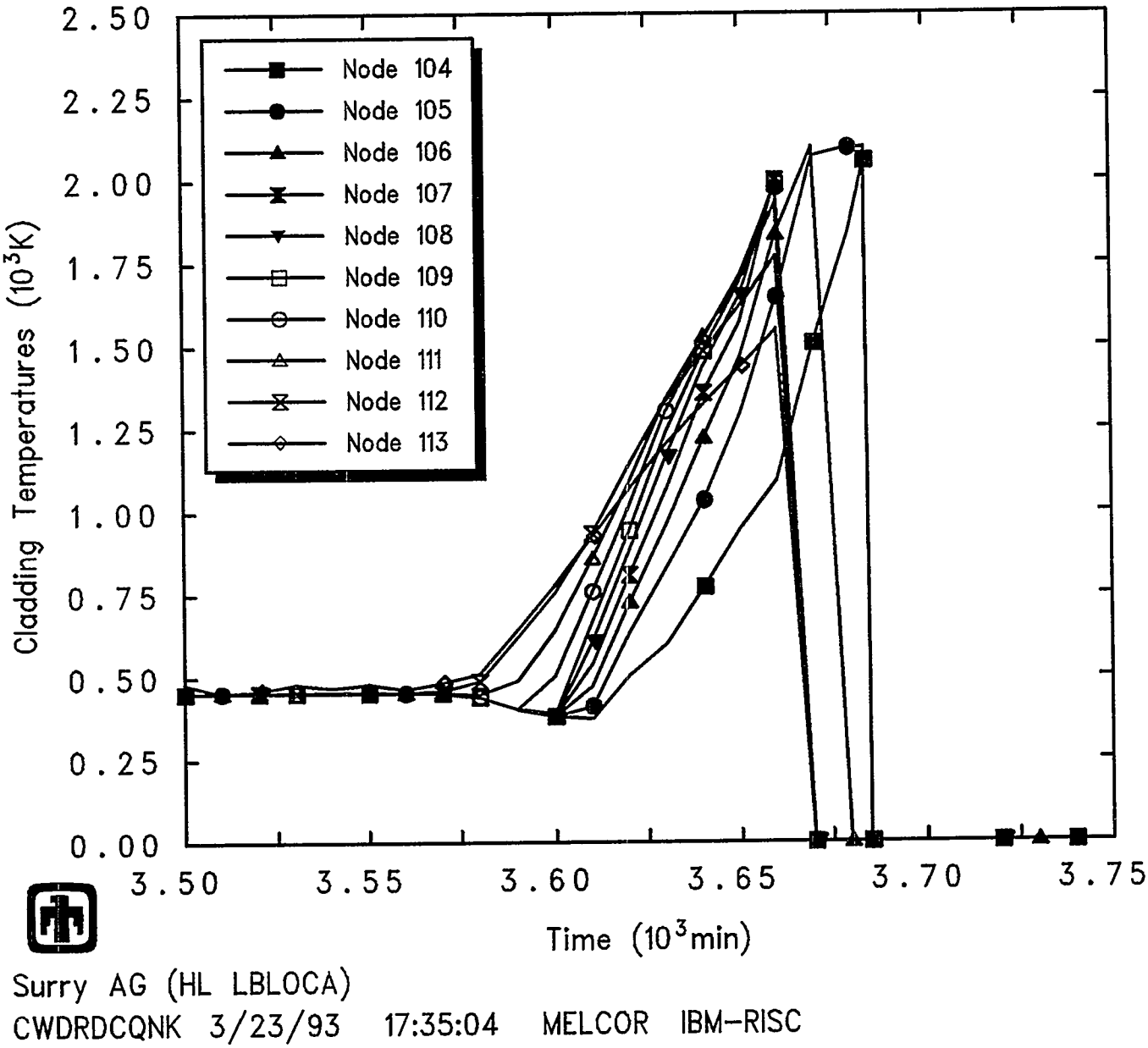

Figure 5.2.7 Core Ring 1 Clad Temperatures Predicted during AG Sequence

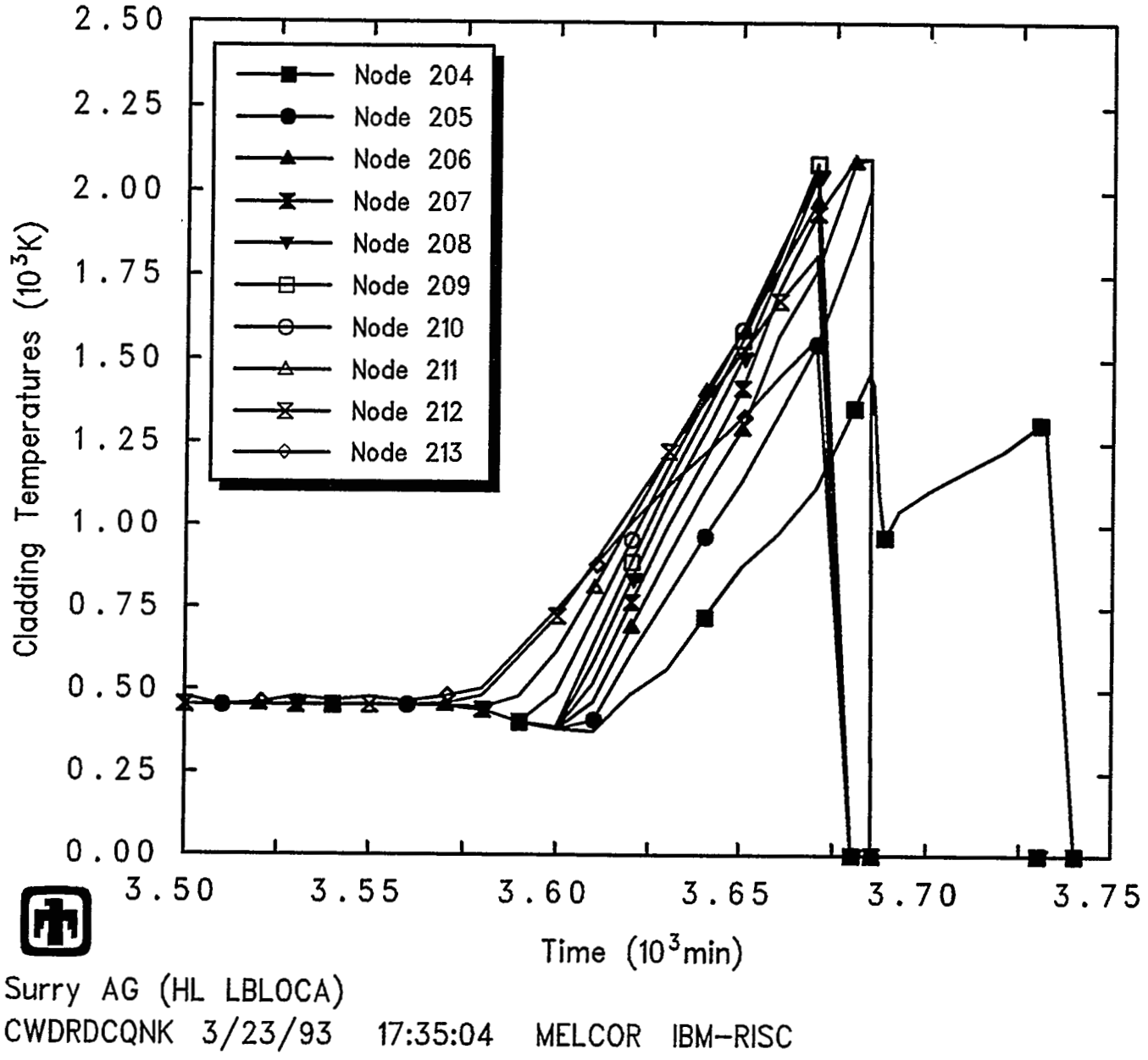

Figure 5.2.8 Core Ring 2 Clad Temperatures Predicted during AG Sequence

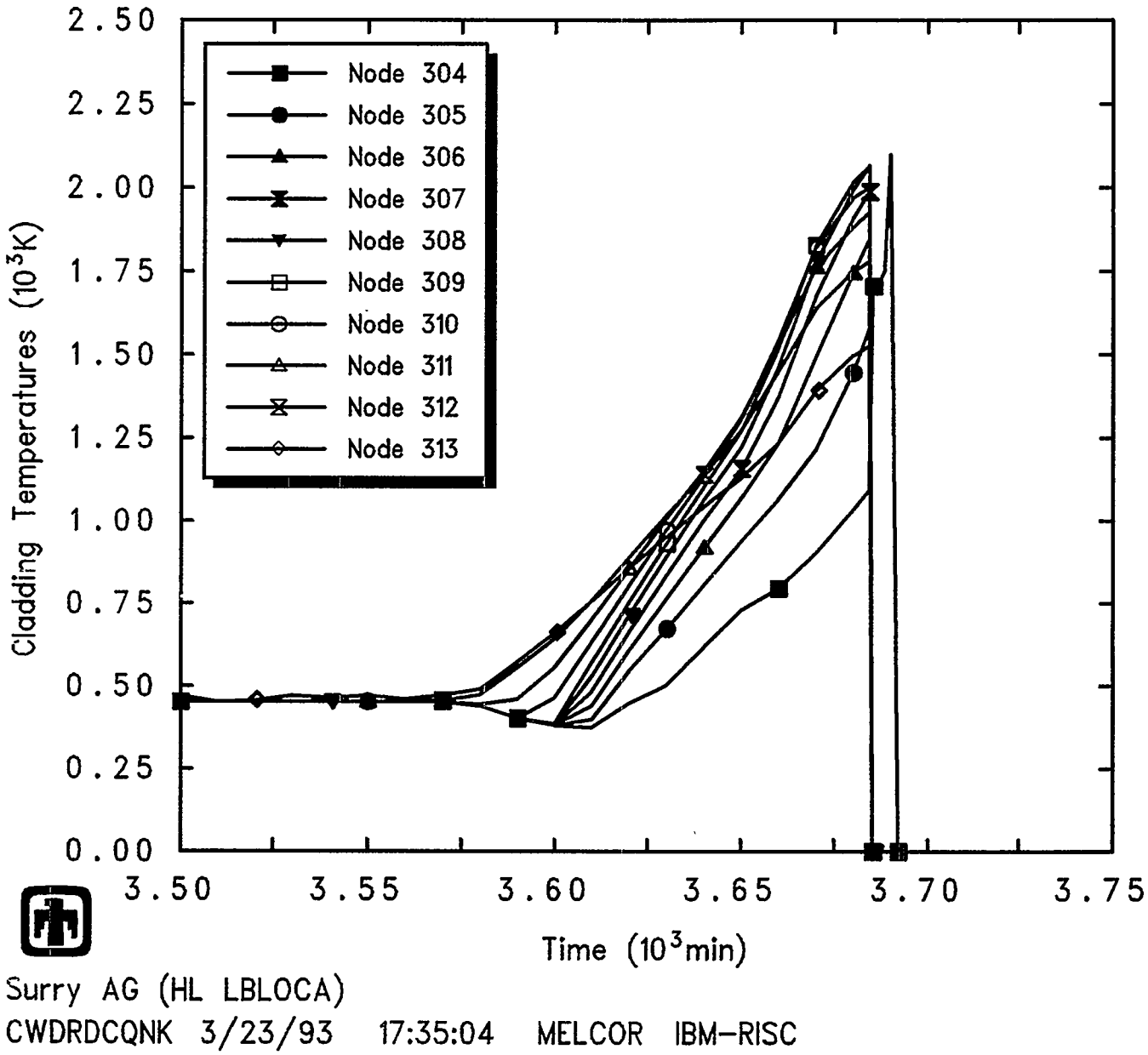

Figure 5.2.9 Core Ring 3 Clad Temperatures Predicted during AG Sequence

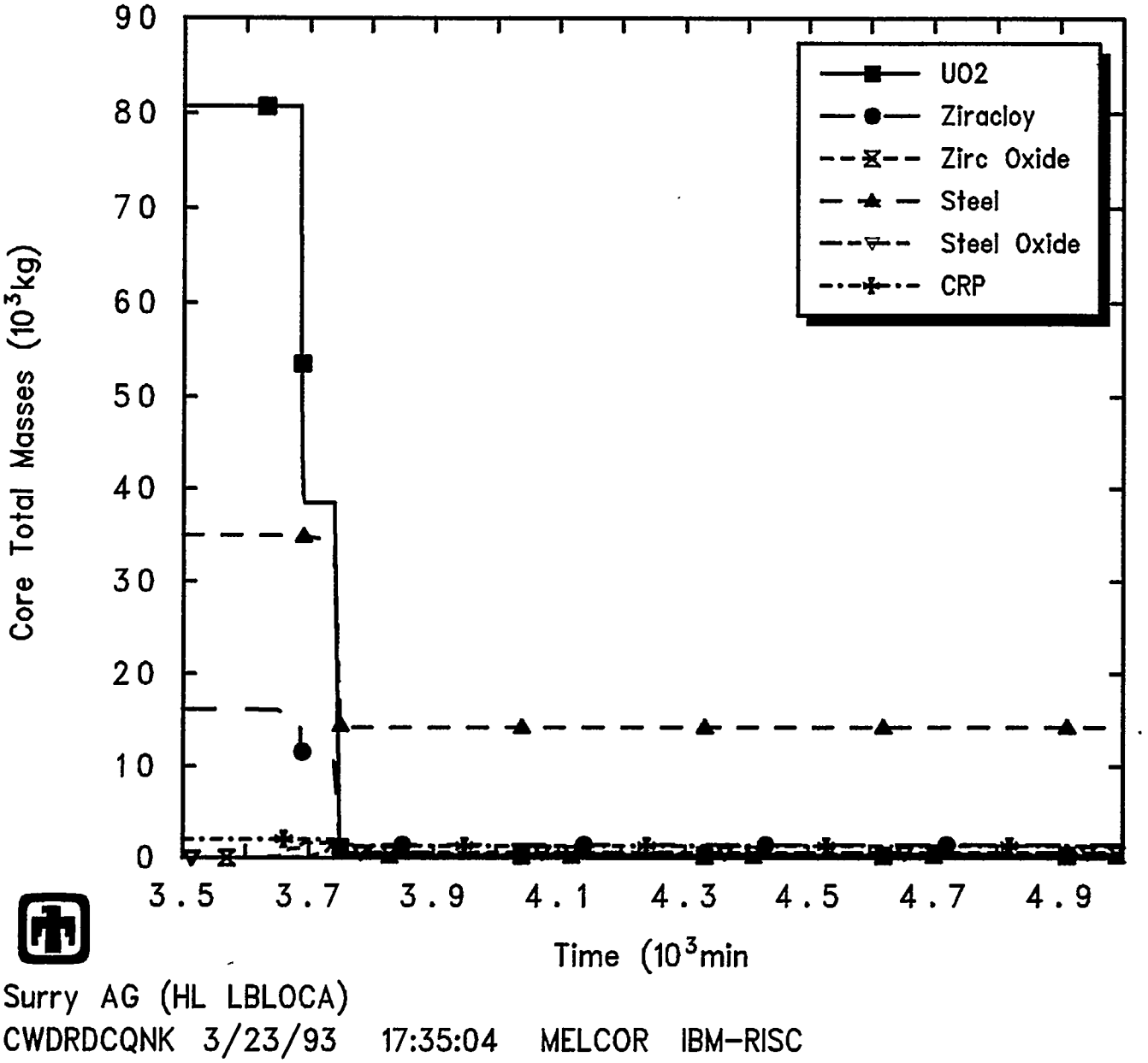

Figure 5.2.10 Core Total Material Masses Predicted during AG Sequence

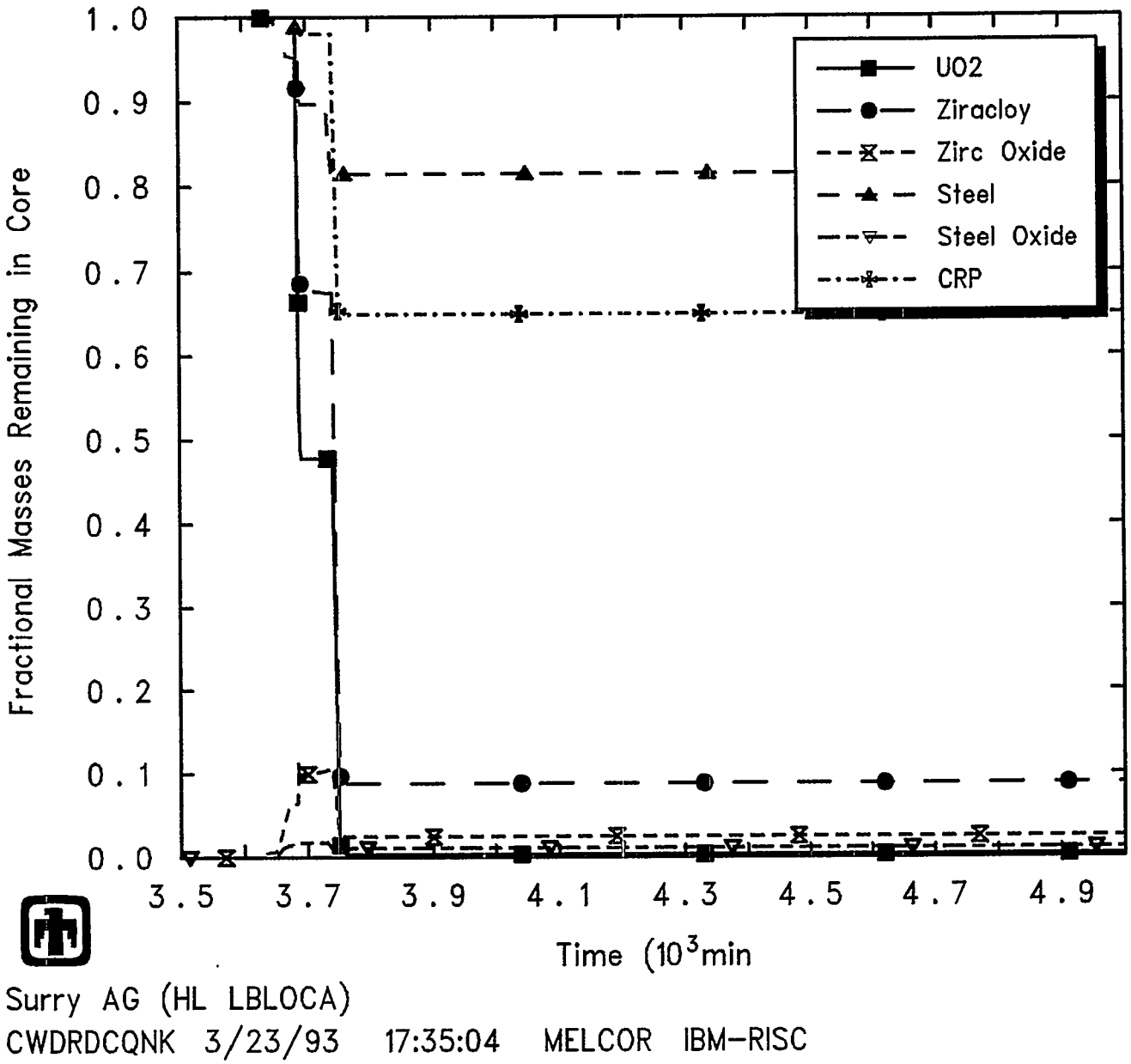

Figure 5.2.11 Core Fractional Material Masses Predicted during AG Sequence

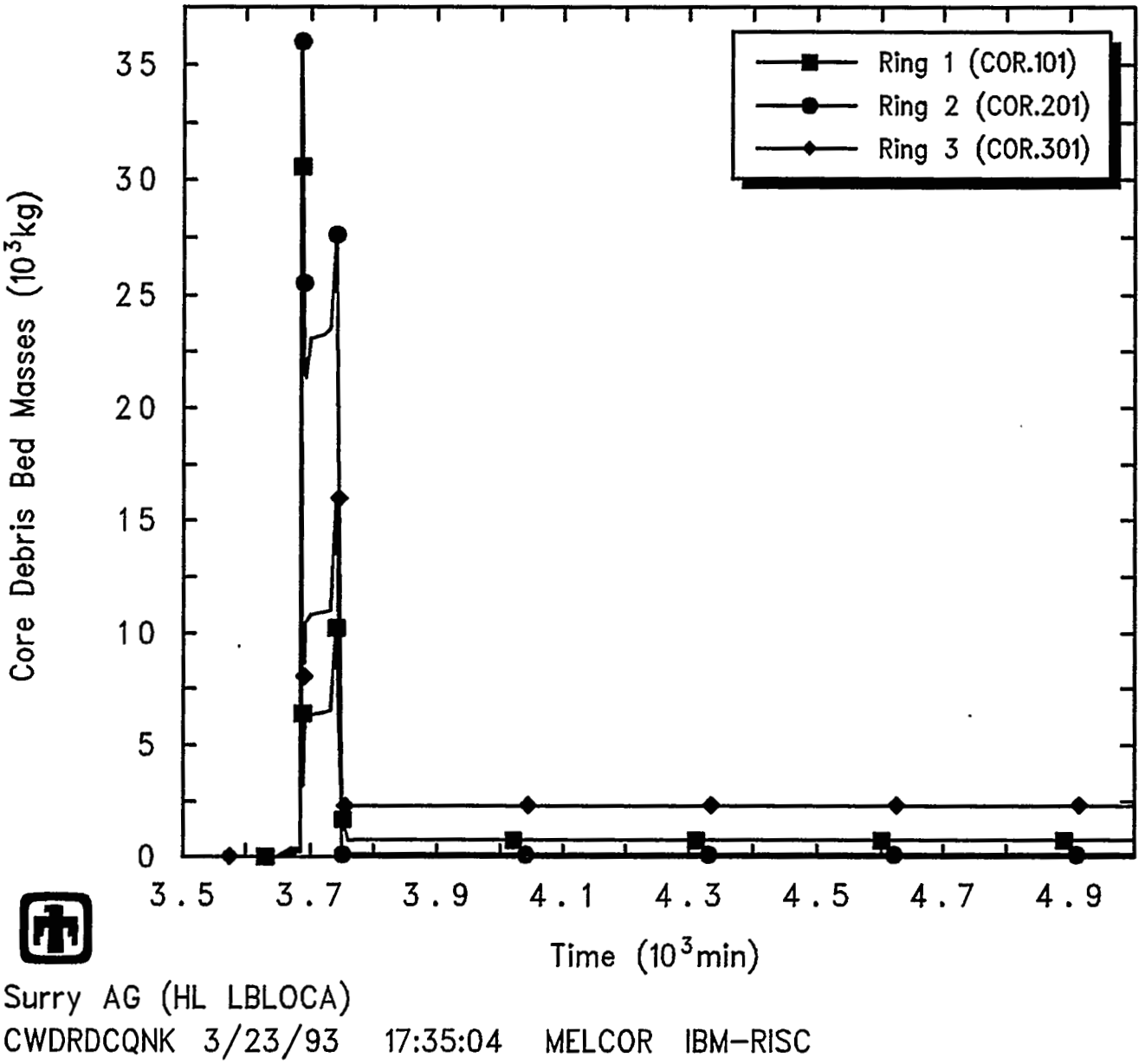

Figure 5.2.12 Lower Plenum Debris Bed Masses Predicted during AG Sequence

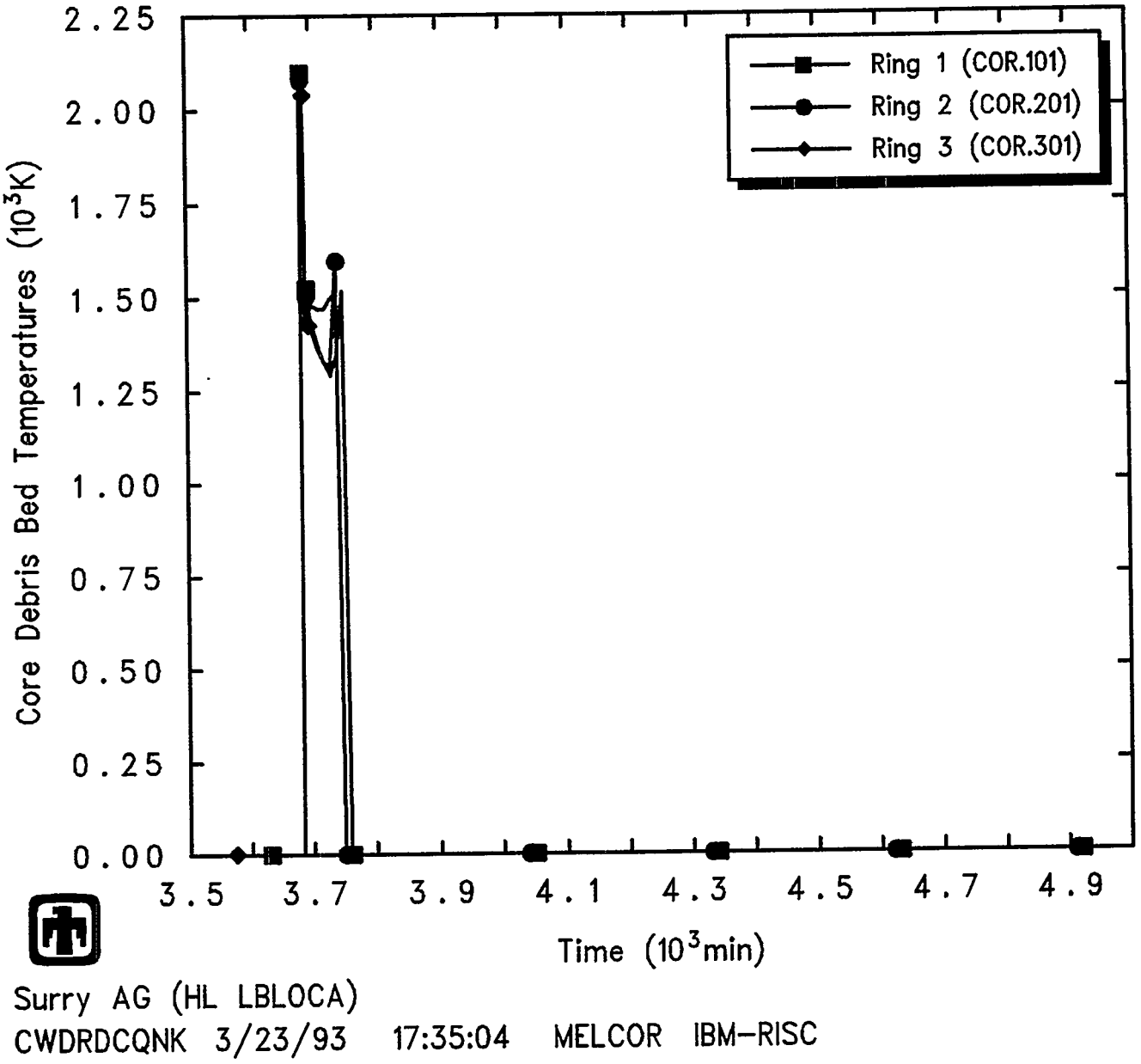

Figure 5.2.13 Lower Plenum Debris Bed Temperatures Predicted during AG Sequence

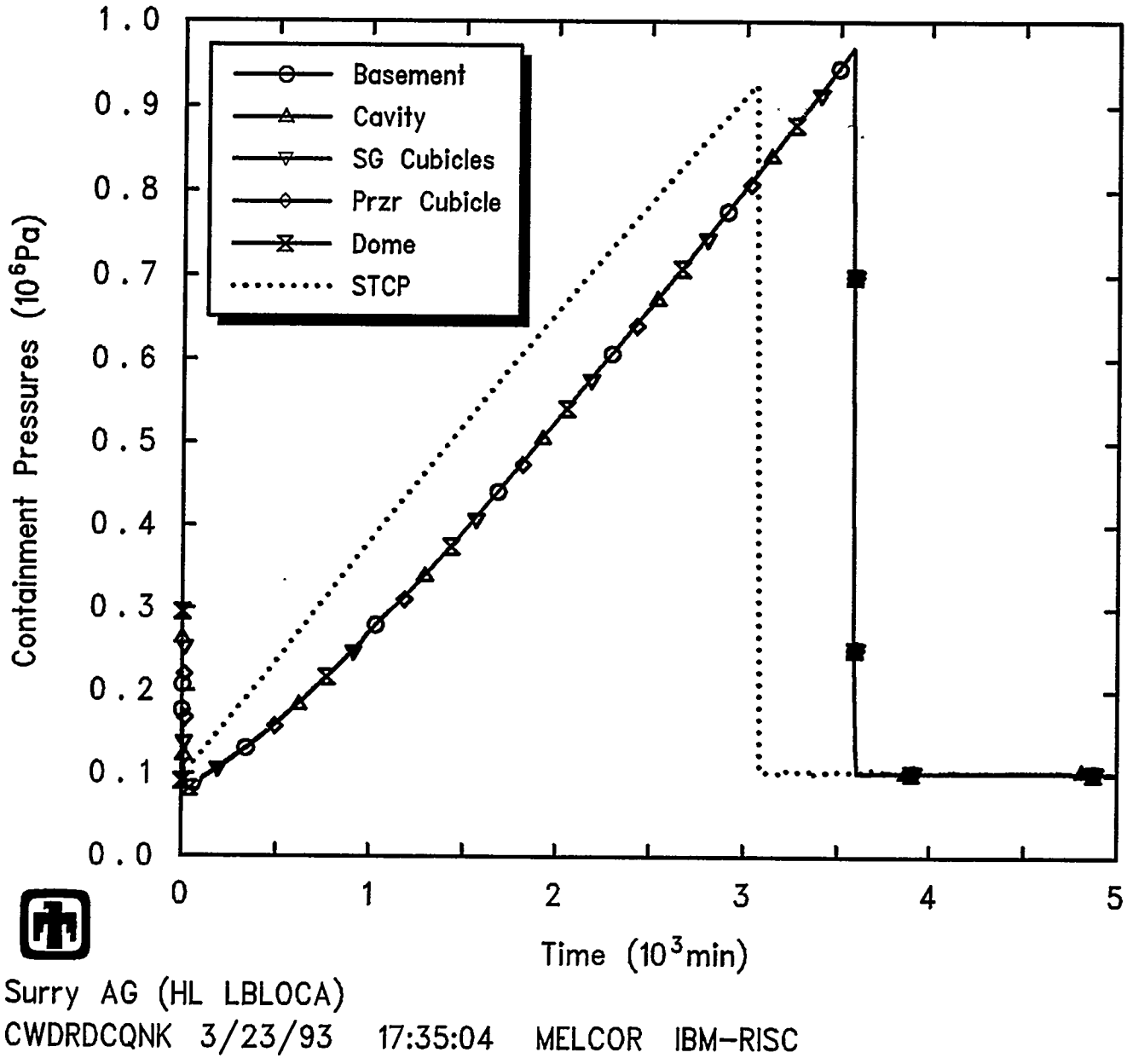

Figure 5.2.14 Containment System Pressures Predicted during AG Sequence

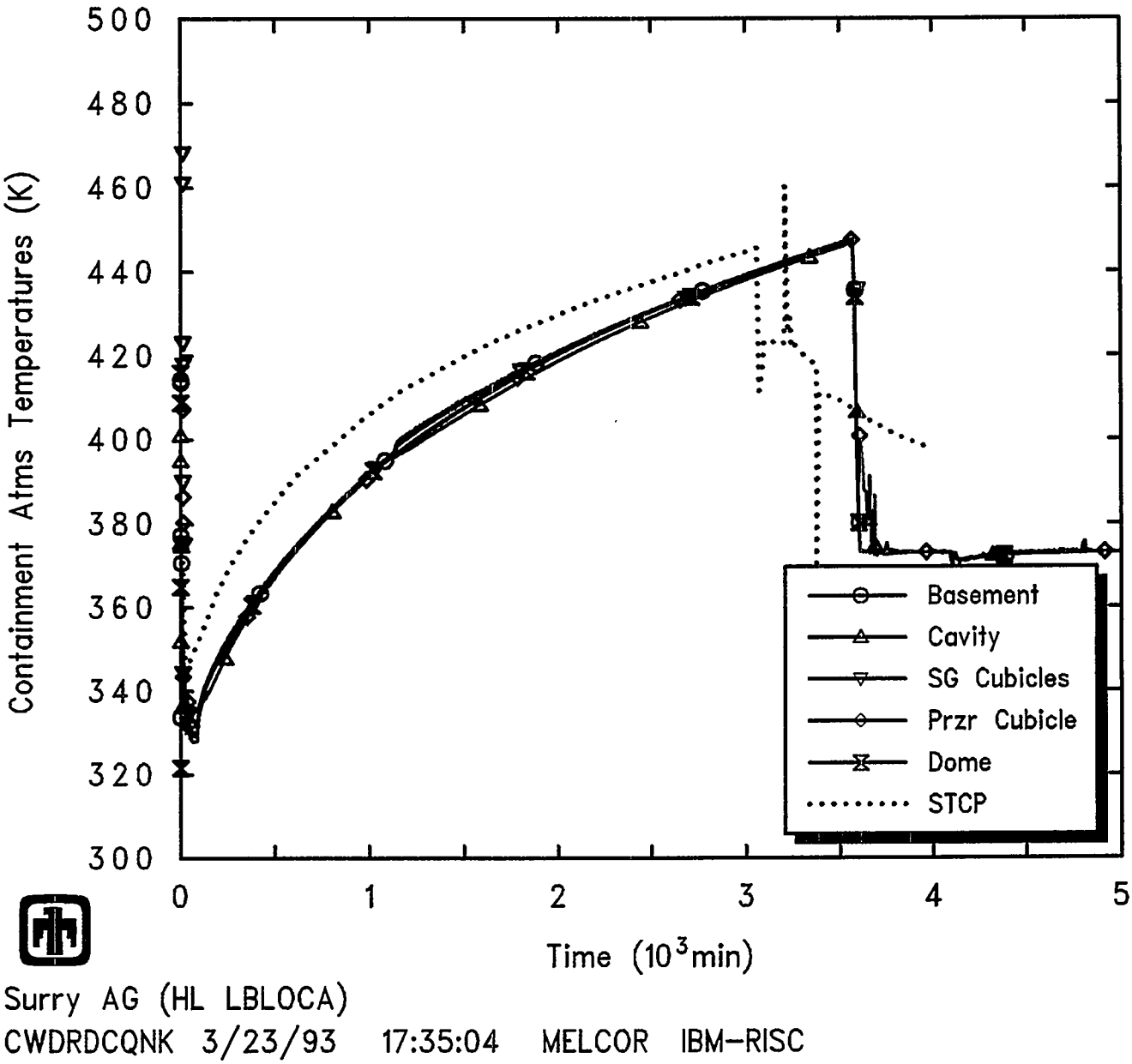

Figure 5.2.15 Containment System Atmosphere Temperatures Predicted during AG Sequence

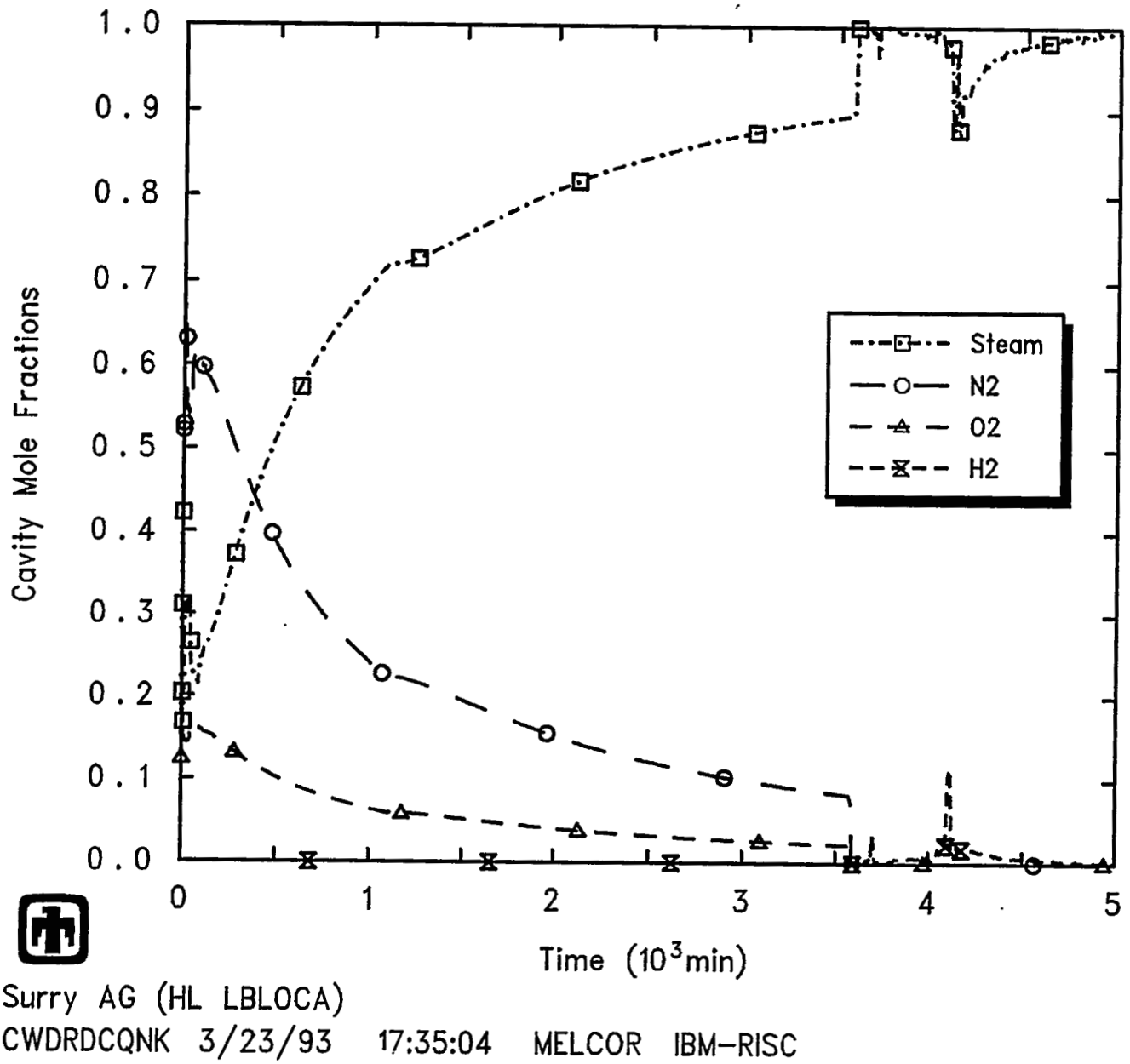

Figure 5.2.16 Cavity Steam and Noncondensable Mole Fractions Predicted during AG Sequence

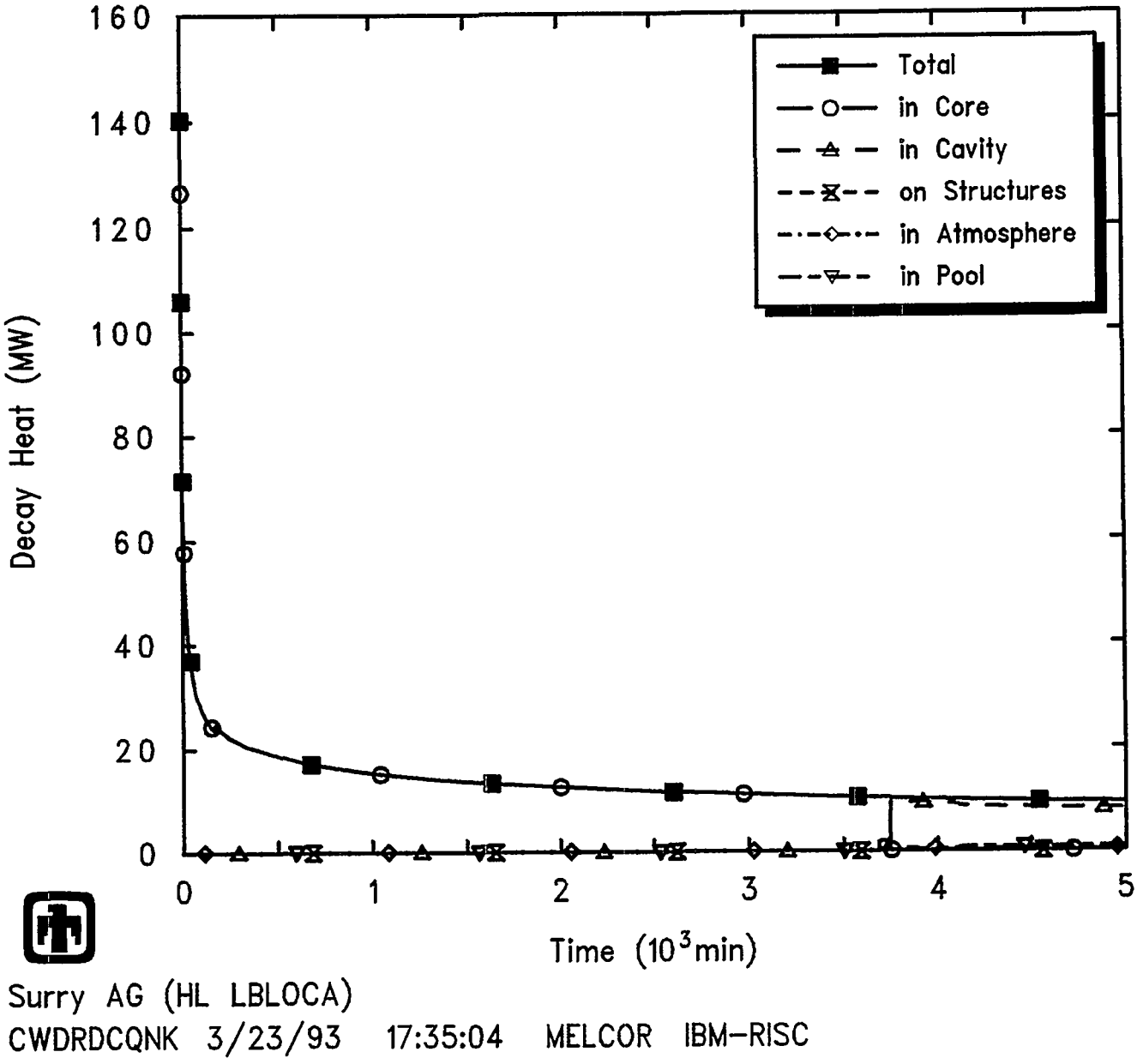

Figure 5.2.17 Decay Heat Predicted during AG Sequence

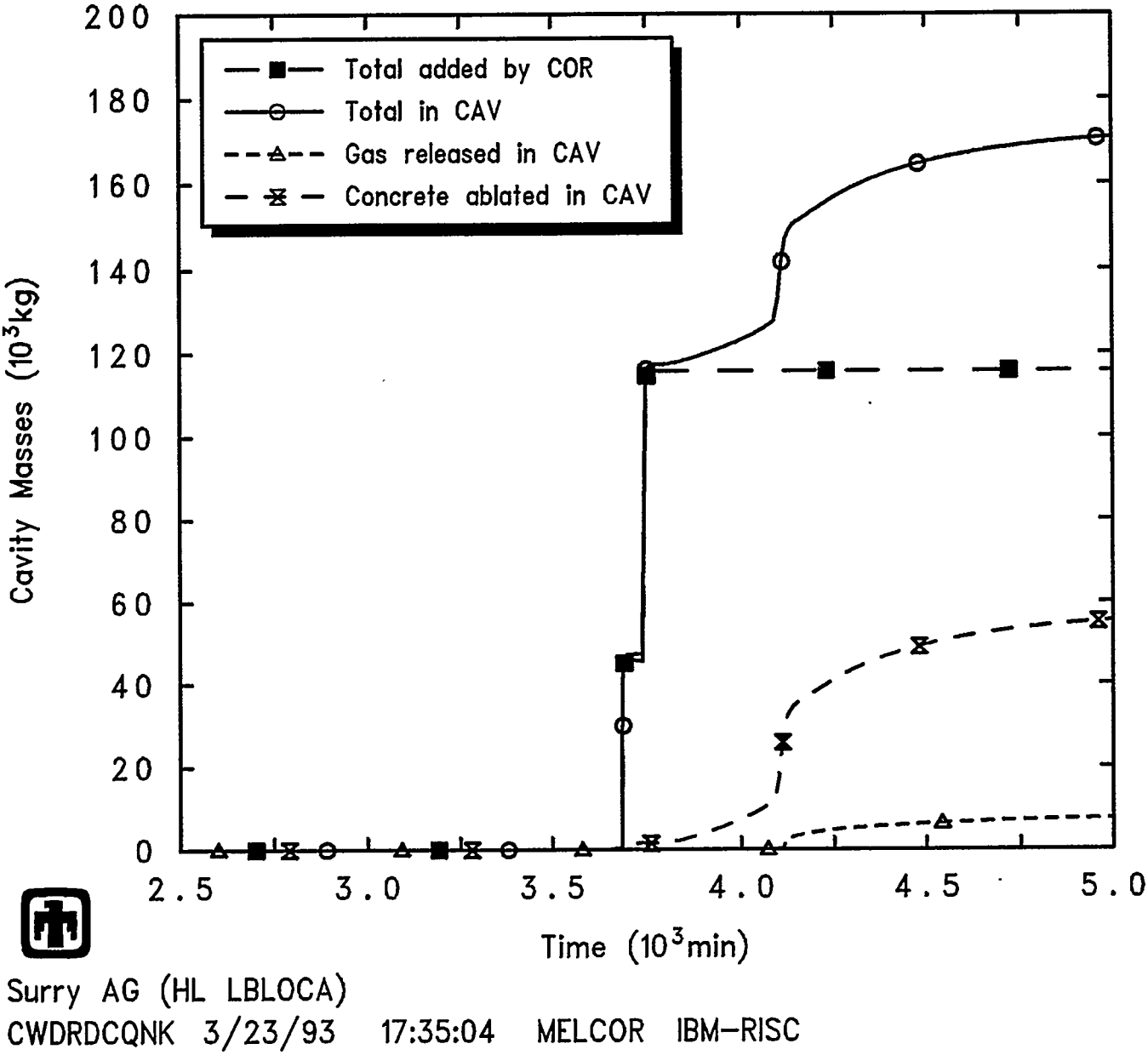

Figure 5.2.18 Total Cavity Masses in Cavity Predicted during AG Sequence

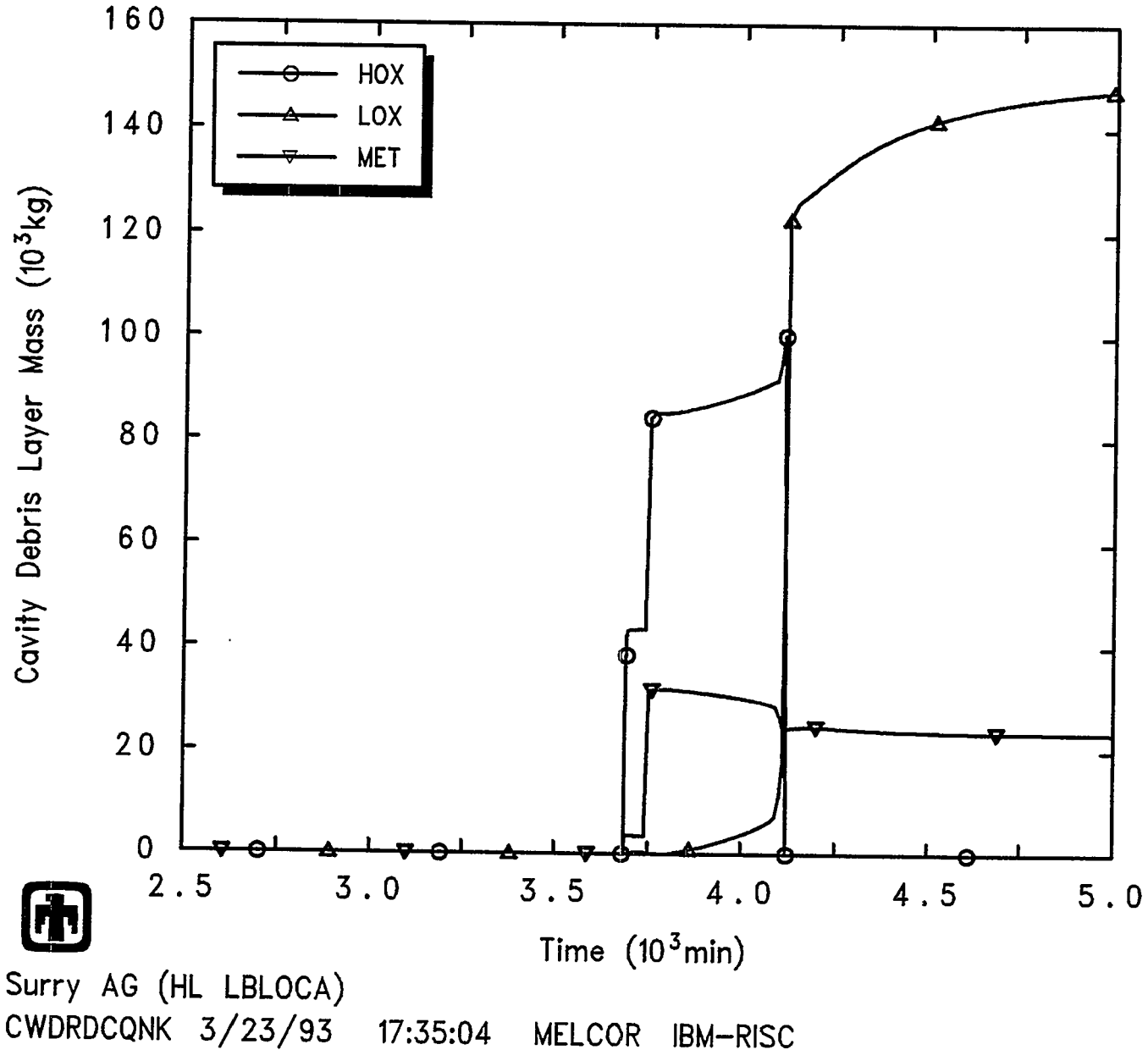

Figure 5.2.19 Cavity Layer Masses Predicted during AG Sequence

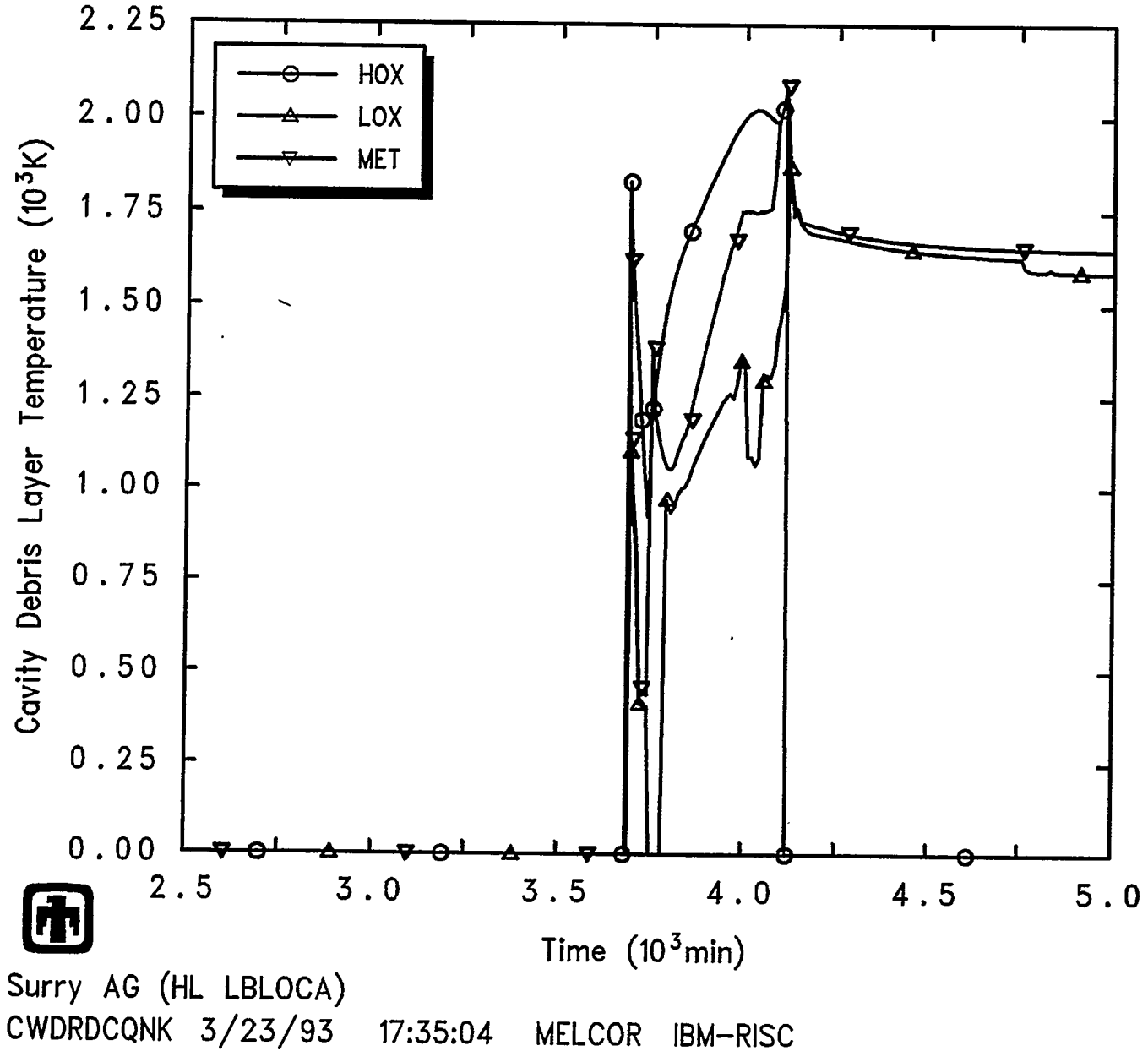

Figure 5.2.20 Cavity Layer Temperatures Predicted during AG Sequence

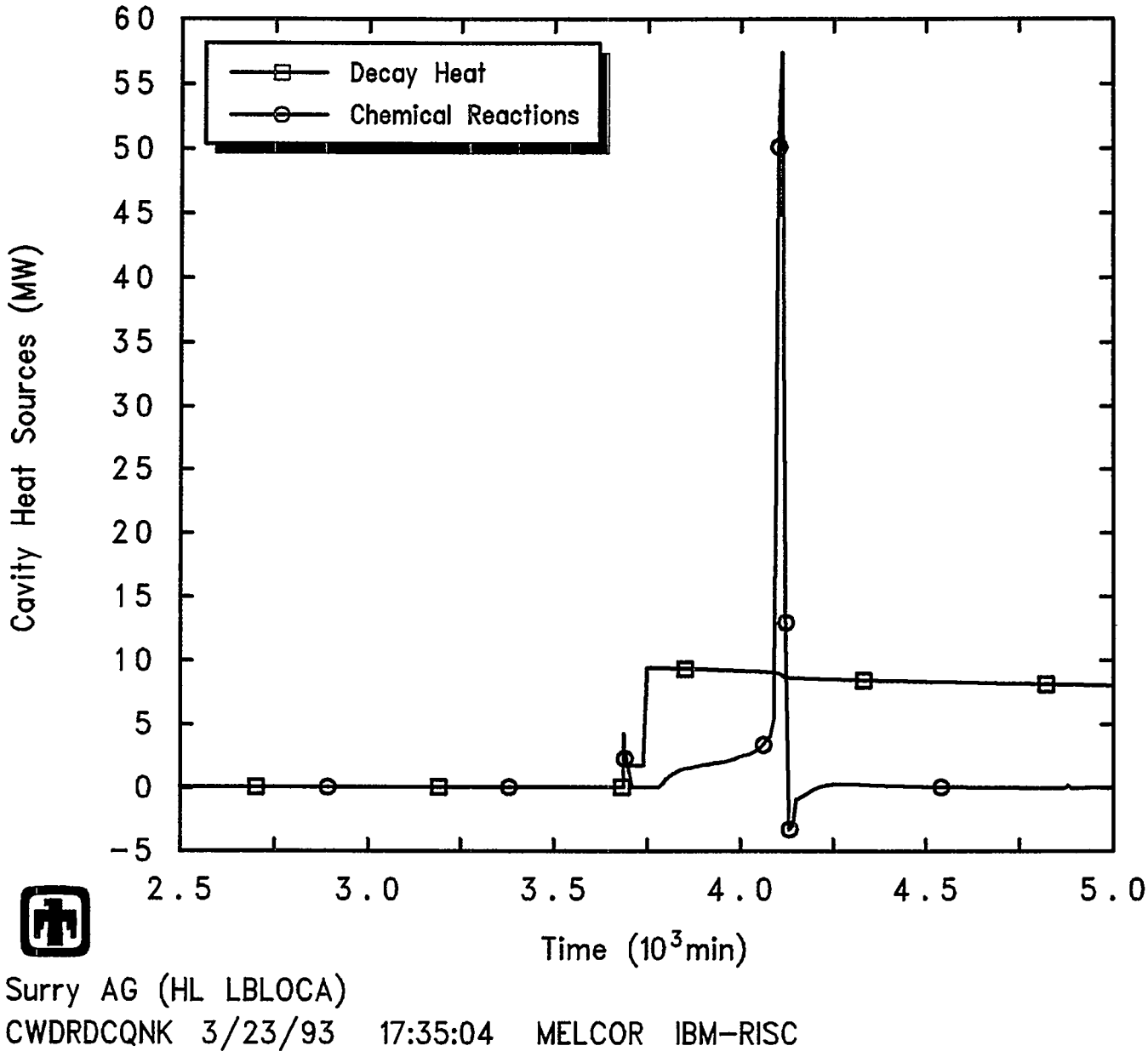

Figure 5.2.21 Decay Heat and Chemical Energy in Cavity Predicted during AG Sequence

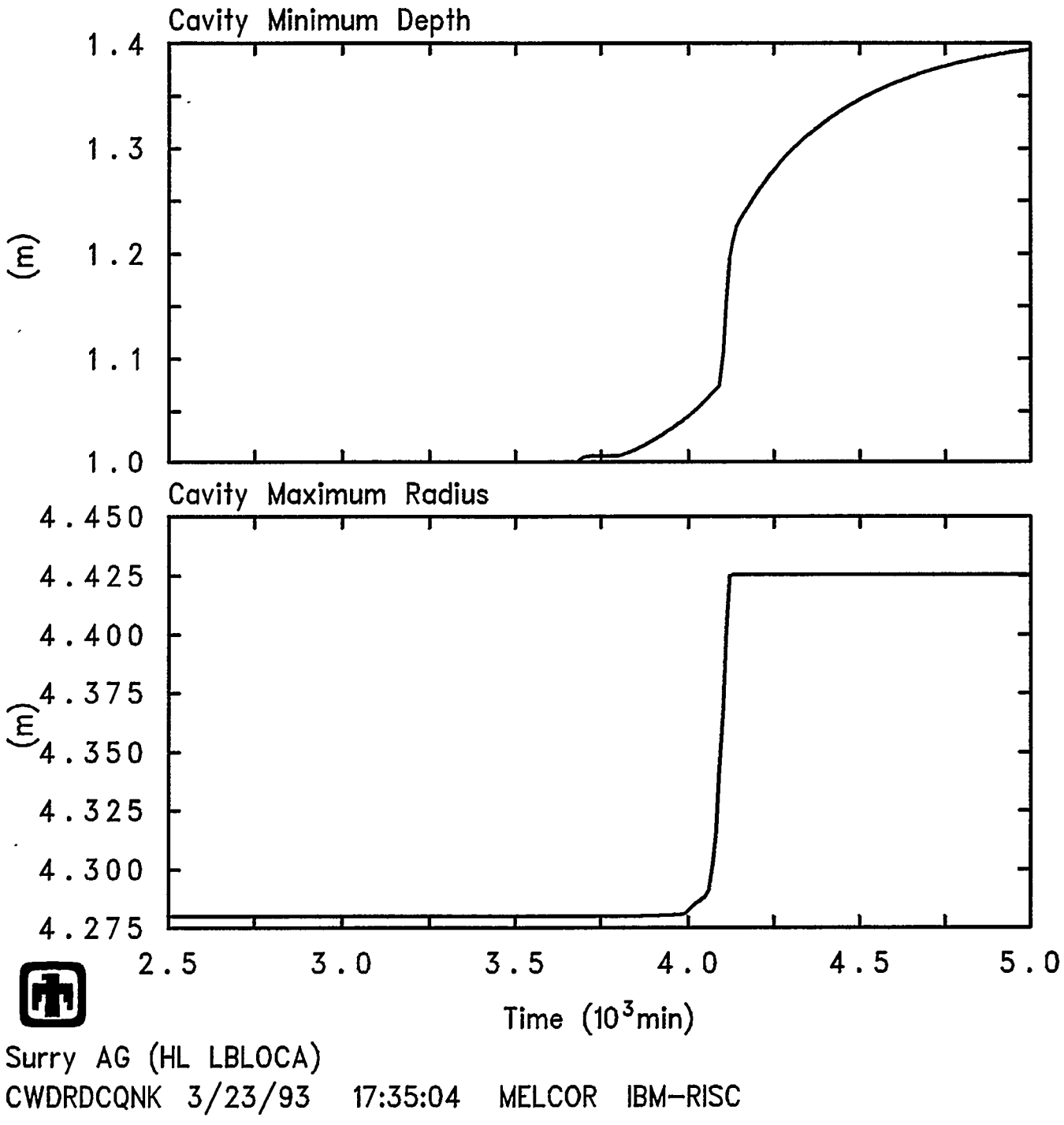

Figure 5.2.22 Cavity Maximum Radius and Minimum Depth Predicted during AG Sequence

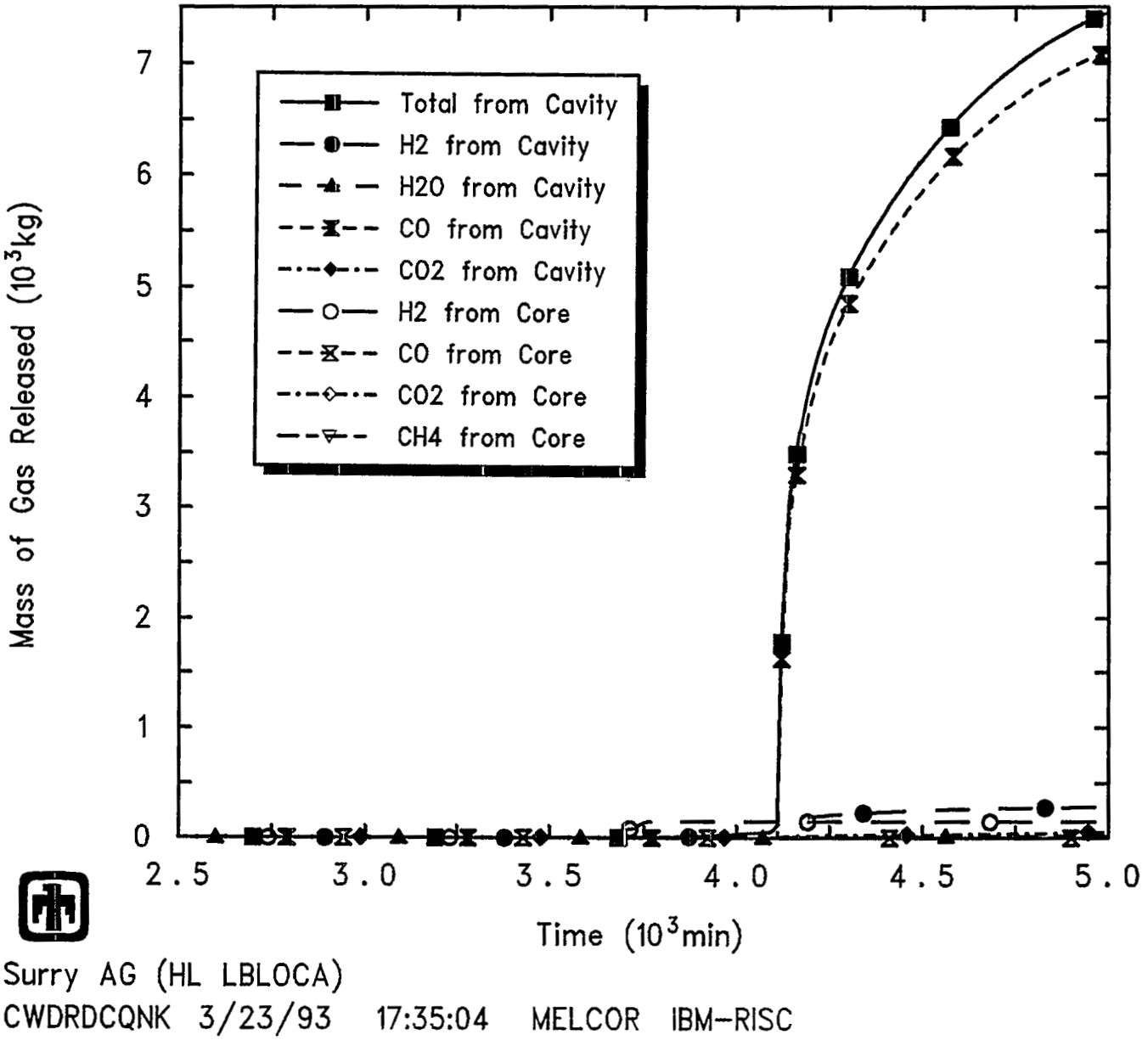

Figure 5.2.23 Gas Generation Predicted in Core and in Cavity during AG Sequence

Table 5.2.2 Radionuclide Distribution in Core, RCS and Cavity Predicted at 5,000min for AG Sequence

Radionuclide Species Group and Representative Element	Core		RCS		Cavity	
	MELCOR	STCP	MELCOR	STCP	MELCOR	STCP
Noble Gases, Xe	8.91E-03		2.93E-04		0	
Alkali Metals, Cs	8.61E-03		0.127	0.13	0	1.6E-04
Alkaline Earths, Ba	1.14E-02		5.74E-03	5.0E-03	0.834	0.98
Halogens, I	1.59E-02		5.13E-04	0.13	0	1.5E-04
Chalcogens, Te	1.14E-02		7.13E-03	0.15	0.755	0.14
Platinoids, Ru	1.15E-02		1.20E-04	3.8E-07	0.988	1.0
Transition Metals, Mo	1.14E-02		5.69E-03		0.958	
Tetravalents, Ce	1.15E-02		4.72E-06	0	0.988	1.0
Trivalents, La	1.15E-02		6.41E-06	4.0E-08	0.988	0.99
Uranium, U	1.53E-02		5.57E-06		0.985	
More Volatile Main Group Metals, Cd	1.13E-02		1.59E-02		0.928	
Less Volatile Main Group Metals, Sn	1.13E-02		1.59E-02		0.919	

Table 5.2.3 Radionuclide Distribution in Containment and Environment Predicted at 5,000min for AG Sequence

Radionuclide Species Group and Representative Element	Containment		Environment		Containment & Environment	
	MELCOR	STCP	MELCOR	STCP	MELCOR	STCP
Noble Gases, Xe	6.75E-05		0.991	0.998	0.99	1.00
Alkali Metals, Cs	0.779	0.28	8.52E-02	0.57	0.86	0.85
Alkaline Earths, Ba	0.145	7.3E-03	4.03E-03	1.4E-02	0.15	2.1E-02
Halogens, I	1.16E-04	0.28	0.983	0.58	0.98	0.86
Chalcogens, Te	0.220	0.24	6.32E-03	0.47	0.23	0.71
Platinoids, Ru	2.78E-04	4.2E-07	7.61E-05	7.9E-07	3.5E-04	1.2E-06
Transition Metals, Mo	2.18E-02		2.87E-03		2.5E-02	
Tetravalents, Ce	1.38E-05	1.8E-05	2.59E-06	4.8E-05	1.6E-05	6.6E-05
Trivalents, La	1.94E-04	6.2E-05	5.82E-06	1.6E-04	2.0E-04	2.2E-04
Uranium, U	2.57E-05		4.30E-06		3.0E-05	
More Volatile Main Group Metals, Cd	3.56E-02		9.61E-03		4.5E-02	
Less Volatile Main Group Metals, Sn	4.36E-02		9.67E-03		5.3E-02	

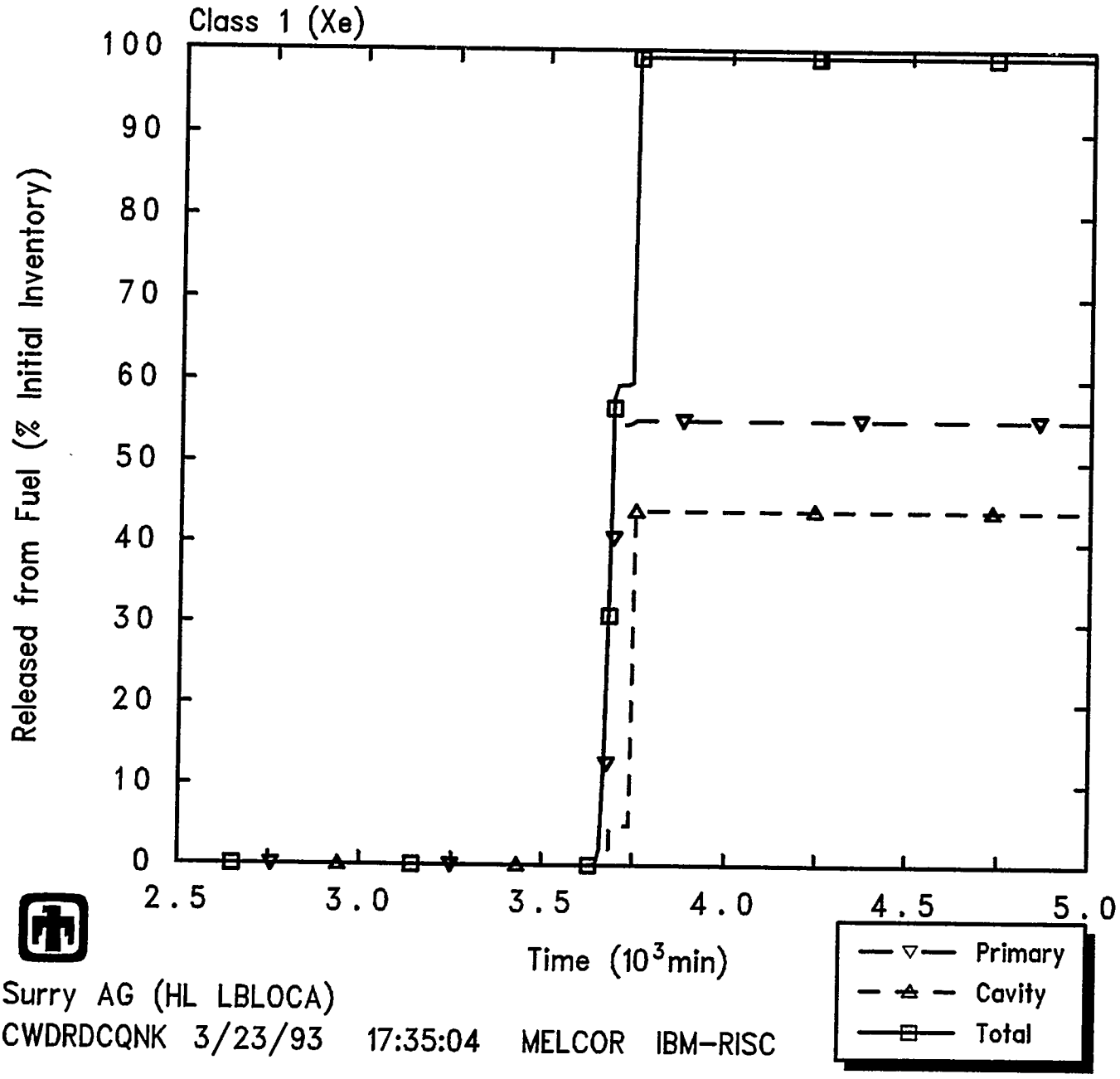

Figure 5.2.24 Release of Class 1 (Xe) Noble Gas Radionuclides from Fuel in Core and in Cavity Predicted during AG Sequence, as Percentage of Initial Inventory in Core

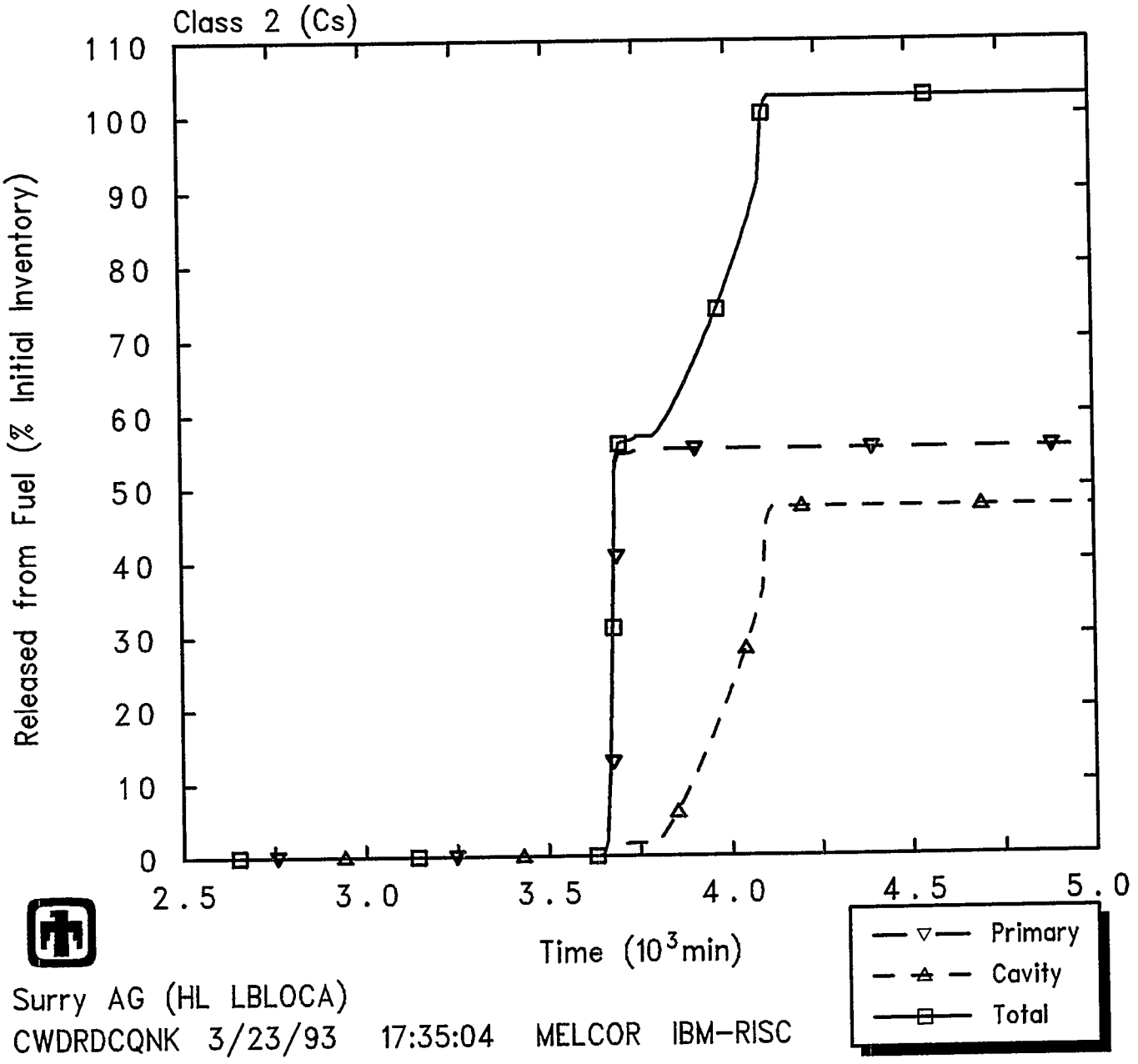

Figure 5.2.25 Release of Class 2 (Cs) Alkali Metal Radionuclides from Fuel in Core and in Cavity Predicted during AG Sequence, as Percentage of Initial Inventory in Core

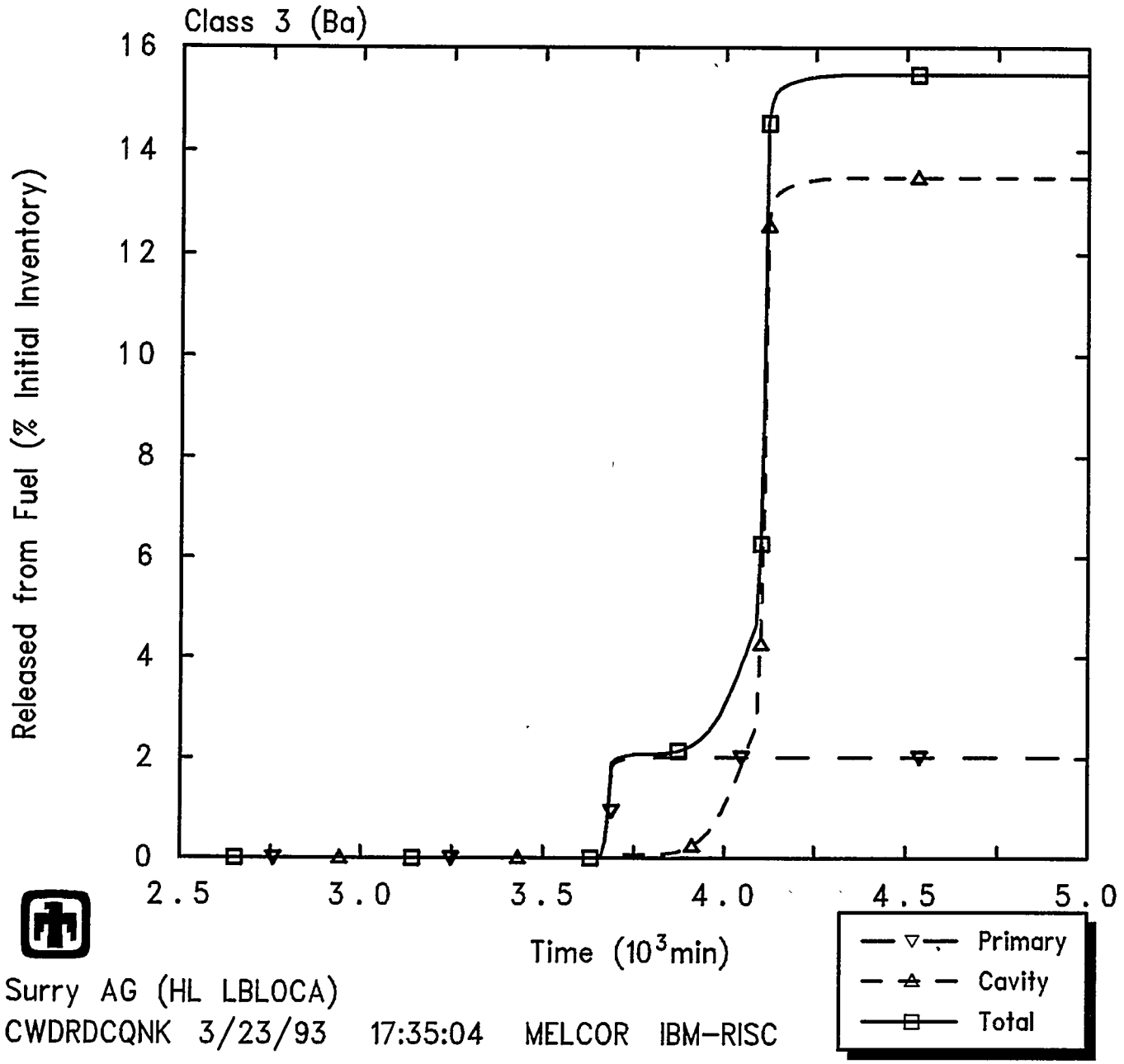

Figure 5.2.26 Release of Class 3 (Ba) Alkaline Earth Radionuclides from Fuel in Core and in Cavity Predicted during AG Sequence, as Percentage of Initial Inventory in Core

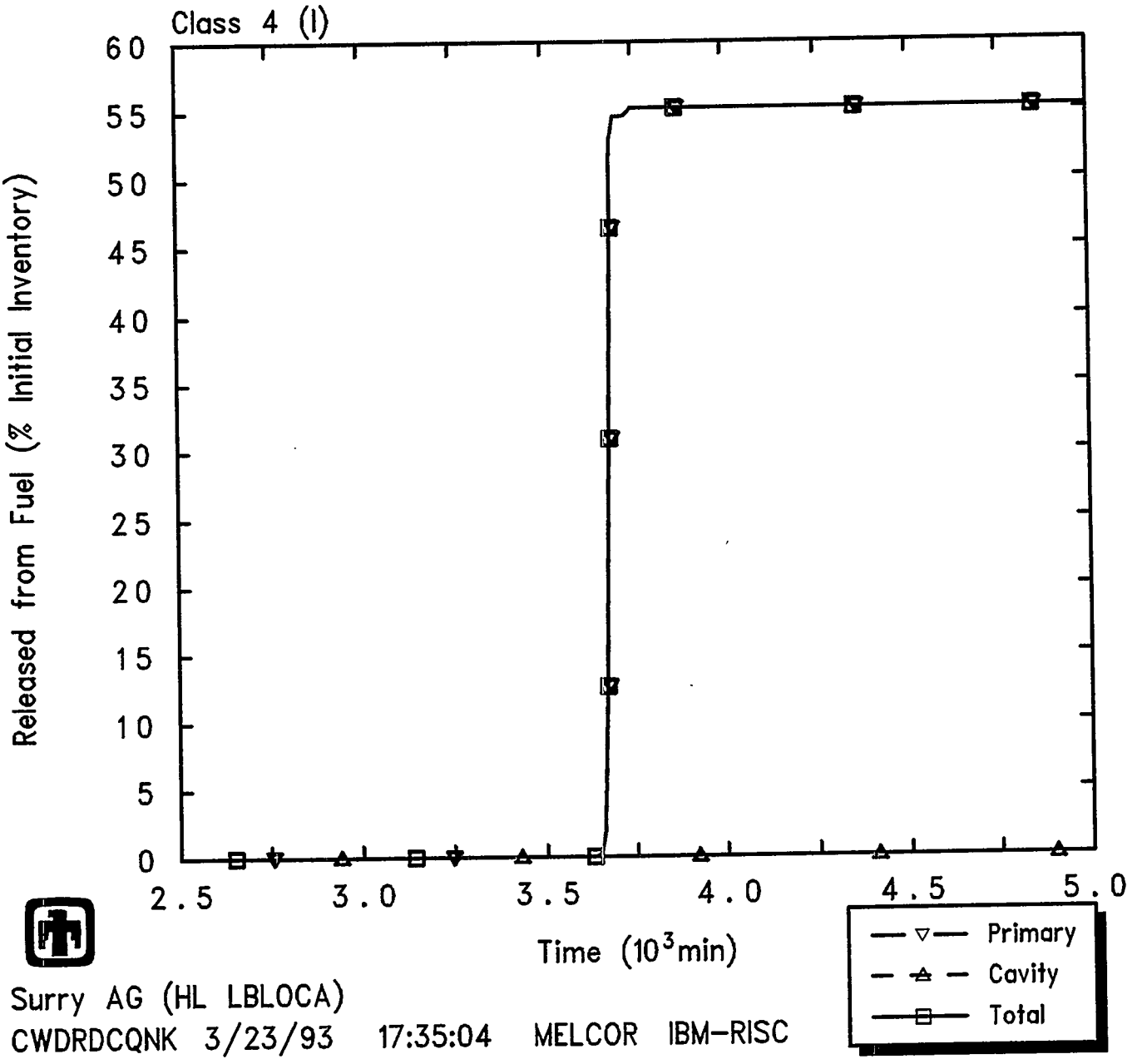

Figure 5.2.27 Release of Class 4 (I) Halogen Radionuclides from Fuel in Core and in Cavity Predicted during AG Sequence, as Percentage of Initial Inventory in Core

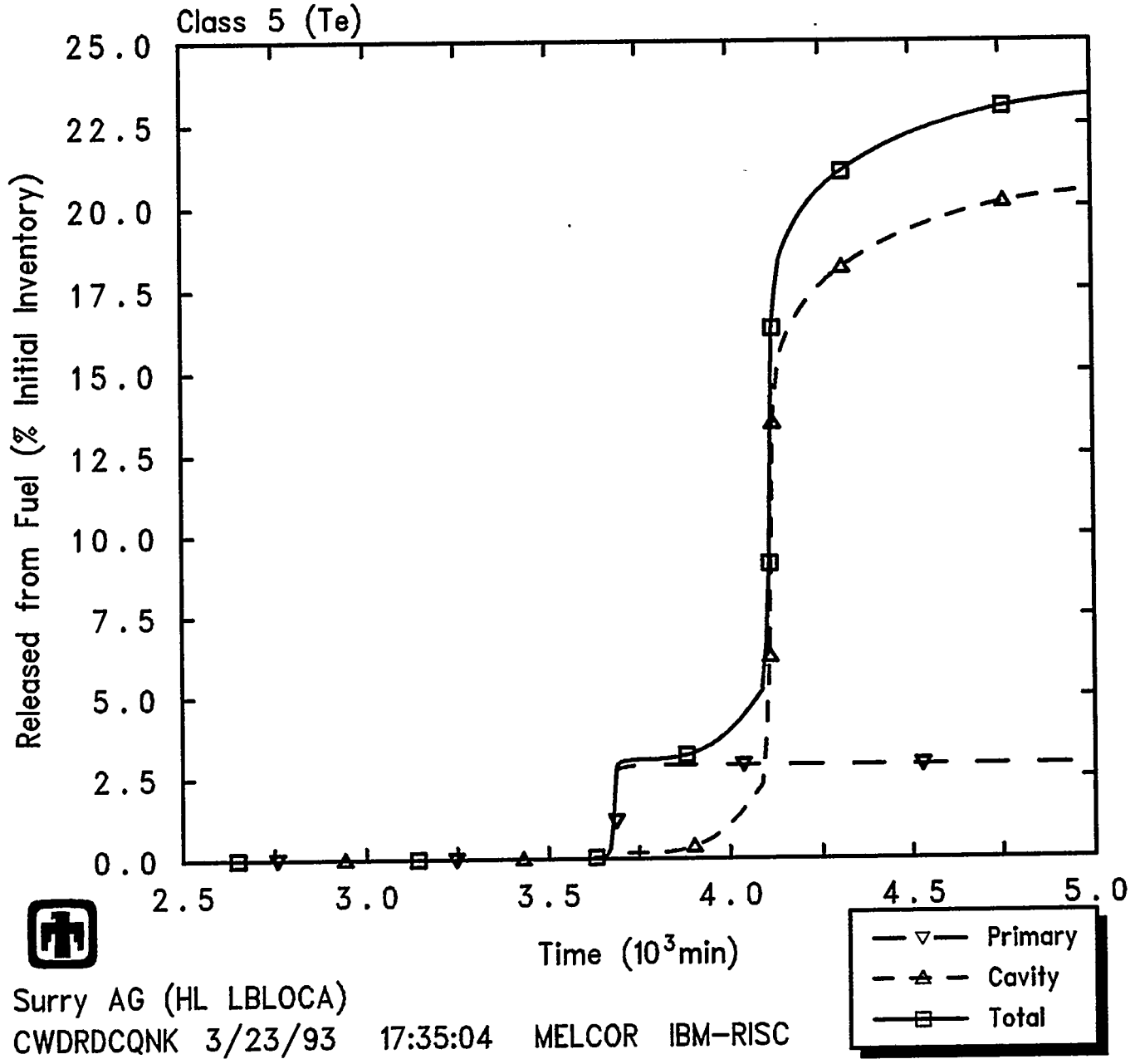

Figure 5.2.28 Release of Class 5 (Te) Chalcogen Radionuclides from Fuel in Core and in Cavity Predicted during AG Sequence, as Percentage of Initial Inventory in Core

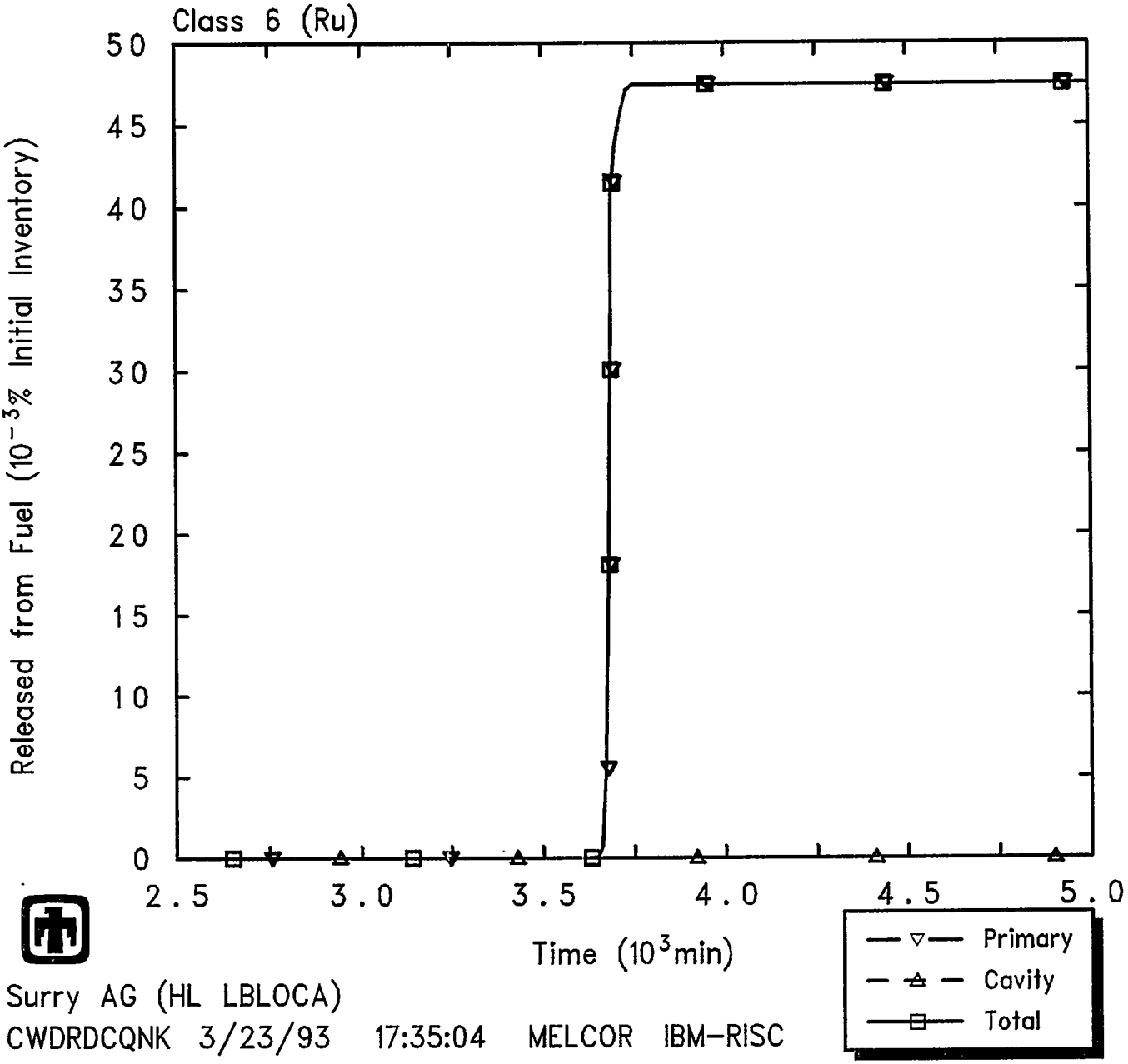

Figure 5.2.29 Release of Class 6 (Ru) Platinoid Radionuclides from Fuel in Core and in Cavity Predicted during AG Sequence, as Percentage of Initial Inventory in Core

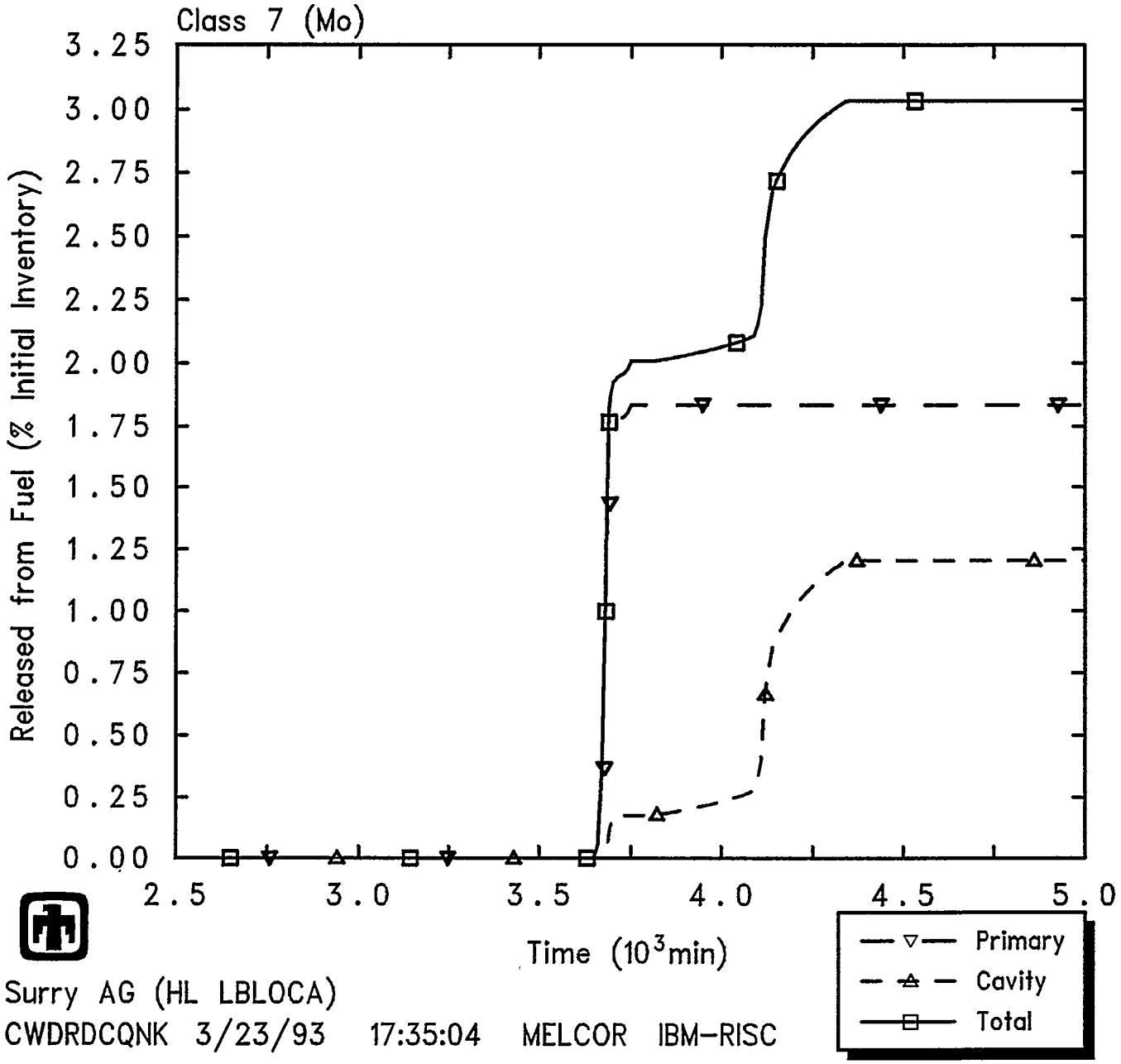

Figure 5.2.30 Release of Class 7 (Mo) Early Transition Element Radionuclides from Fuel in Core and in Cavity Predicted during AG Sequence, as Percentage of Initial Inventory in Core

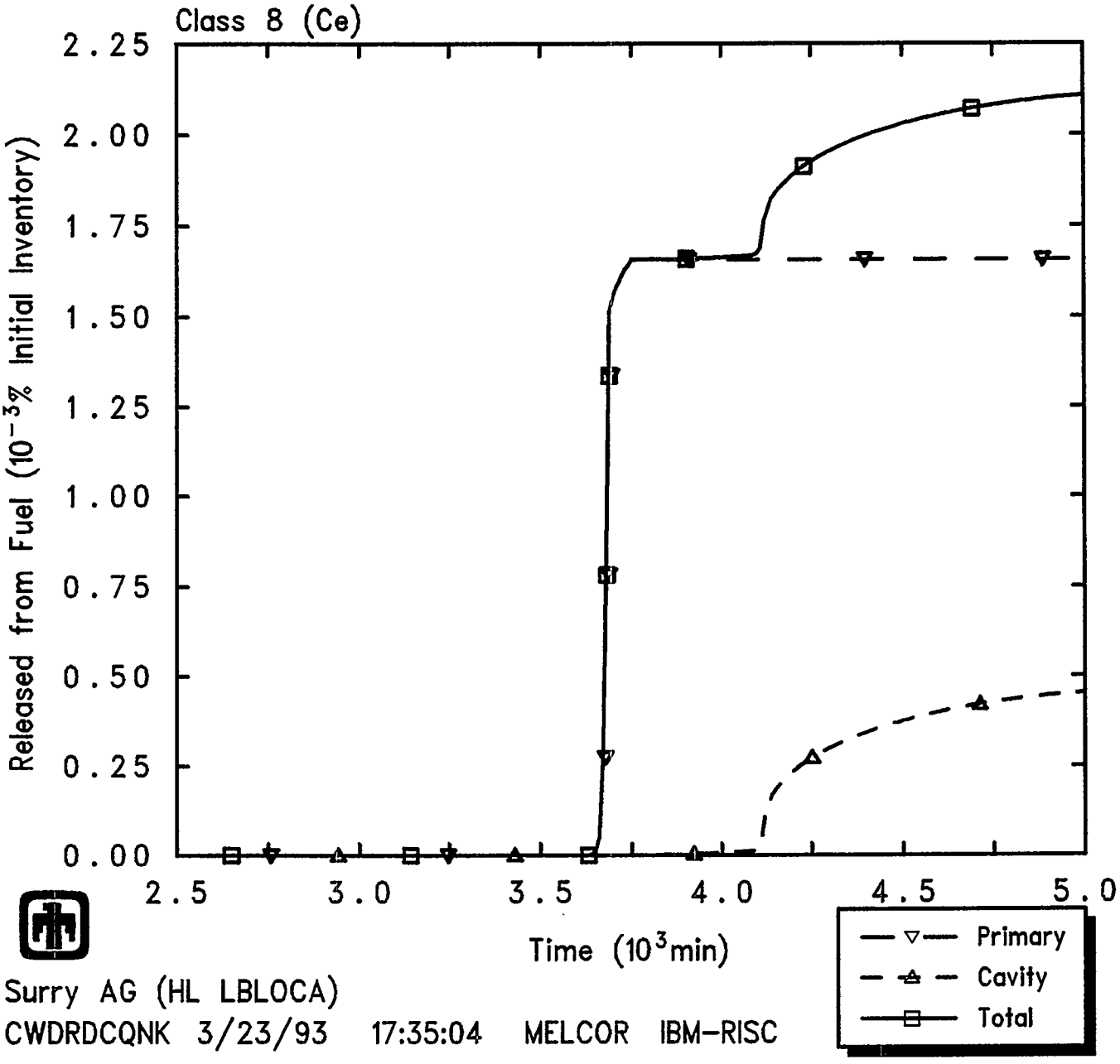

Figure 5.2.31 Release of Class 8 (Ce) Tetravalent Radionuclides from Fuel in Core and in Cavity Predicted during AG Sequence, as Percentage of Initial Inventory in Core

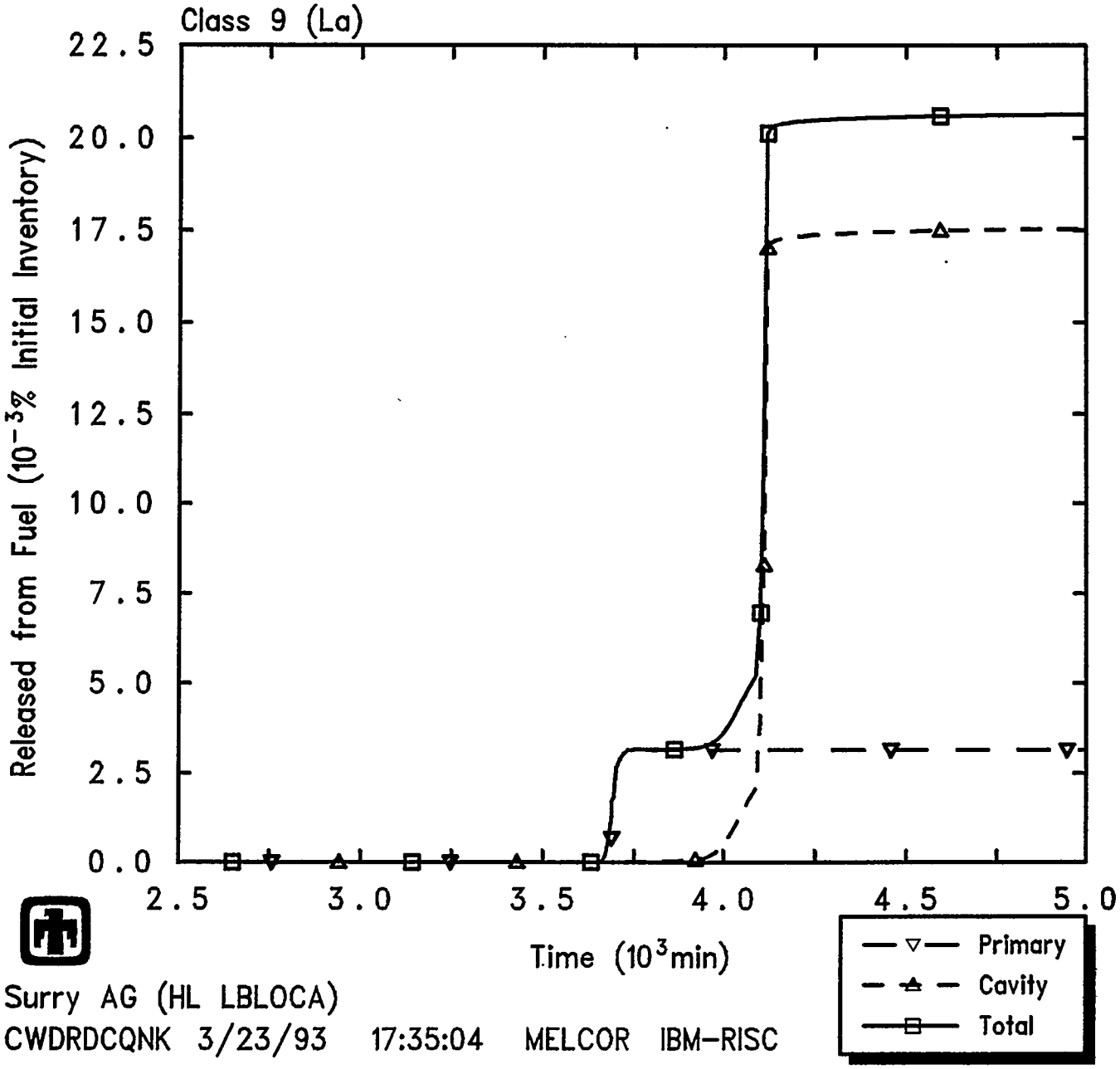

Figure 5.2.32 Release of Class 9 (La) Trivalent Radionuclides from Fuel in Core and in Cavity Predicted during AG Sequence, as Percentage of Initial Inventory in Core

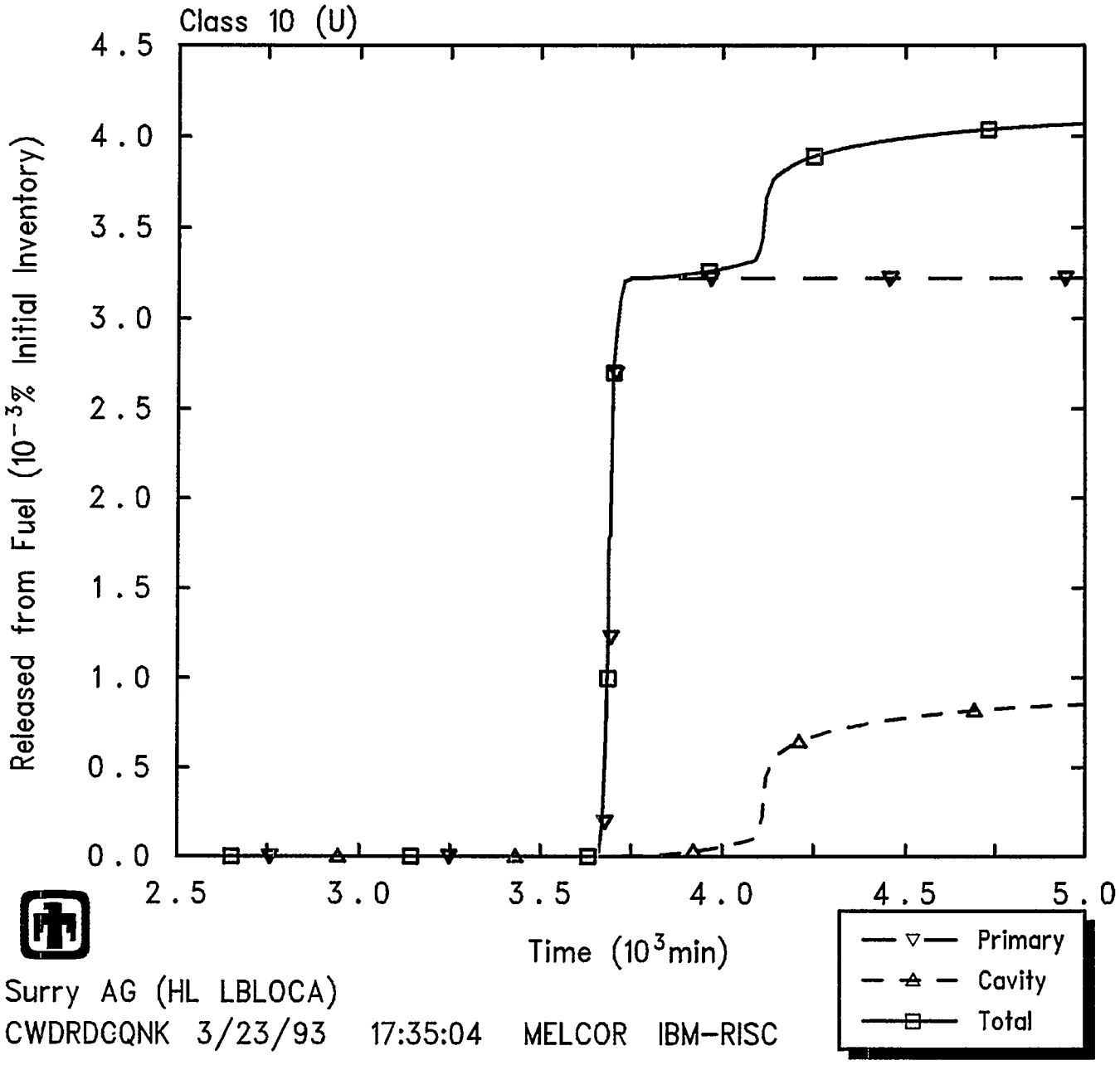

Figure 5.2.33 Release of Class 10 (U) Uranium Radionuclides from Fuel in Core and in Cavity Predicted during AG Sequence, as Percentage of Initial Inventory in Core

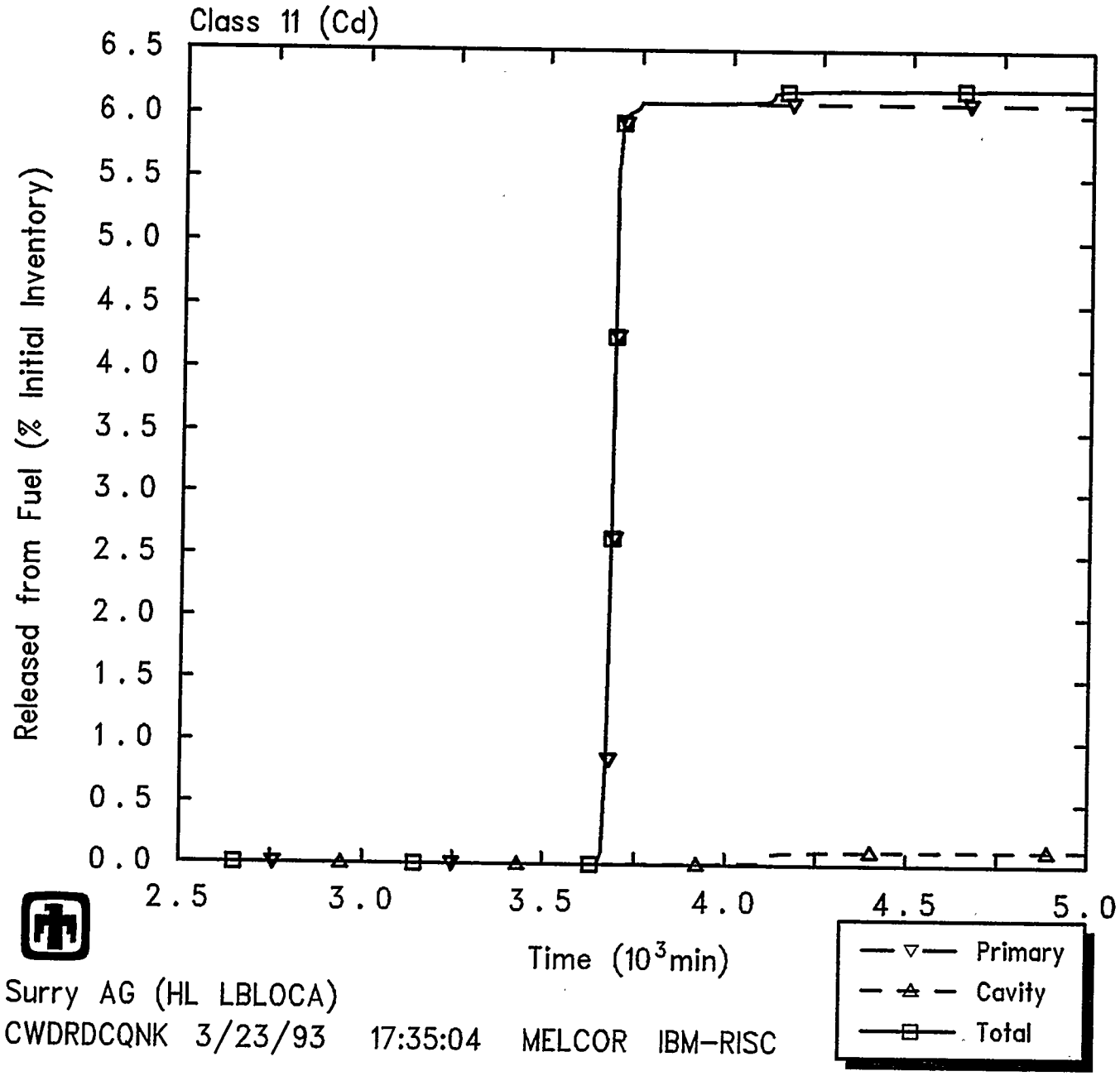

Figure 5.2.34 Release of Class 11 (Cd) More Volatile Main Group Radionuclides from Fuel in Core and in Cavity Predicted during AG Sequence, as Percentage of Initial Inventory in Core

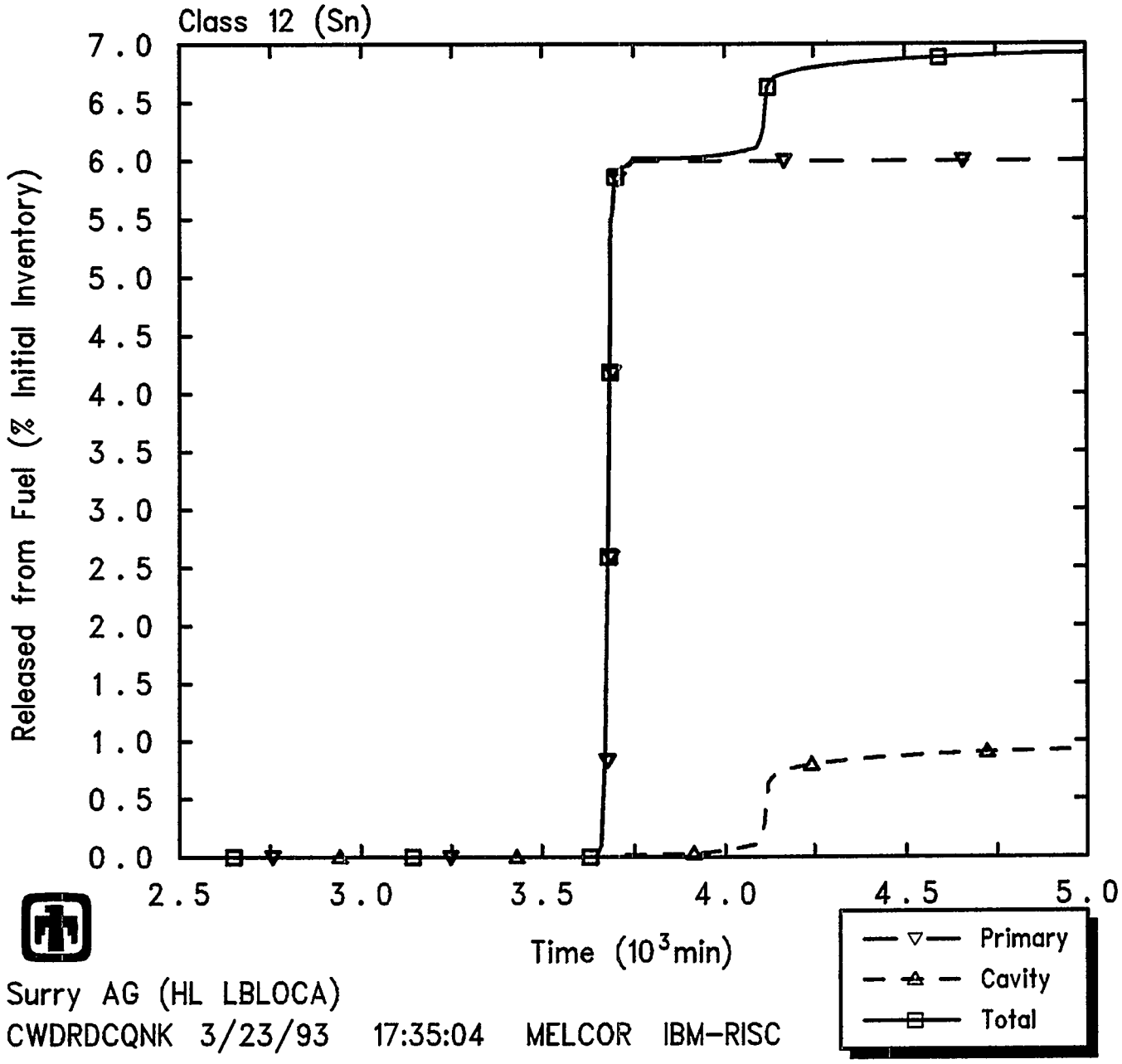

Figure 5.2.35 Release of Class 12 (Sn) Less Volatile Main Group Radionuclides from Fuel in Core and in Cavity Predicted during AG Sequence, as Percentage of Initial Inventory in Core

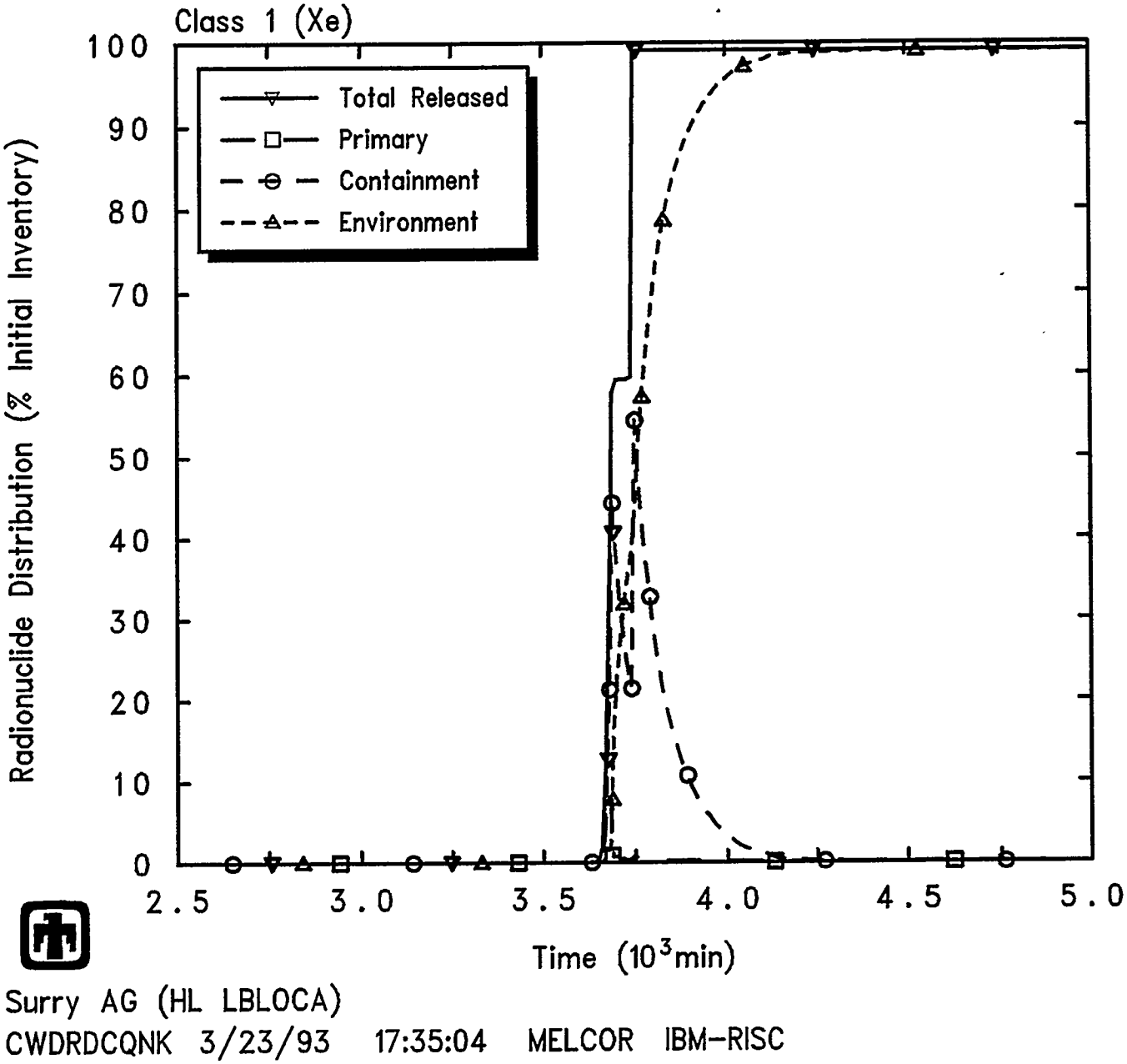

Figure 5.2.36 Distribution of Class 1 (Xe) Noble Gas Radionuclides in Primary System, Containment and Environment Predicted during AG Sequence, as Percentage of Initial Inventory in Core

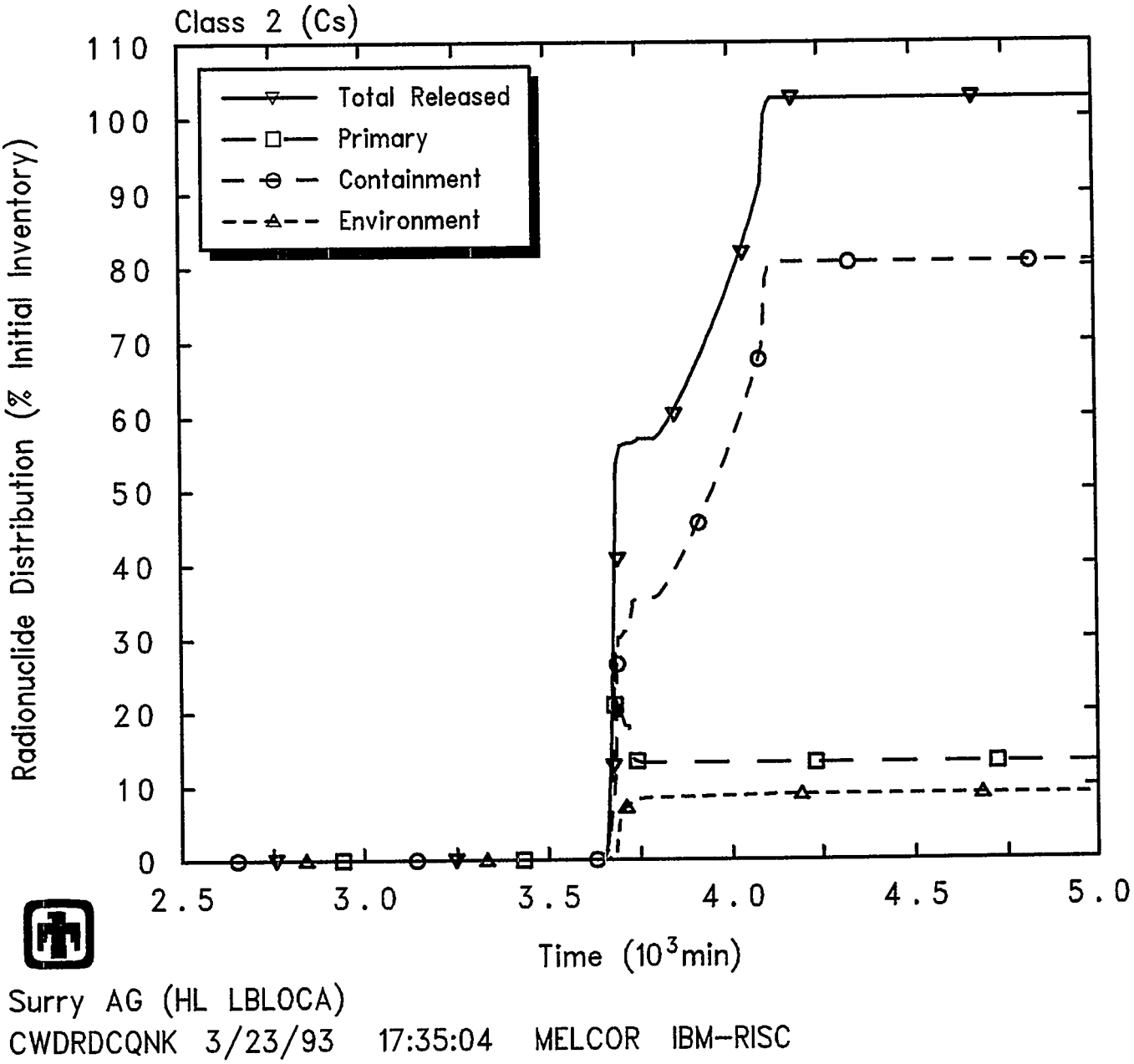

Figure 5.2.37 Distribution of Class 2 (Cs) Alkali Metal Radionuclides in Primary System, Containment and Environment Predicted during AG Sequence, as Percentage of Initial Inventory in Core

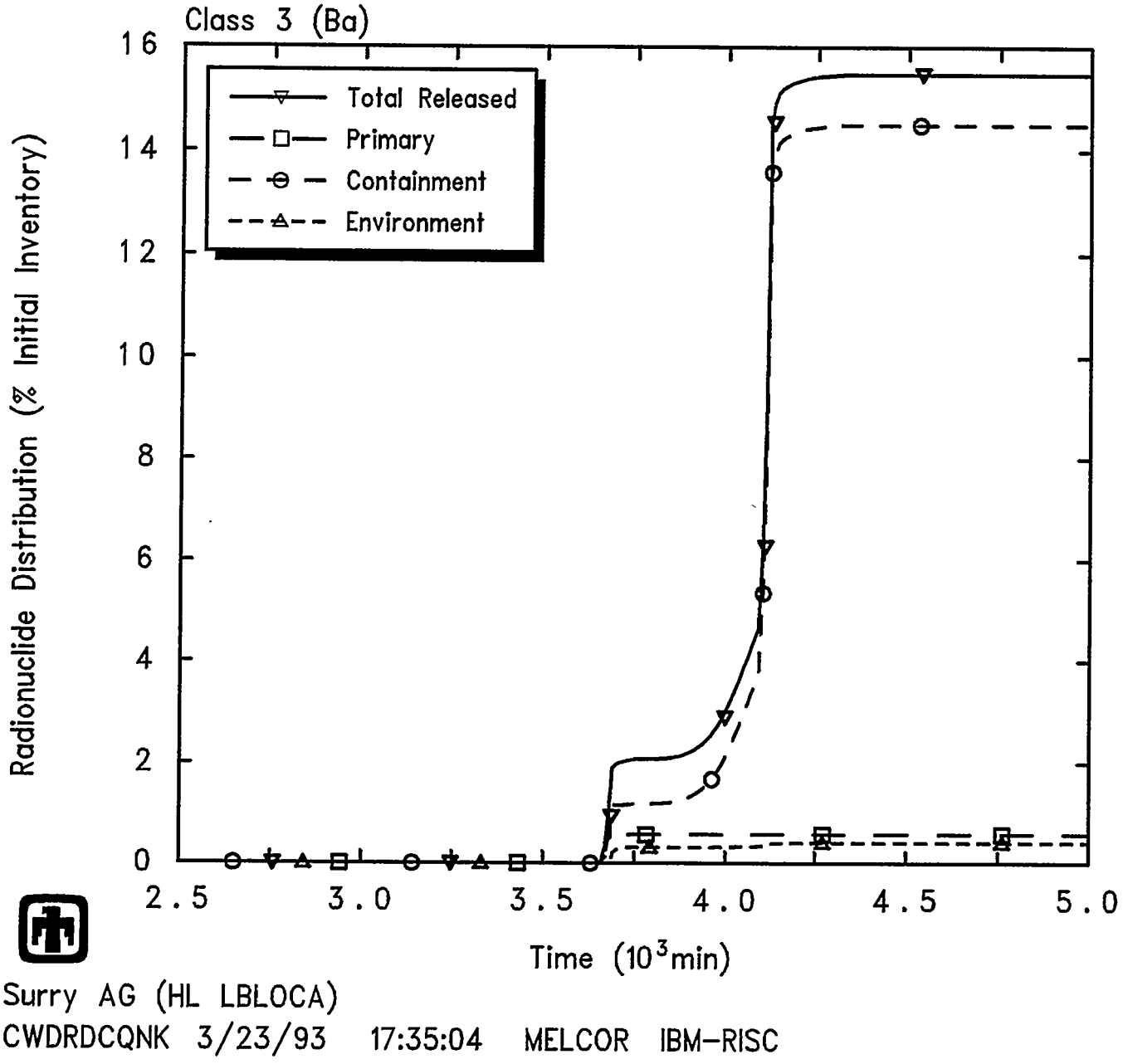

Figure 5.2.38 Distribution of Class 3 (Ba) Alkaline Earth Radionuclides in Primary System, Containment and Environment during AG Sequence, as Percentage of Initial Inventory in Core

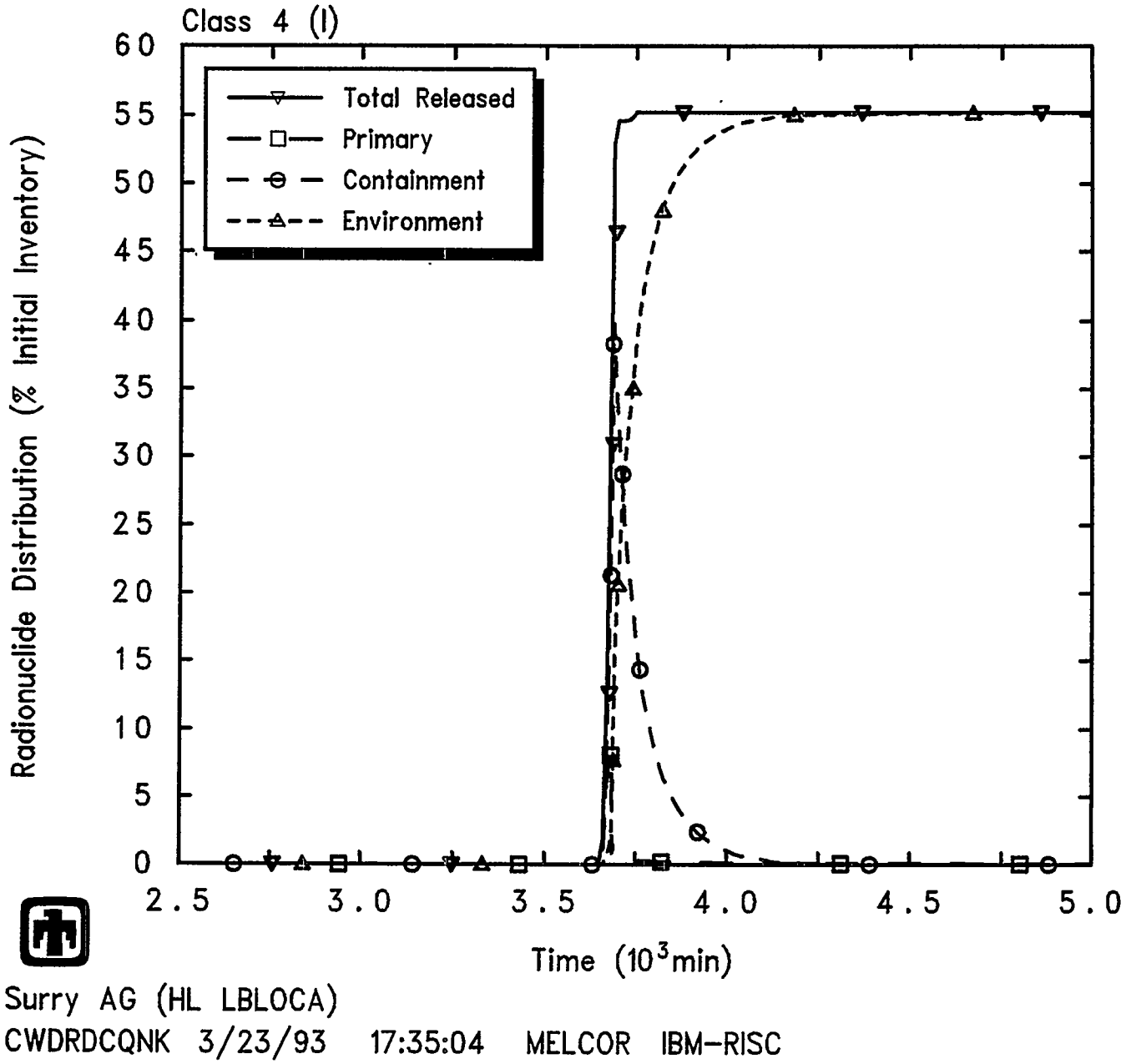

Figure 5.2.39 Distribution of Class 4 (I) Halogen Radionuclides in Primary System, Containment and Environment Predicted during AG Sequence, as Percentage of Initial Inventory in Core

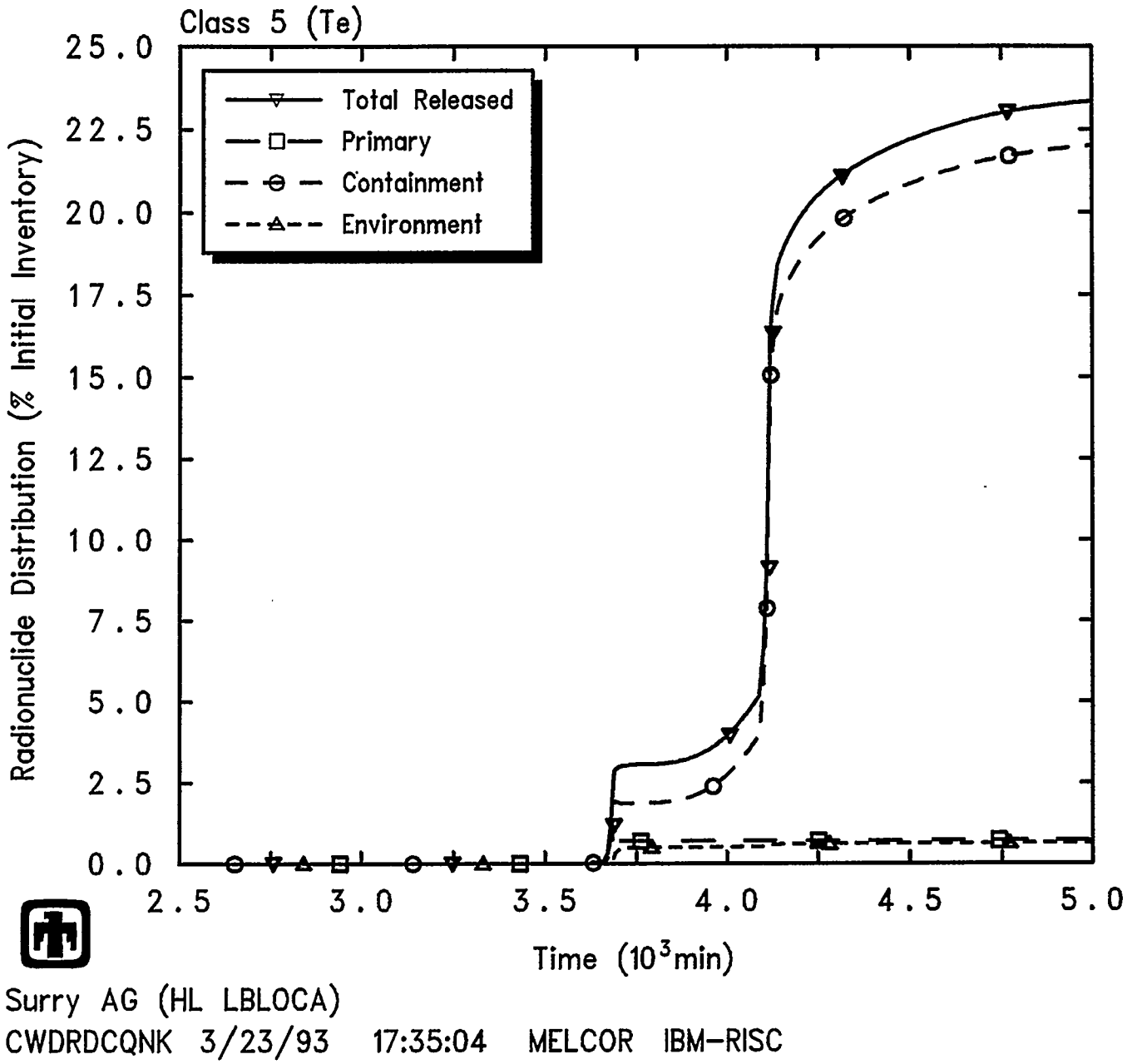

Figure 5.2.40 Distribution of Class 5 (Te) Chalcogen Radionuclides in Primary System, Containment and Environment Predicted during AG Sequence, as Percentage of Initial Inventory in Core

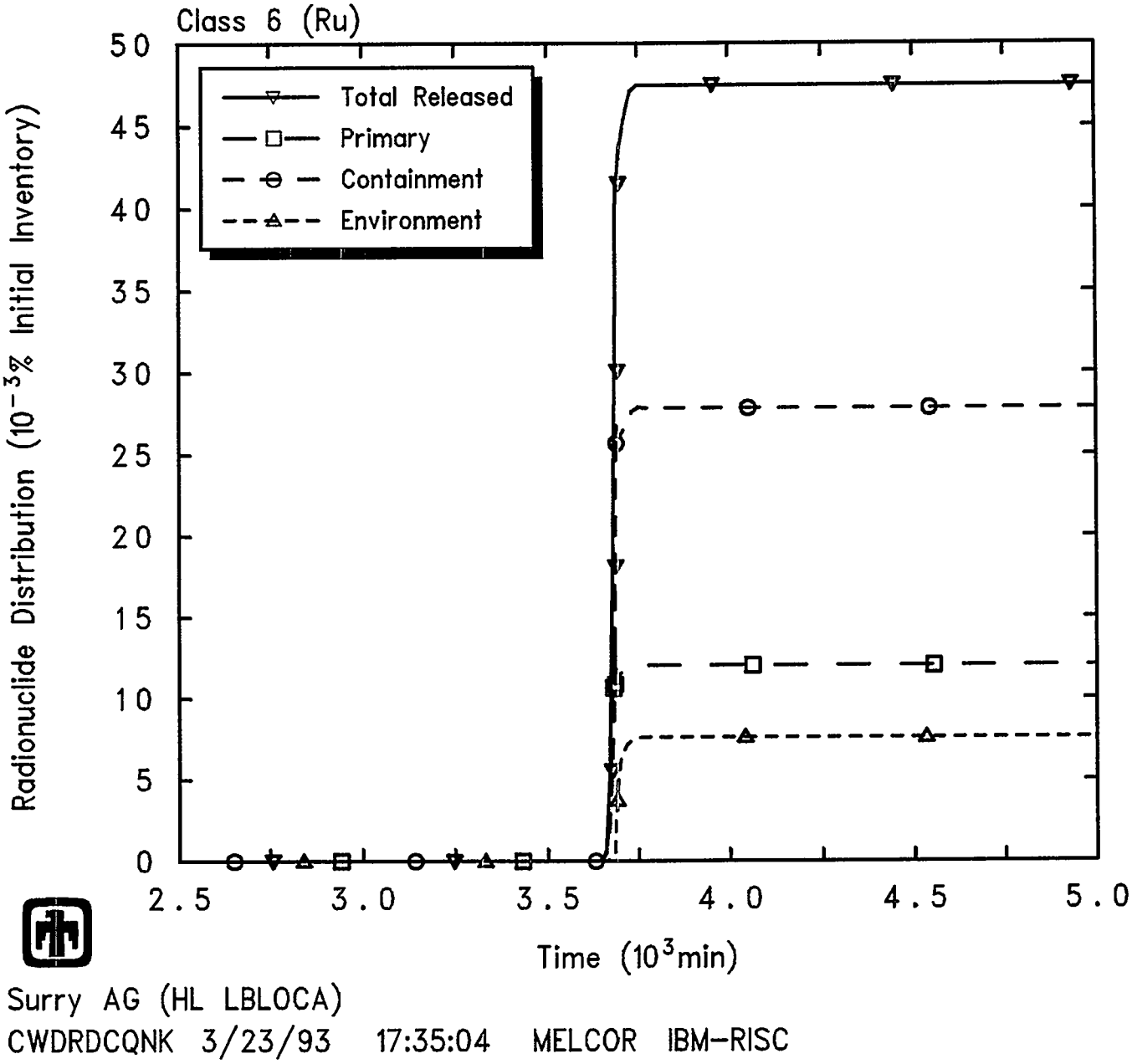

Figure 5.2.41 Distribution of Class 6 (Ru) Platinoid Radionuclides in Primary System, Containment and Environment Predicted during AG Sequence, as Percentage of Initial Inventory in Core

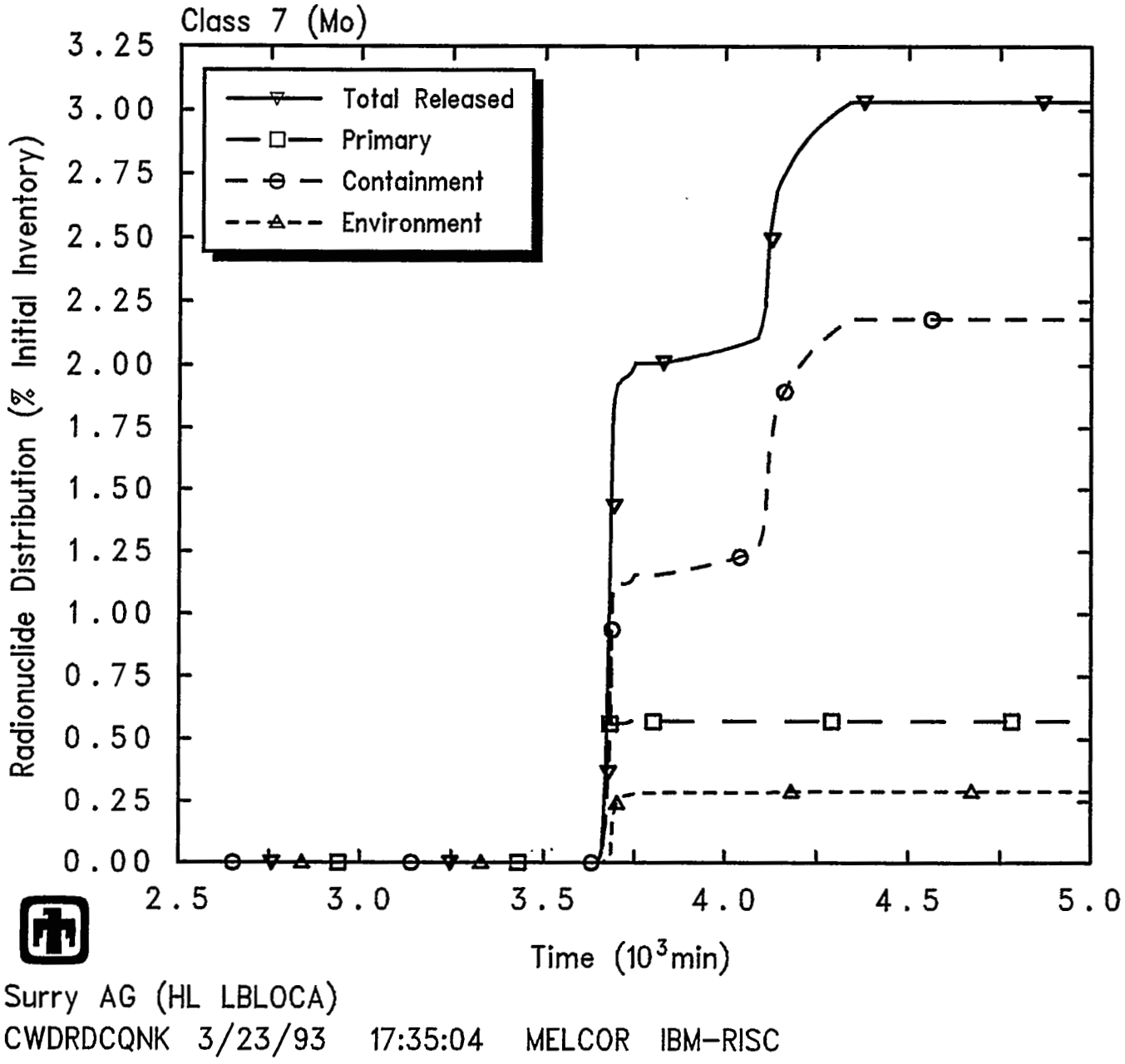

Figure 5.2.42 Distribution of Class 7 (Mo) Early Transition Element Radionuclides in Primary System, Containment and Environment Predicted during AG Sequence, as Percentage of Initial Inventory in Core

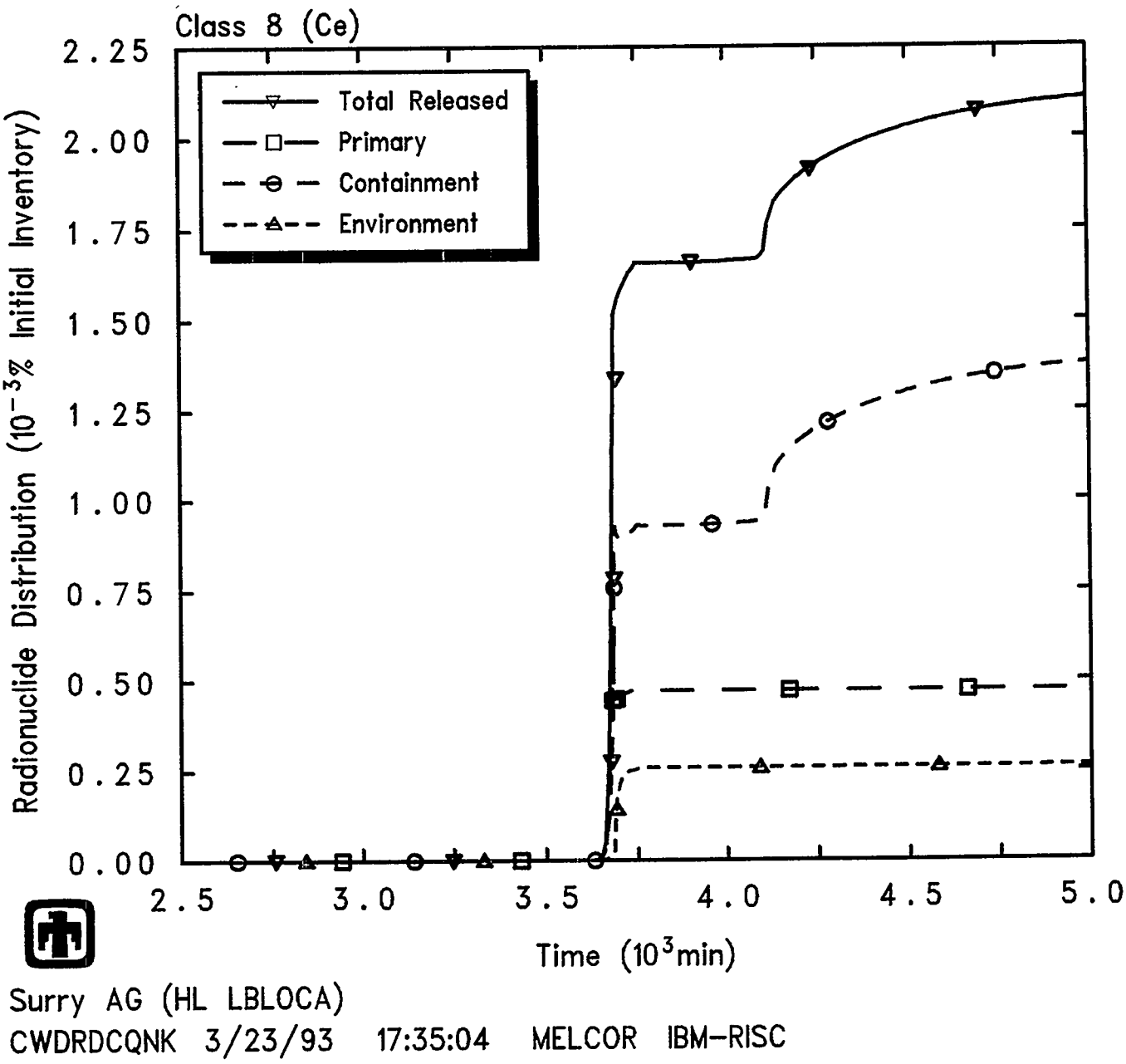

Figure 5.2.43 Distribution of Class 8 (Ce) Tetravalent Radionuclides in Primary System, Containment and Environment Predicted during AG Sequence, as Percentage of Initial Inventory in Core

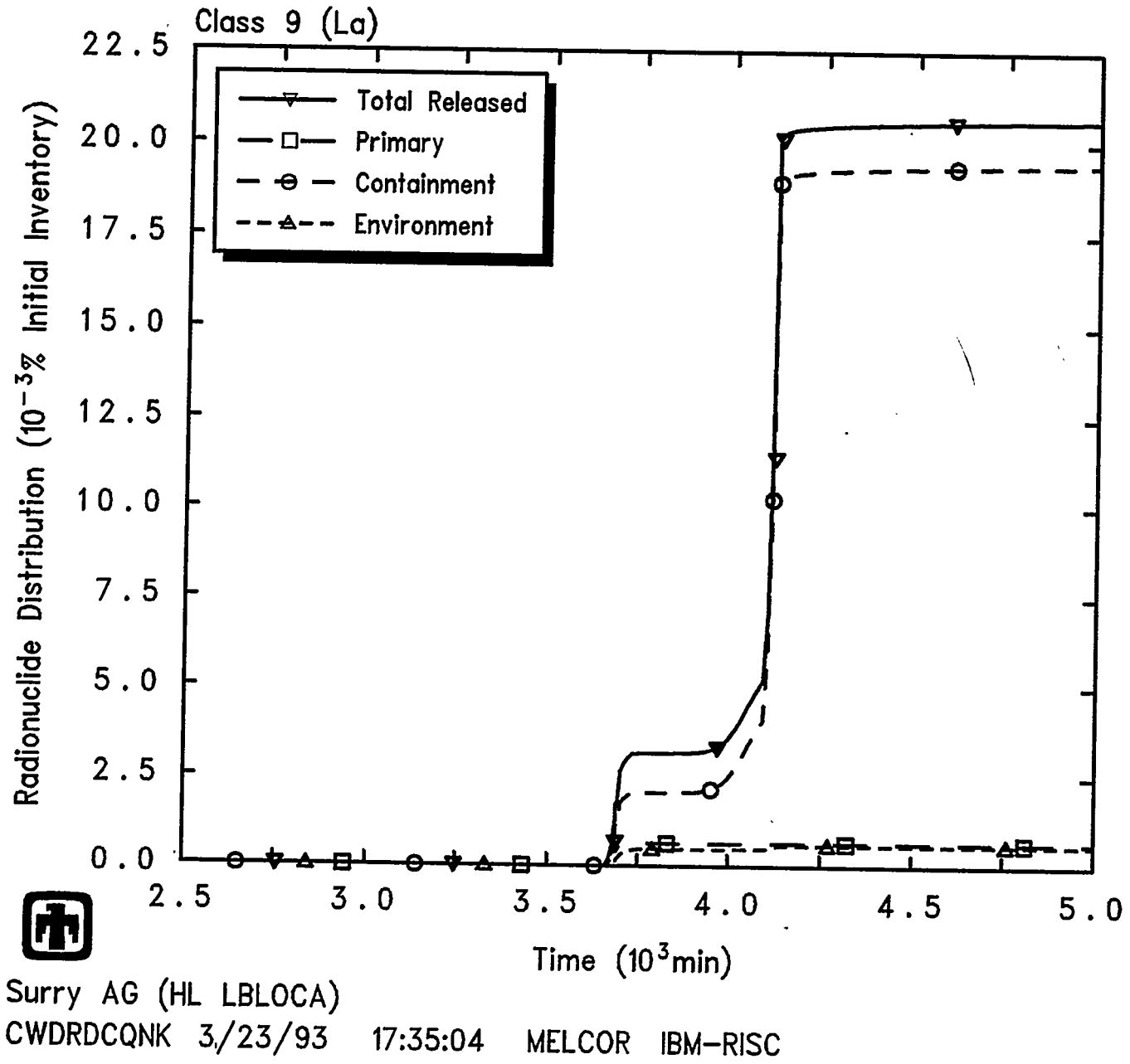

Figure 5.2.44 Distribution of Class 9 (La) Trivalent Radionuclides in Primary System, Containment and Environment Predicted during AG Sequence, as Percentage of Initial Inventory in Core

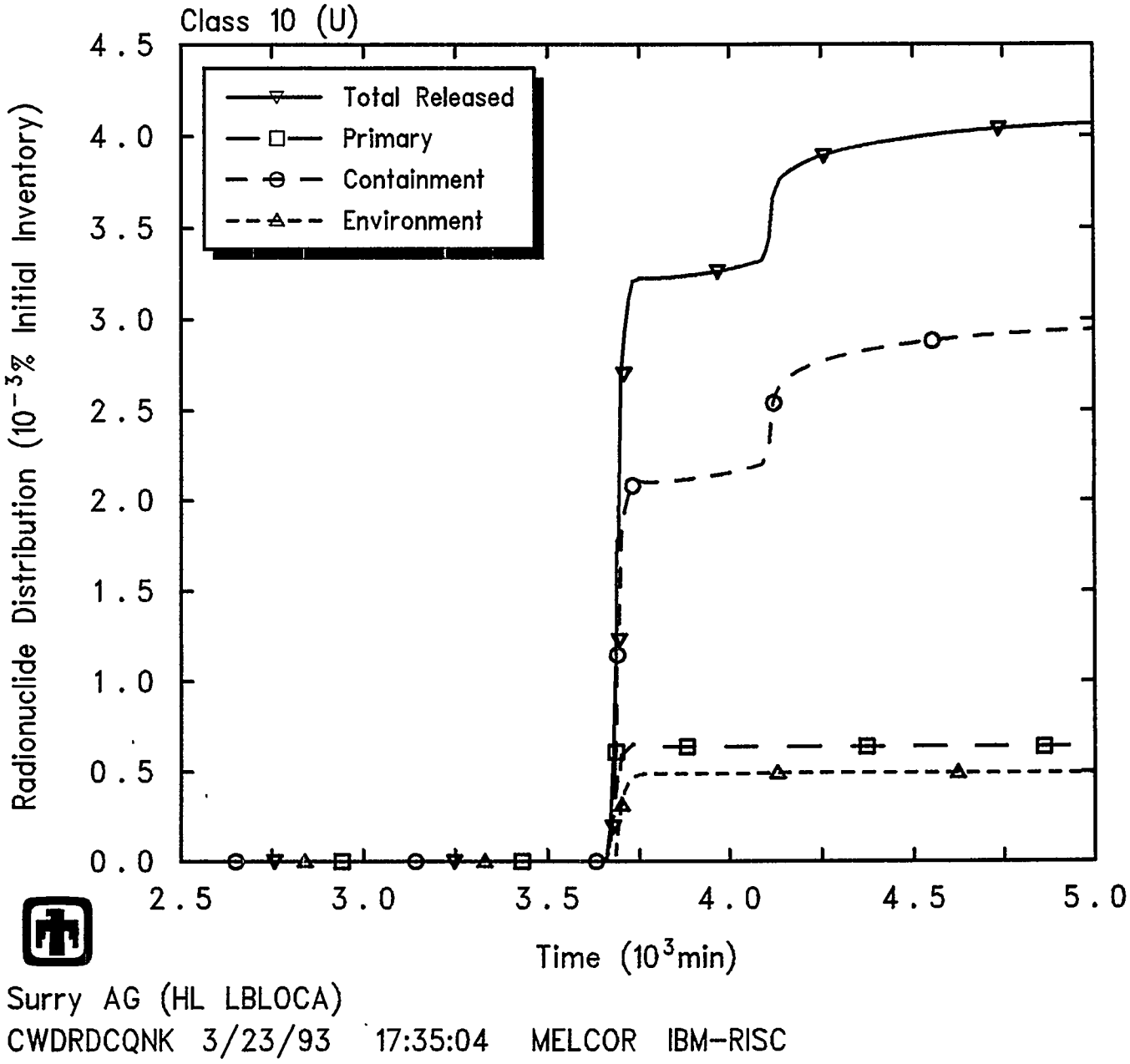

Figure 5.2.45 Distribution of Class 10 (U) Uranium Radionuclides in Primary System, Containment and Environment Predicted during AG Sequence, as Percentage of Initial Inventory in Core

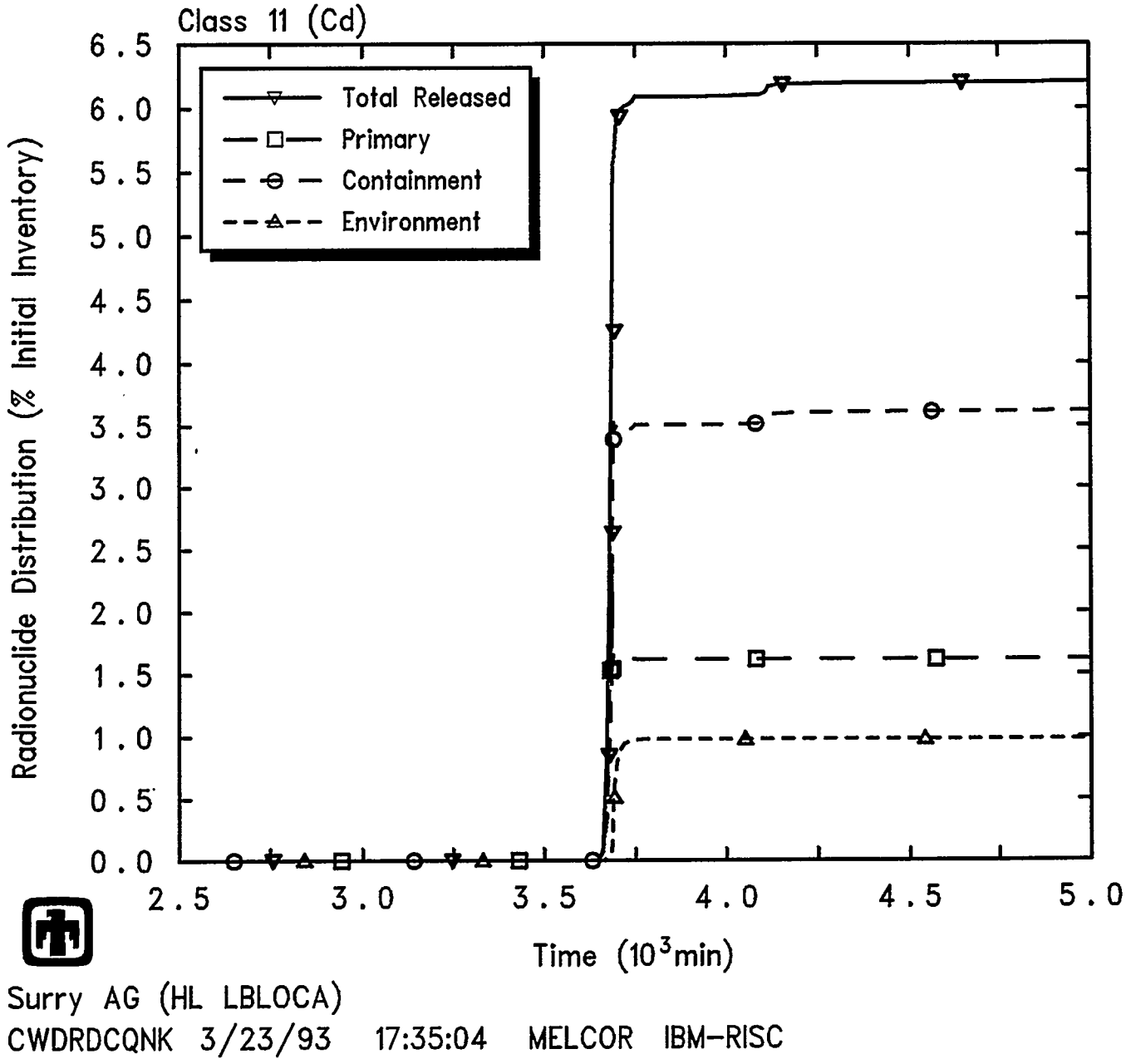

Figure 5.2.46 Distribution of Class 11 (Cd) More Volatile Main Group Radionuclides in Primary System, Containment and Environment Predicted during AG Sequence, as Percentage of Initial Inventory in Core

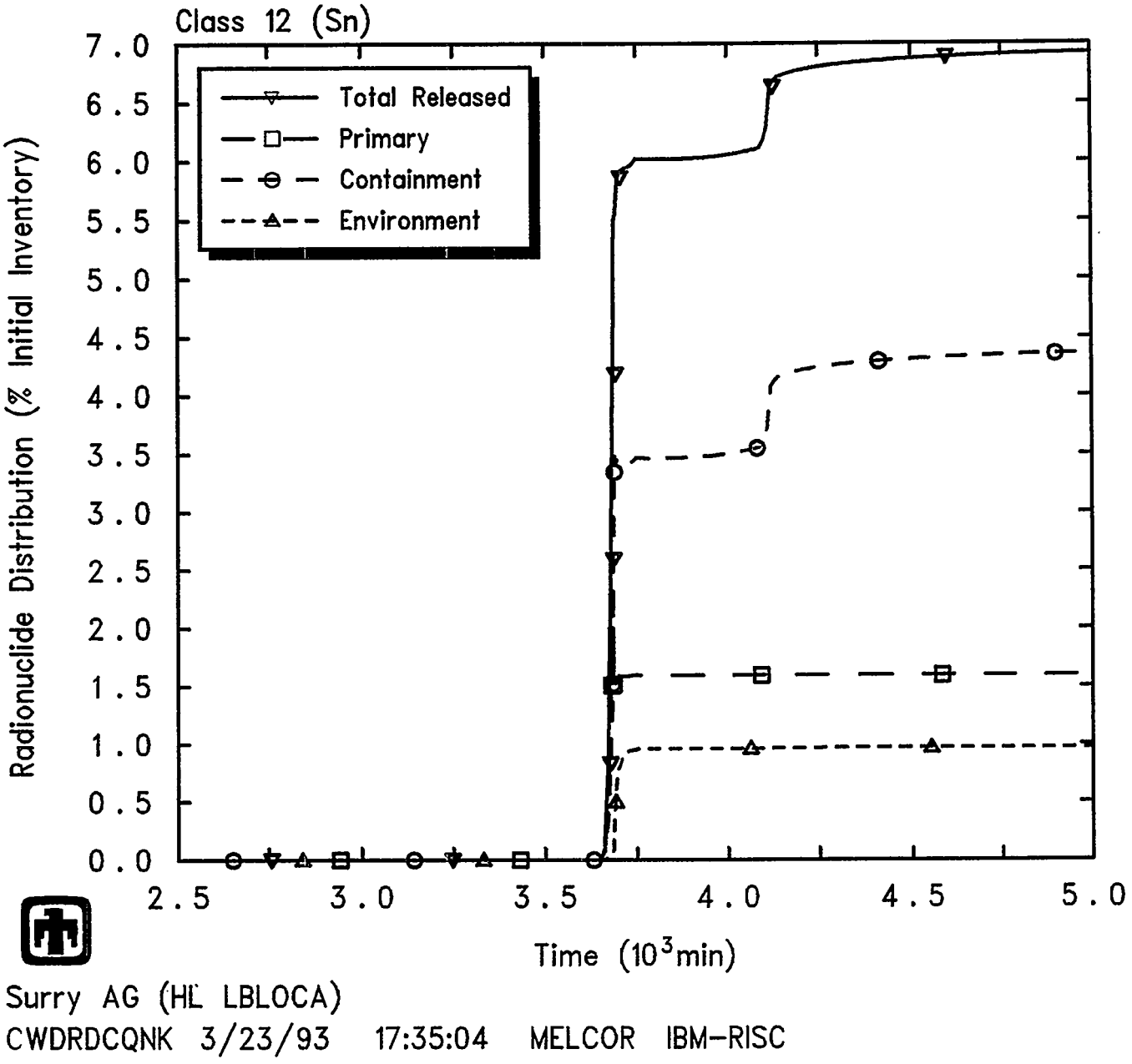

Figure 5.2.47 Distribution of Class 12 (Sn) Less Volatile Main Group Radionuclides in Primary System, Containment and Environment Predicted during AG Sequence, as Percentage of Initial Inventory in Core

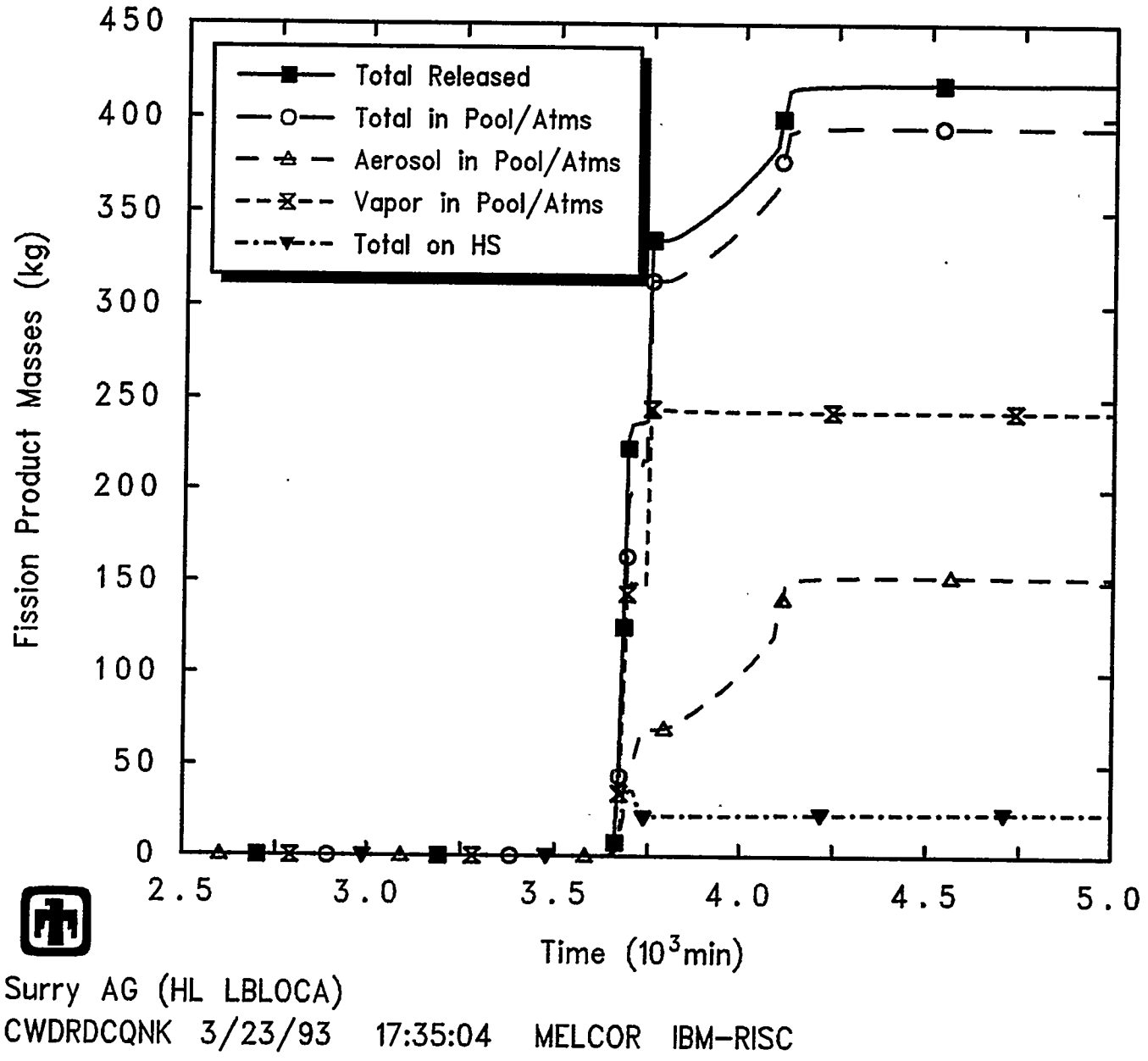

Figure 5.2.48 Total Fission Product Mass Released, and Overall Distribution, Predicted during AG Sequence

Table 5.3.1 Sequence of Events Predicted during S2D Sequence, Compared to STCP

Key Event	Time (min)	
	STCP	MELCOR
Accident initiation	0.0	0.0
Containment coolers on	1.0	0.3
Start steam generator depressurization	30.0*	30.0*
Initial core uncovery begins	41.3	35.6
Accumulators deliver until depleted	44.0 - 65.0	38.8 - 68.6 (First Flow) 158.0 - 158.5 (Second Flow)
End steam generator depressurization	60.0*	68.6
Gap release, Ring-1		46.5
Gap release, Ring-2		48.1
Begin zircaloy oxidation		61.7
Second core uncovery begins	114.7	101.9
Gap release, Ring-3		135.7
Primary system PORVs open	148.0	49.0
Core melt starts	161.6	130.0
Core slump	176.8	140.0
Core collapse	180.6	146.7 (Partial) Ring-1
Containment coolers trip off		267.0
Containment injection sprays on	188.0	267.0
Bottom head dryout	209.2	Does not occur prior to failure of bottom head.
RWST depleted		363.6
Containment injection sprays off		363.6
Containment recirculation sprays on	282.4	272.0
Bottom head failure	314.4	148.3 (Partial) Ring-1
Commence debris ejection		164.4
Begin concrete attack	315.5	227.6
Corium layers invert	372.5	333.3
End of calculation	915.5	833.4

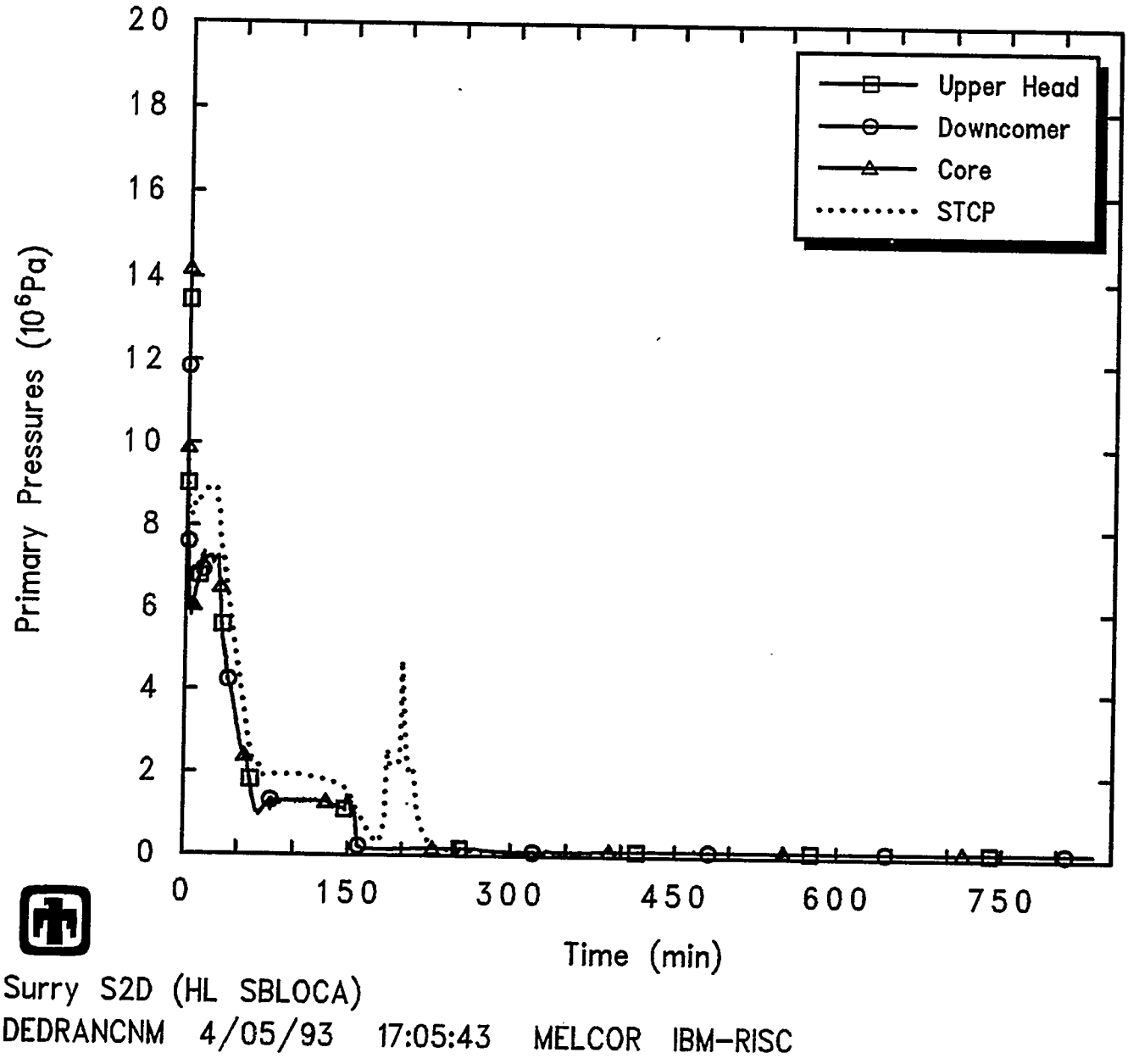

Figure 5.3.1 Primary System Pressures Predicted during S2D Sequence

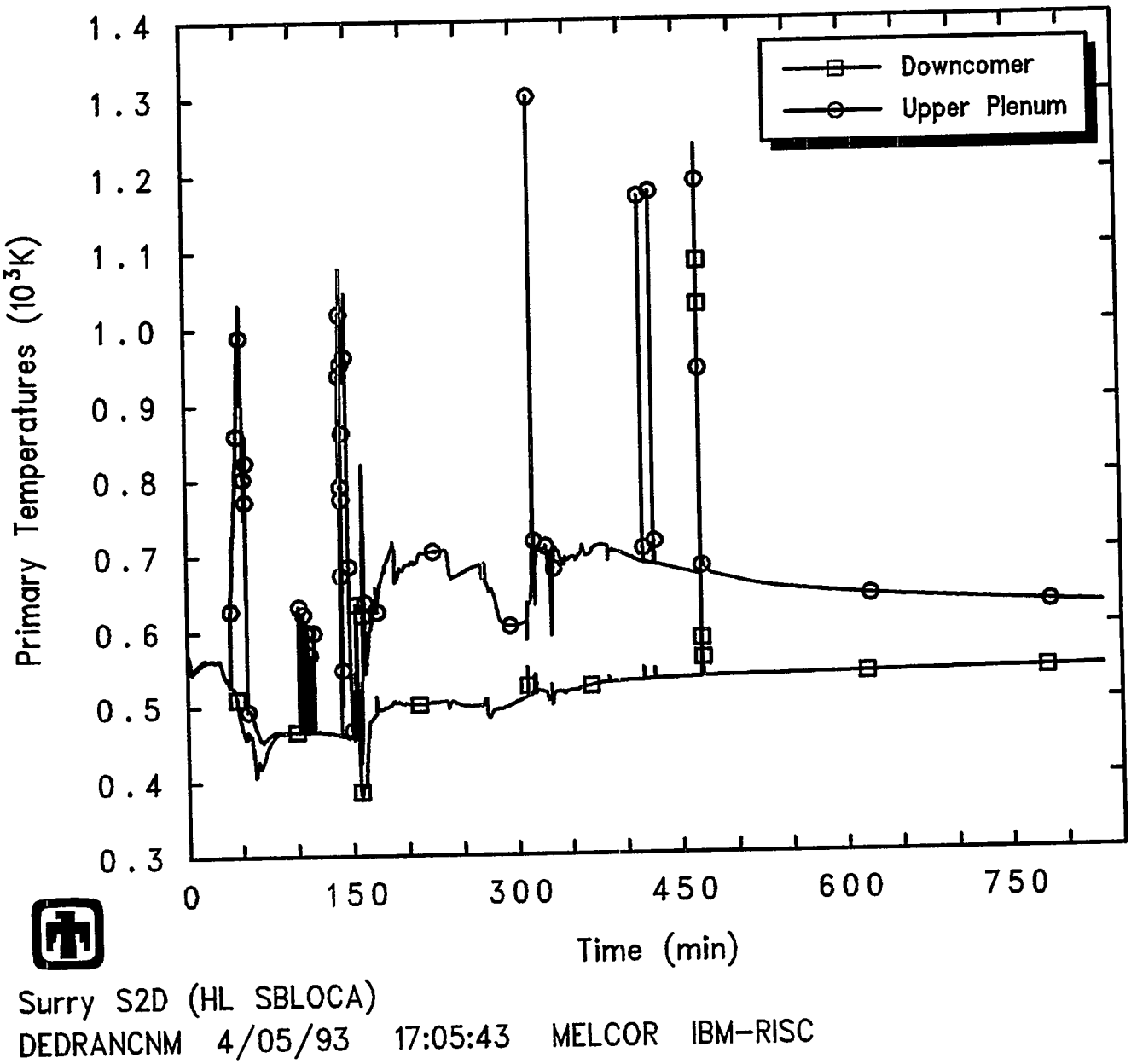

Figure 5.3.2 Primary System Temperatures, in Downcomer and in Upper Plenum Predicted during S2D Sequence

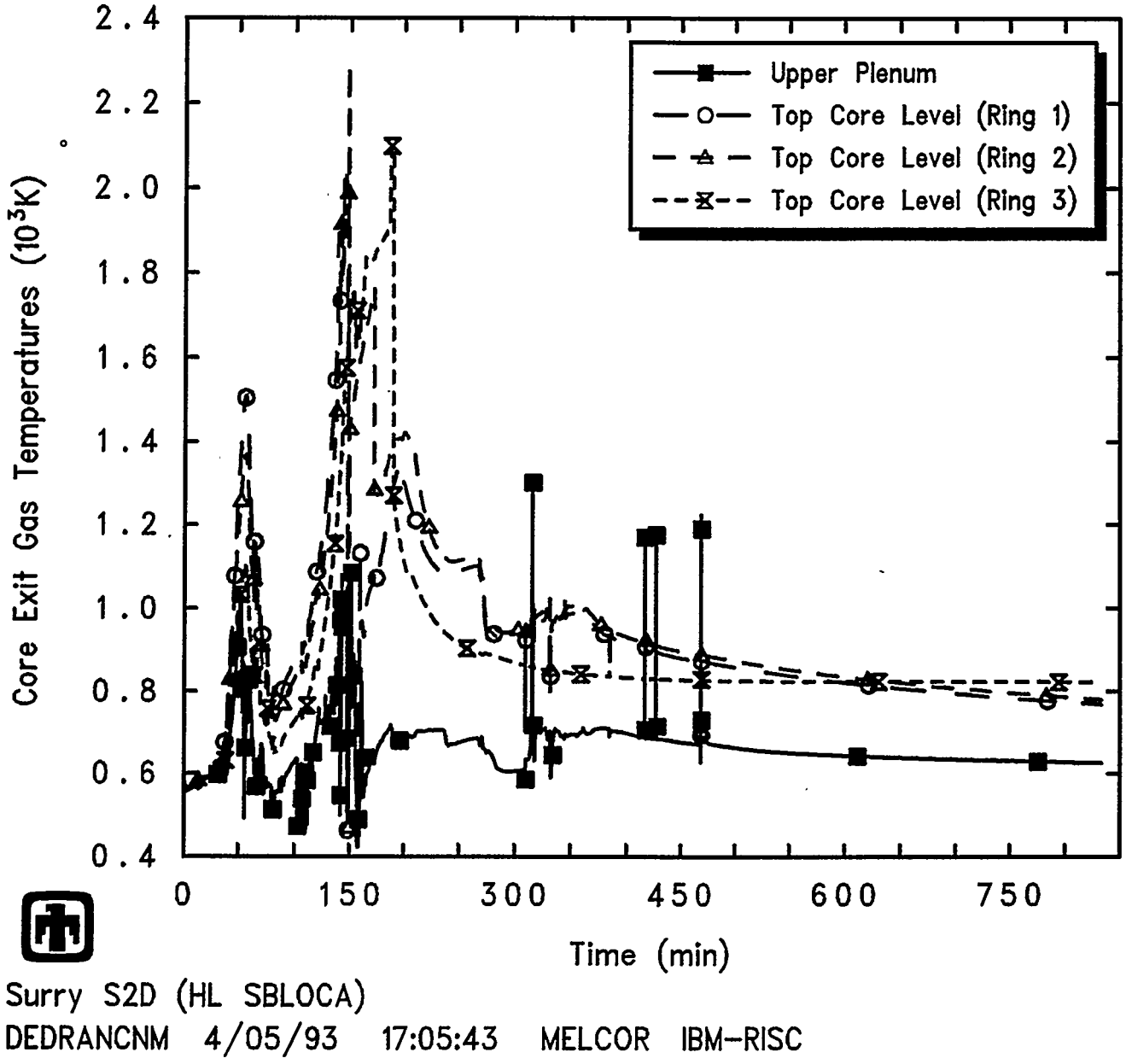

Figure 5.3.3 Core Exit Gas Temperatures, in Upper Plenum and in Uppermost Core Cells, Predicted during S2D Sequence

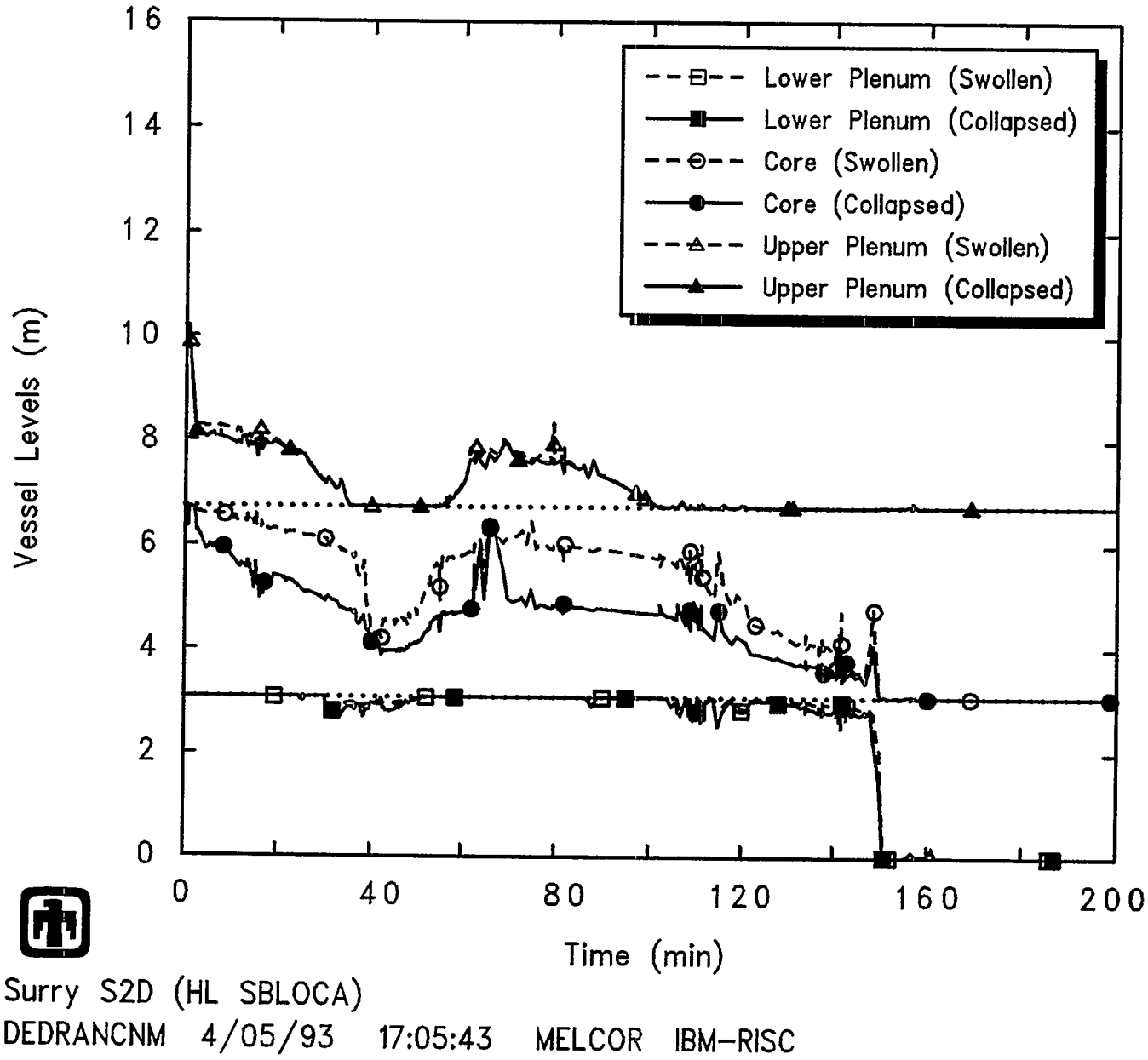

Figure 5.3.4 Reactor Vessel Liquid Levels Predicted during S2D Sequence

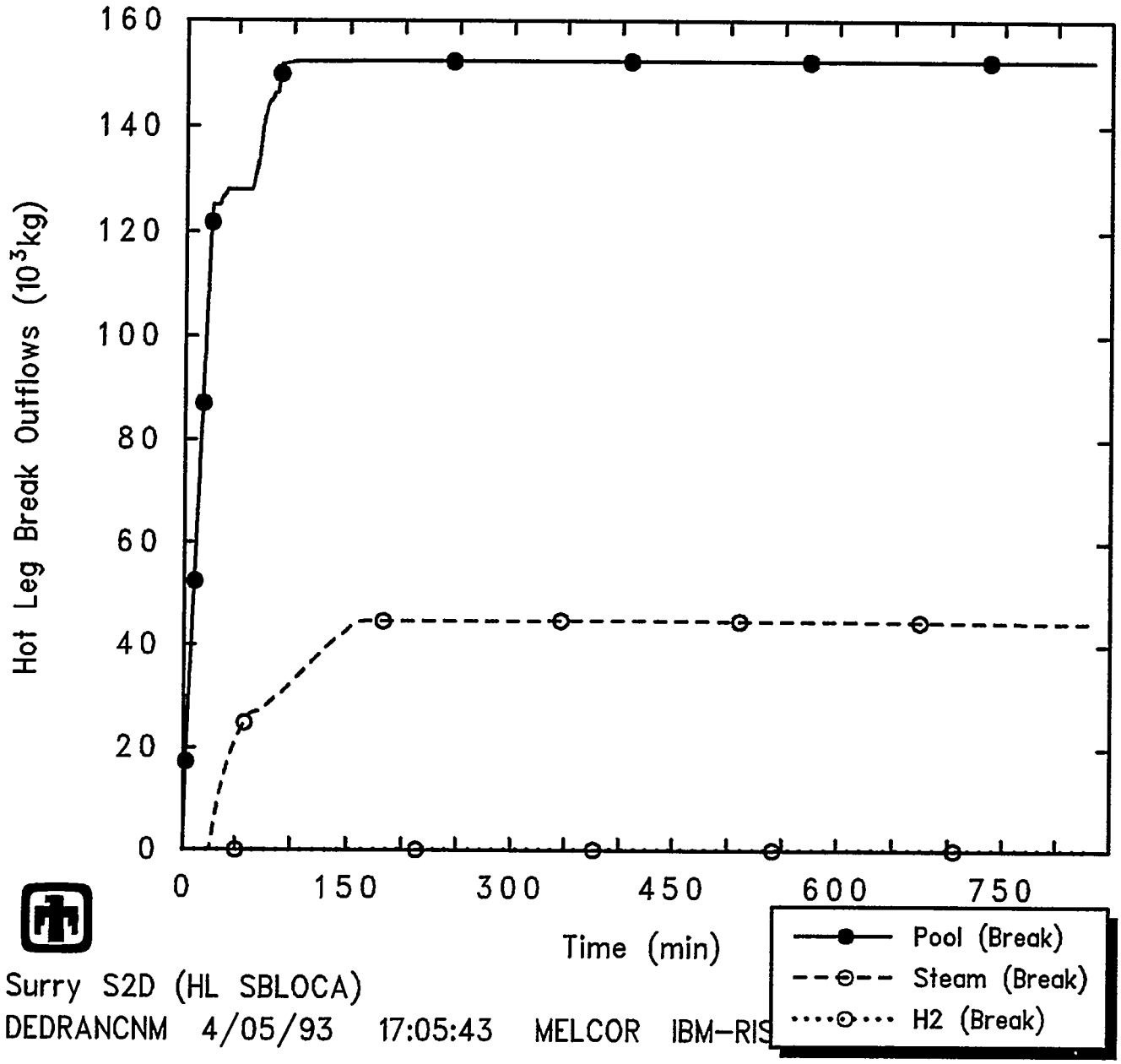

Figure 5.3.5 Integrated Outflows of Liquid, Steam and Hydrogen through the Hot Leg Break Predicted during S2D Sequence

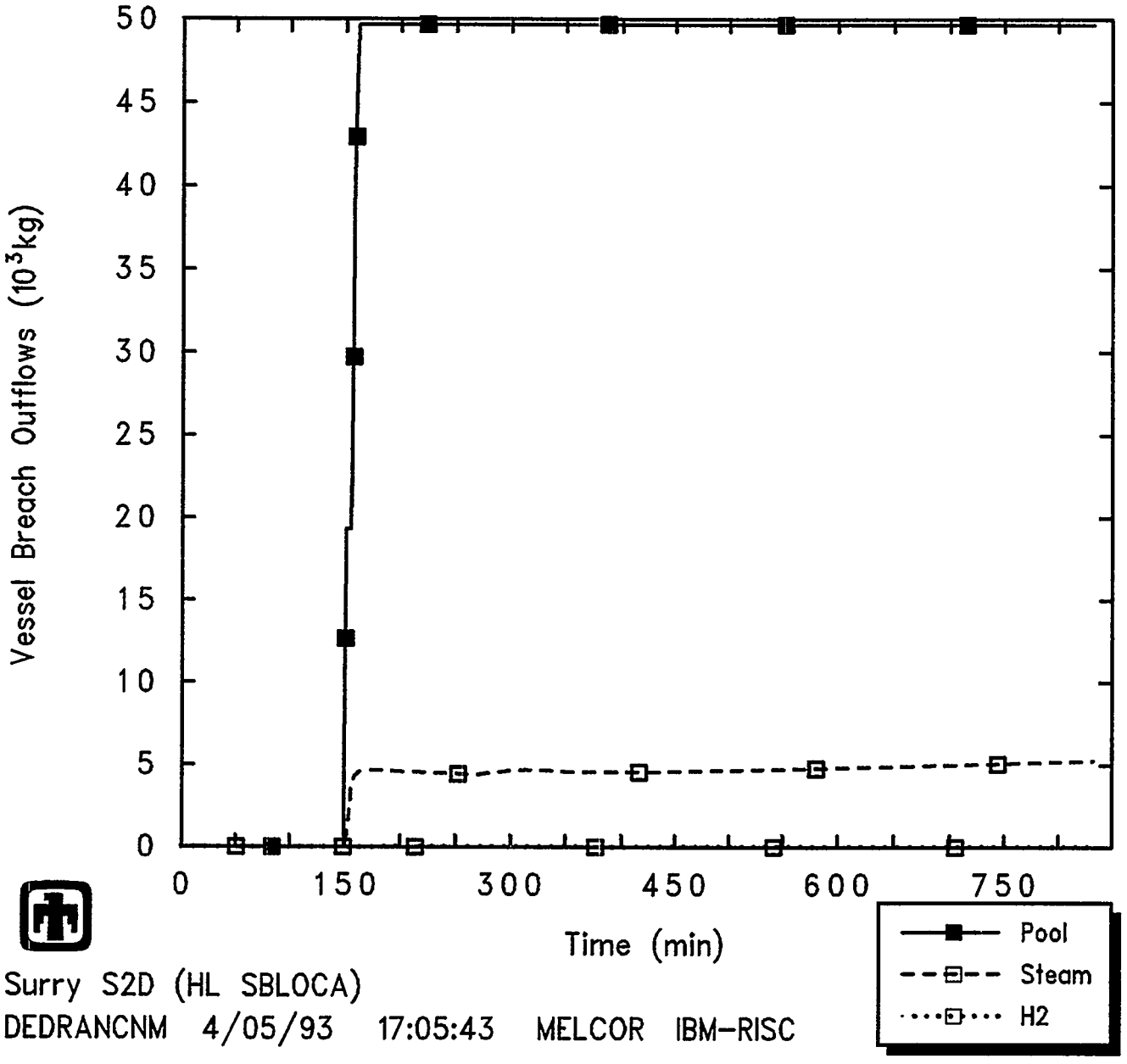

Figure 5.3.6 Integrated Outflows of Liquid, Steam and Hydrogen through the Vessel Breach Predicted during S2D Sequence

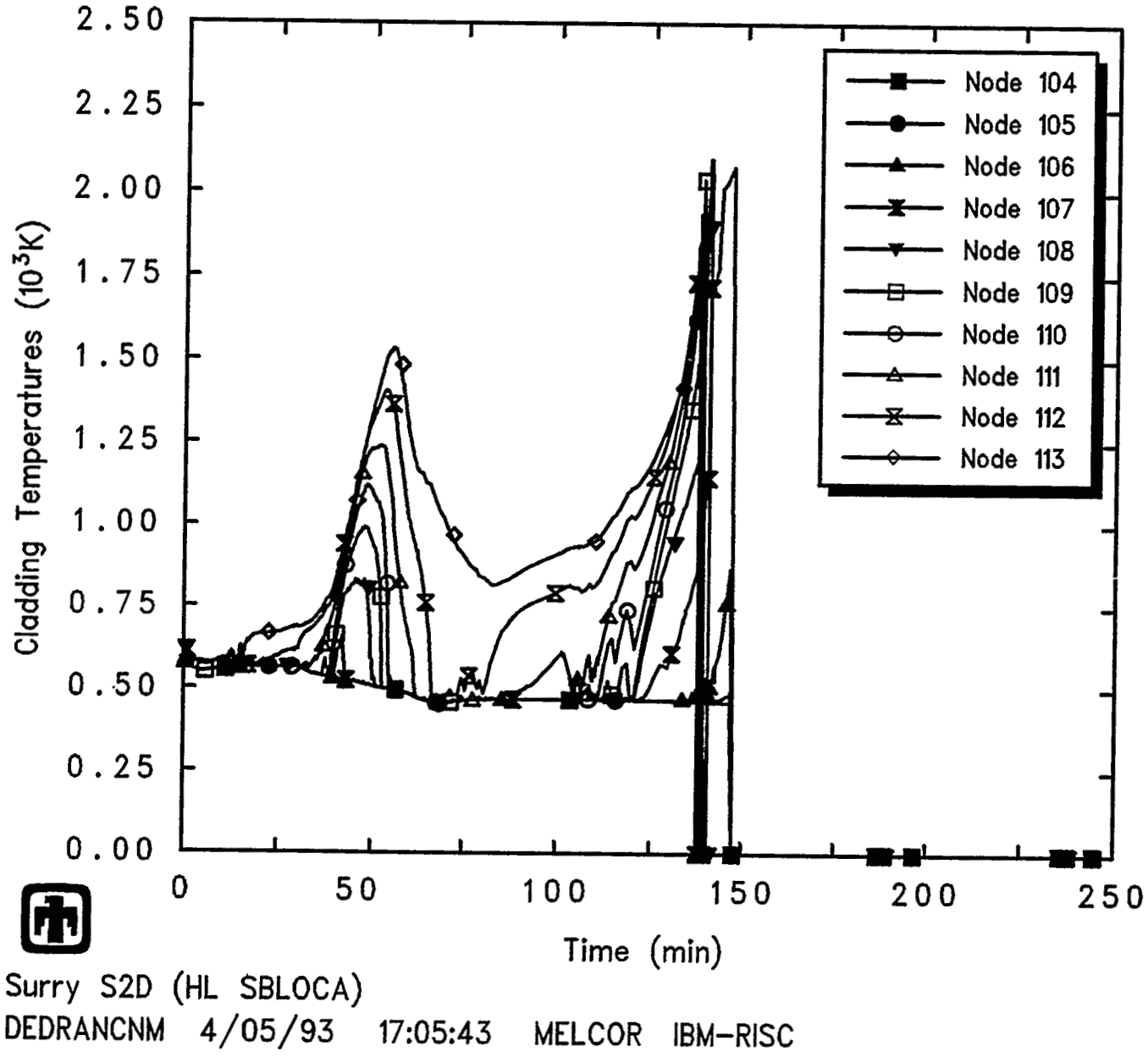

Figure 5.3.7 Core Ring 1 Clad Temperatures Predicted during S2D Sequence

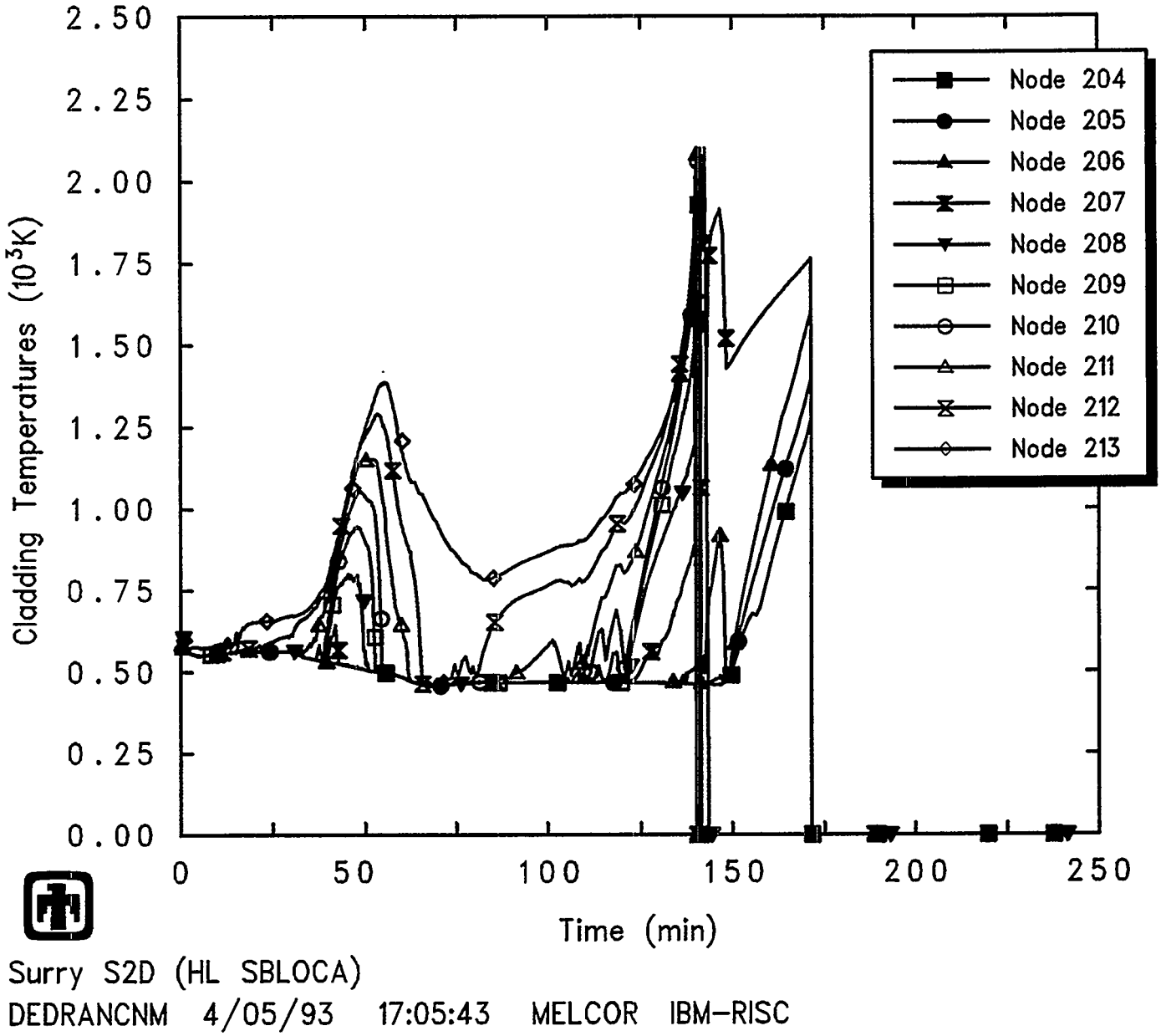

Figure 5.3.8 Core Ring 2 Clad Temperatures Predicted during S2D Sequence

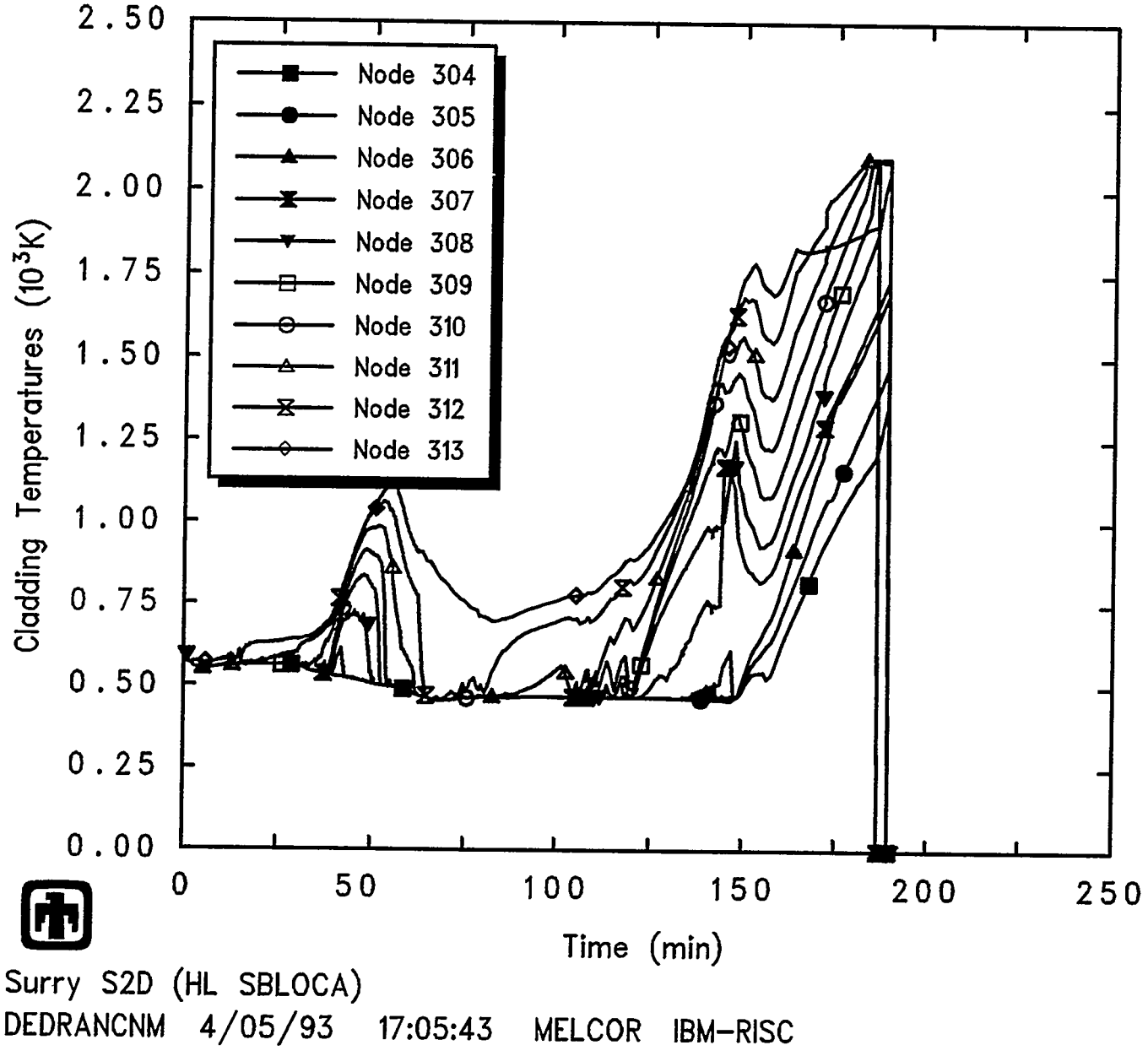

Figure 5.3.9 Core Ring 3 Clad Temperatures Predicted during S2D Sequence

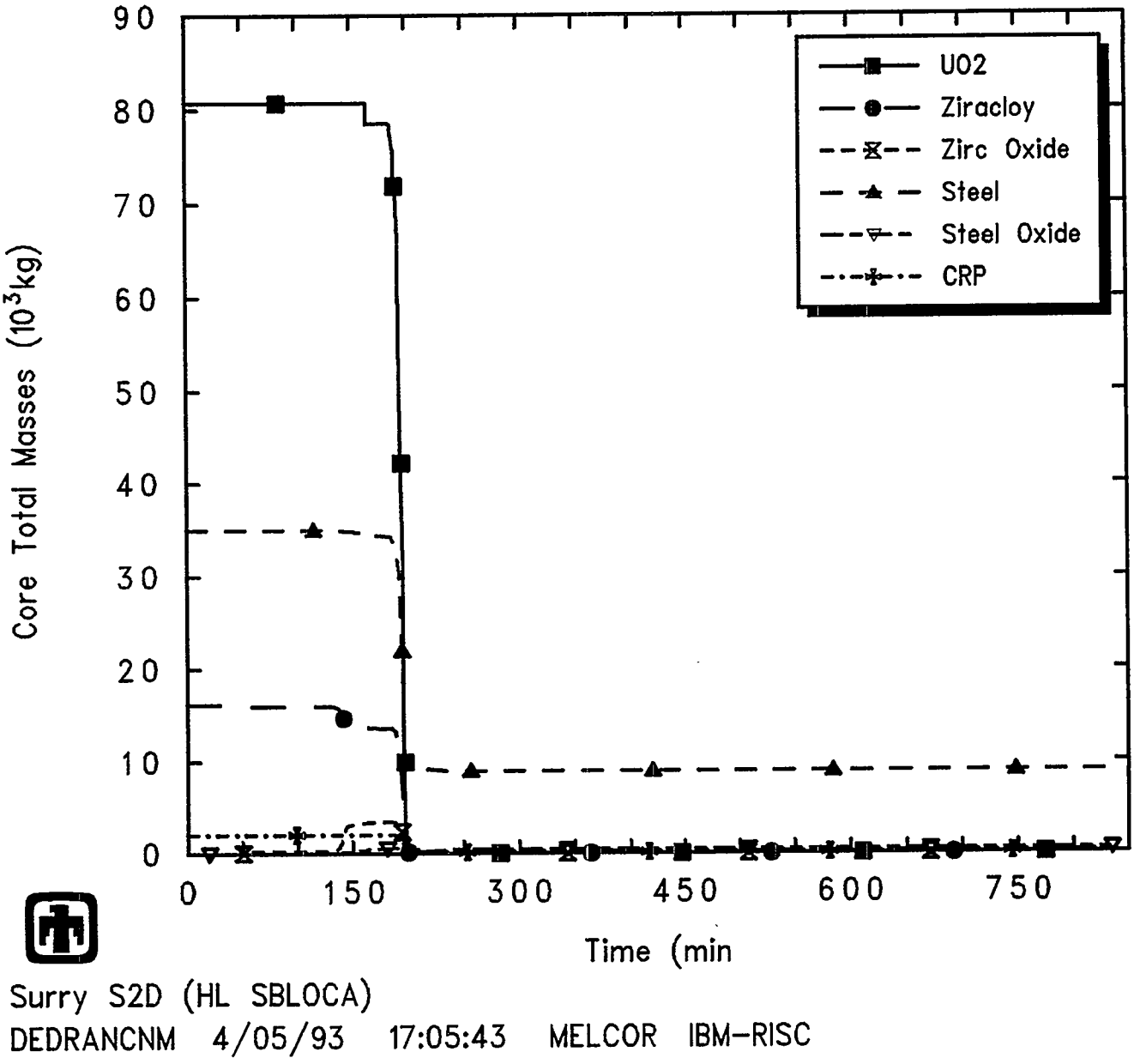

Figure 5.3.10 Core Total Material Masses Predicted during S2D Sequence

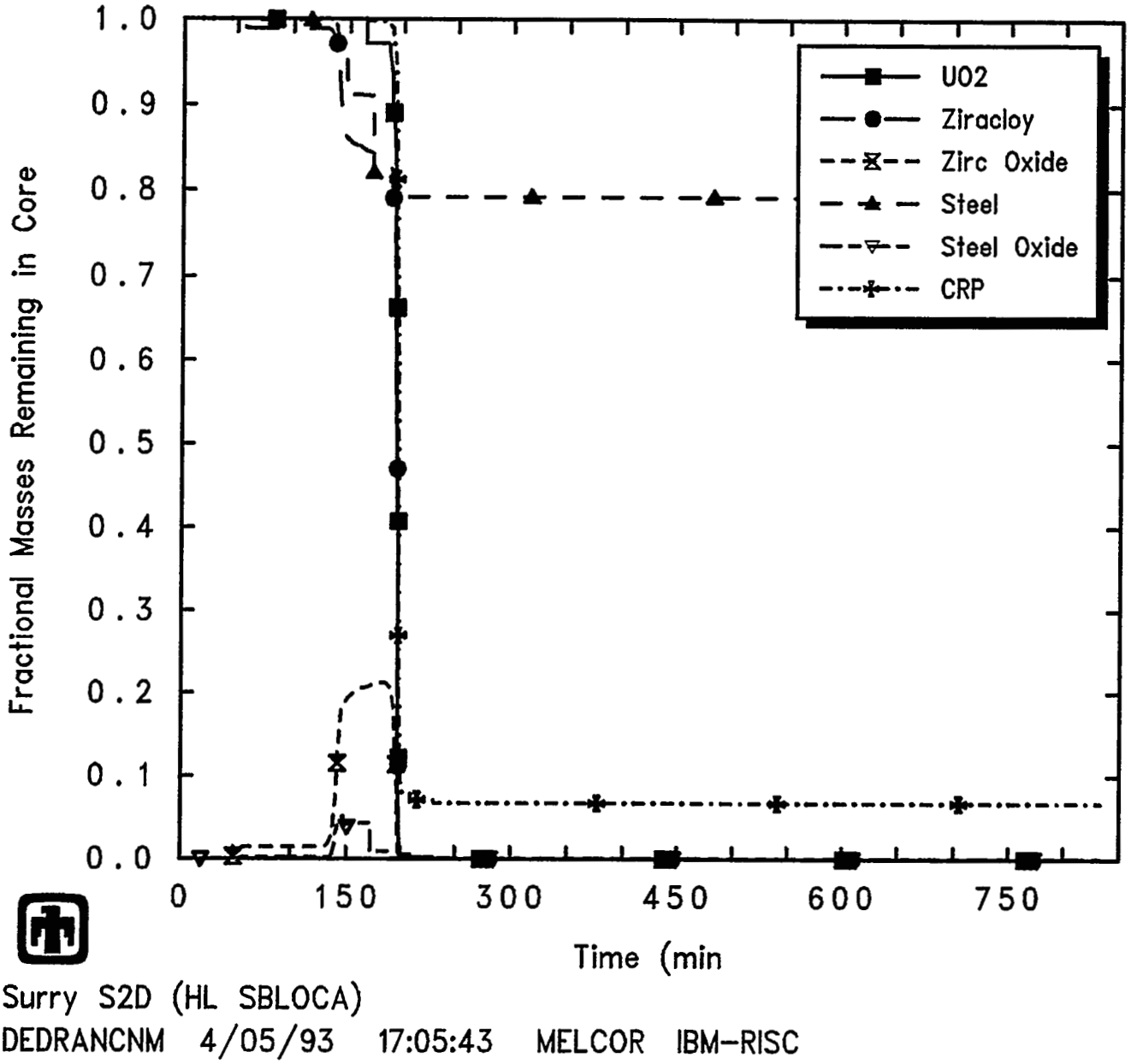

Figure 5.3.11 Core Fractional Material Masses Predicted during S2D Sequence

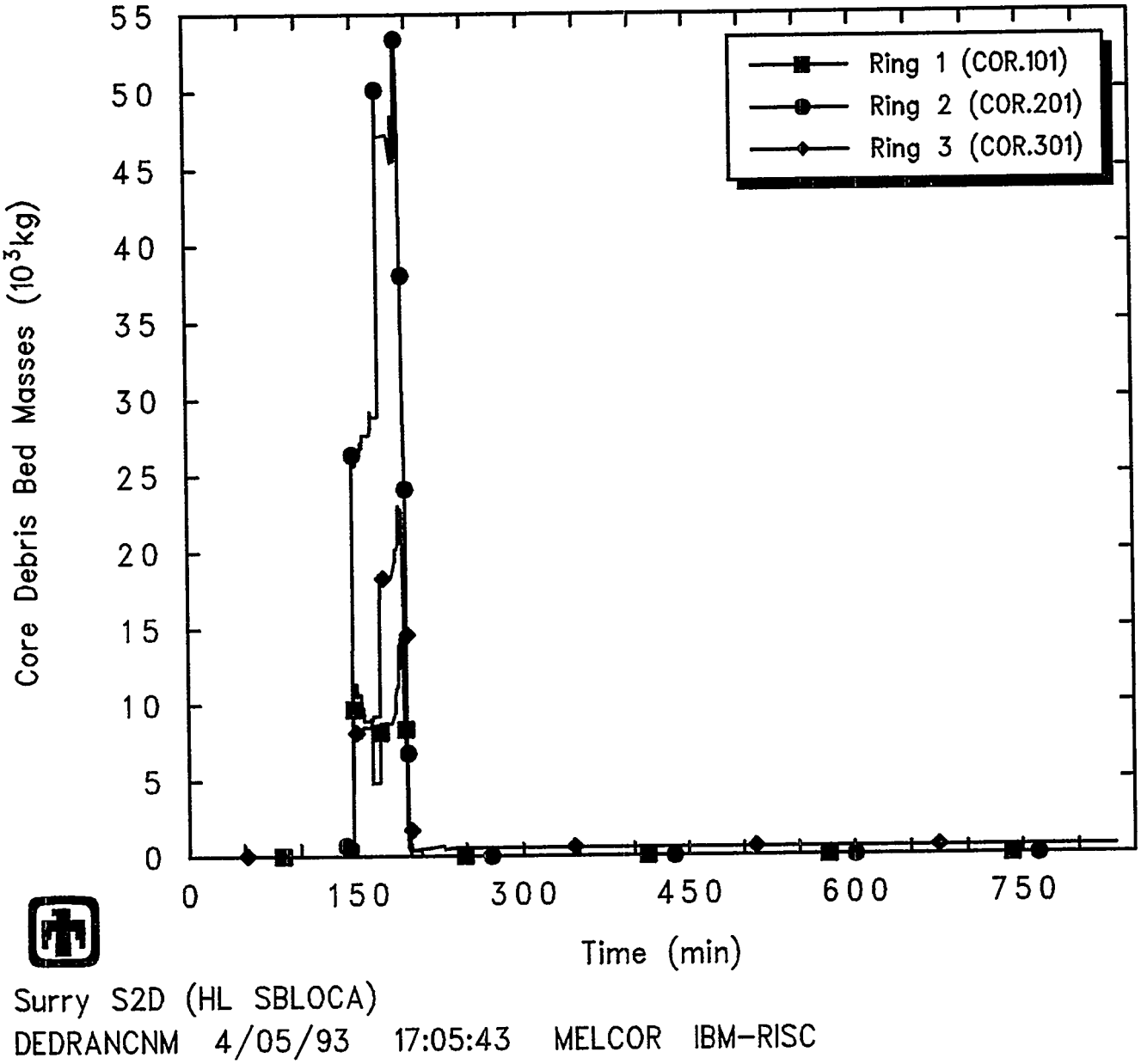

Figure 5.3.12 Lower Plenum Debris Bed Masses Predicted during S2D Sequence

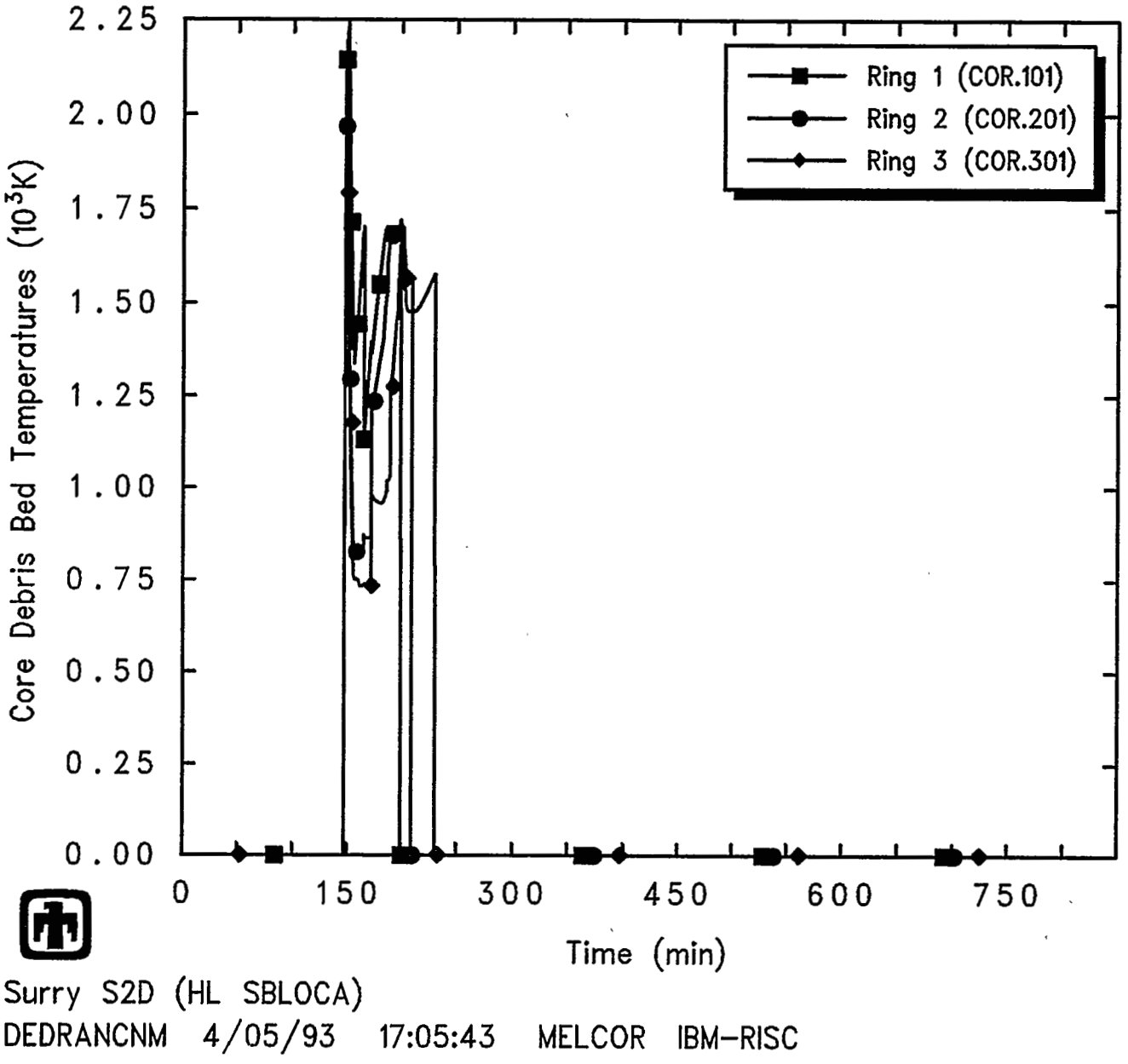

Figure 5.3.13 Lower Plenum Debris Bed Temperatures Predicted during S2D Sequence

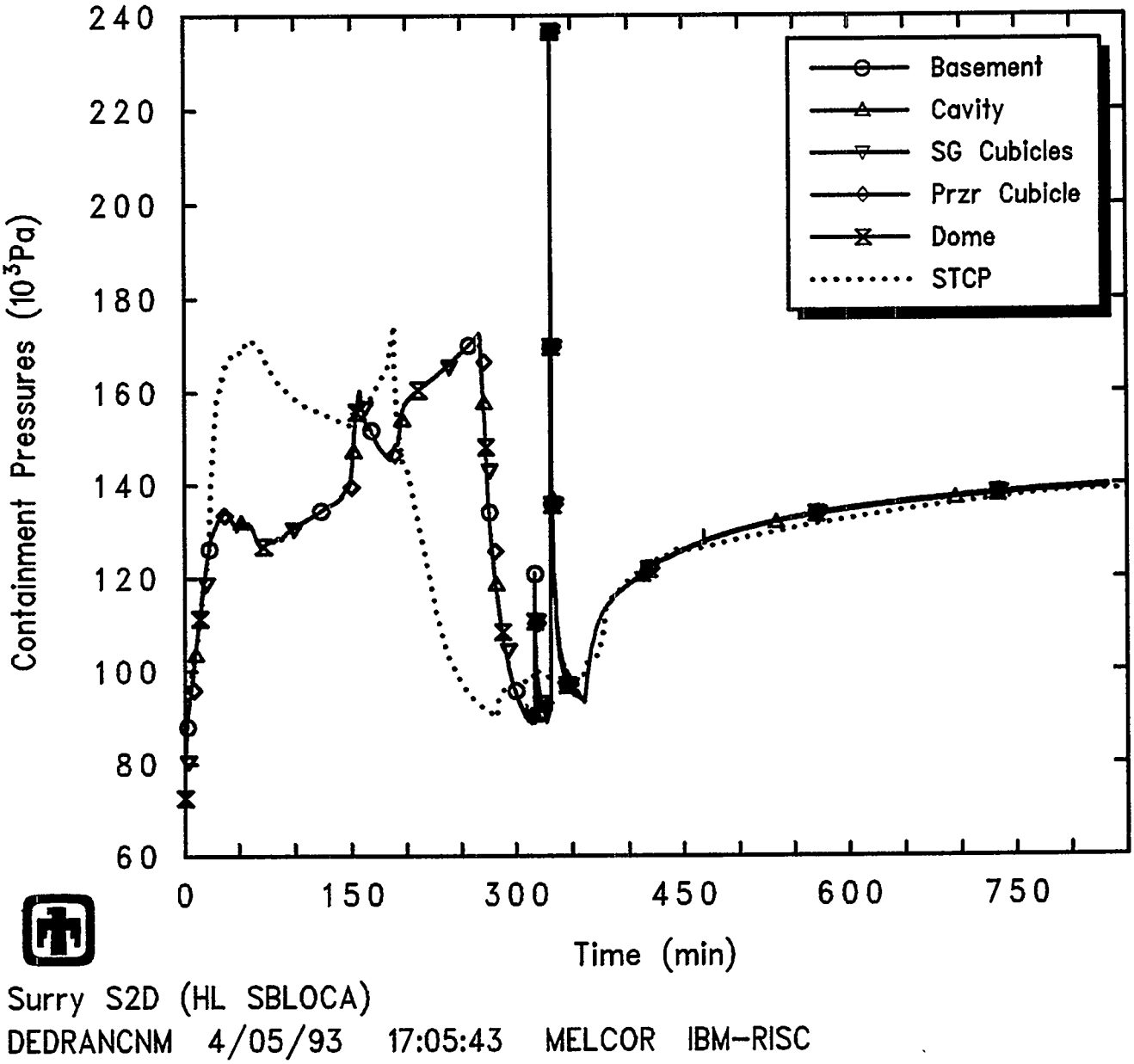

Figure 5.3.14 Containment System Pressures Predicted during S2D Sequence

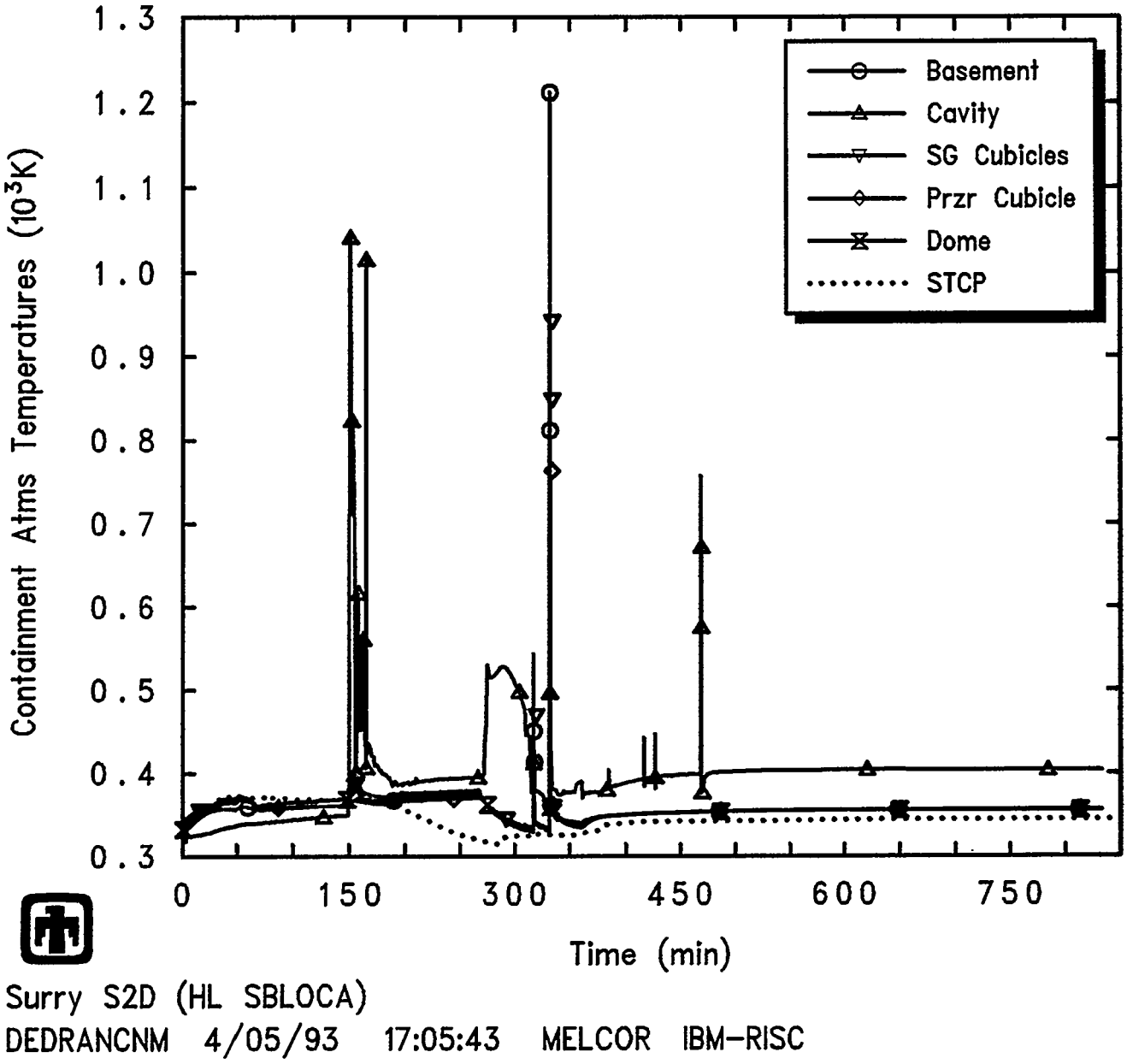

Figure 5.3.15 Containment System Atmosphere Temperatures Predicted during S2D Sequence

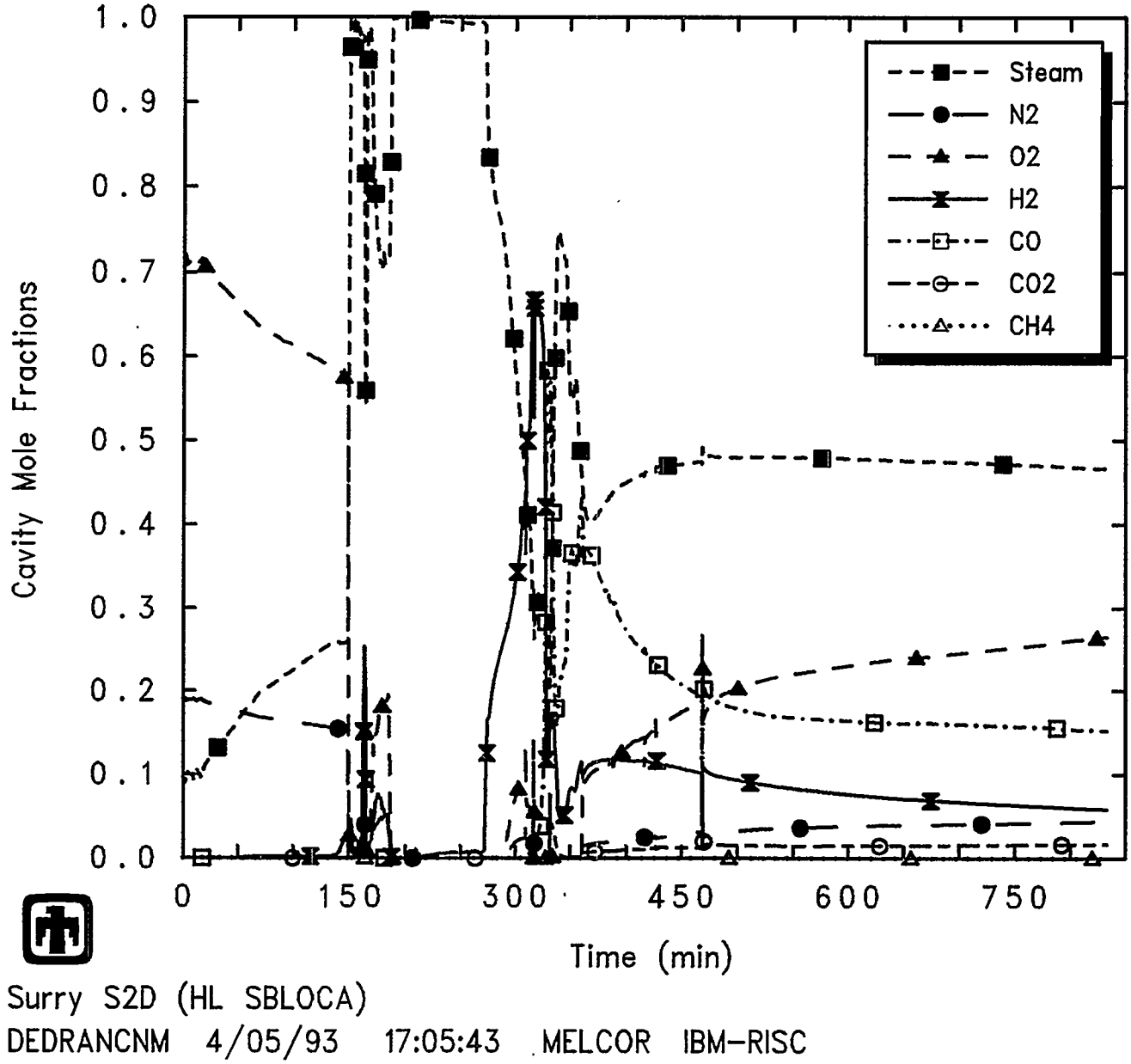

Figure 5.3.16 Cavity Steam and Noncondensable Mole Fractions Predicted during S2D Sequence

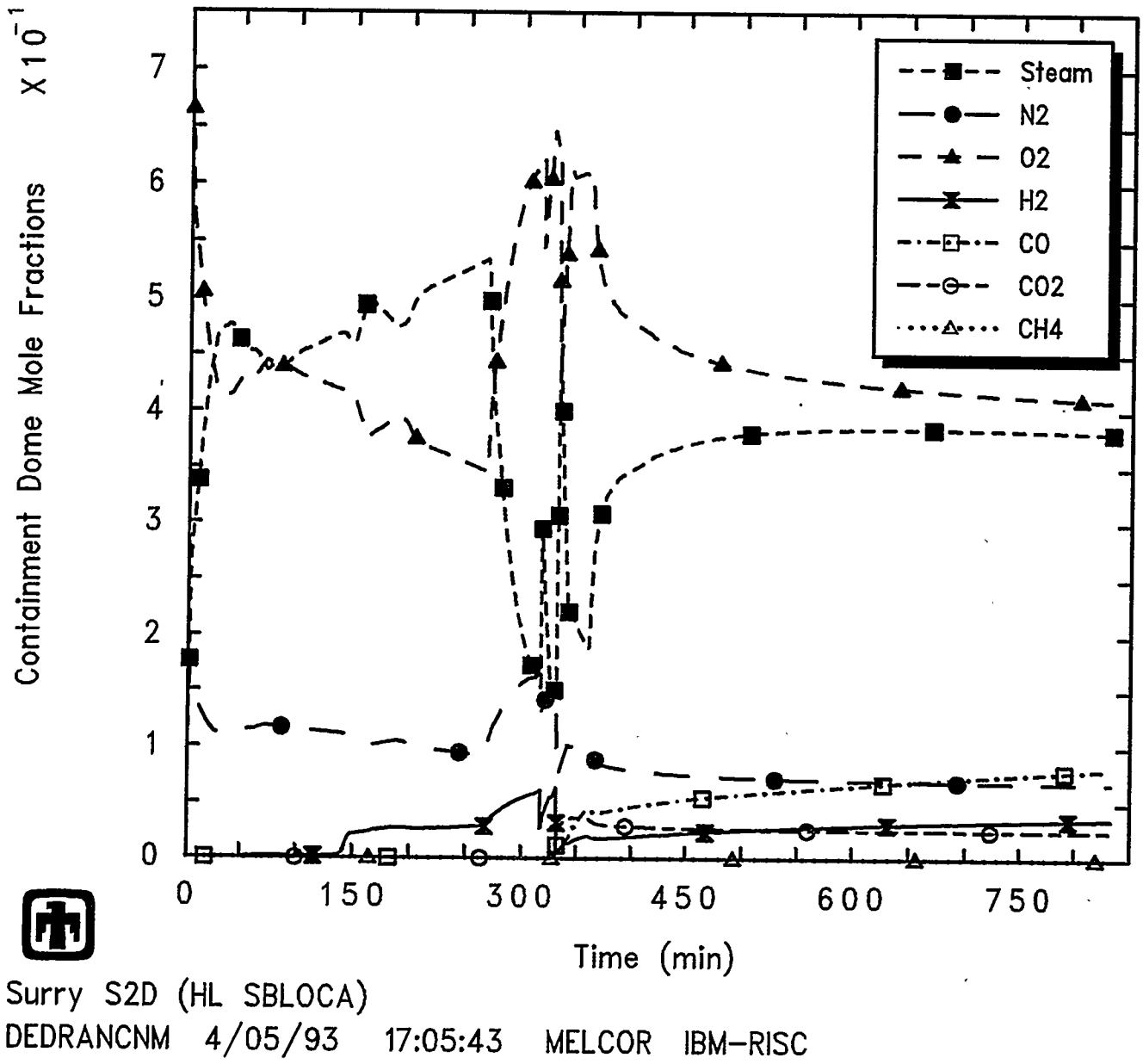

Figure 5.3.17 Containment Dome Steam and Noncondensable Mole Fractions Predicted during S2D Sequence

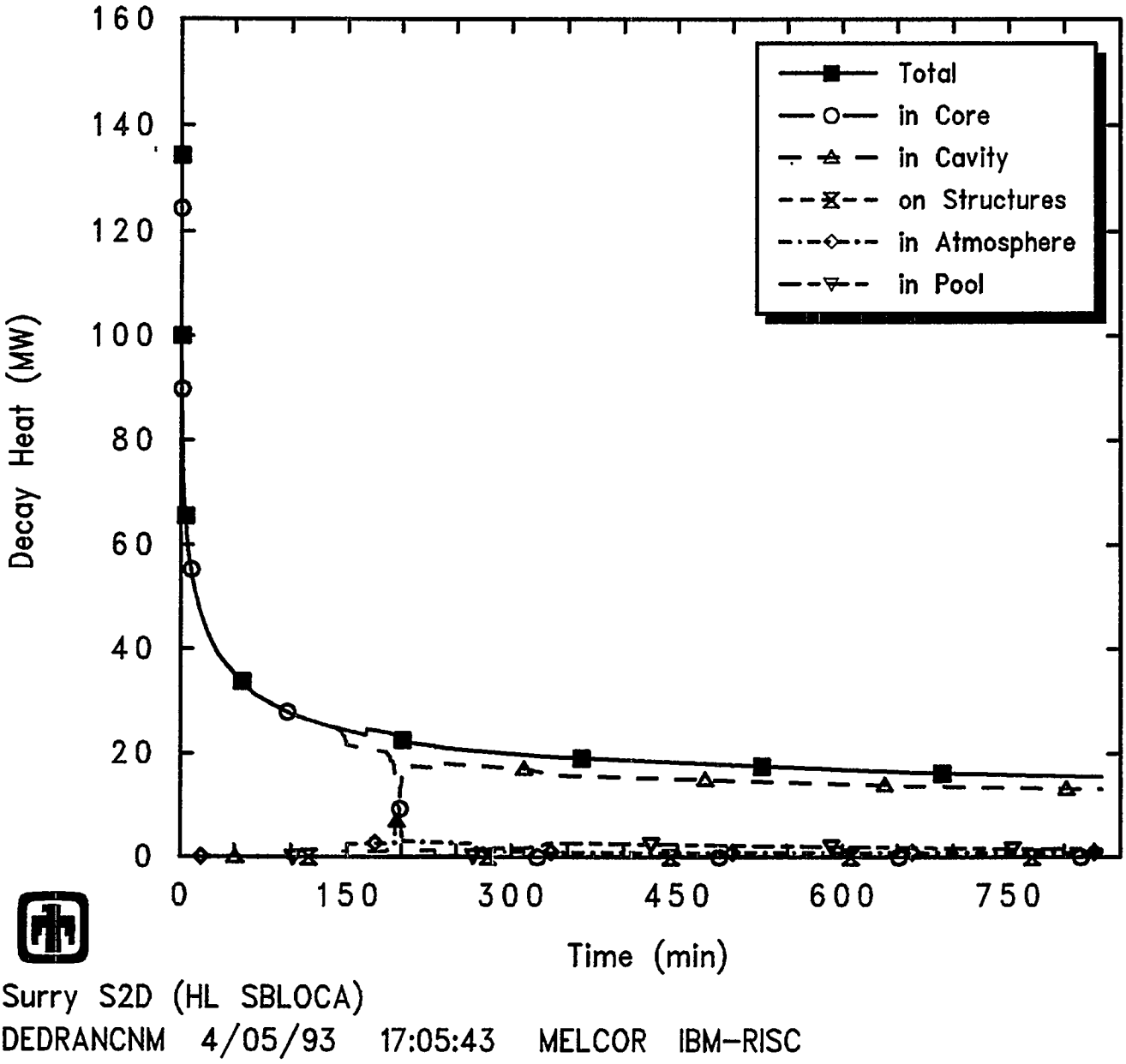

Figure 5.3.18 Decay Heat Predicted during S2D Sequence

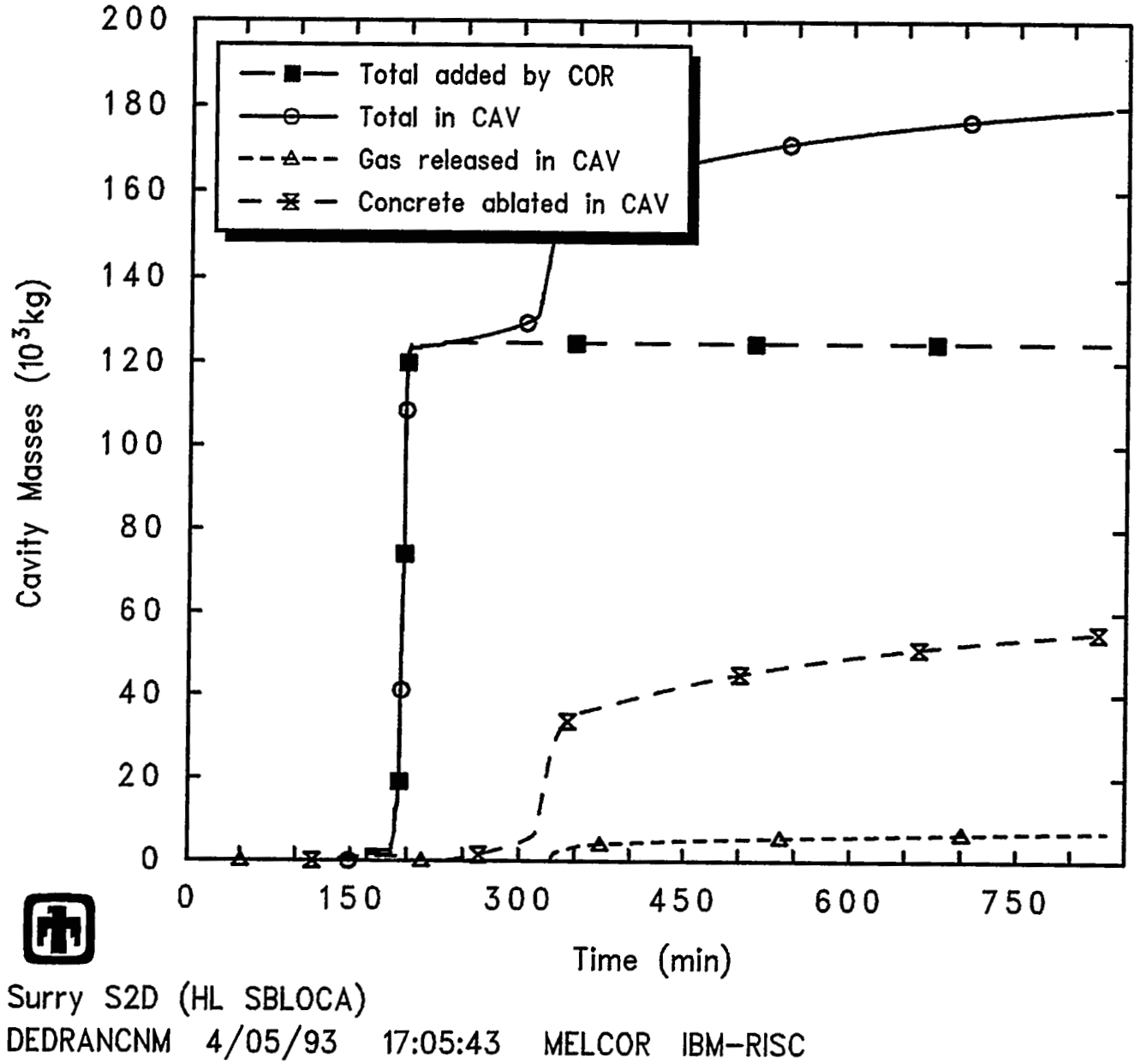

Figure 5.3.19 Total Cavity Masses in Cavity Predicted during S2D Sequence

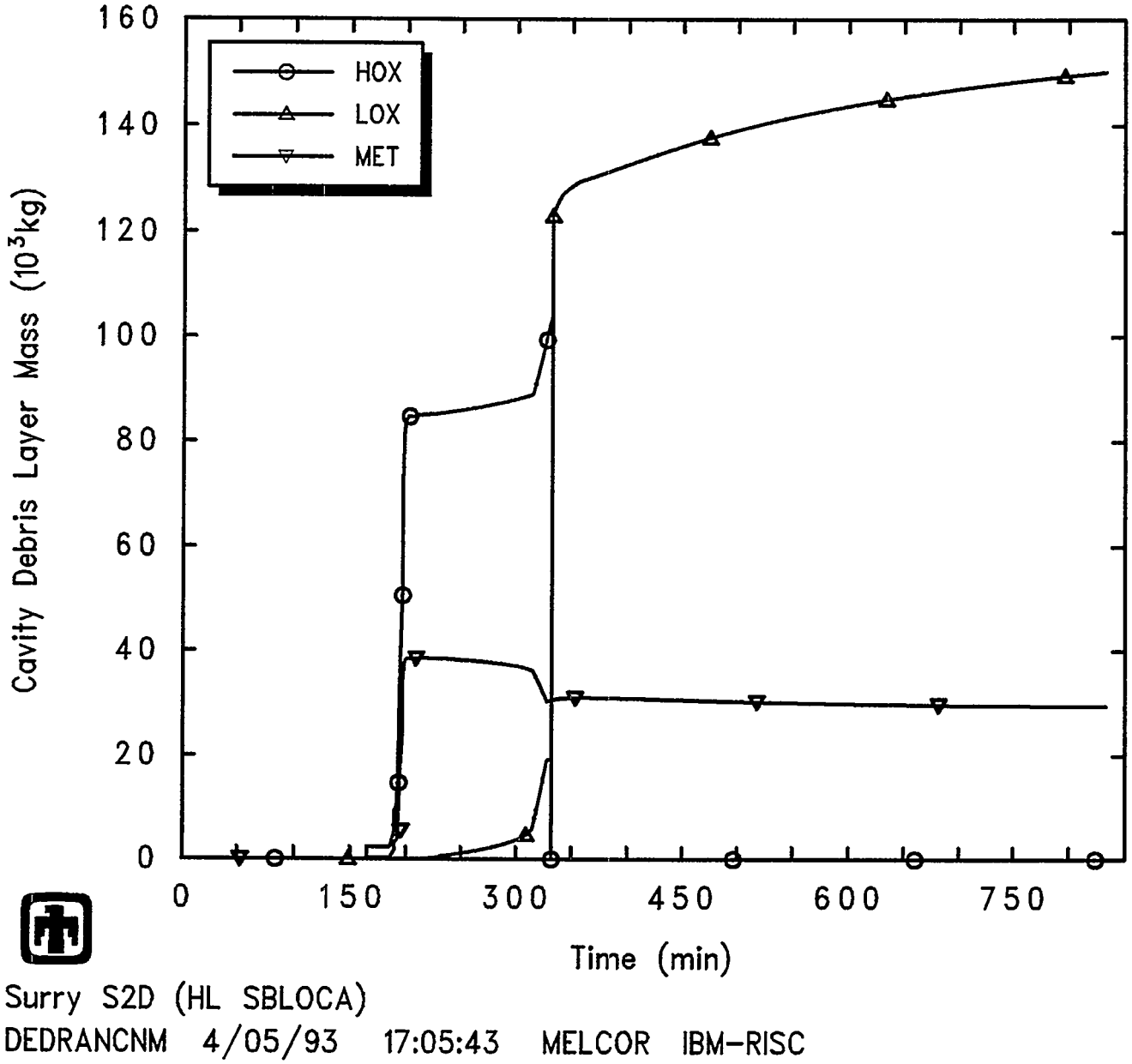

Figure 5.3.20 Cavity Layer Masses Predicted during S2D Sequence

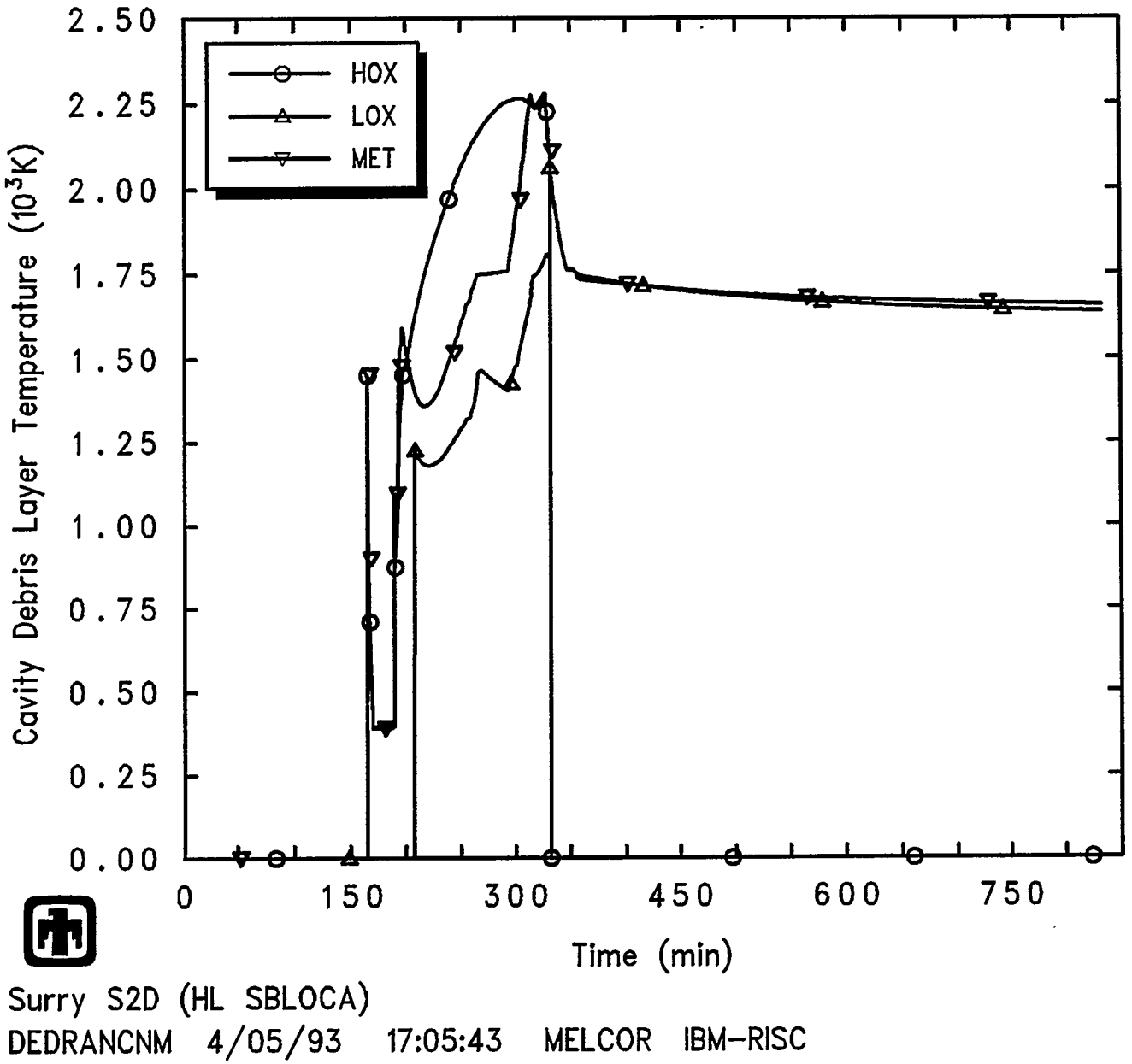

Figure 5.3.21 Cavity Layer Temperatures Predicted during S2D Sequence

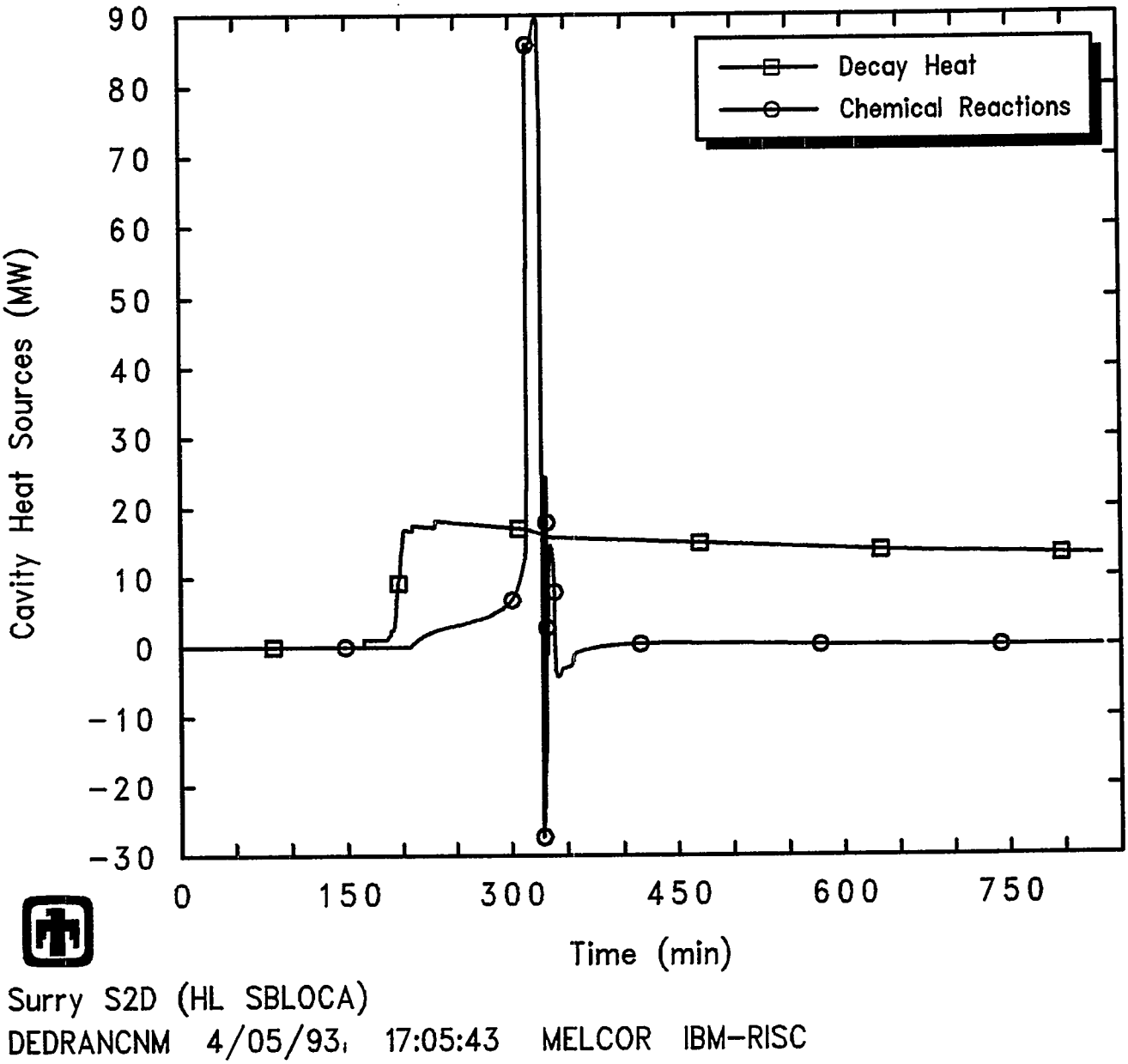

Figure 5.3.22 Decay Heat and Chemical Energy in Cavity Predicted during S2D Sequence

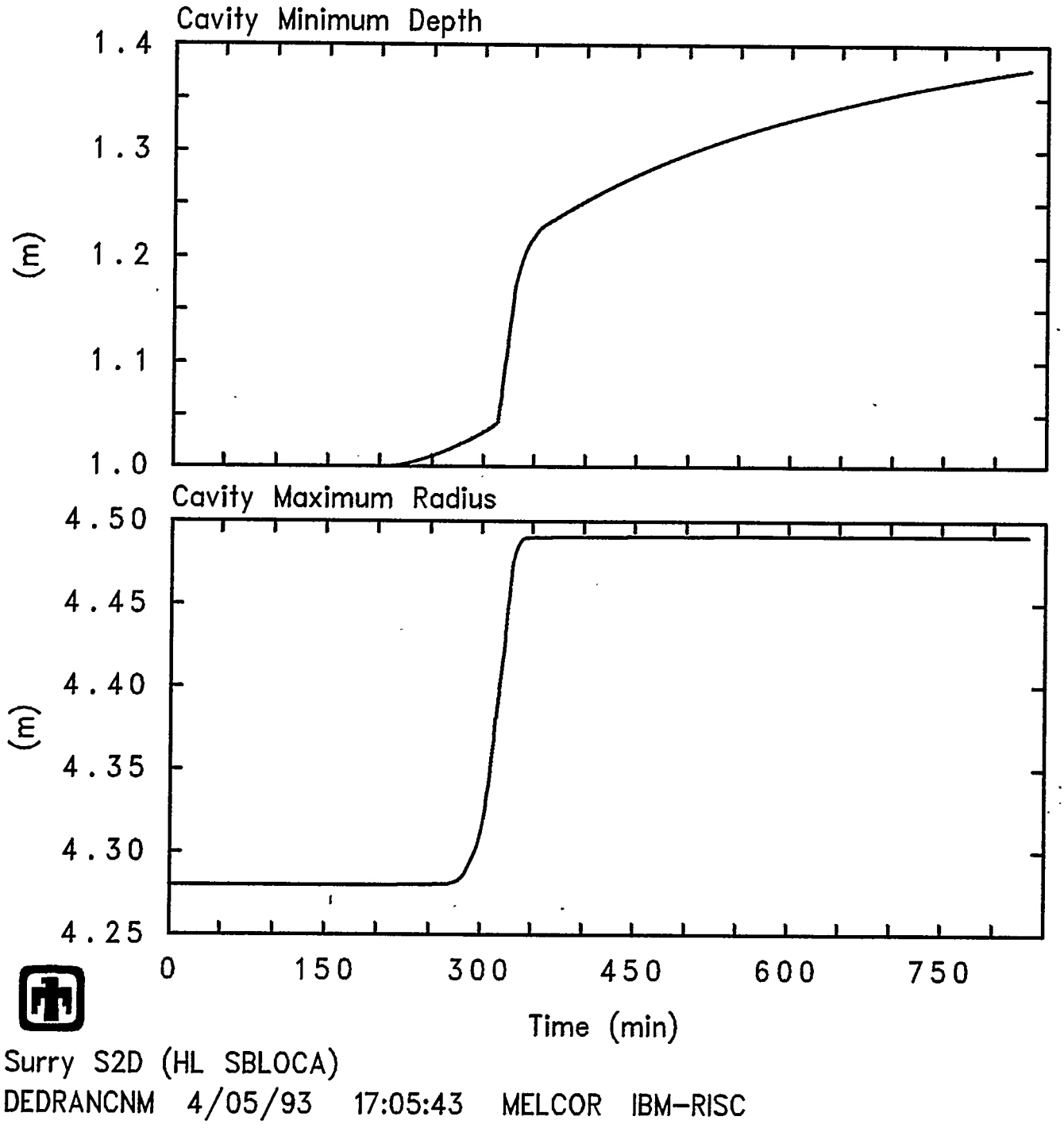

Figure 5.3.23 Cavity Maximum Radius and Minimum Depth Predicted during S2D Sequence

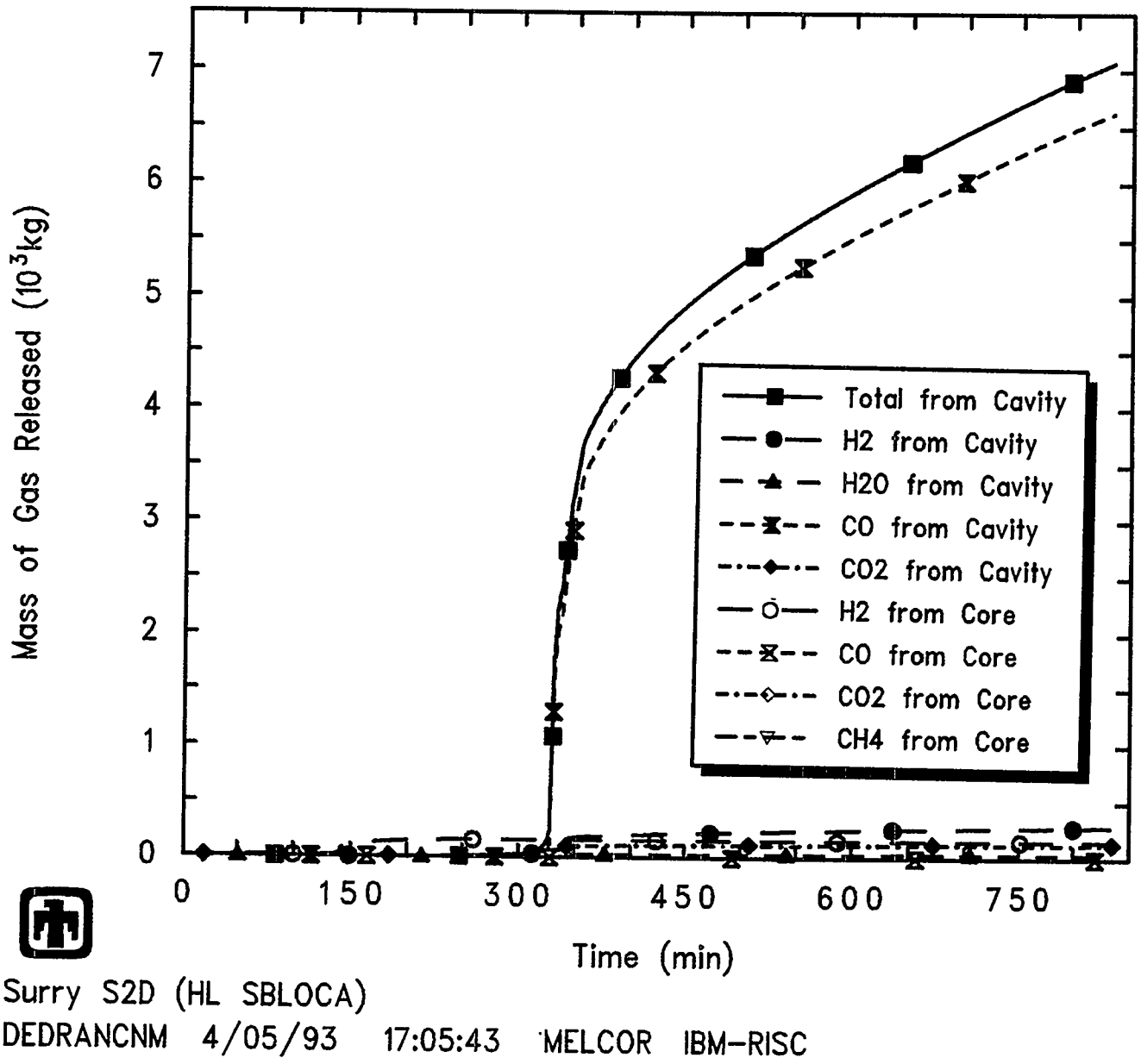

Figure 5.3.24 Gas Generation Predicted in Core and in Cavity during S2D Sequence

Table 5.3.2 Radionuclide Distribution at 833 min for S2D Sequence

Radionuclide Species Group and Representative Element	Core	RCS	Cavity	Containment
Noble Gases, Xe	3.06E-04	3.34E-03	0	0.996
Alkali Metals, Cs	2.94E-04	0.139	2.54E-18	0.860
Alkaline Earths, Ba	4.63E-04	7.56E-03	0.703	0.289
Halogens, I	6.04E-04	1.99E-03	0	0.997
Chalcogens, Te	4.67E-04	8.97E-03	0.685	0.306
Platinoids, Ru	4.68E-04	2.12E-04	0.999	7.45E-04
Transition Metals, Mo	4.63E-04	5.13E-03	0.974	1.99E-02
Tetravalents, Ce	4.68E-04	5.59E-06	1.0	2.07E-05
Trivalents, La	4.68E-04	5.52E-05	0.997	2.79E-03
Uranium, U	7.04E-04	5.08E-05	0.999	2.48E-04
More Volatile Main Group Metals, Cd	4.56E-04	2.93E-02	0.873	9.78E-02
Less Volatile Main Group Metals, Sn	4.56E-04	2.93E-02	0.861	0.109

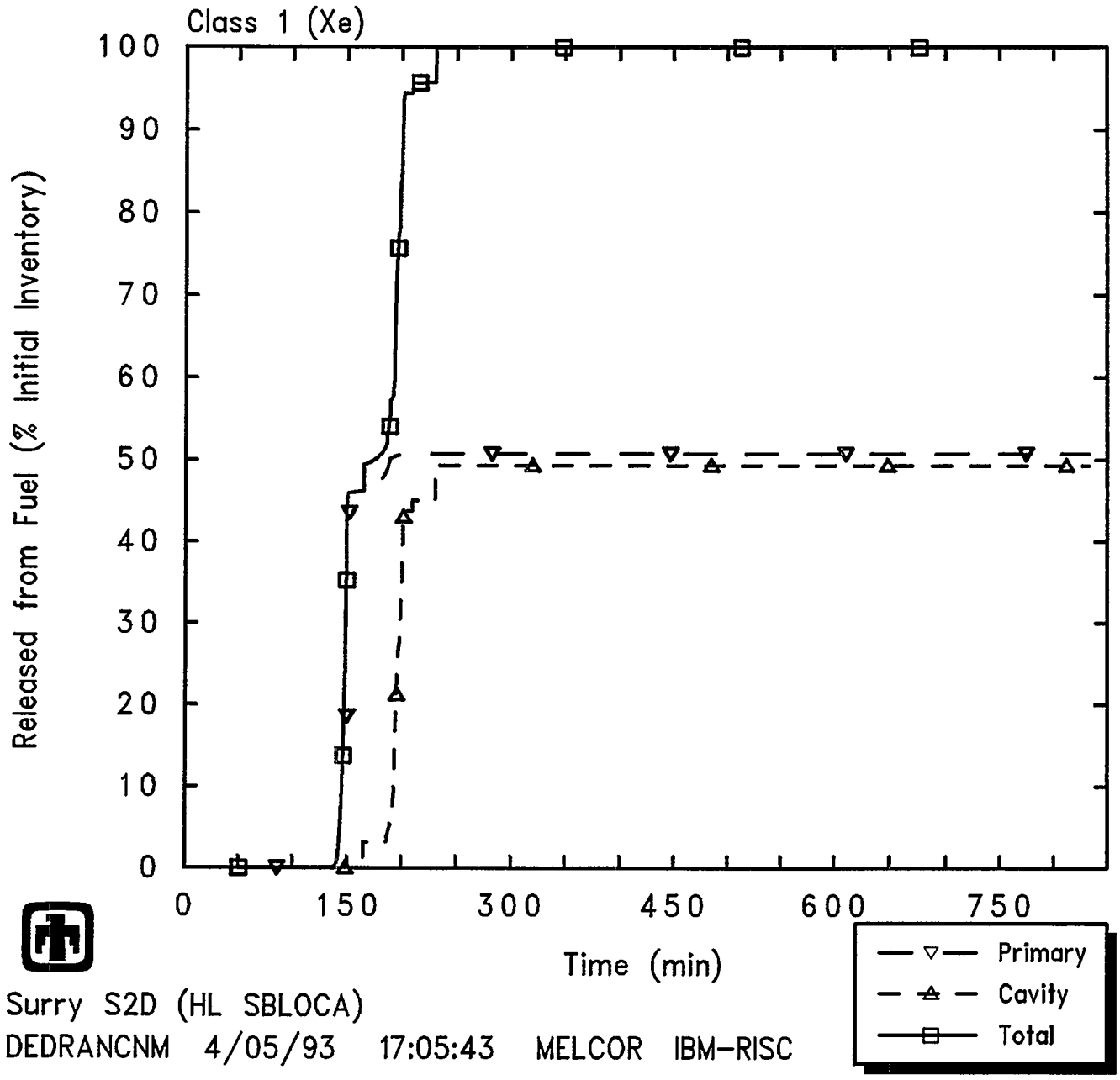

Figure 5.3.25 Release of Class 1 (Xe) Noble Gas Radionuclides from Fuel in Core and in Cavity Predicted during S2D Sequence, as Percentage of Initial Inventory in Core

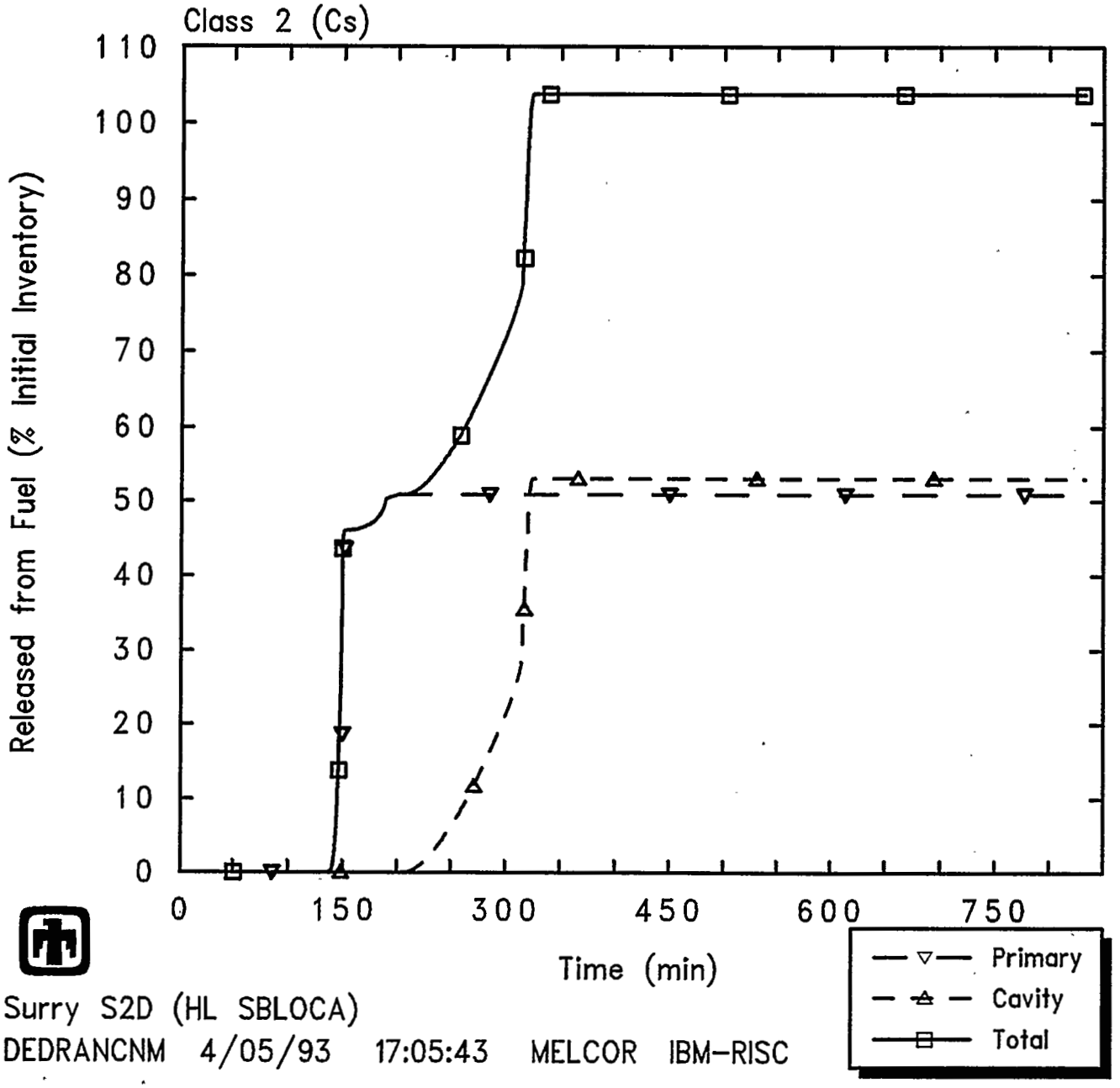

Figure 5.3.26 Release of Class 2 (Cs) Alkali Metal Radionuclides from Fuel in Core and in Cavity Predicted during S2D Sequence, as Percentage of Initial Inventory in Core

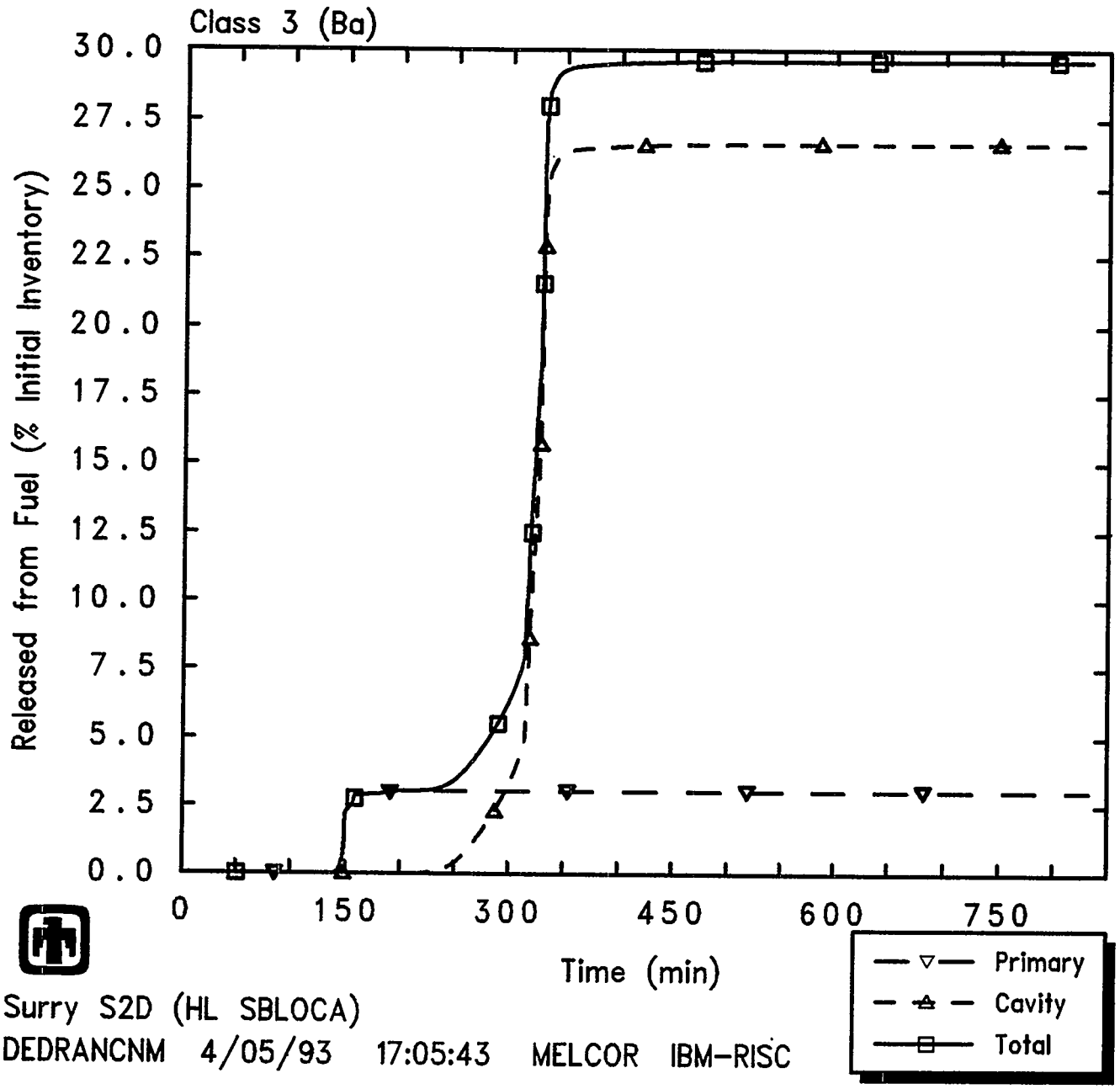

Figure 5.3.27 Release of Class 3 (Ba) Alkaline Earth Radionuclides from Fuel in Core and in Cavity during S2D Sequence, as Percentage of Initial Inventory in Core

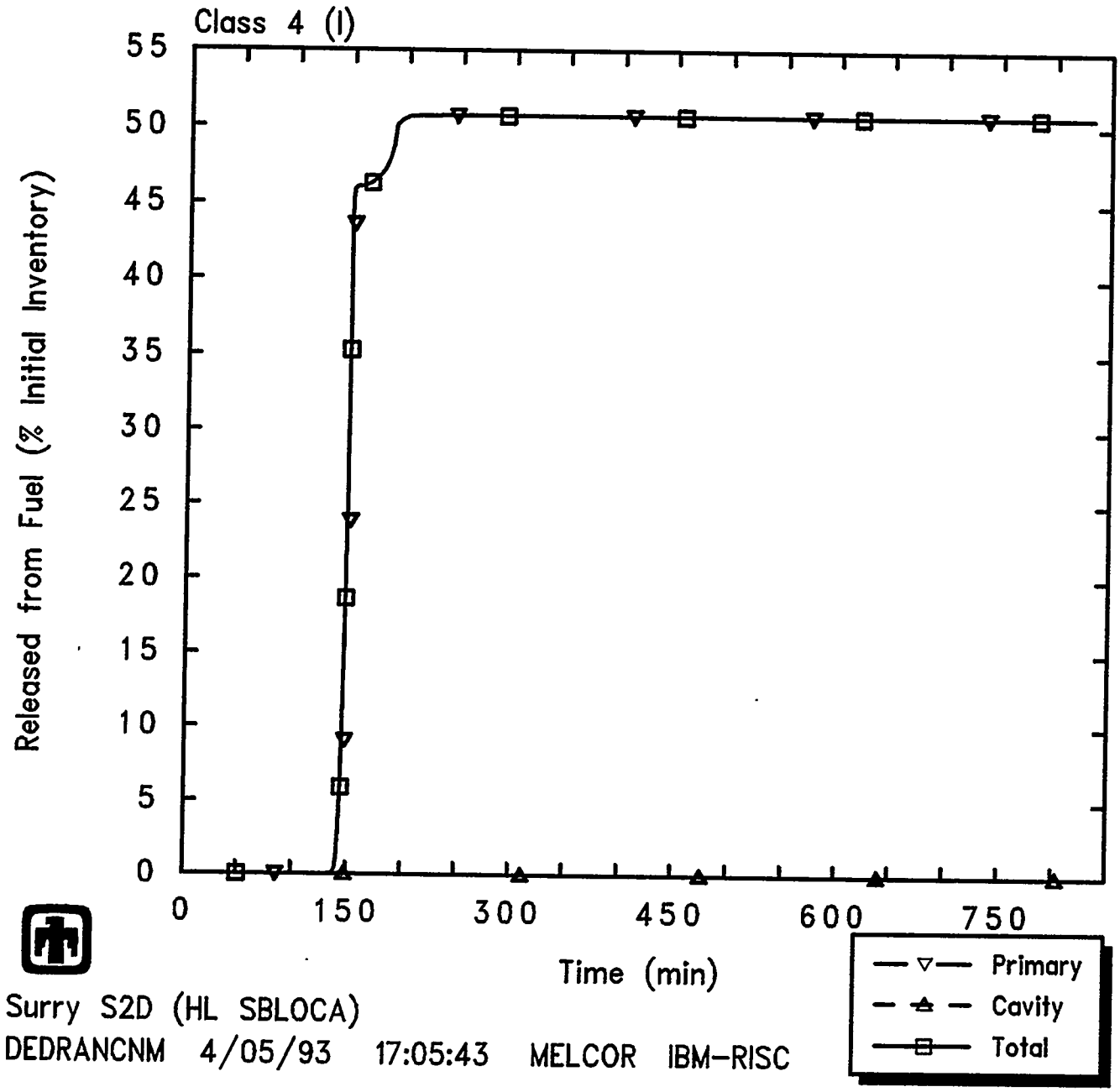

Figure 5.3.28 Release of Class 4 (I) Halogen Radionuclides from Fuel in Core and in Cavity Predicted during S2D Sequence, as Percentage of Initial Inventory in Core

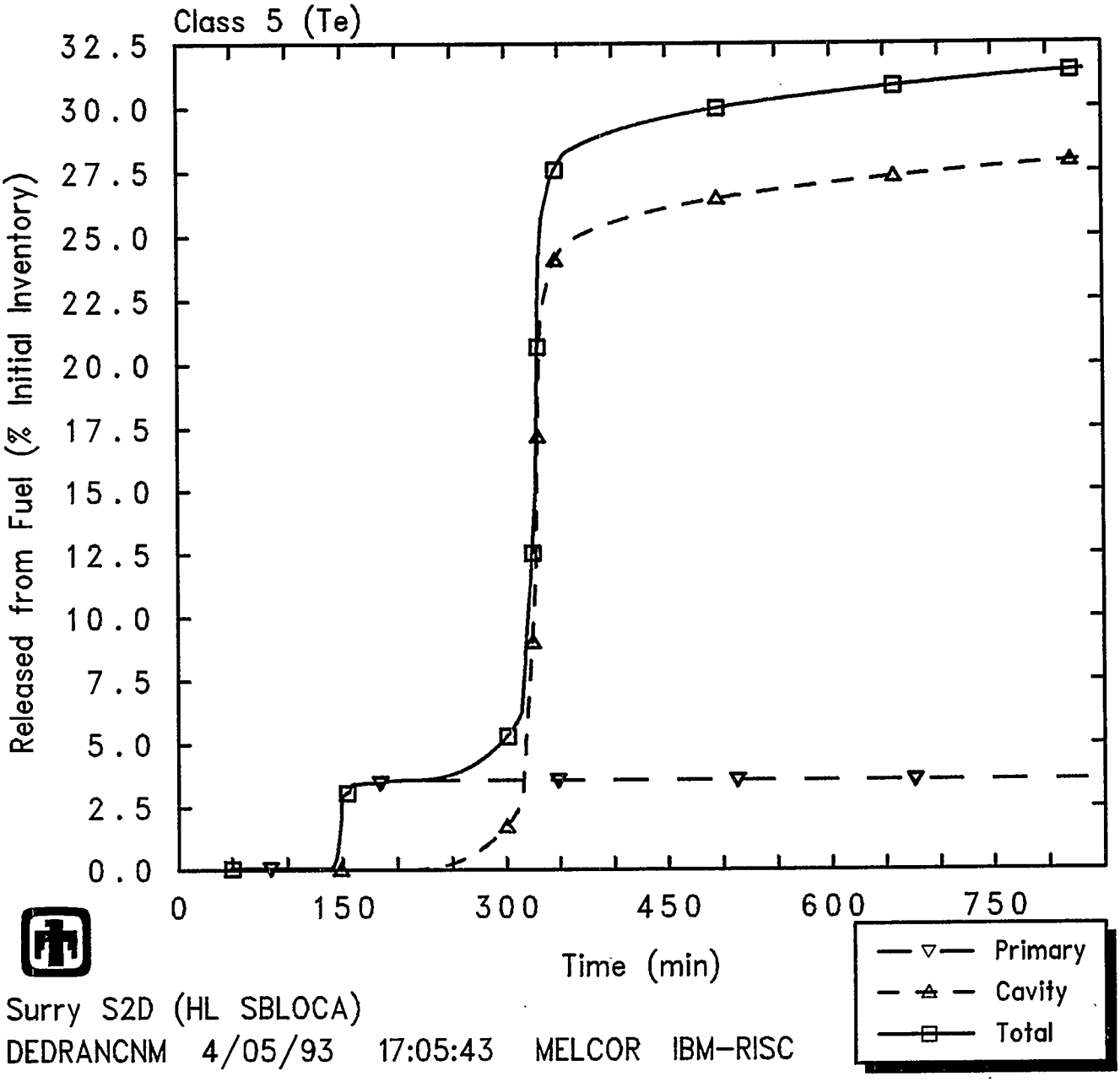

Figure 5.3.29 Release of Class 5 (Te) Chalcogen Radionuclides from Fuel in Core and in Cavity Predicted during S2D Sequence, as Percentage of Initial Inventory in Core

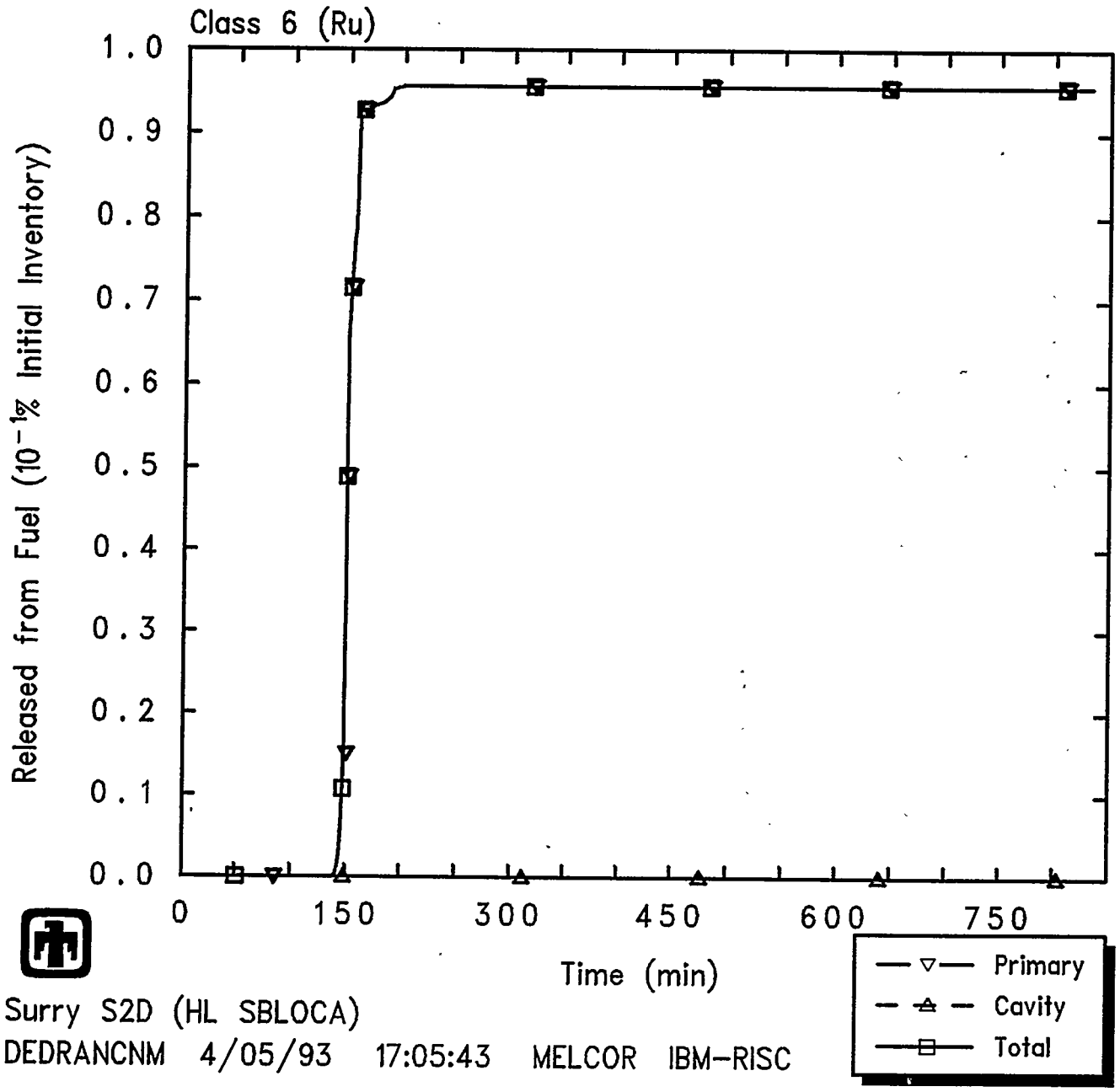

Figure 5.3.30 Release of Class 6 (Ru) Platinoid Radionuclides from Fuel in Core and in Cavity Predicted during S2D Sequence, as Percentage of Initial Inventory in Core

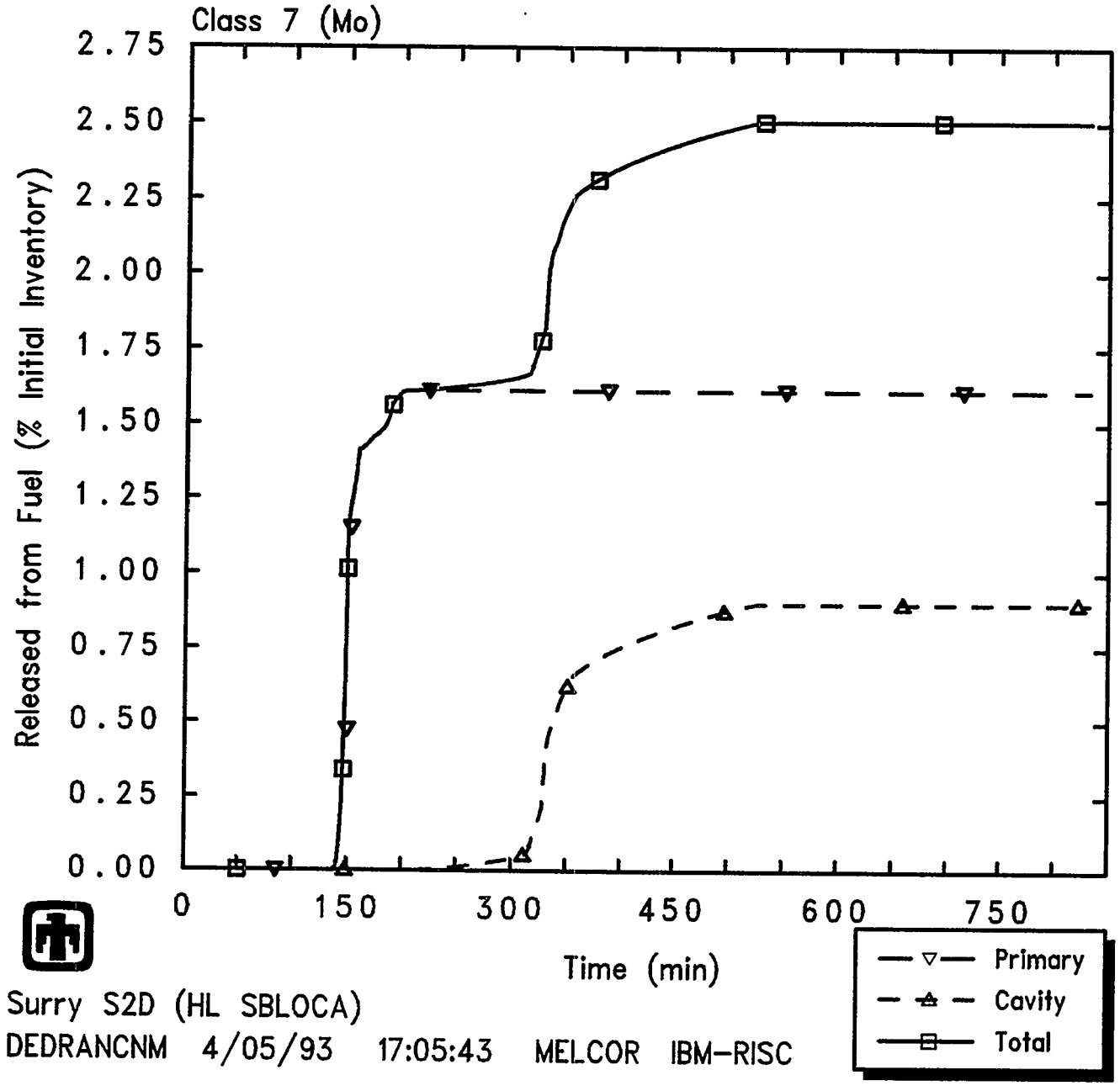

Figure 5.3.31 Release of Class 7 (Mo) Early Transition Element Radionuclides from Fuel in Core and in Cavity Predicted during S2D Sequence, as Percentage of Initial Inventory in Core

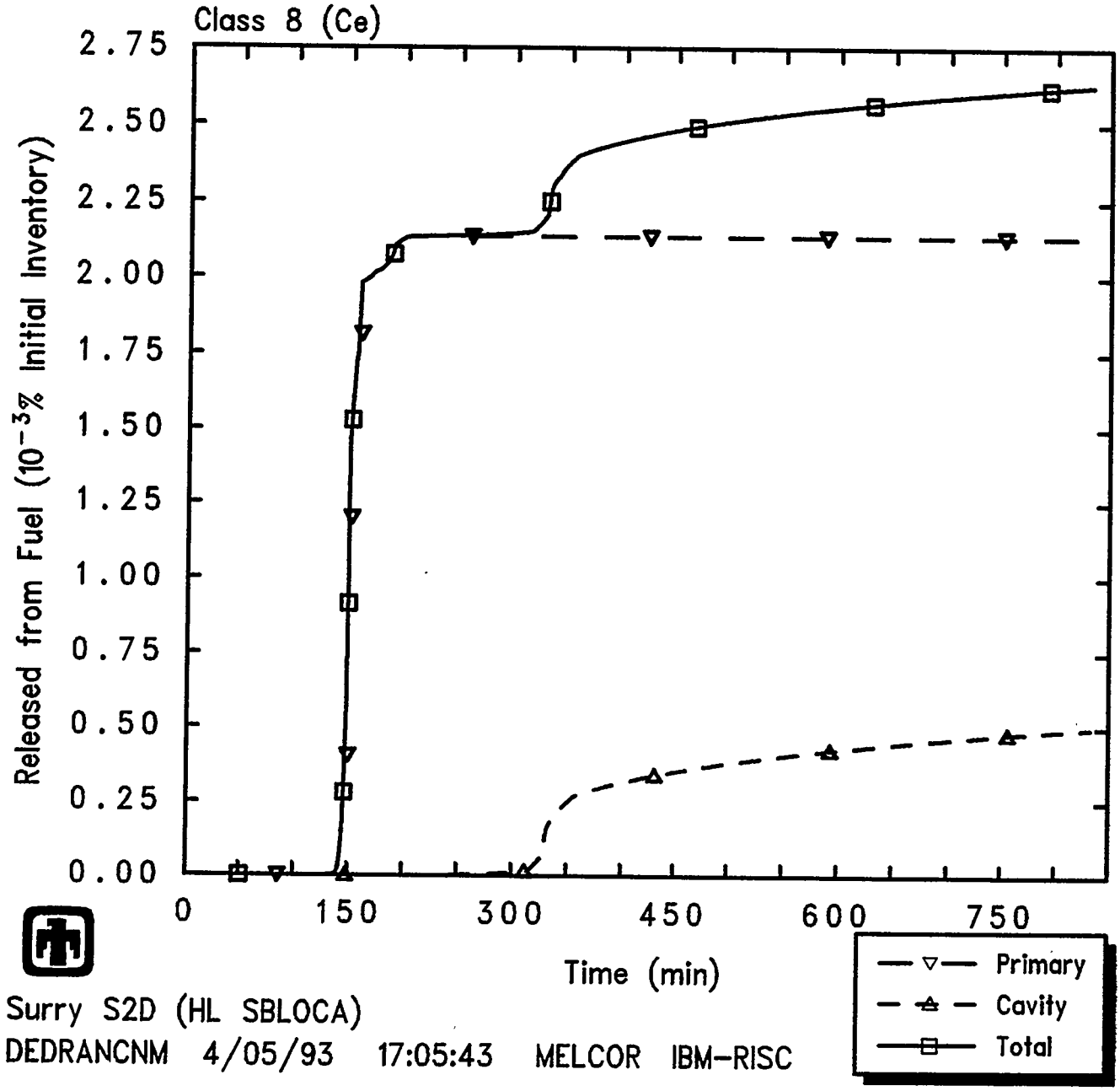

Figure 5.3.32 Release of Class 8 (Ce) Tetravalent Radionuclides from Fuel in Core and in Cavity Predicted during S2D Sequence, as Percentage of Initial Inventory in Core

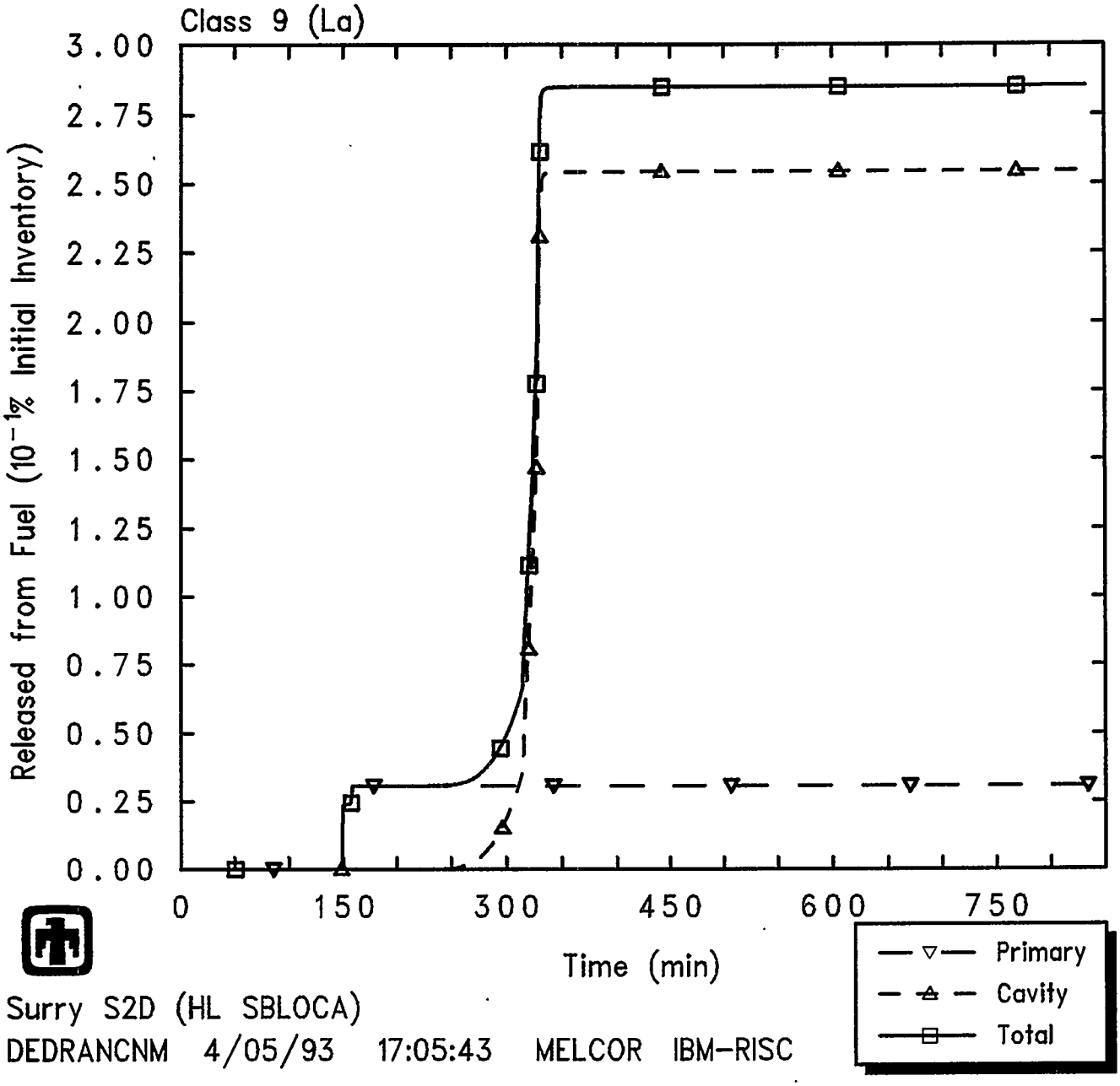

Figure 5.3.33 Release of Class 9 (La) Trivalent Radionuclides from Fuel in Core and in Cavity Predicted during S2D Sequence, as Percentage of Initial Inventory in Core

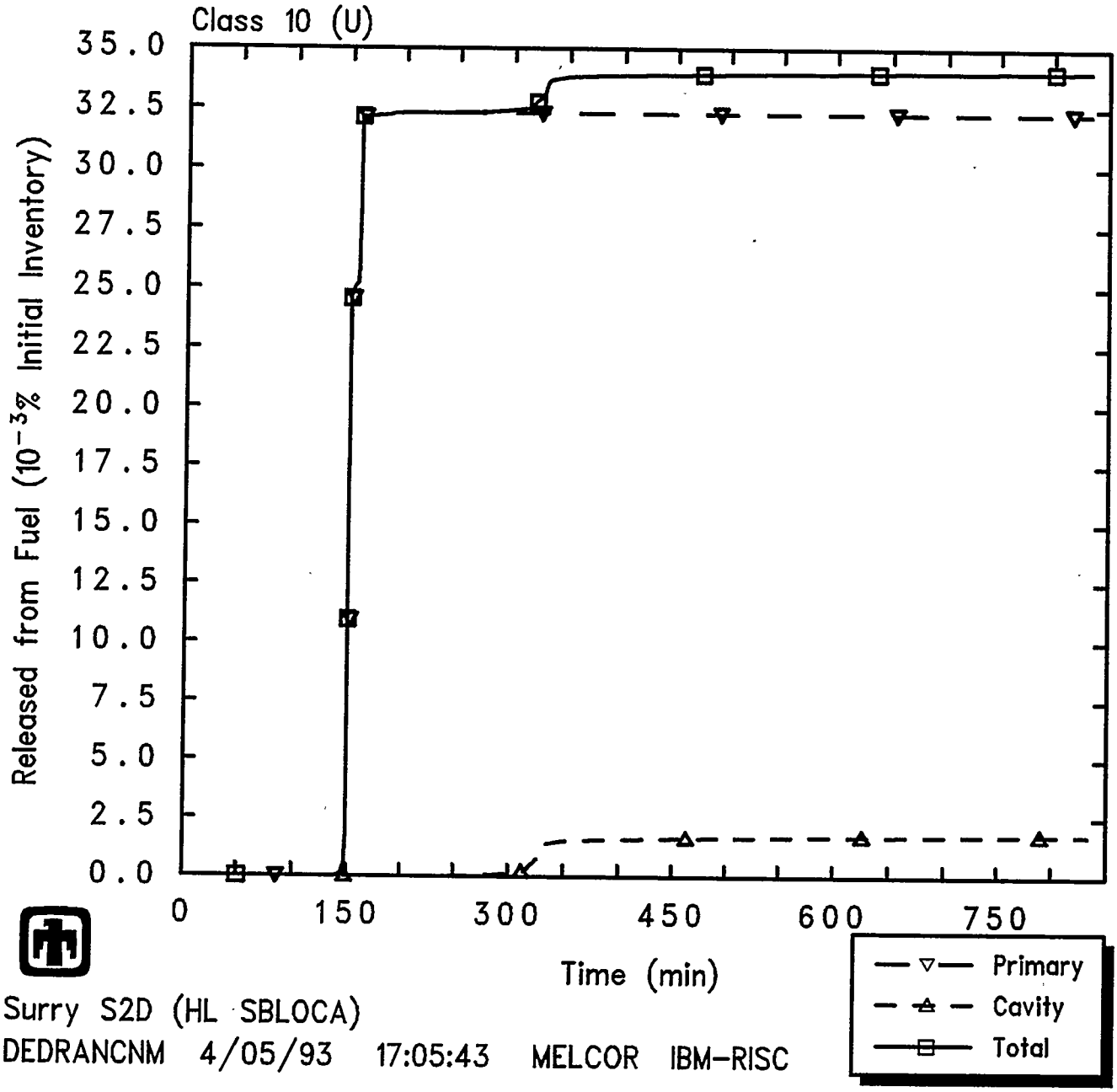

Figure 5.3.34 Release of Class 10 (U) Uranium Radionuclides from Fuel in Core and in Cavity Predicted during S2D Sequence, as Percentage of Initial Inventory in Core

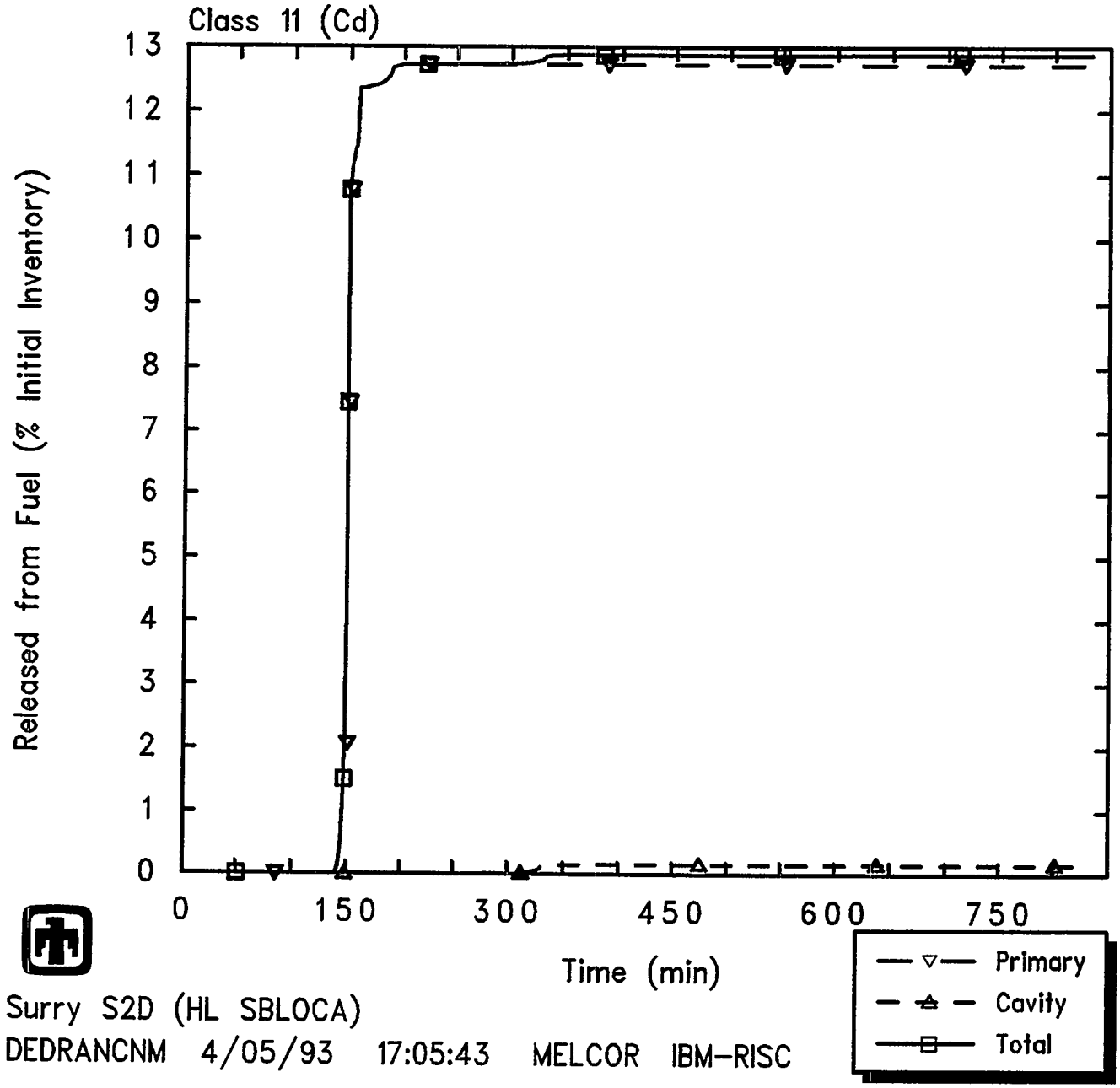

Figure 5.3.35 Release of Class 11 (Cd) More Volatile Main Group Radionuclides from Fuel in Core and in Cavity Predicted during S2D Sequence, as Percentage of Initial Inventory in Core

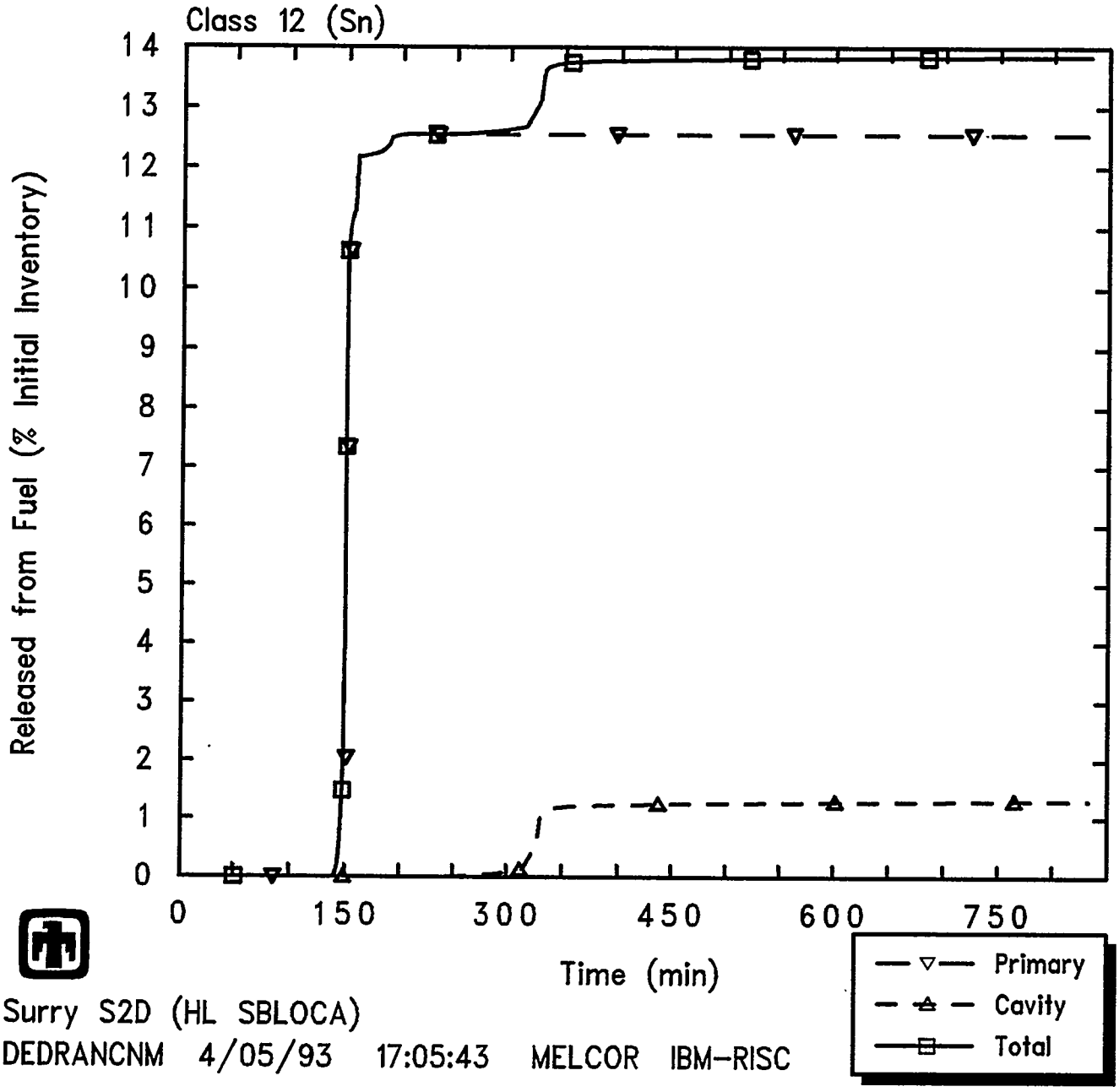

Figure 5.3.36 Release of Class 12 (Sn) Less Volatile Main Group Radionuclides from Fuel in Core and in Cavity Predicted during S2D Sequence, as Percentage of Initial Inventory in Core

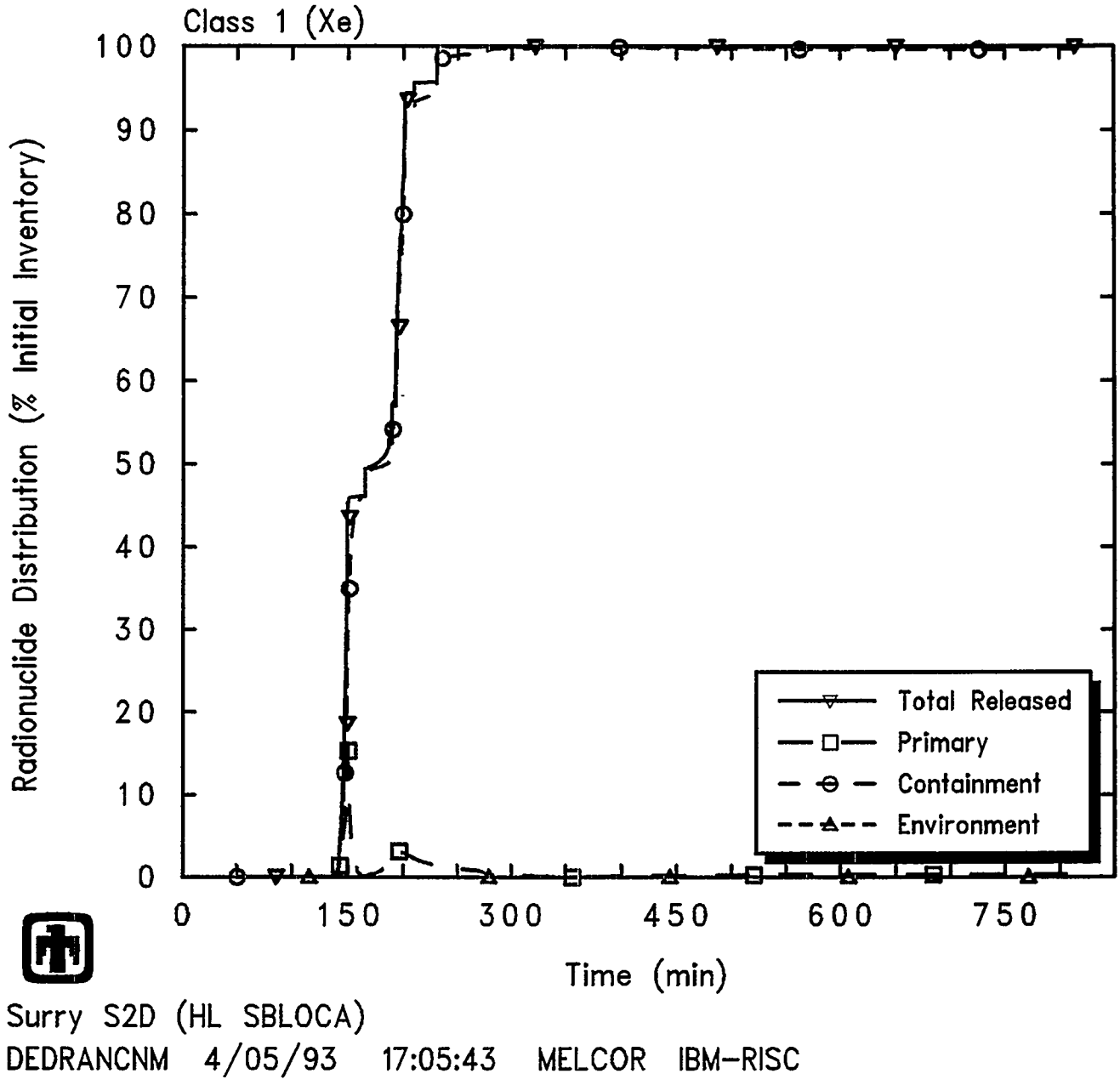

Figure 5.3.37 Distribution of Class 1 (Xe) Noble Gas Radionuclides in Primary System, Containment and Environment Predicted during S2D Sequence, as Percentage of Initial Inventory in Core

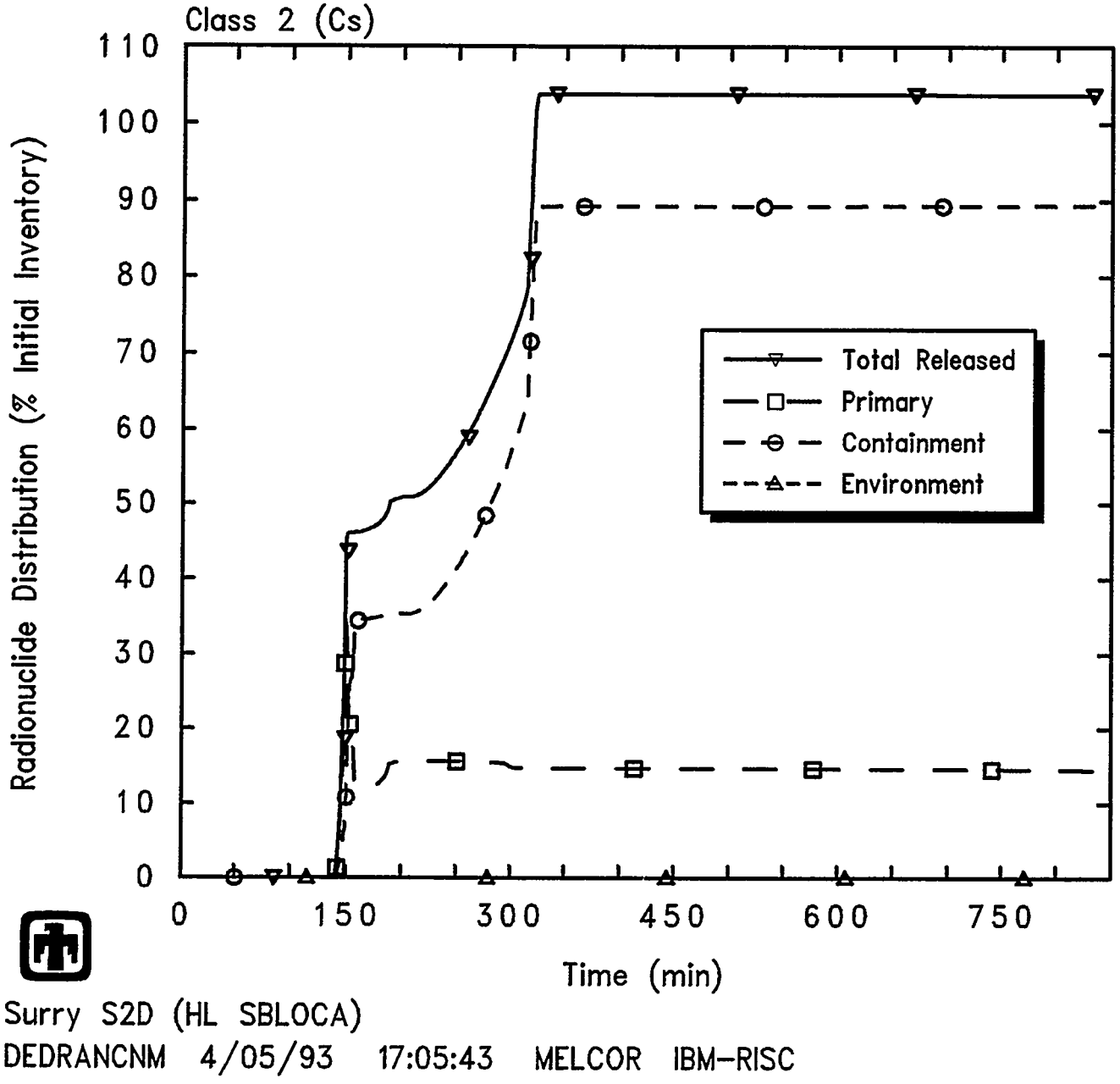

Figure 5.3.38 Distribution of Class 2 (Cs) Alkali Metal Radionuclides in Primary System, Containment and Environment Predicted during S2D Sequence, as Percentage of Initial Inventory in Core

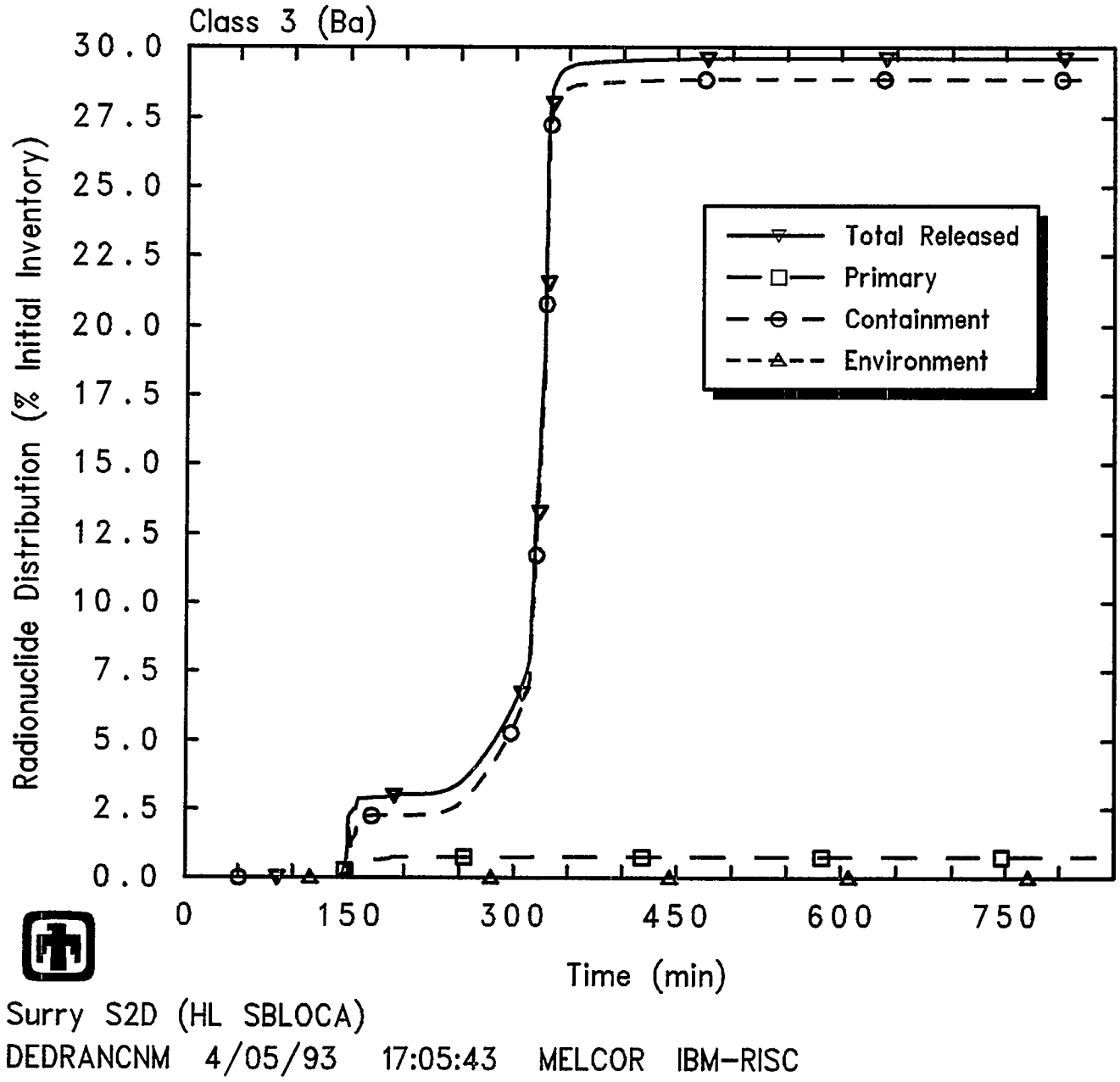

Figure 5.3.39 Distribution of Class 3 (Ba) Alkaline Earth Radionuclides in Primary System, Containment and Environment during S2D Sequence, as Percentage of Initial Inventory in Core

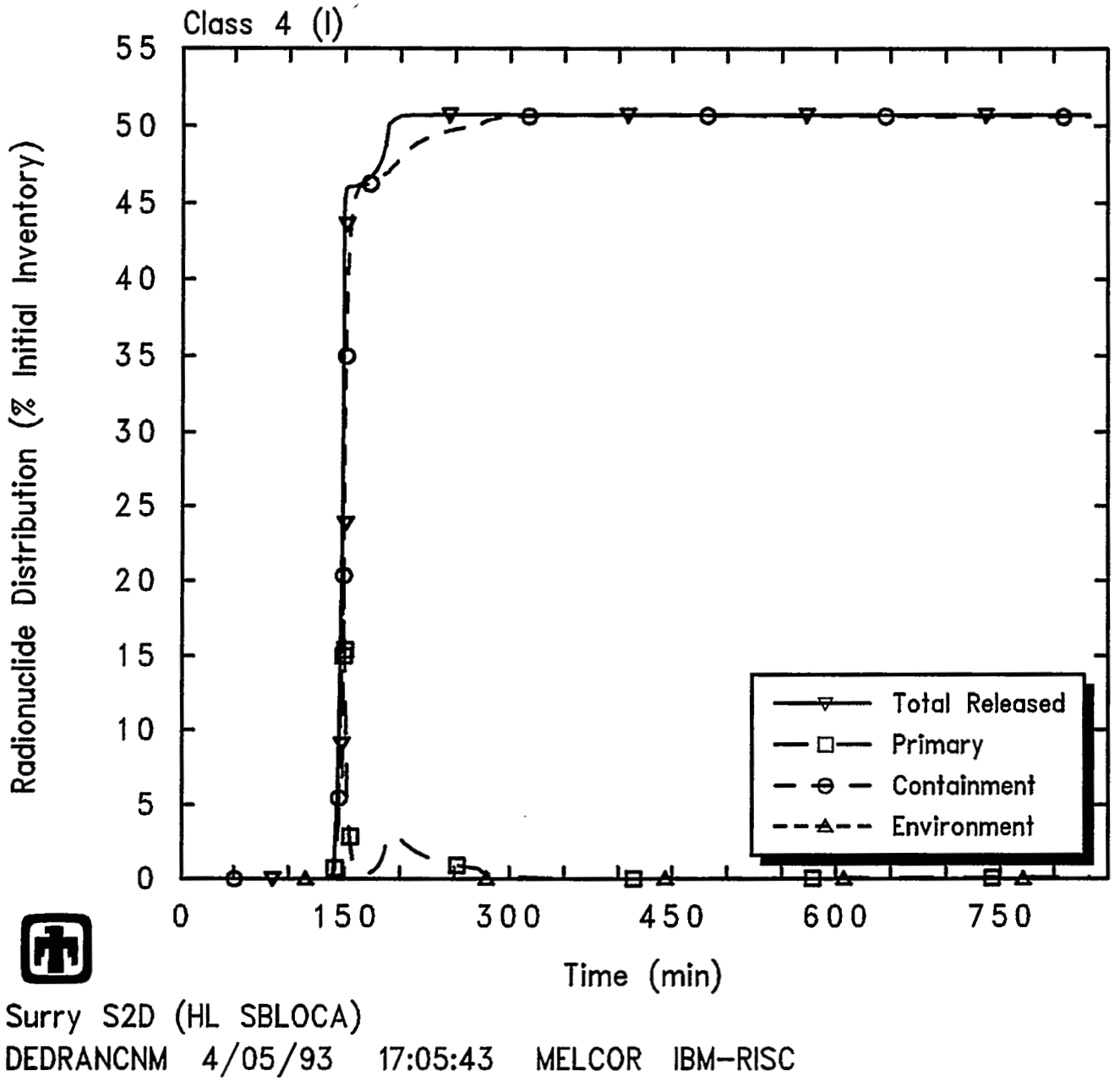

Figure 5.3.40 Distribution of Class 4 (I) Halogen Radionuclides in Primary System, Containment and Environment Predicted during S2D Sequence, as Percentage of Initial Inventory in Core

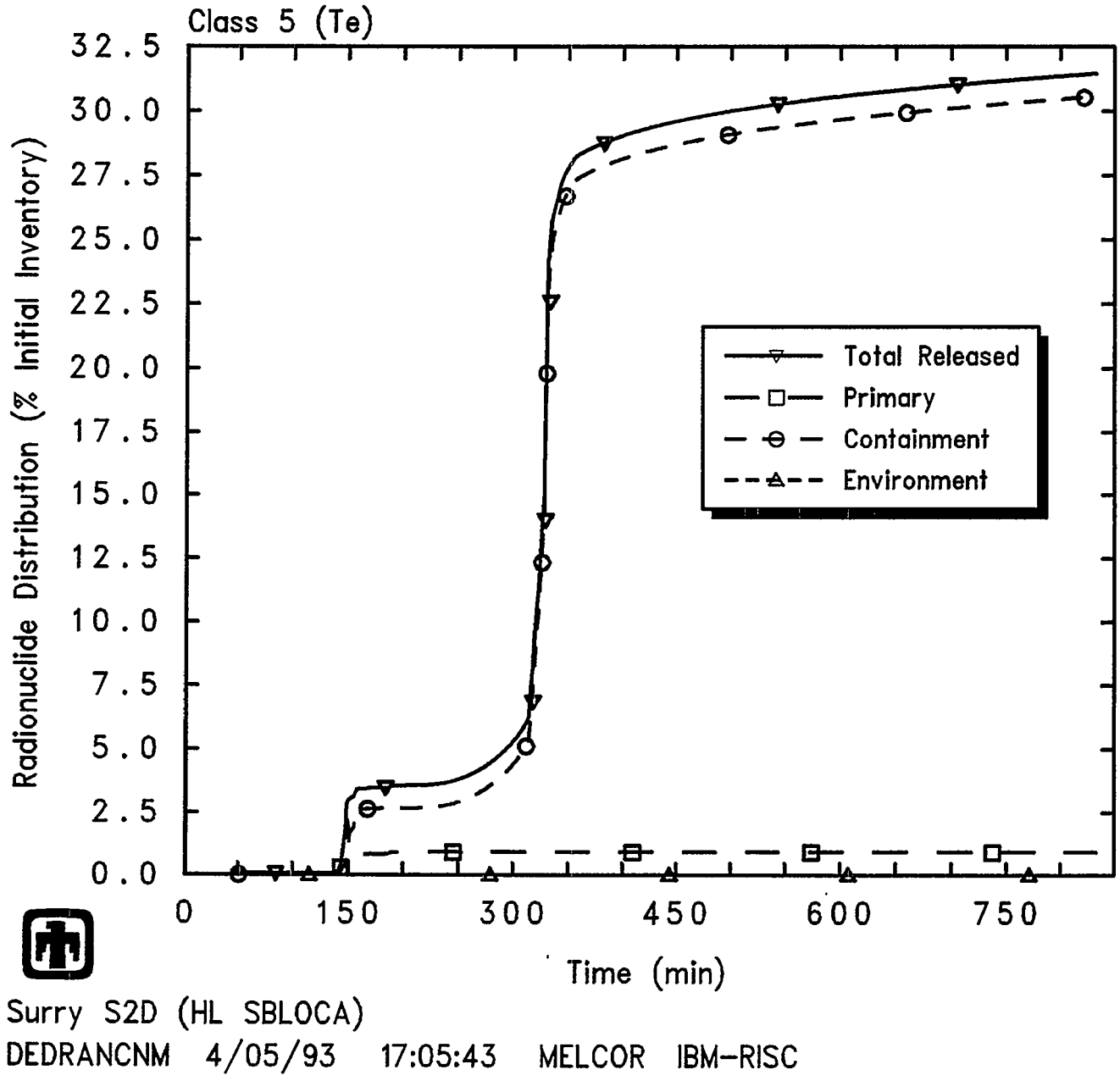

Figure 5.3.41 Distribution of Class 5 (Te) Chalcogen Radionuclides in Primary System, Containment and Environment Predicted during S2D Sequence, as Percentage of Initial Inventory in Core

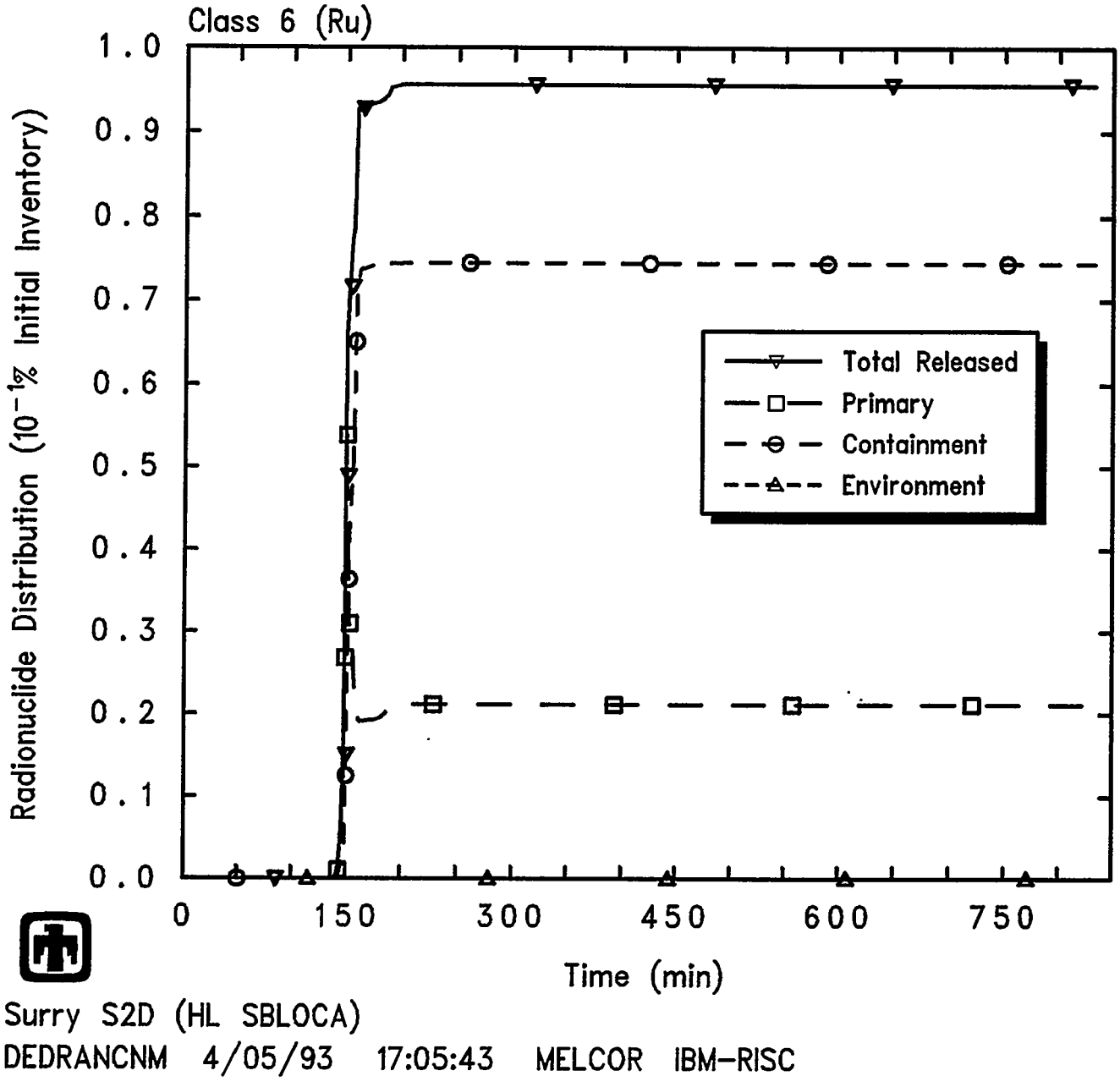

Figure 5.3.42 Distribution of Class 6 (Ru) Platinoid Radionuclides in Primary System, Containment and Environment Predicted during S2D Sequence, as Percentage of Initial Inventory in Core

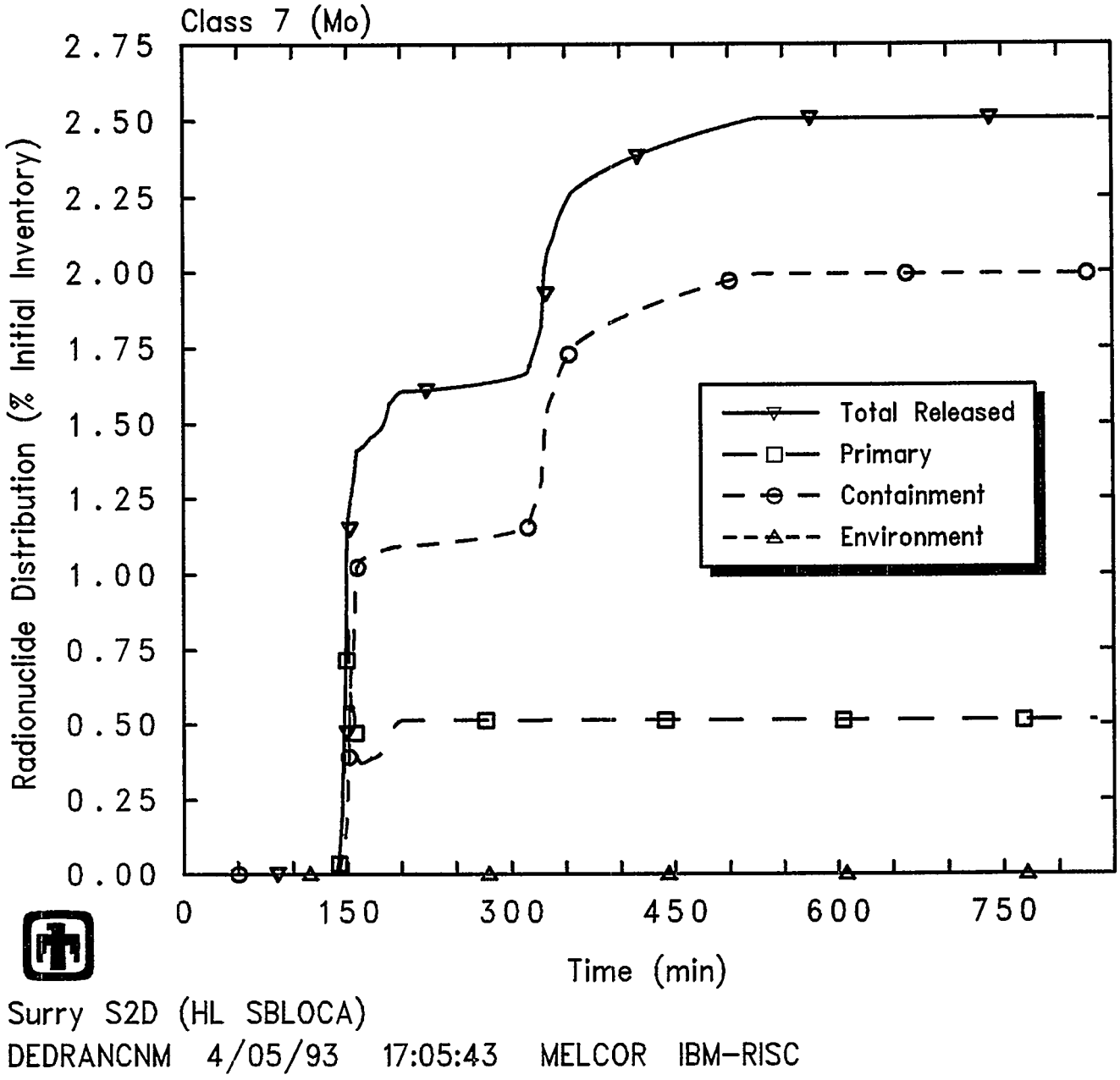

Figure 5.3.43 Distribution of Class 7 (Mo) Early Transition Element Radionuclides in Primary System, Containment and Environment Predicted during S2D Sequence, as Percentage of Initial Inventory in Core

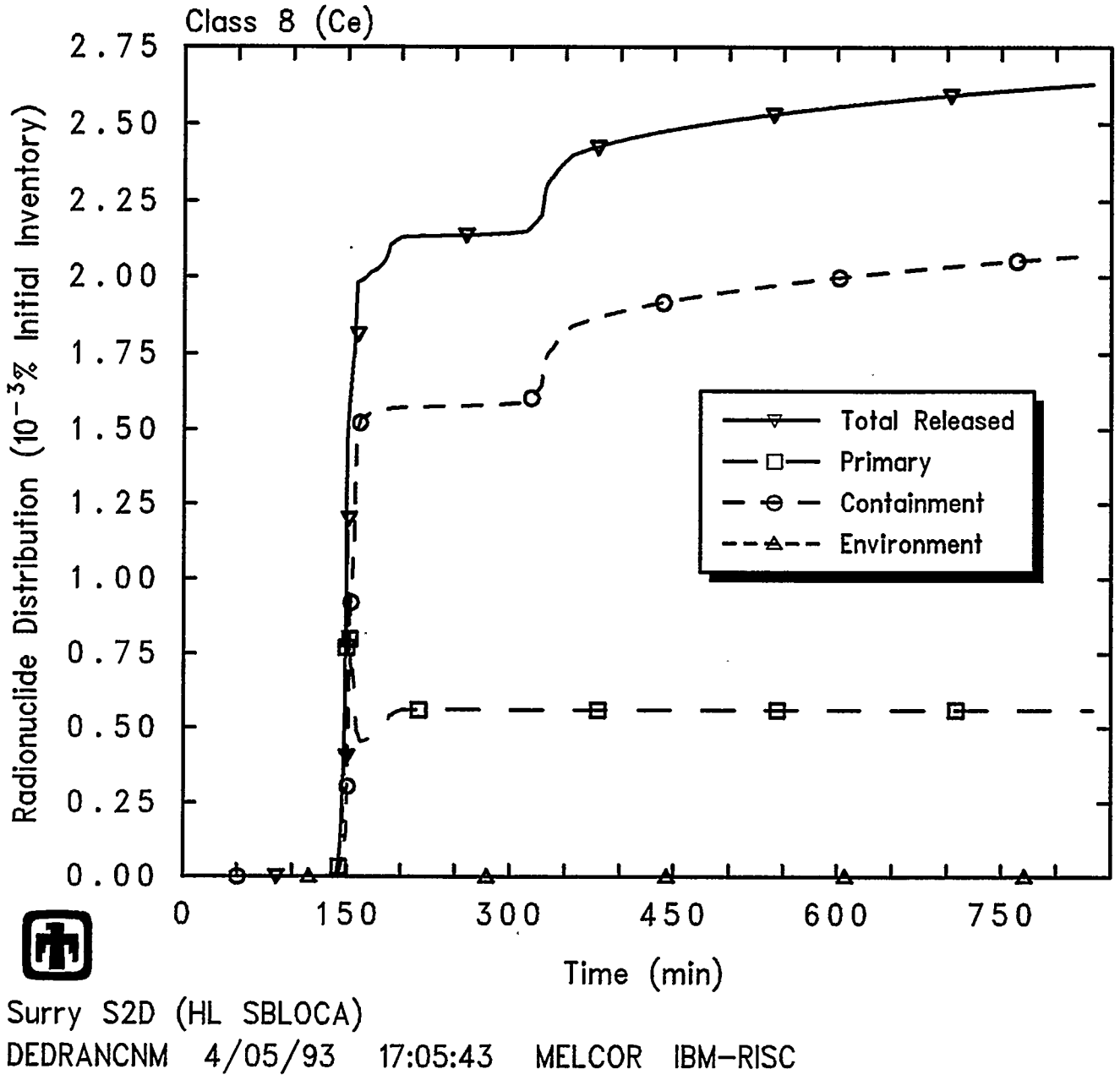

Figure 5.3.44 Distribution of Class 8 (Ce) Tetravalent Radionuclides in Primary System, Containment and Environment Predicted during S2D Sequence, as Percentage of Initial Inventory in Core

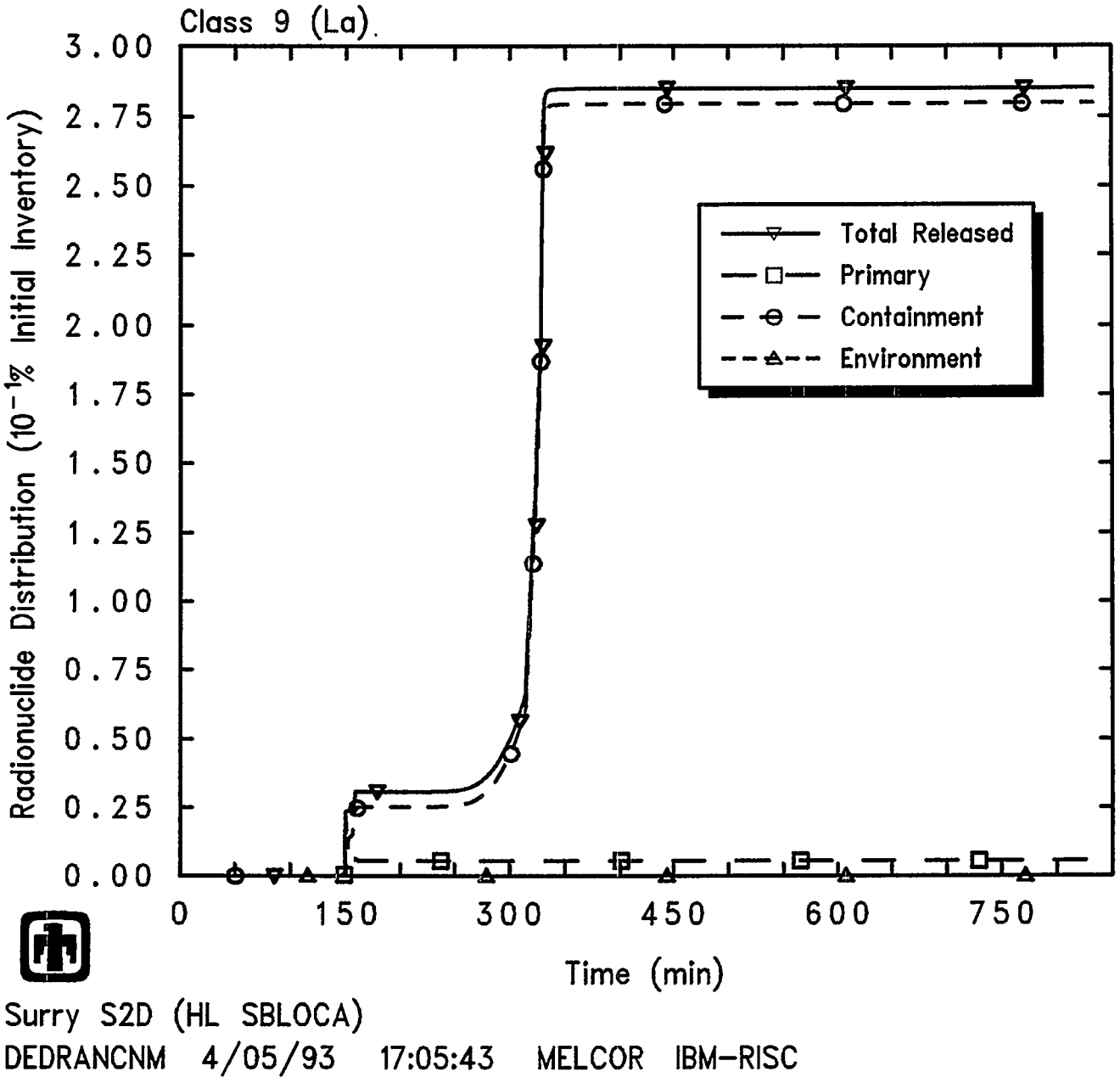

Figure 5.3.45 Distribution of Class 9 (La) Trivalent Radionuclides in Primary System, Containment and Environment Predicted during S2D Sequence, as Percentage of Initial Inventory in Core

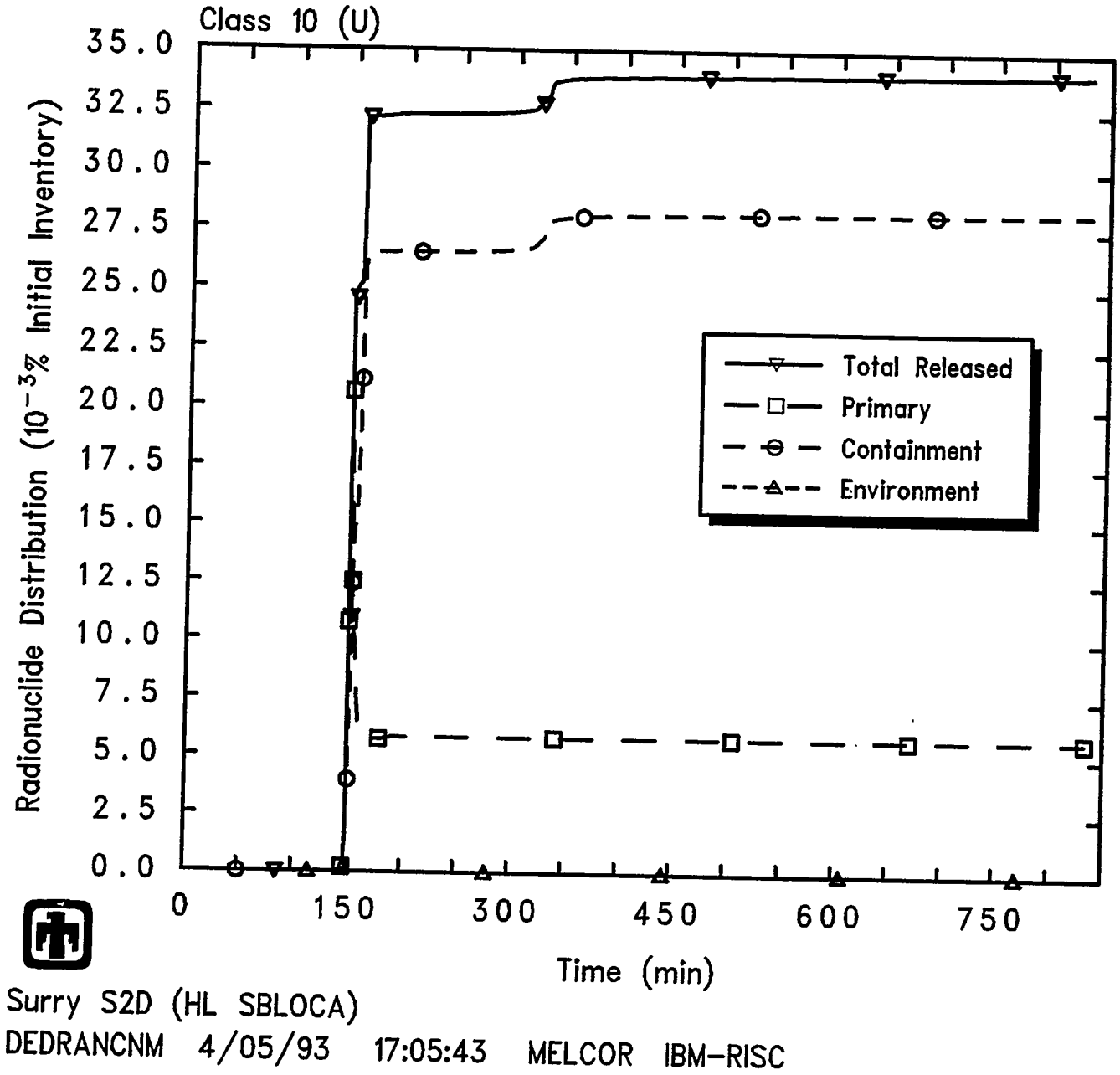

Figure 5.3.46 Distribution of Class 10 (U) Uranium Radionuclides in Primary System, Containment and Environment Predicted during S2D Sequence, as Percentage of Initial Inventory in Core

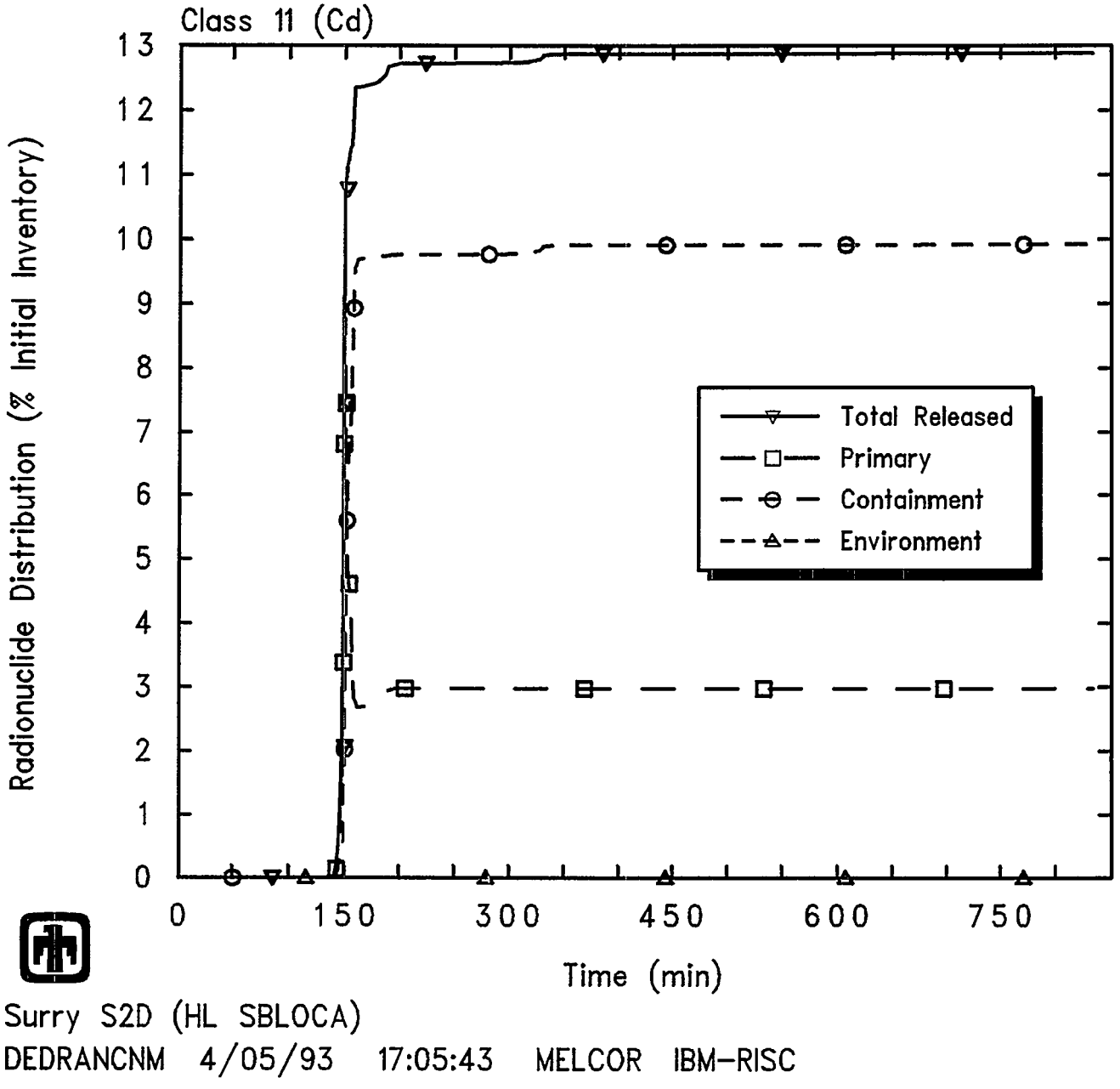

Figure 5.3.47 Distribution of Class 11 (Cd) More Volatile Main Group Radionuclides in Primary System, Containment and Environment Predicted during S2D Sequence, as Percentage of Initial Inventory in Core

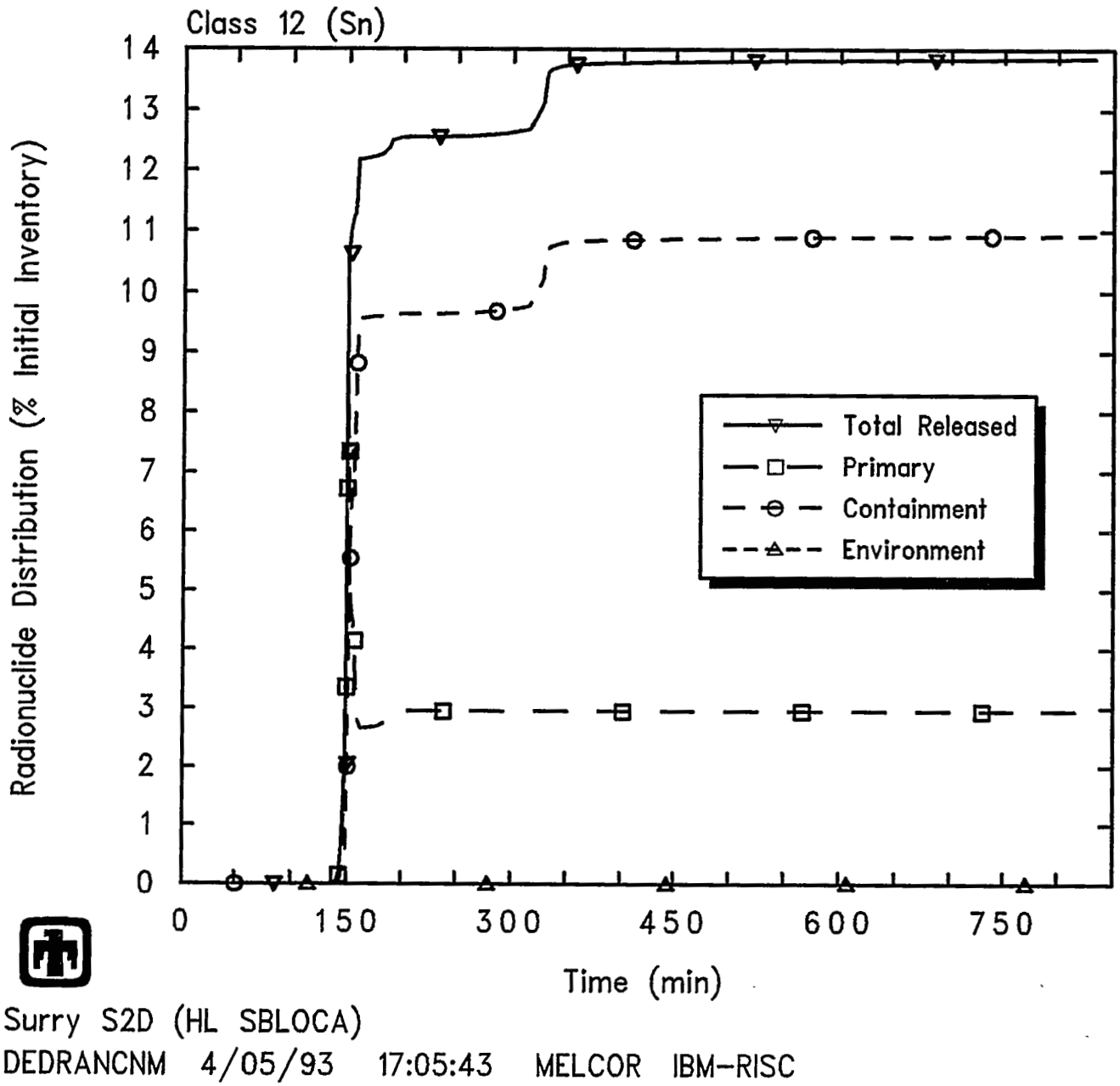

Figure 5.3.48 Distribution of Class 12 (Sn) Less Volatile Main Group Radionuclides in Primary System, Containment and Environment Predicted during S2D Sequence, as Percentage of Initial Inventory in Core

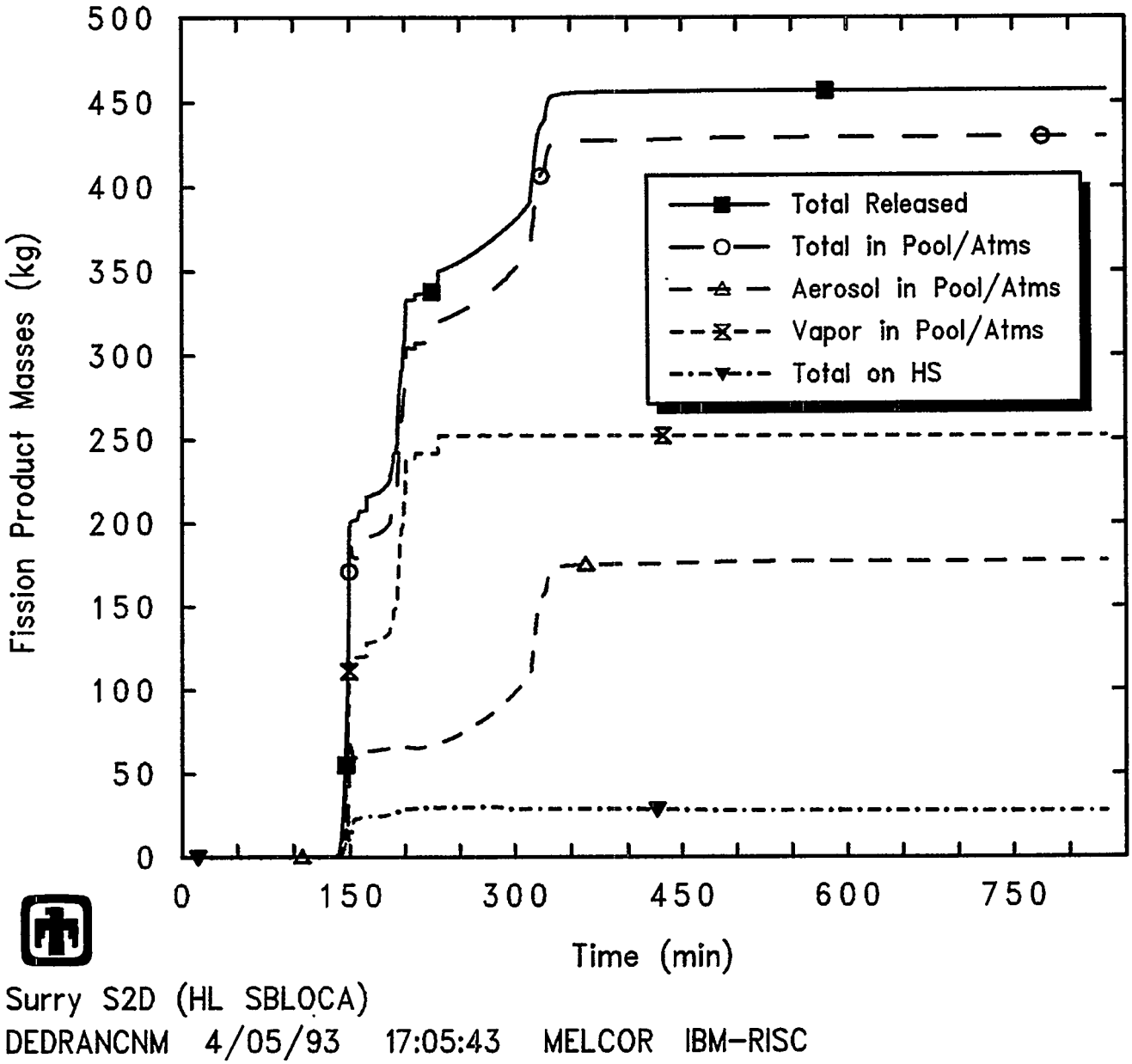

Figure 5.3.49 Total Fission Product Mass Released, and Overall Distribution, Predicted during S2D Sequence

Table 5.4.1 Sequence of Events Predicted during S3D Sequence, Compared to STCP

Key Event	Time (min)	
	STCP	MELCOR
Accident initiation	0.0	0.0
Containment coolers on	1.0	0.4
Start steam generator depressurization	30.0*	30.0*
Accumulators deliver until depleted	40.0 - 80.5	38.8 - 113.3 (First Flow) 656.0 - 701.0 (Second Flow
End steam generator depressurization	60.0*	110.1
Initial core uncovery begins	525.4	590.6
Gap release, Ring-1		606.2
Gap release, Ring-2		608.6
Gap release, Ring-3		617.3
Primary system PORVs open	658.0	616.7
Begin zircaloy oxidation		620.1
Core melt starts	687.3	625.0
Core slump	707.9	630.0
Core collapse	716.7	739.0 (Partial) Ring-2
Containment injection sprays on		850.9
Containment recirculation sprays on		855.1
Bottom head dryout	740.6	Does not occur prior to failure of bottom head
Bottom head failure	849.1	739.9 (Partial) Ring-2
Commence debris ejection		739.9
Begin concrete attack	850.1	740.0
Corium layers invert	921.1	900.0
RWST depleted		944.4
Containment injection sprays off		944.4
End of calculation	1,450.1	1,666.8

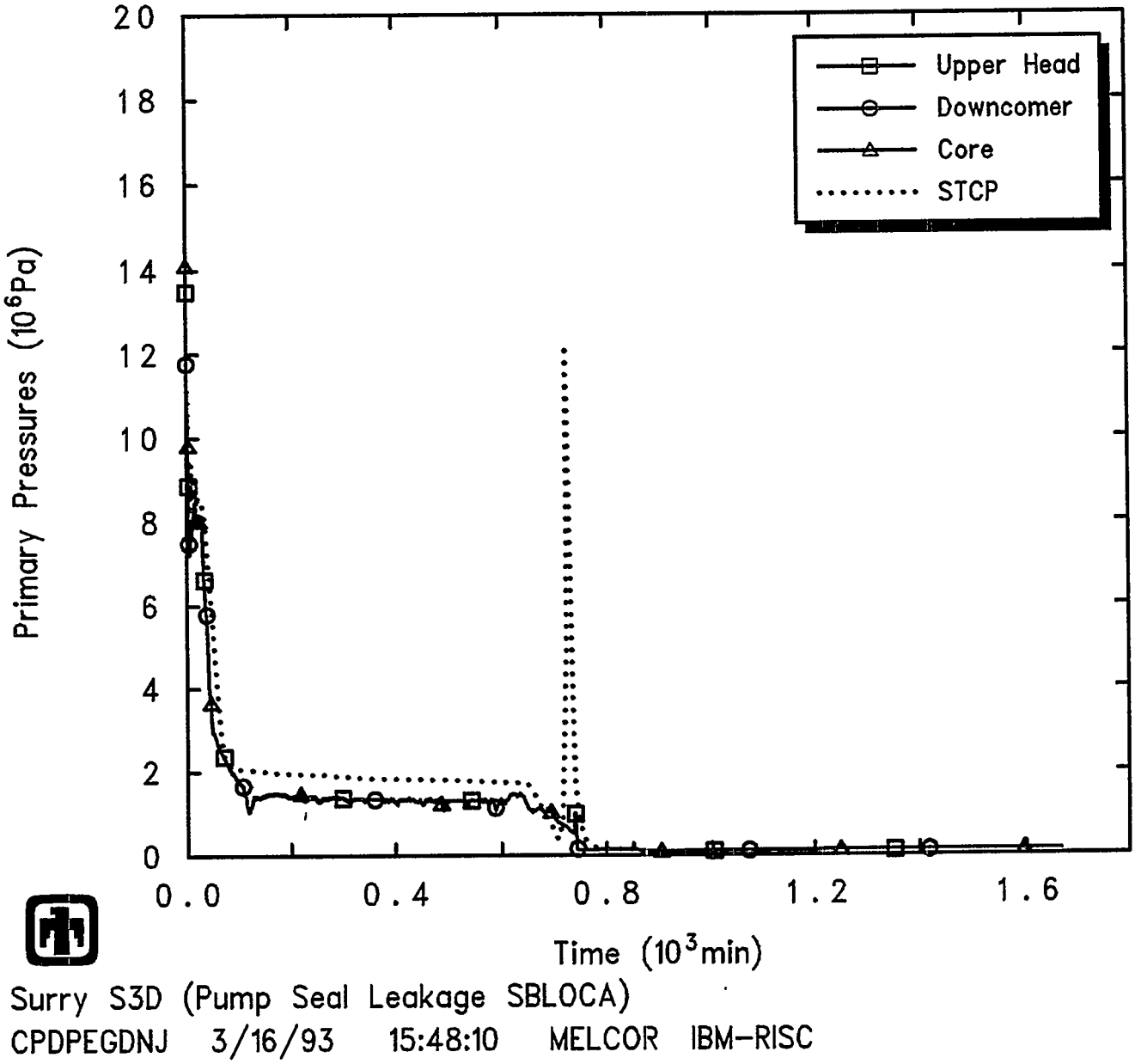

Figure 5.4.1 Primary System Pressures Predicted during S3D Sequence

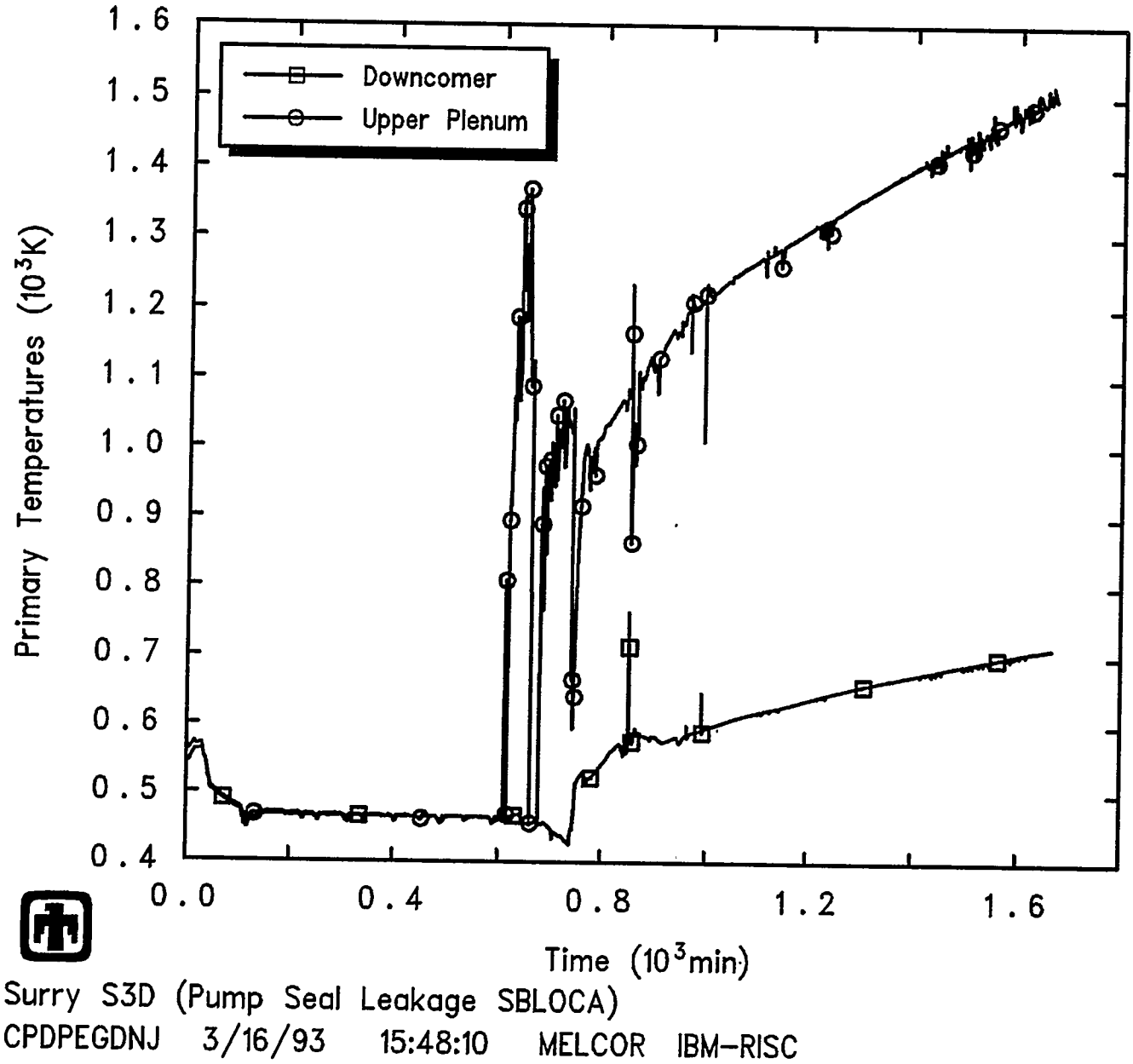

Figure 5.4.2 Primary System Temperatures, in Downcomer and in Upper Plenum, Predicted during S3D Sequence

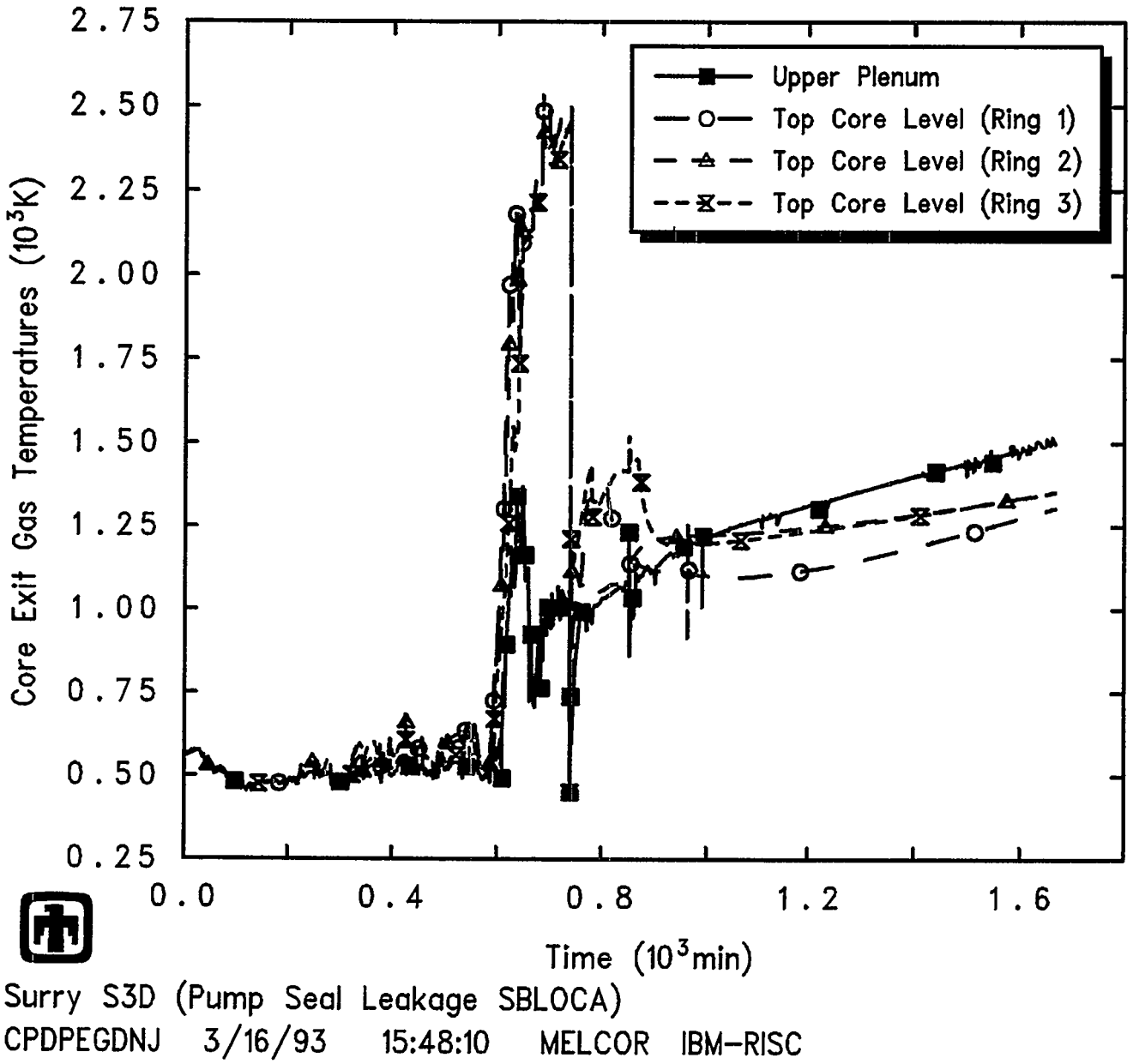

Figure 5.4.3 Core Exit Gas Temperatures, in Upper Plenum and in Uppermost Core Cells Predicted during S3D Sequence

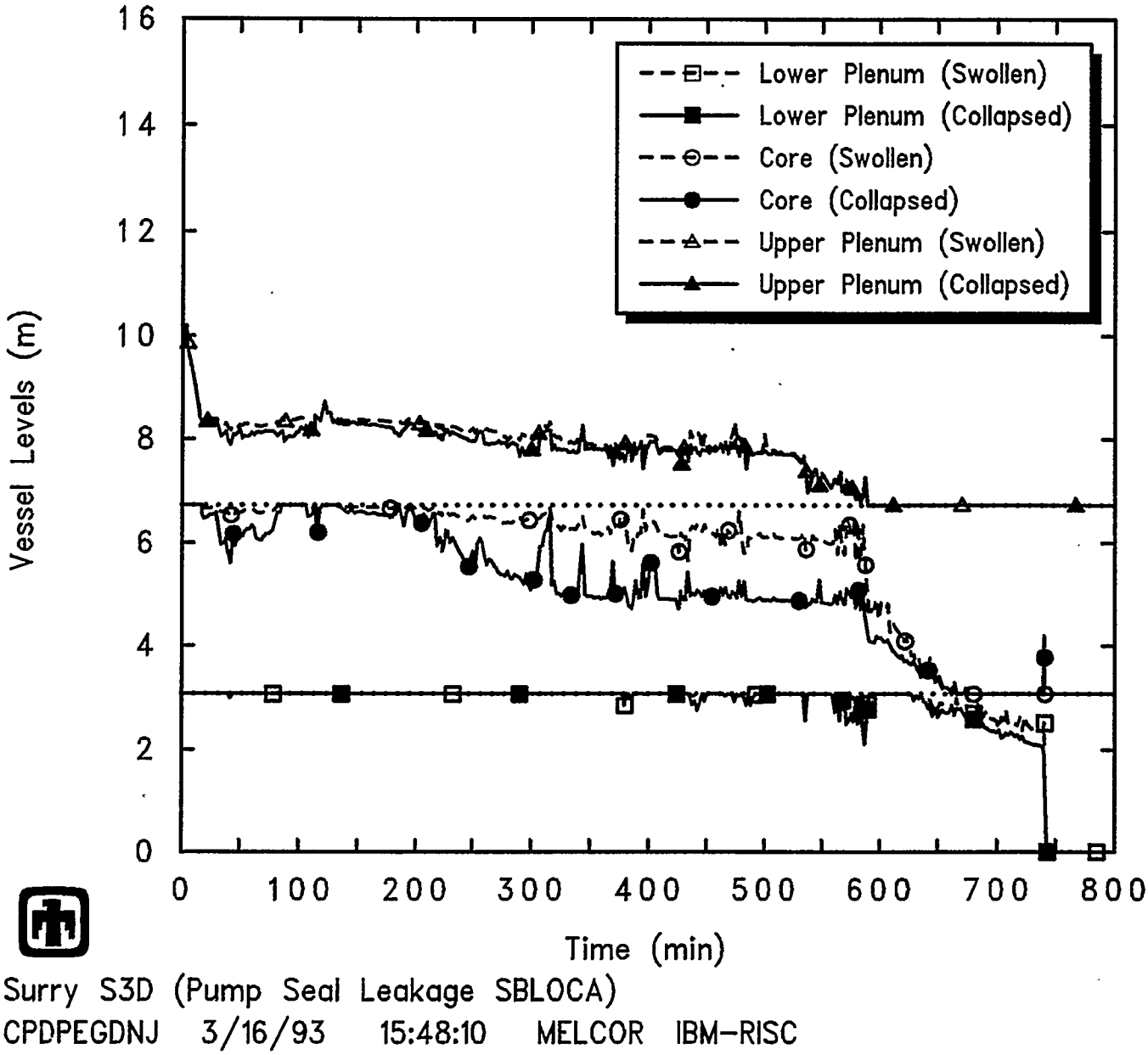

Figure 5.4.4 Reactor Vessel Liquid Levels Predicted during S3D Sequence

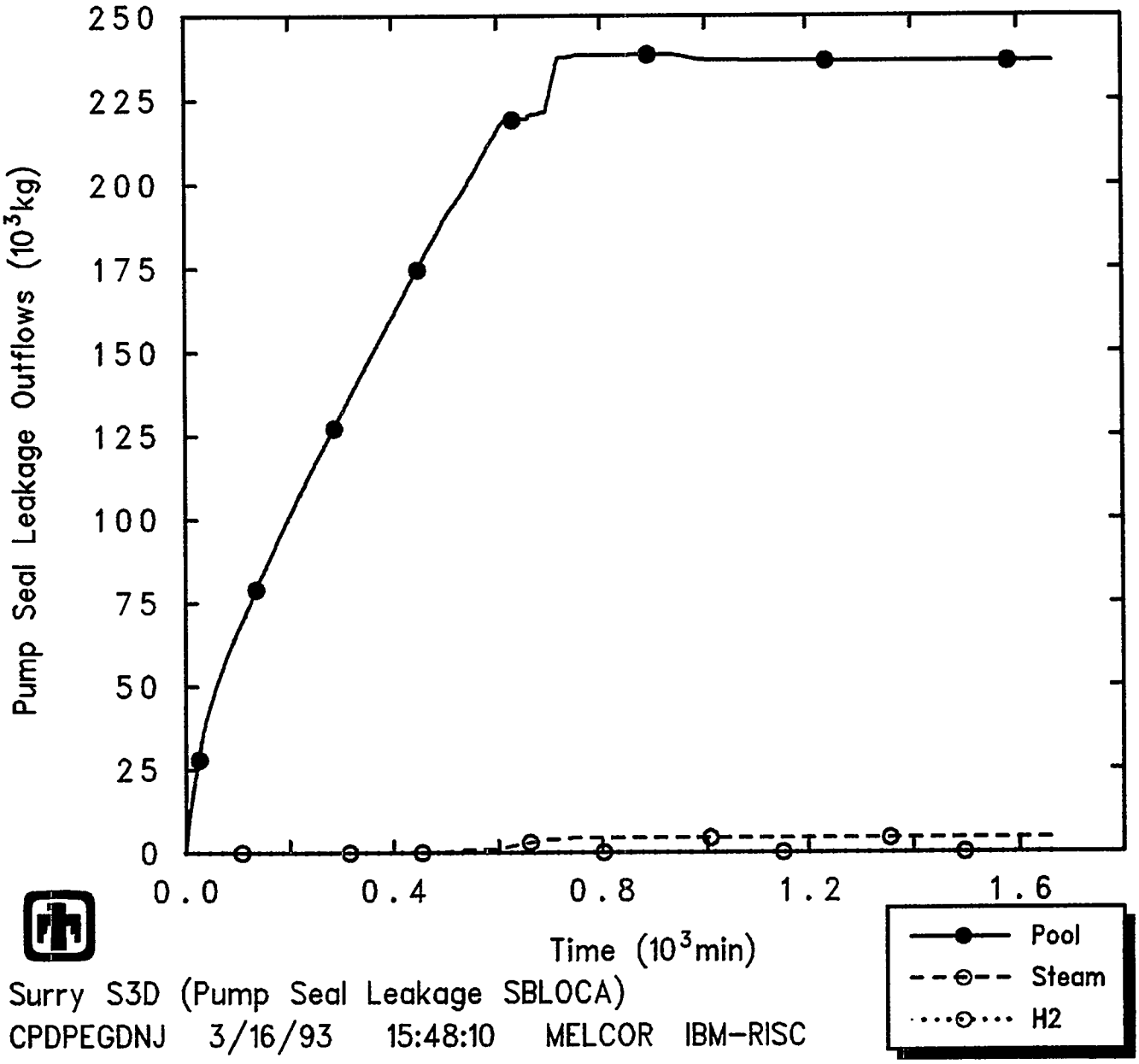

Figure 5.4.5 Integrated Outflows of Liquid, Steam and Hydrogen through the Hot Leg Break Predicted during S3D Sequence

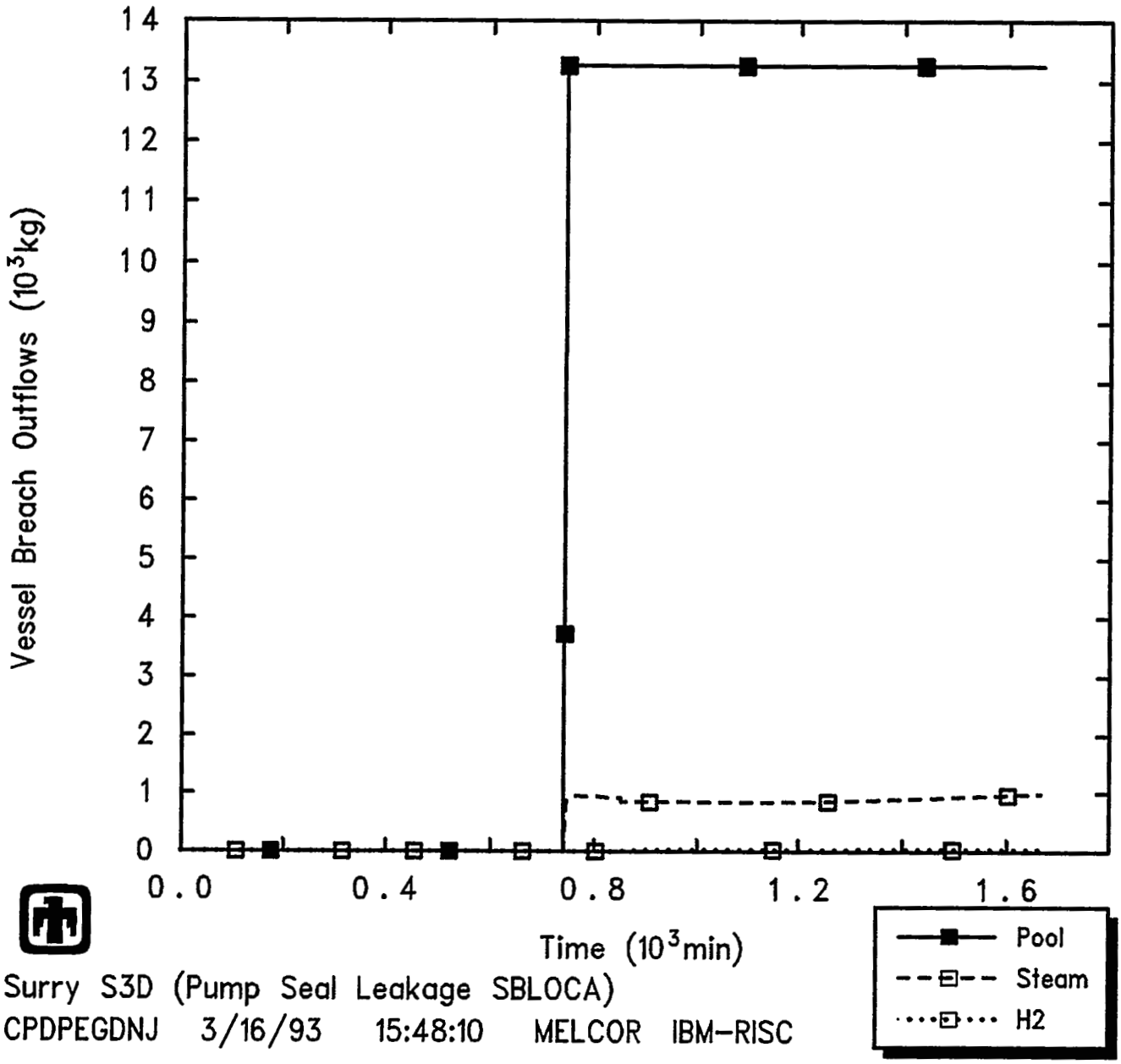

Figure 5.4.6 Integrated Outflows of Liquid, Steam and Hydrogen through the Vessel Breach Predicted during S3D Sequence

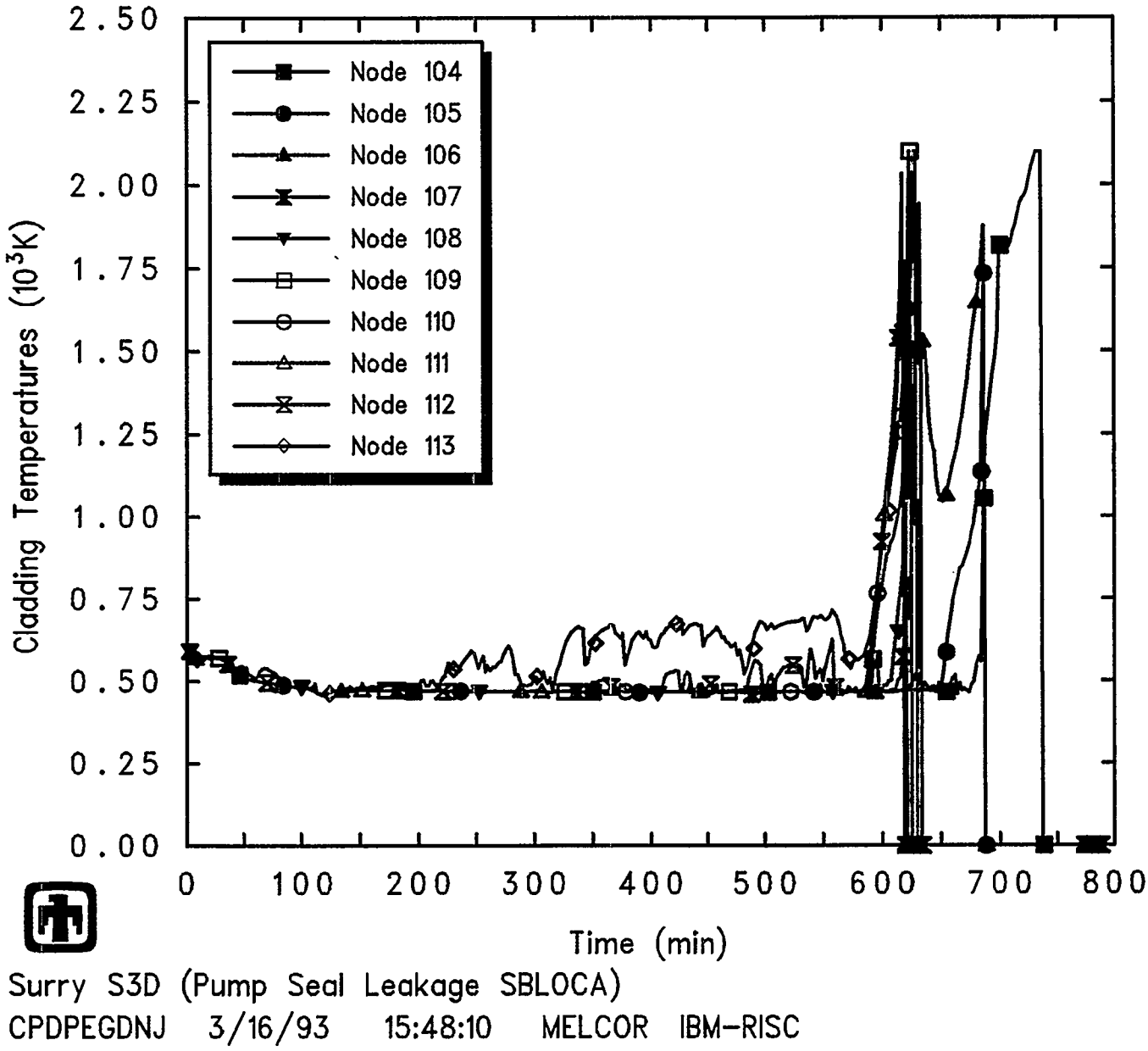

Figure 5.4.7 Core Ring 1 Clad Temperatures Predicted during S3D Sequence

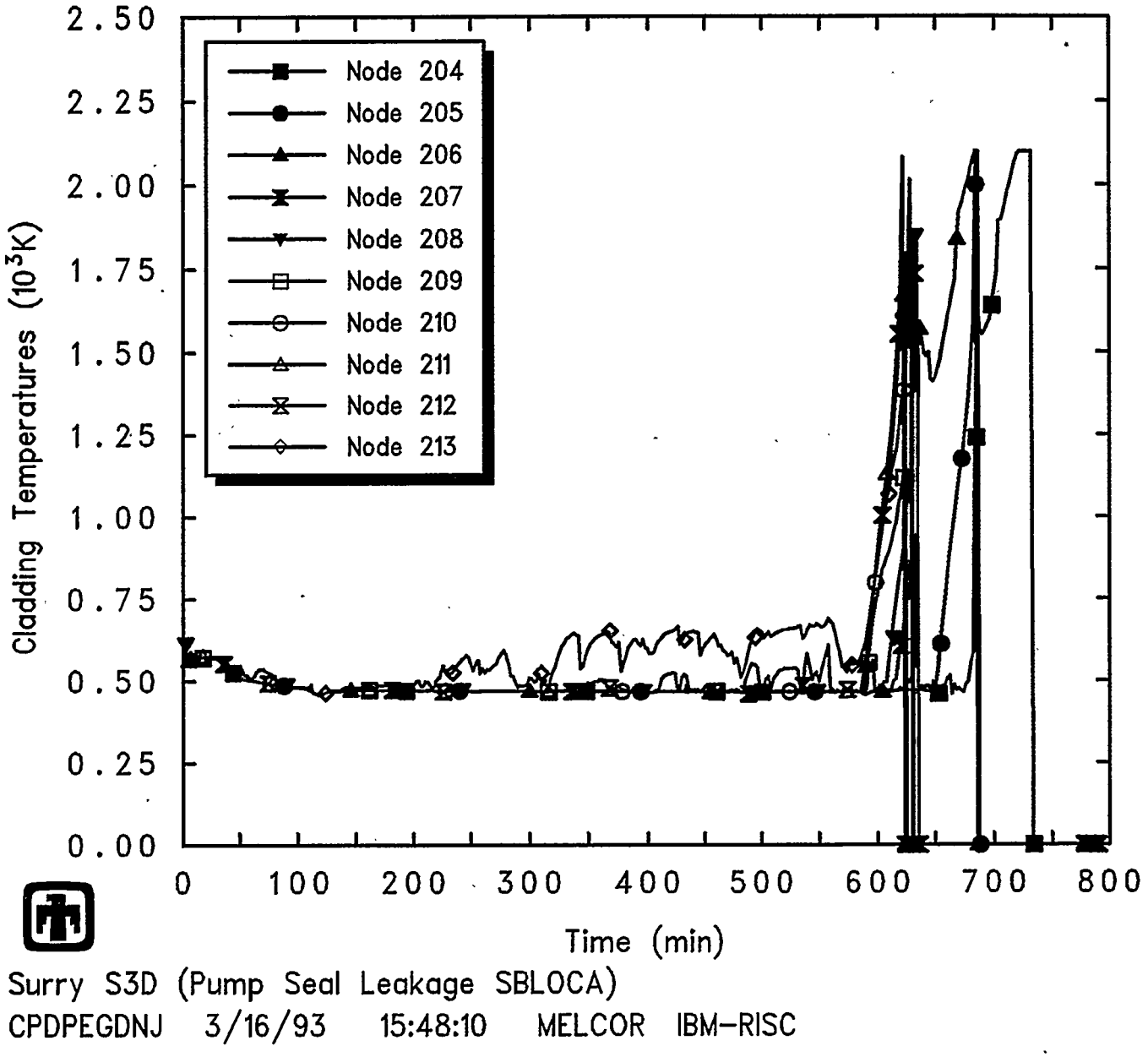

Figure 5.4.8 Core Ring 2 Clad Temperatures Predicted during S3D Sequence

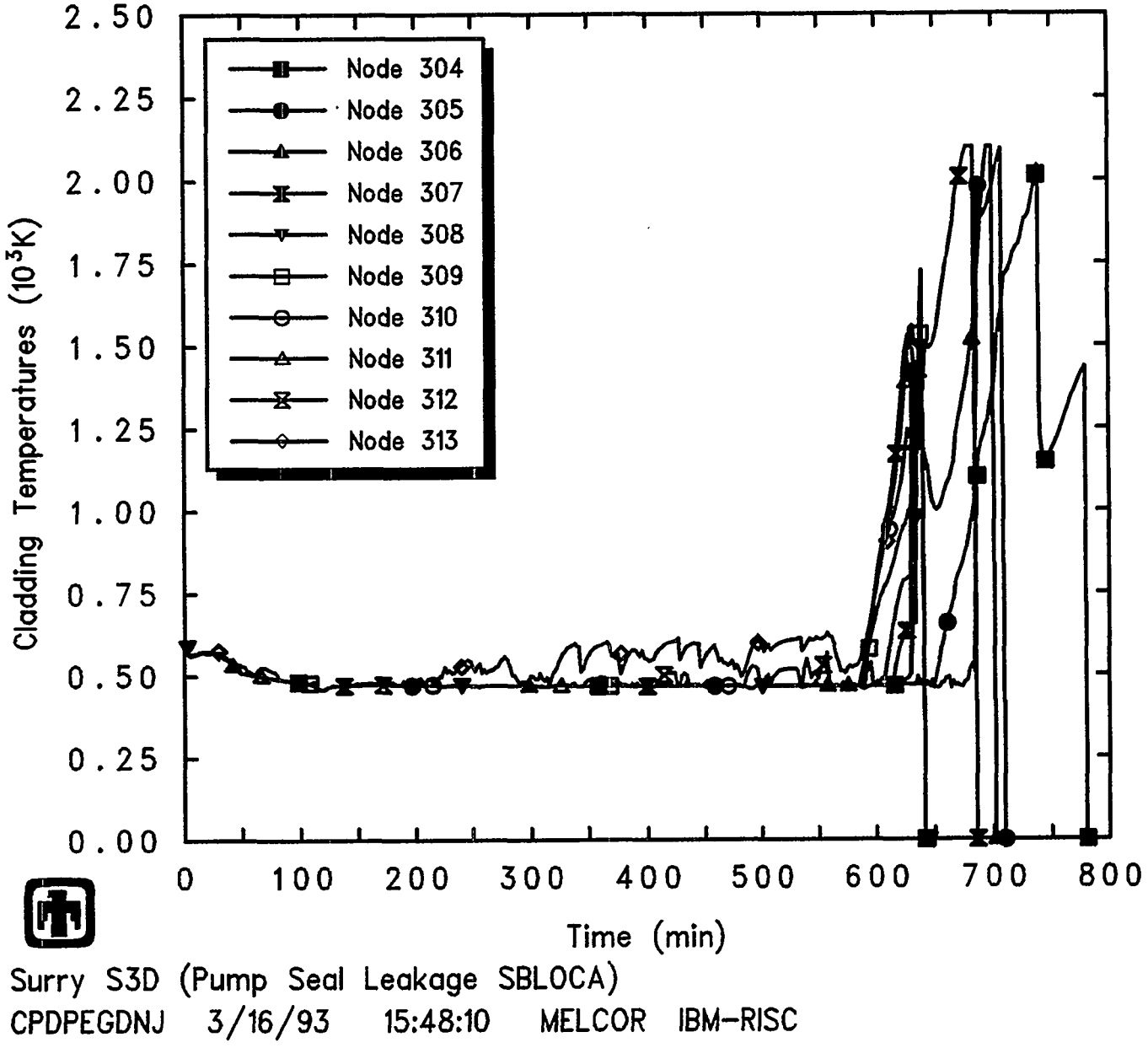

Figure 5.4.9 Core Ring 3 Clad Temperatures Predicted during S3D Sequence

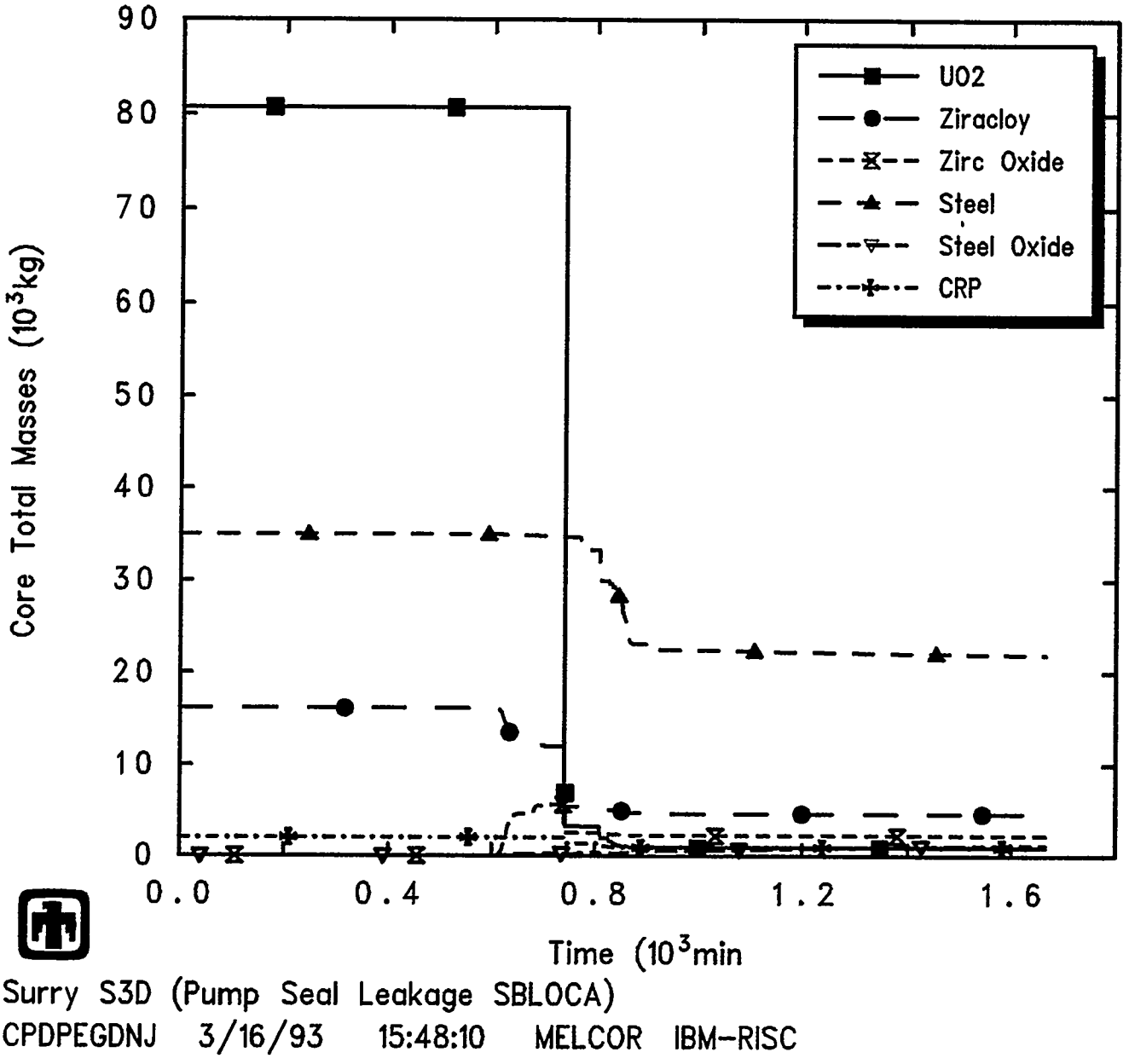

Figure 5.4.10 Core Total Material Masses Predicted during S3D Sequence

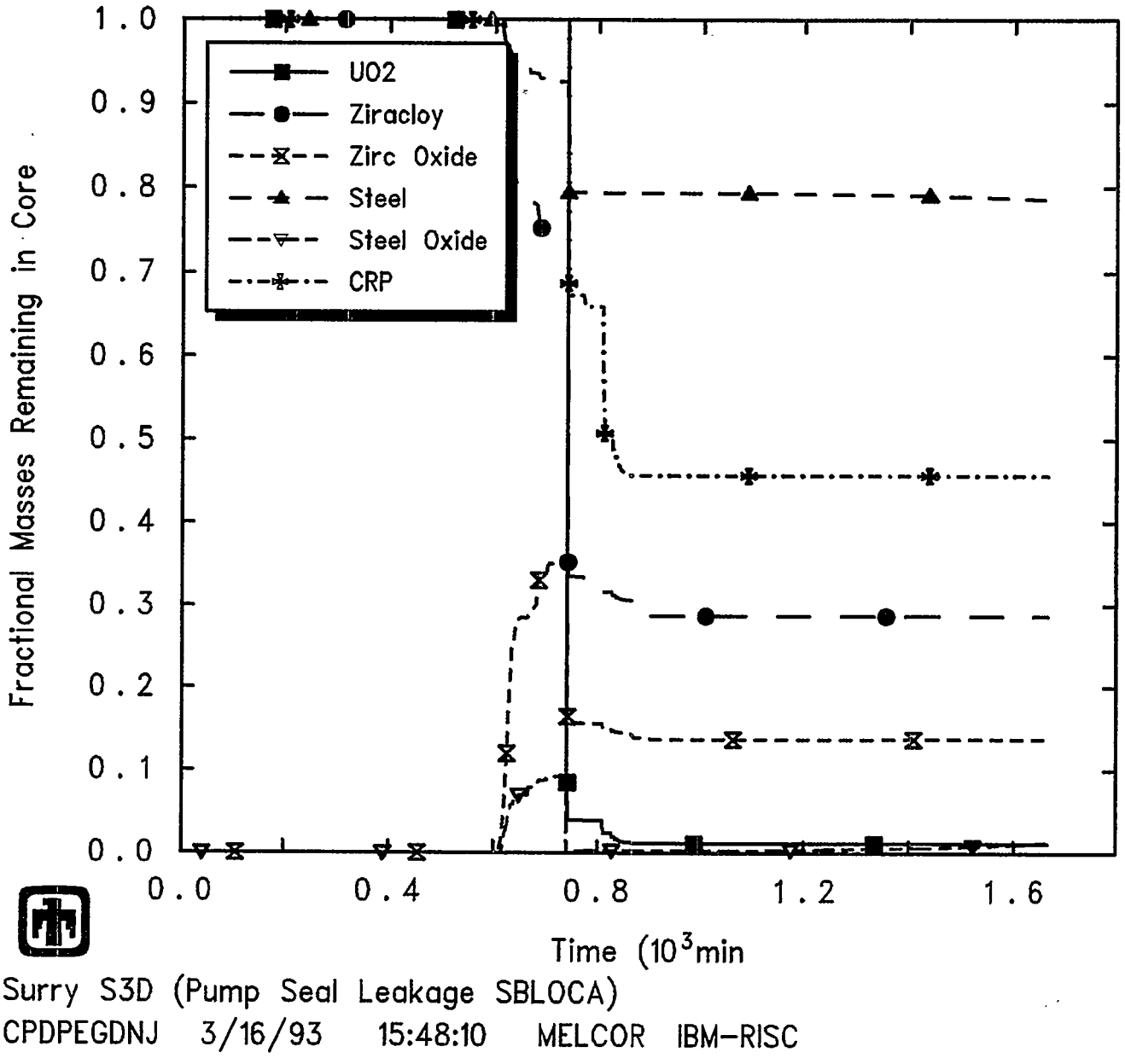

Figure 5.4.11 Core Fractional Material Masses Predicted during S3D Sequence

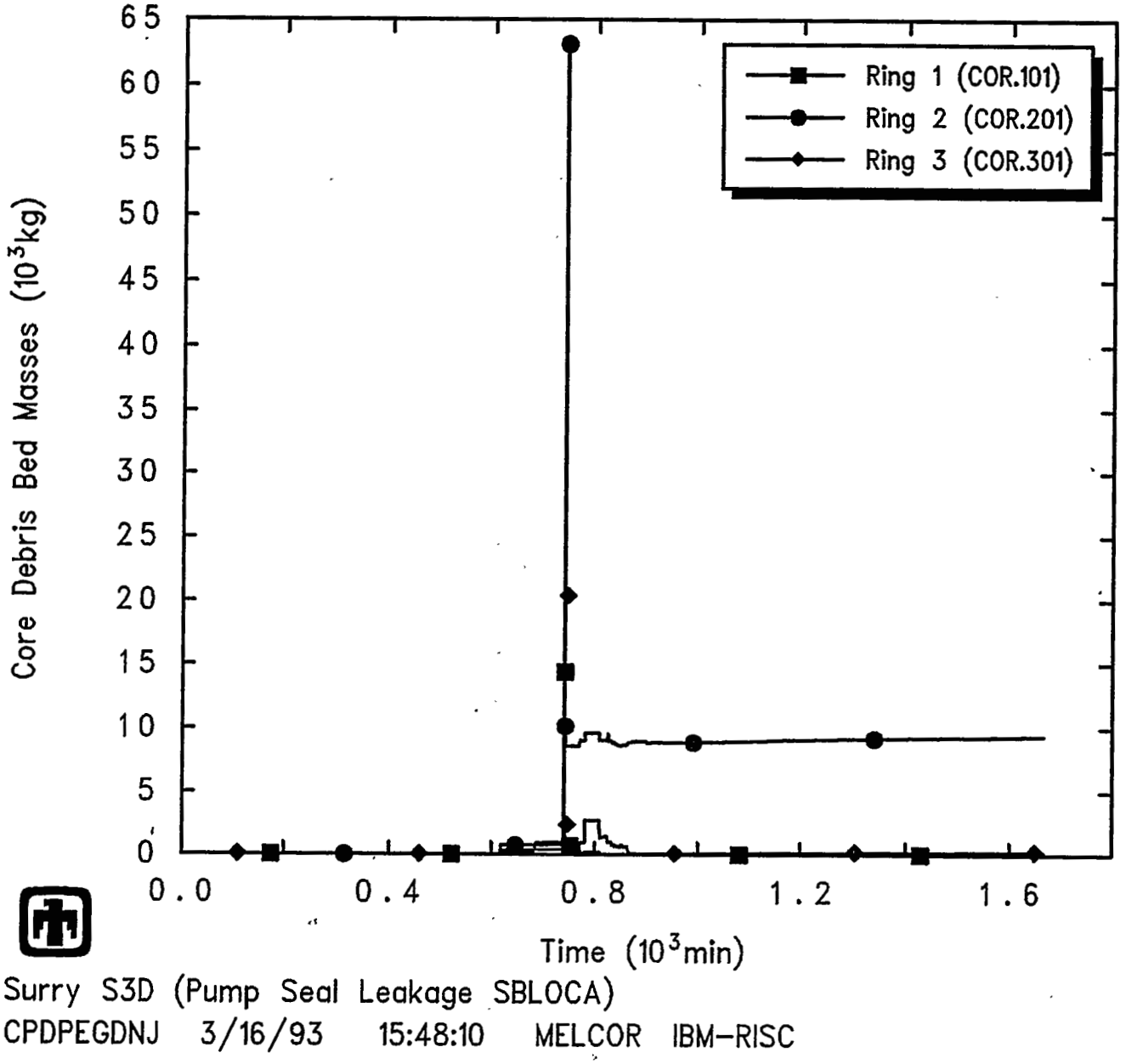

Figure 5.4.12 Lower Plenum Debris Bed Masses Predicted during S3D Sequence

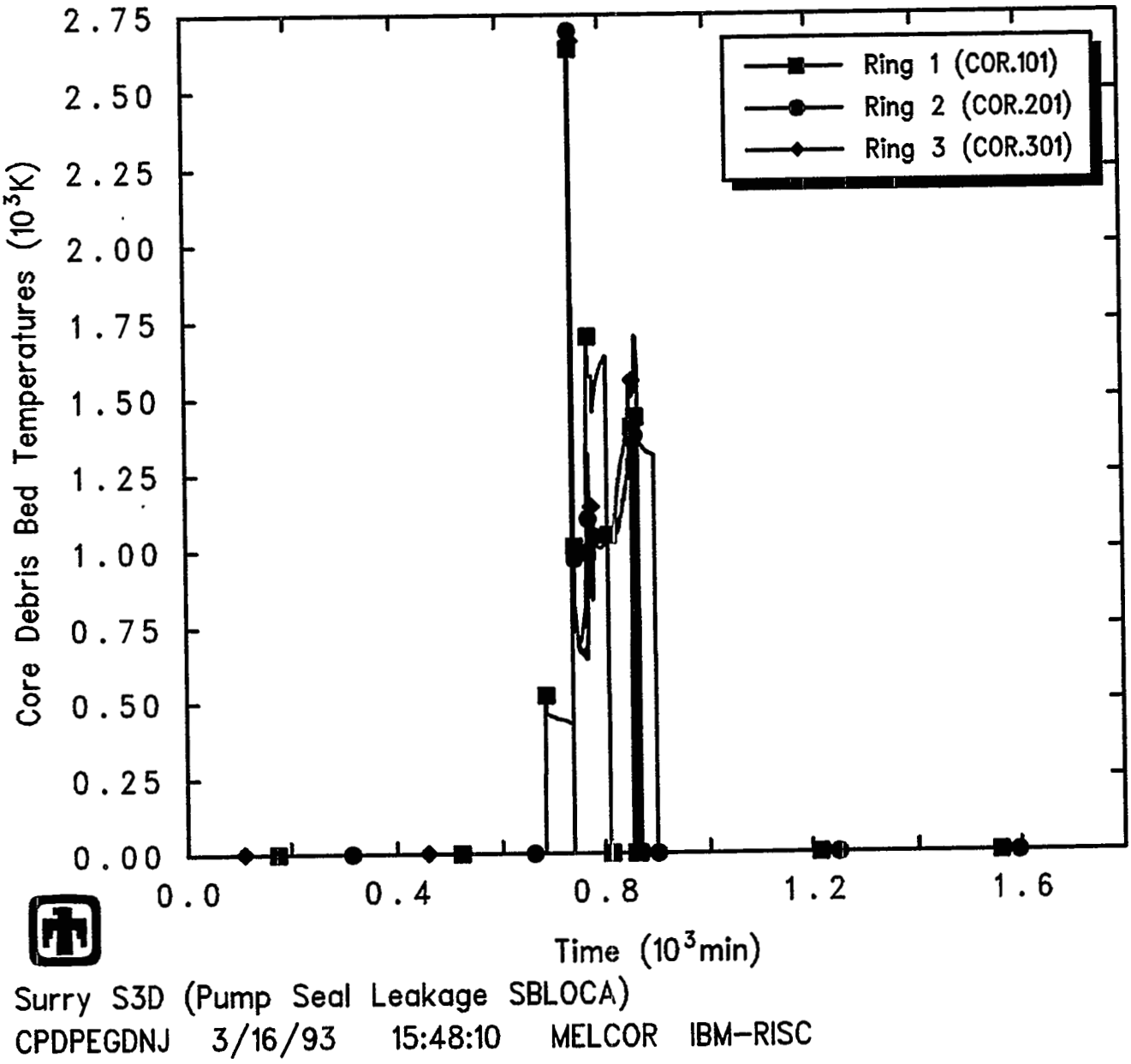

Figure 5.4.13 Lower Plenum Debris Bed Temperatures Predicted during S3D Sequence

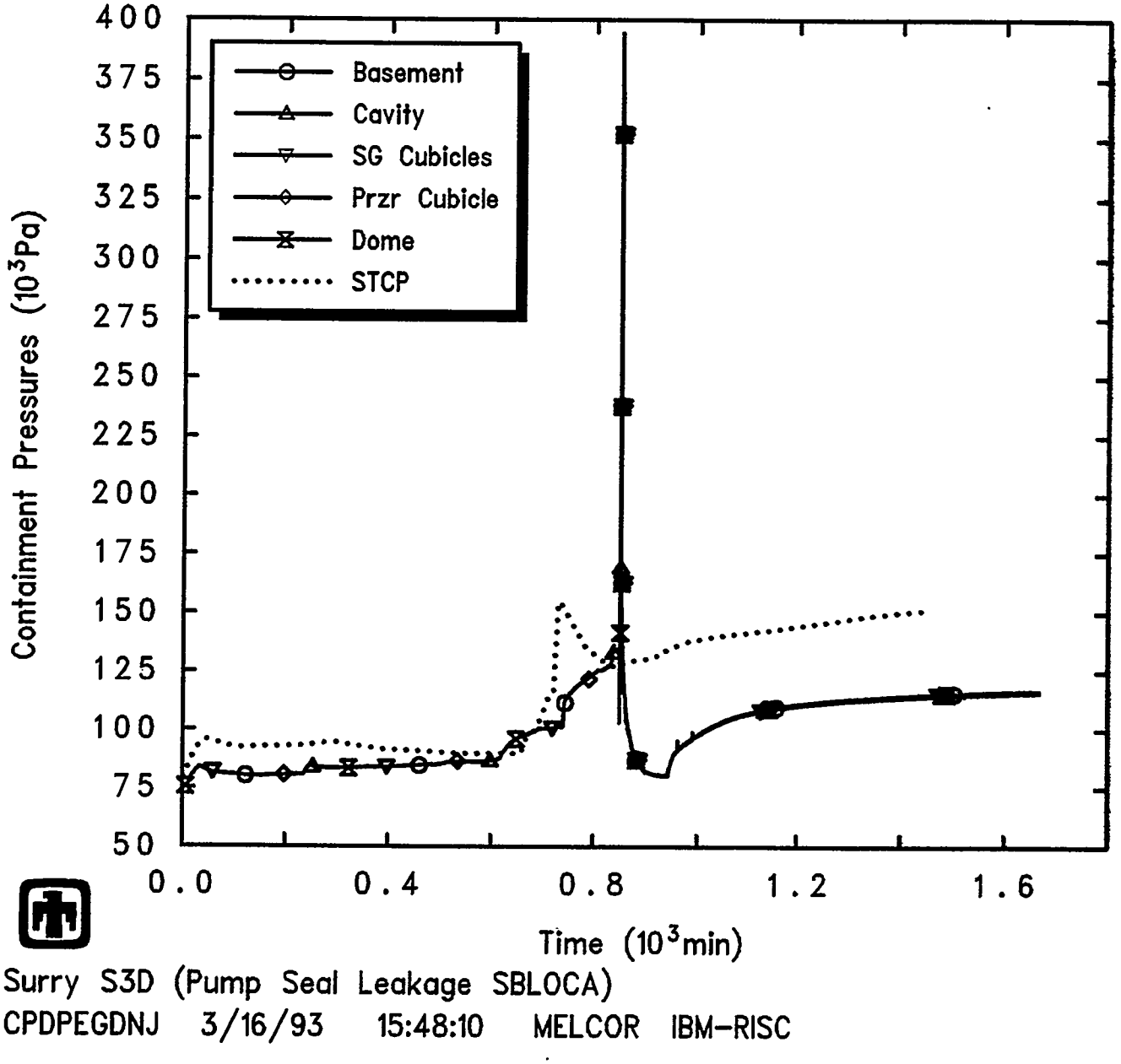

Figure 5.4.14 Containment System Pressures Predicted during S3D Sequence

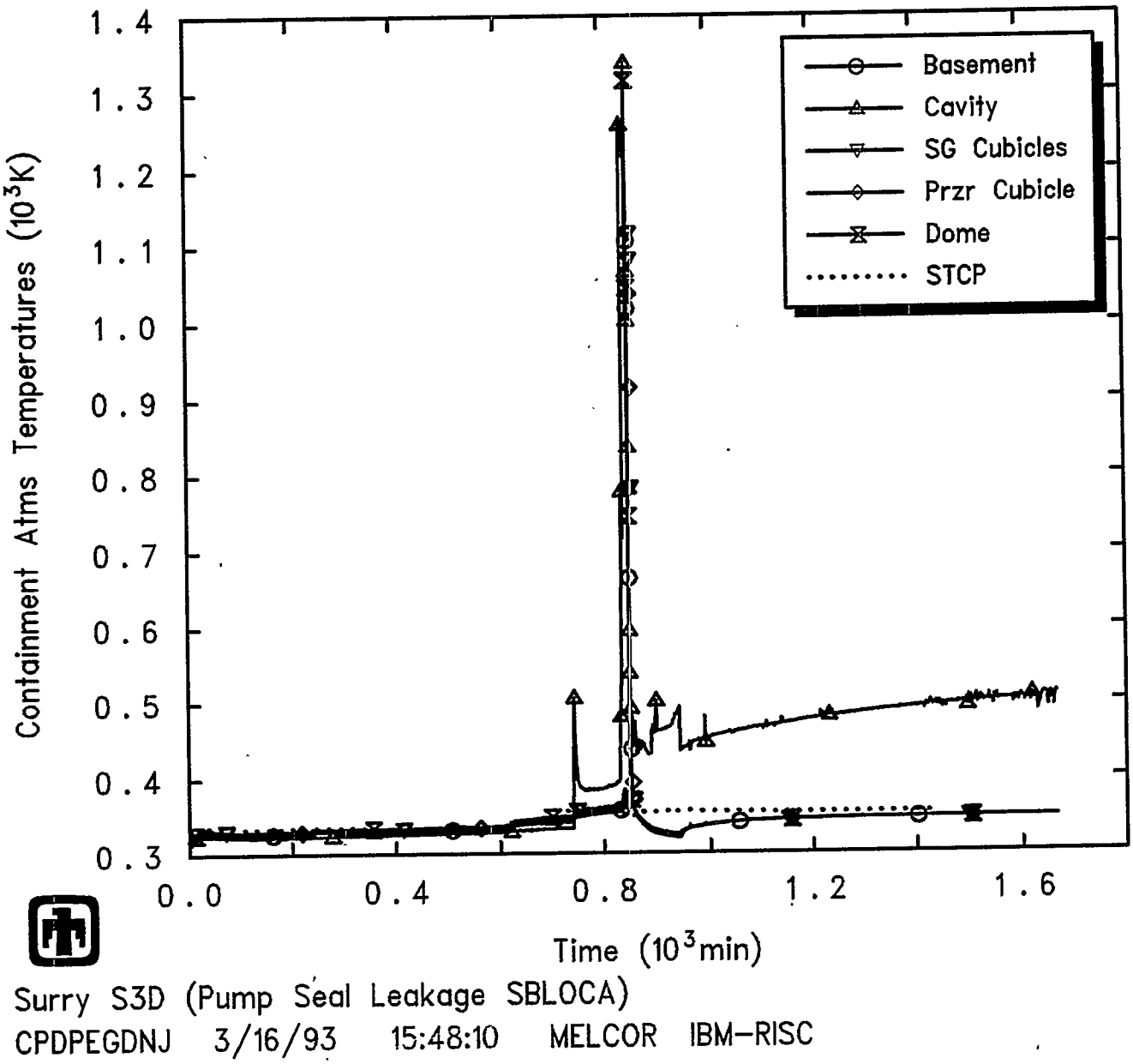

Figure 5.4.15 Containment System Atmosphere Temperatures Predicted during S3D Sequence

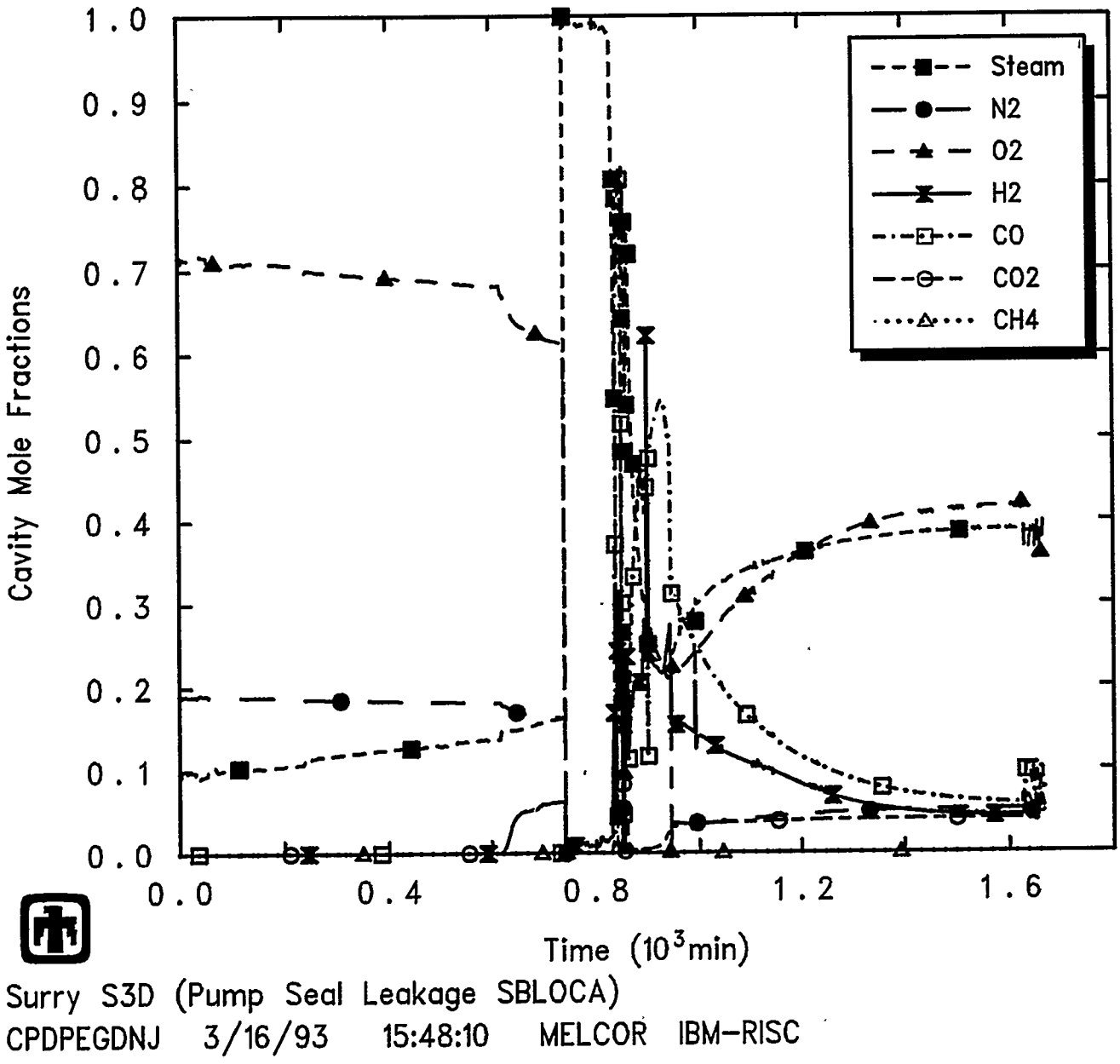

Figure 5.4.16 Cavity Steam and Noncondensable Mole Fractions Predicted during S3D Sequence

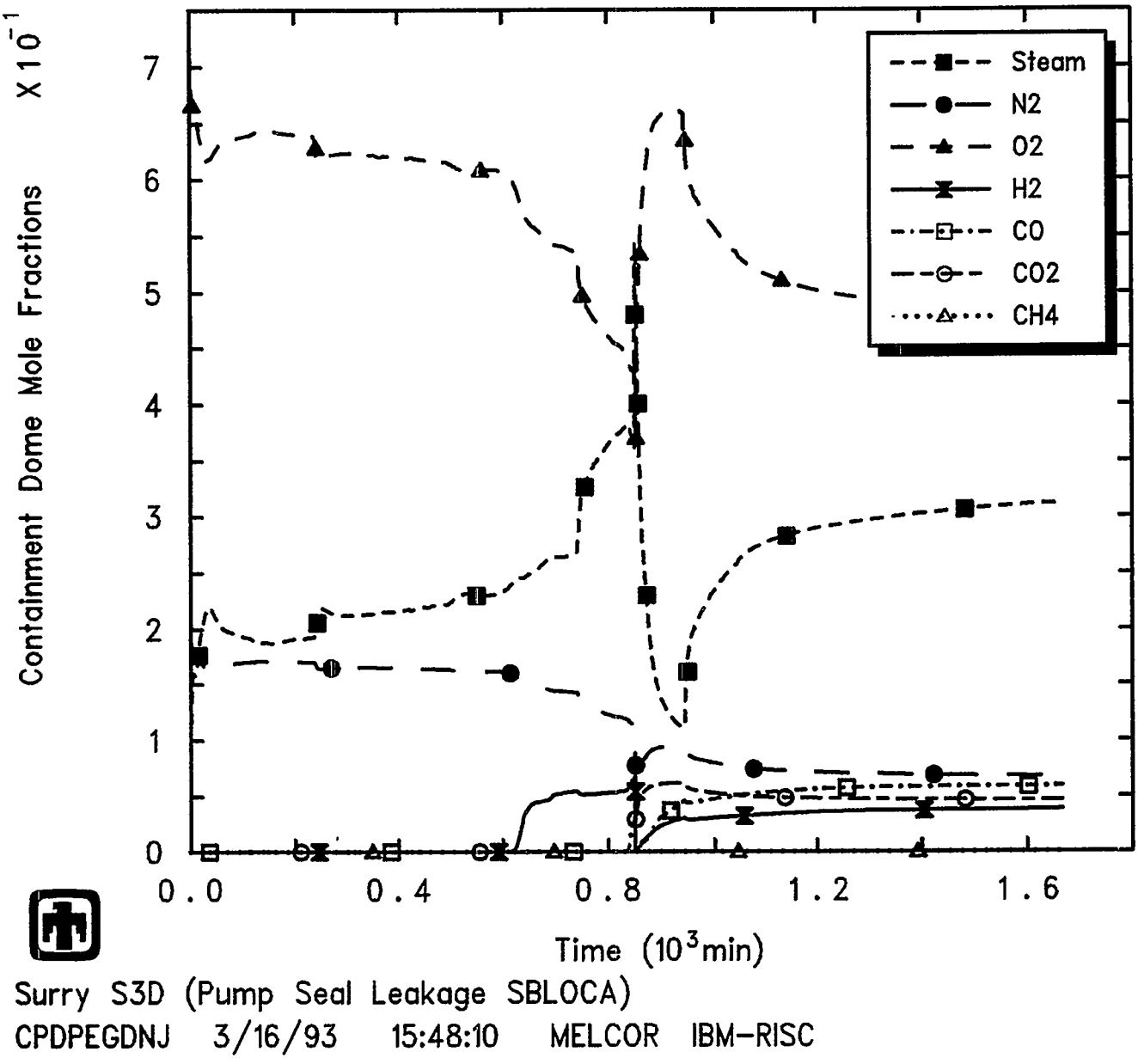

Figure 5.4.17 Containment Dome Steam and Noncondensable Mole Fractions Predicted during S3D Sequence

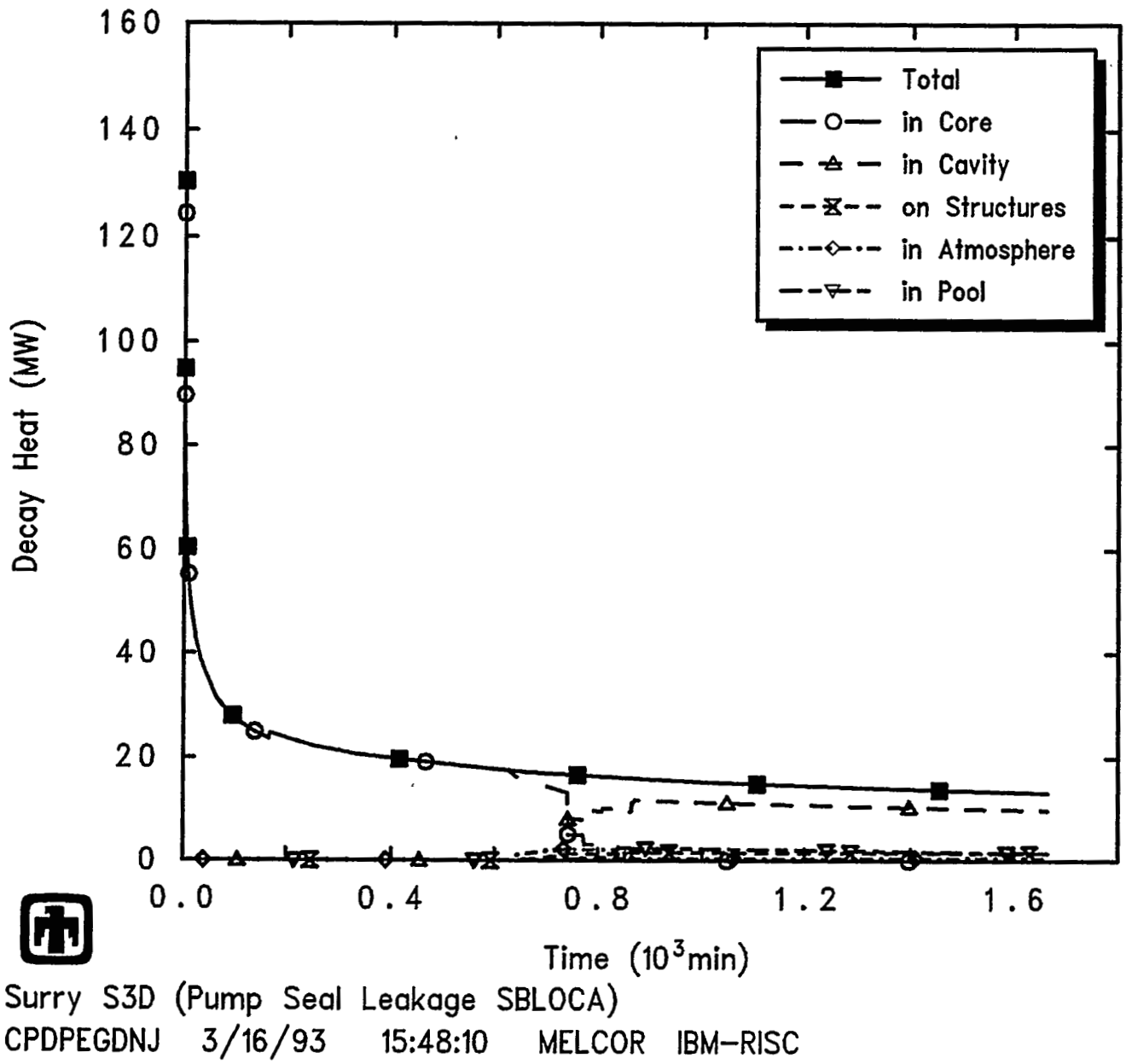

Figure 5.4.18 Decay Heat Predicted during S3D Sequence

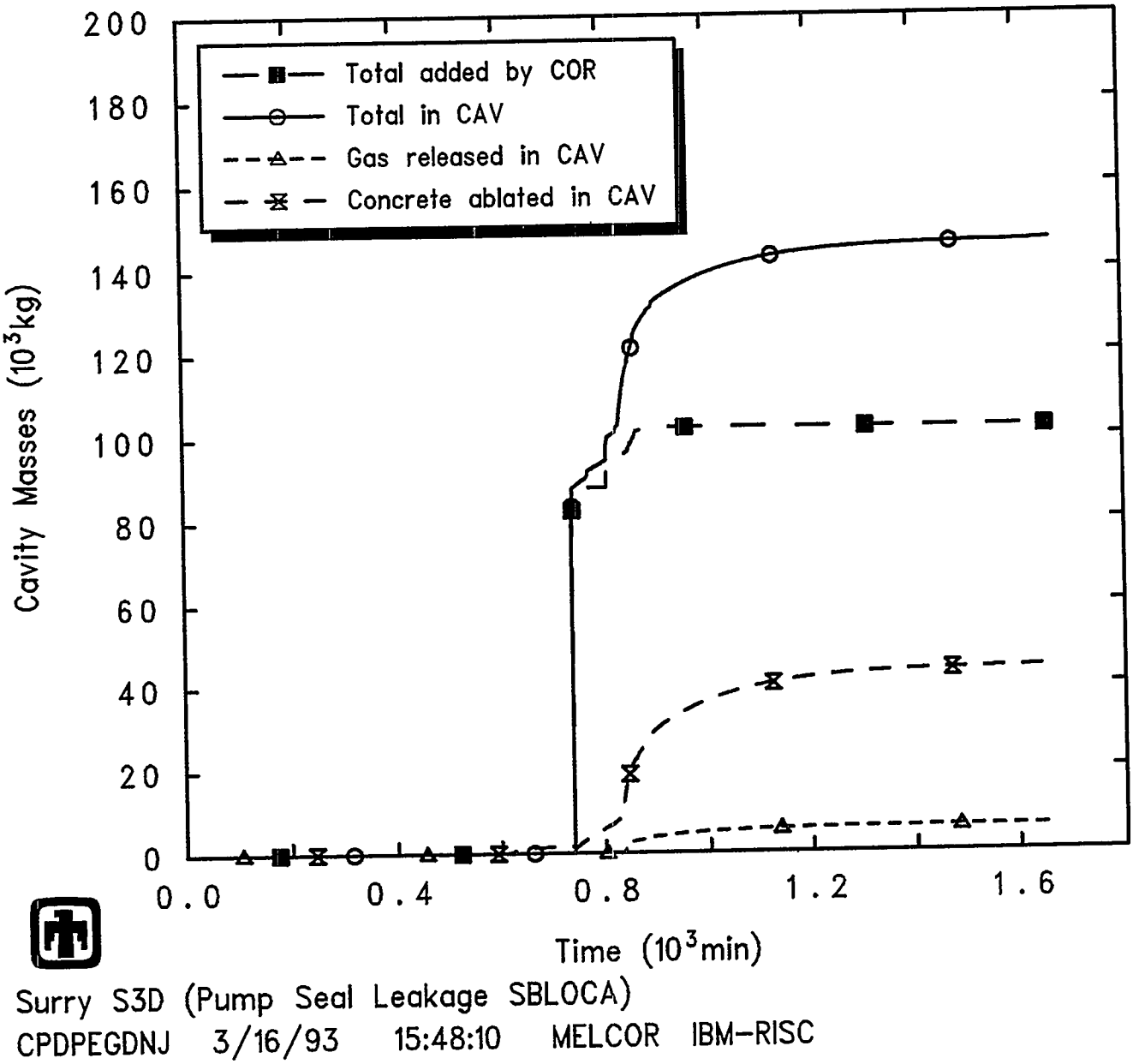

Figure 5.4.19 Total Cavity Masses in Cavity Predicted during S3D Sequence

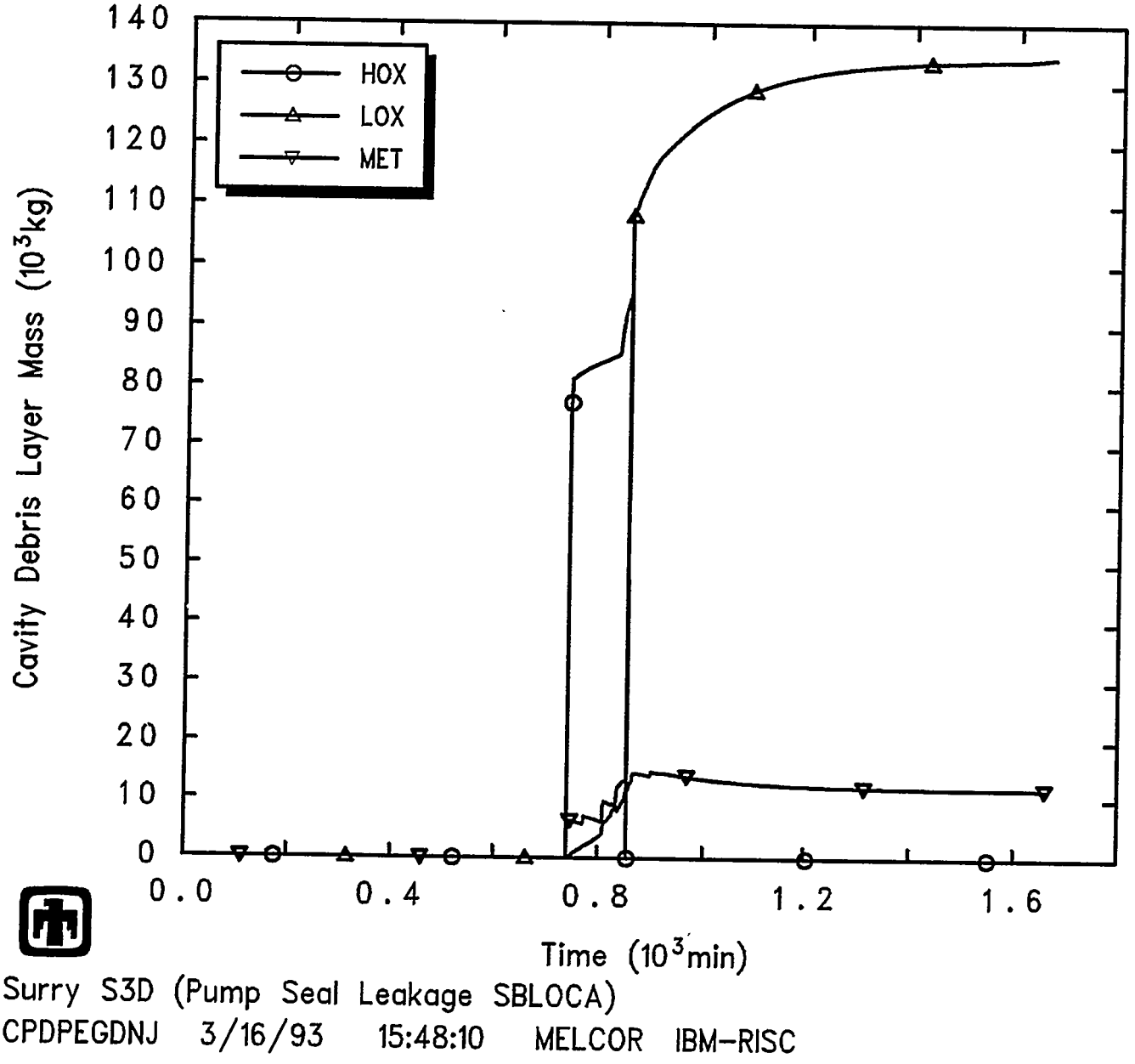

Figure 5.4.20 Cavity Layer Masses Predicted during S3D Sequence

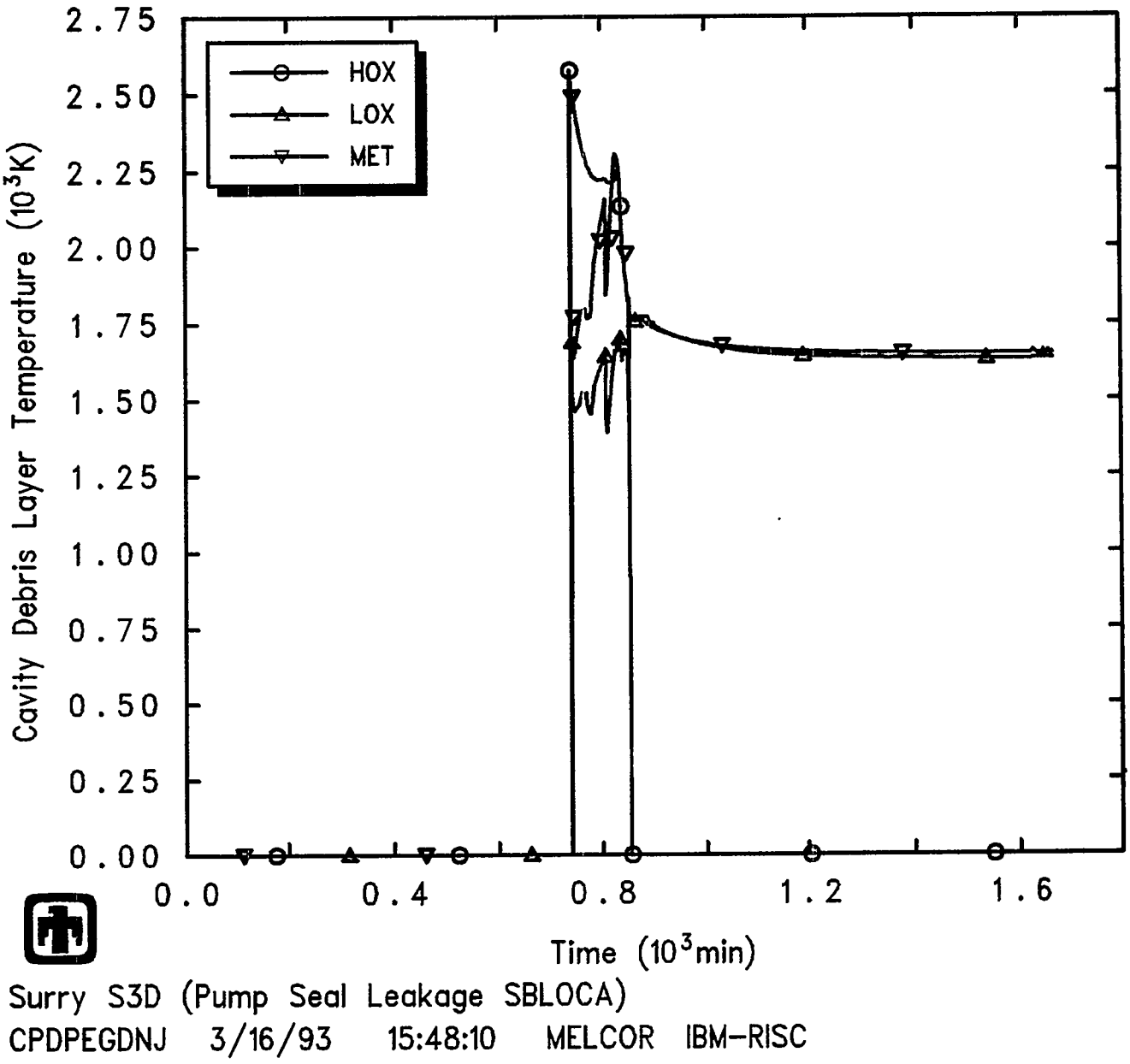

Figure 5.4.21 Cavity Layer Temperatures Predicted during S3D Sequence

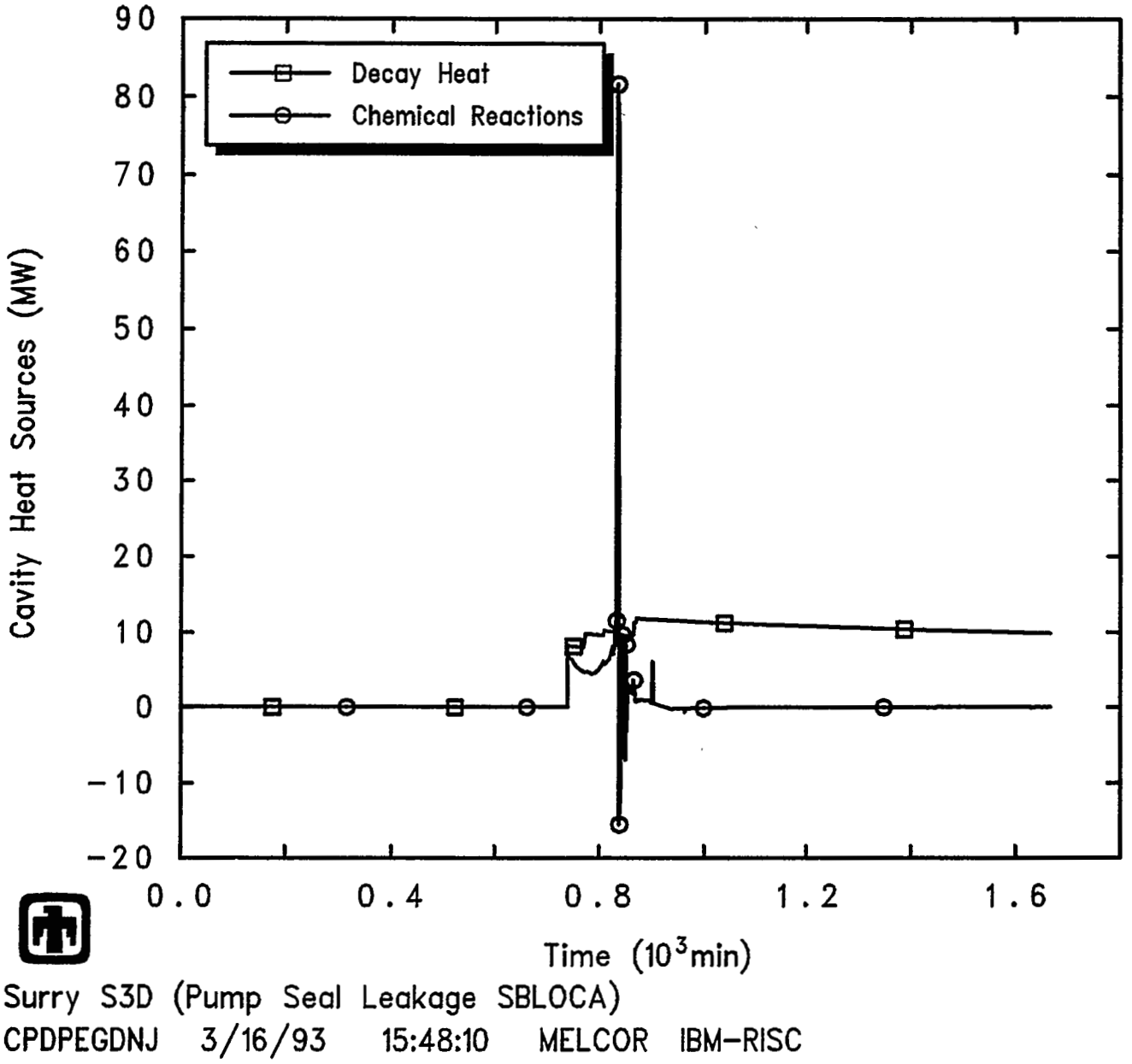

Figure 5.4.22 Decay Heat and Chemical Energy in Cavity Predicted during S3D Sequence

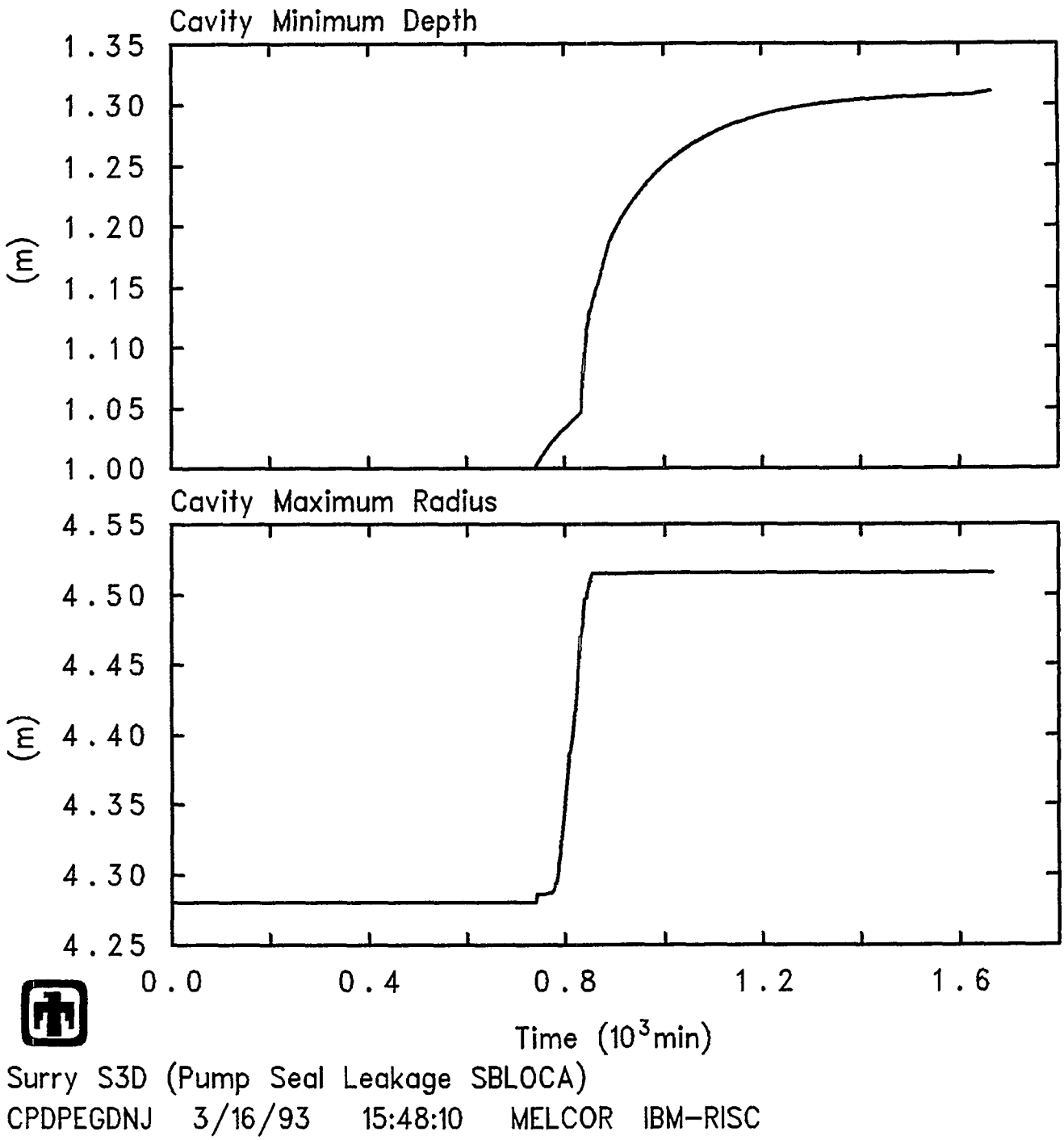

Figure 5.4.23 Cavity Maximum Radius and Minimum Depth Predicted during S3D Sequence

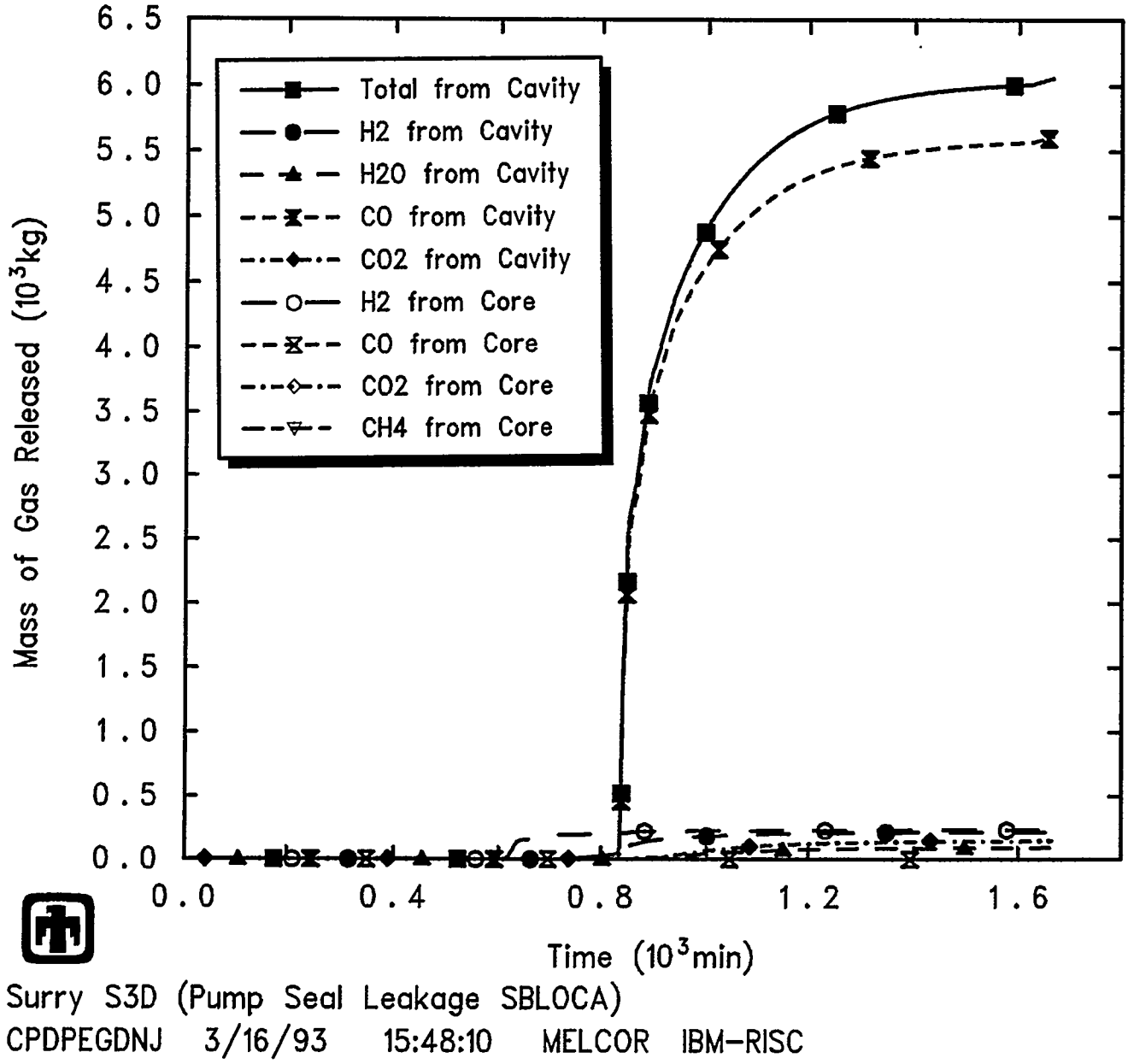

Figure 5.4.24 Gas Generation Predicted in Core and in Cavity during S3D Sequence

Table 5.4.2 Radionuclide Distribution at 1,668min for S3D Sequence

Radionuclides Species Group and Representative Element	Core	RCS	Cavity	Containment
Noble Gases, Xe	5.59E-12	2.36E-03	0	0.998
Alkali Metals, Cs	1.21E-11	0.528	3.88E-10	0.472
Alkaline Earths, Ba	1.23E-11	0.270	0.510	0.220
Halogens, I	8.51E-12	2.36E-03	0	0.998
Chalcogens, Te	1.29E-11	0.218	0.372	0.410
Platinoids, Ru	1.69E-11	1.29E-02	0.983	3.77E-03
Transition Metals, Mo	4.80E-12	0.128	0.812	6.02E-02
Tetravalents, Ce	1.38E-11	2.64E-04	1.0	8.57E-05
Trivalents, La	5.79E-12	1.63E-03	0.995	3.75E-03
Uranium, U	8.89E-12	1.47E-03	0.998	4.33E-04
More Volatile Main Group Metals, Cd	5.36E-12	0.554	0.262	0.184
Less Volatile Main Group Metals, Sn	1.17E-11	0.554	0.253	0.193

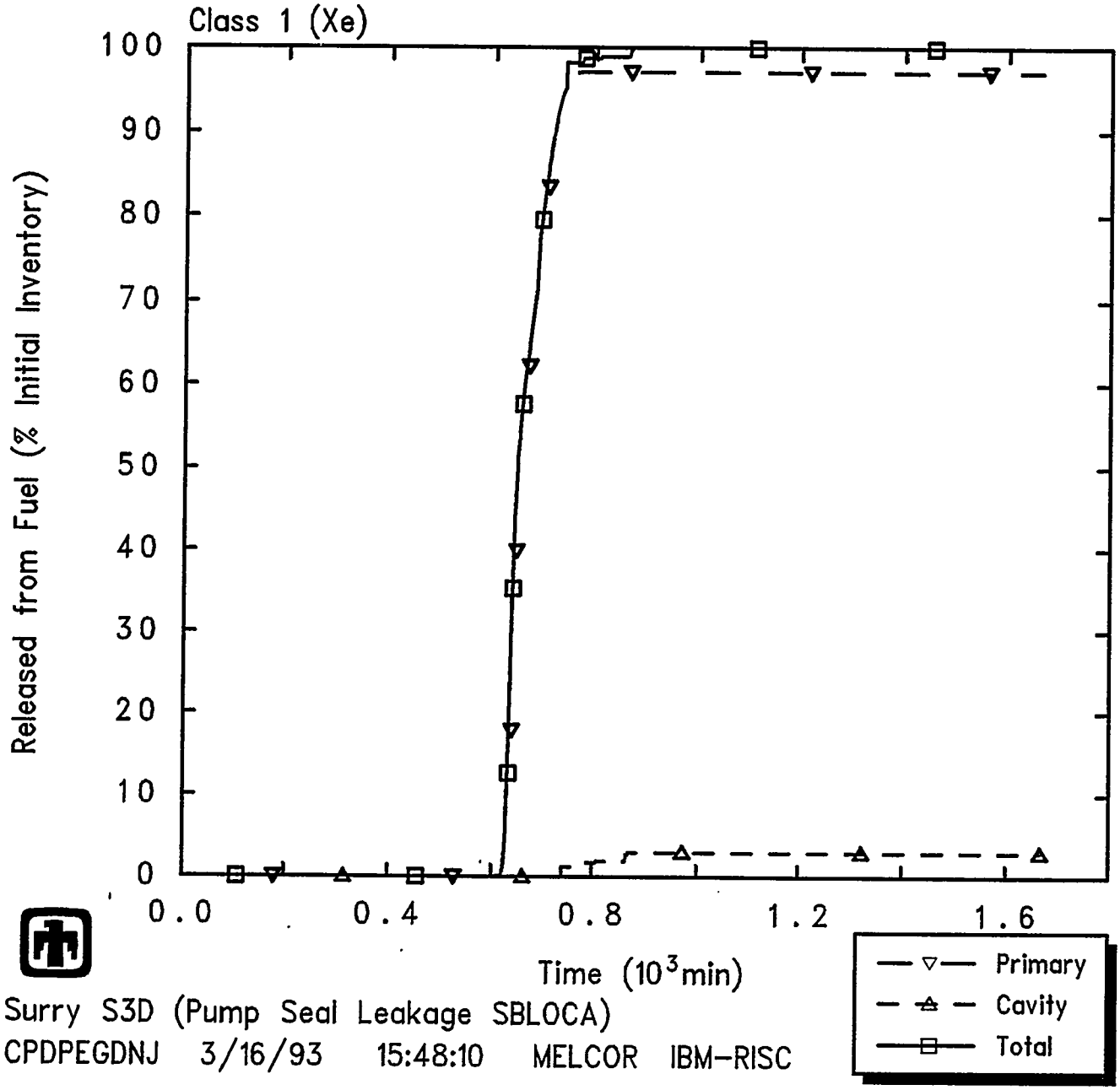

Figure 5.4.25 Release of Class 1 (Xe) Noble Gas Radionuclides from Fuel in Core and in Cavity Predicted during S3D Sequence, as Percentage of Initial Inventory in Core

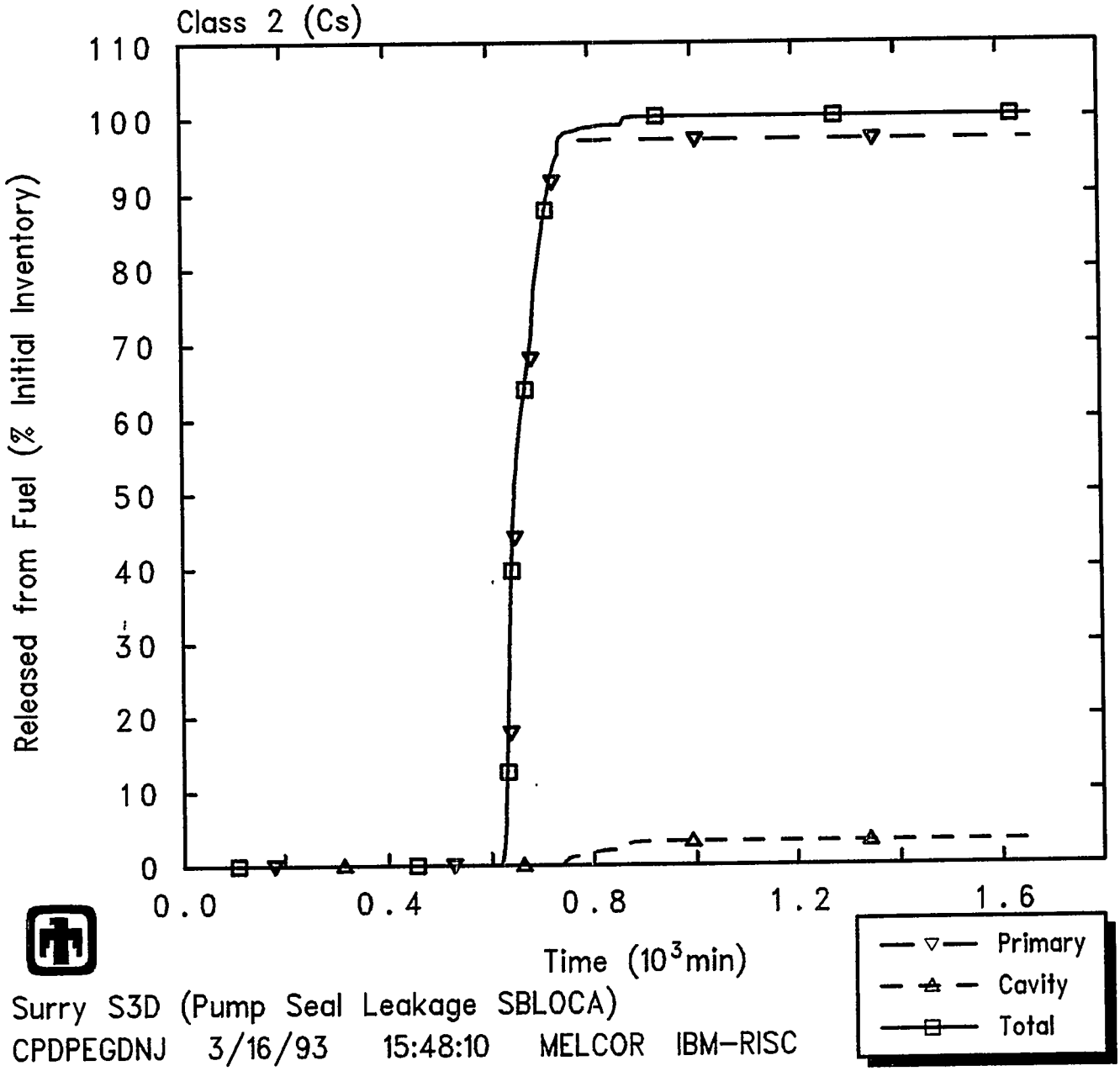

Figure 5.4.26 Release of Class 2 (Cs) Alkali Metal Radionuclides from Fuel in Core and in Cavity Predicted during S3D Sequence, as Percentage of Initial Inventory in Core

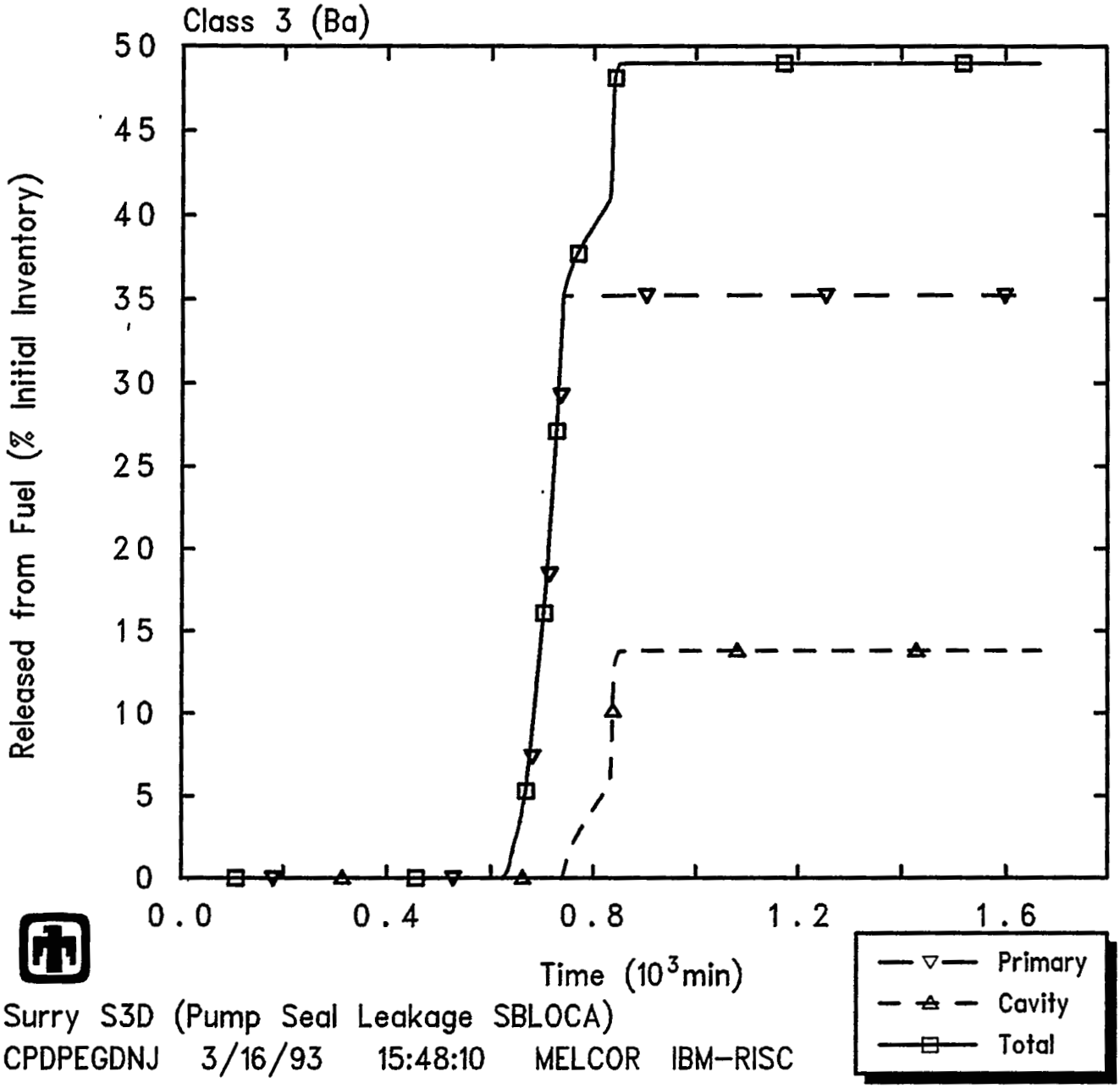

Figure 5.4.27 Release of Class 3 (Ba) Alkaline Earth Radionuclides from Fuel in Core and in Cavity during S3D Sequence, as Percentage of Initial Inventory in Core

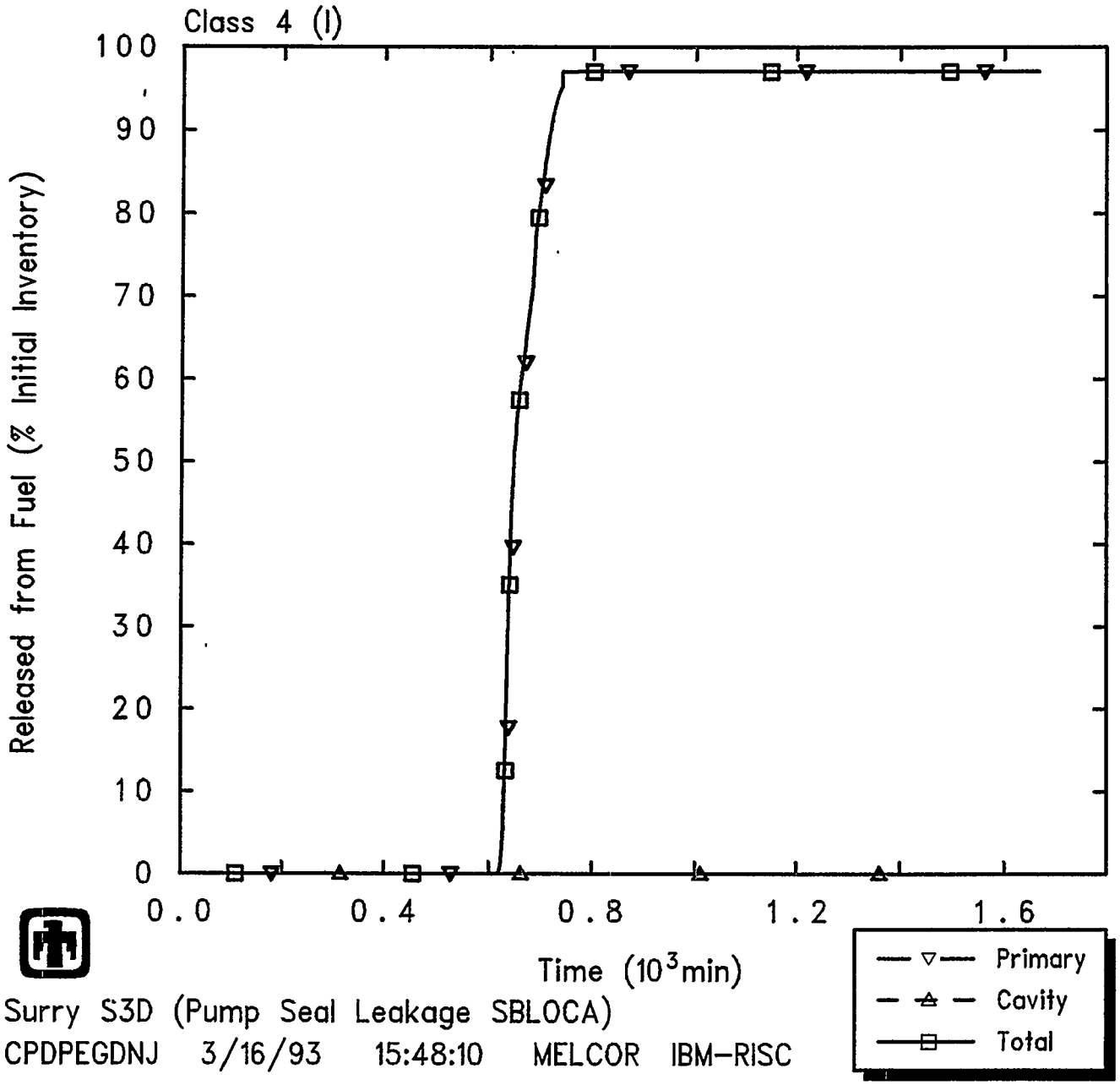

Figure 5.4.28 Release of Class 4 (I) Halogen Radionuclides from Fuel in Core and in Cavity Predicted during S3D Sequence, as Percentage of Initial Inventory in Core

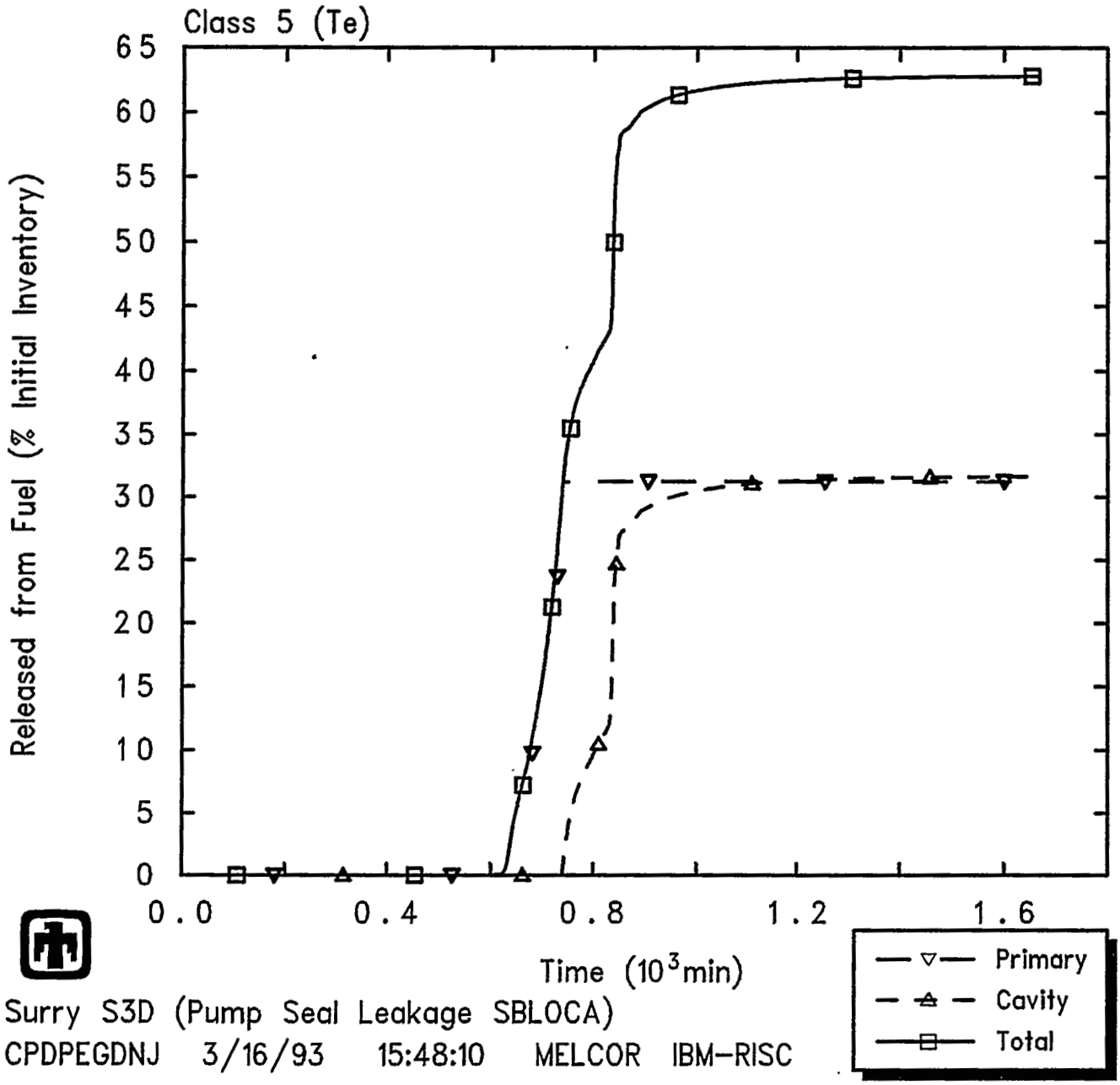

Figure 5.4.29 Release of Class 5 (Te) Chalcogen Radionuclides from Fuel in Core and in Cavity Predicted during S3D Sequence, as Percentage of Initial Inventory in Core

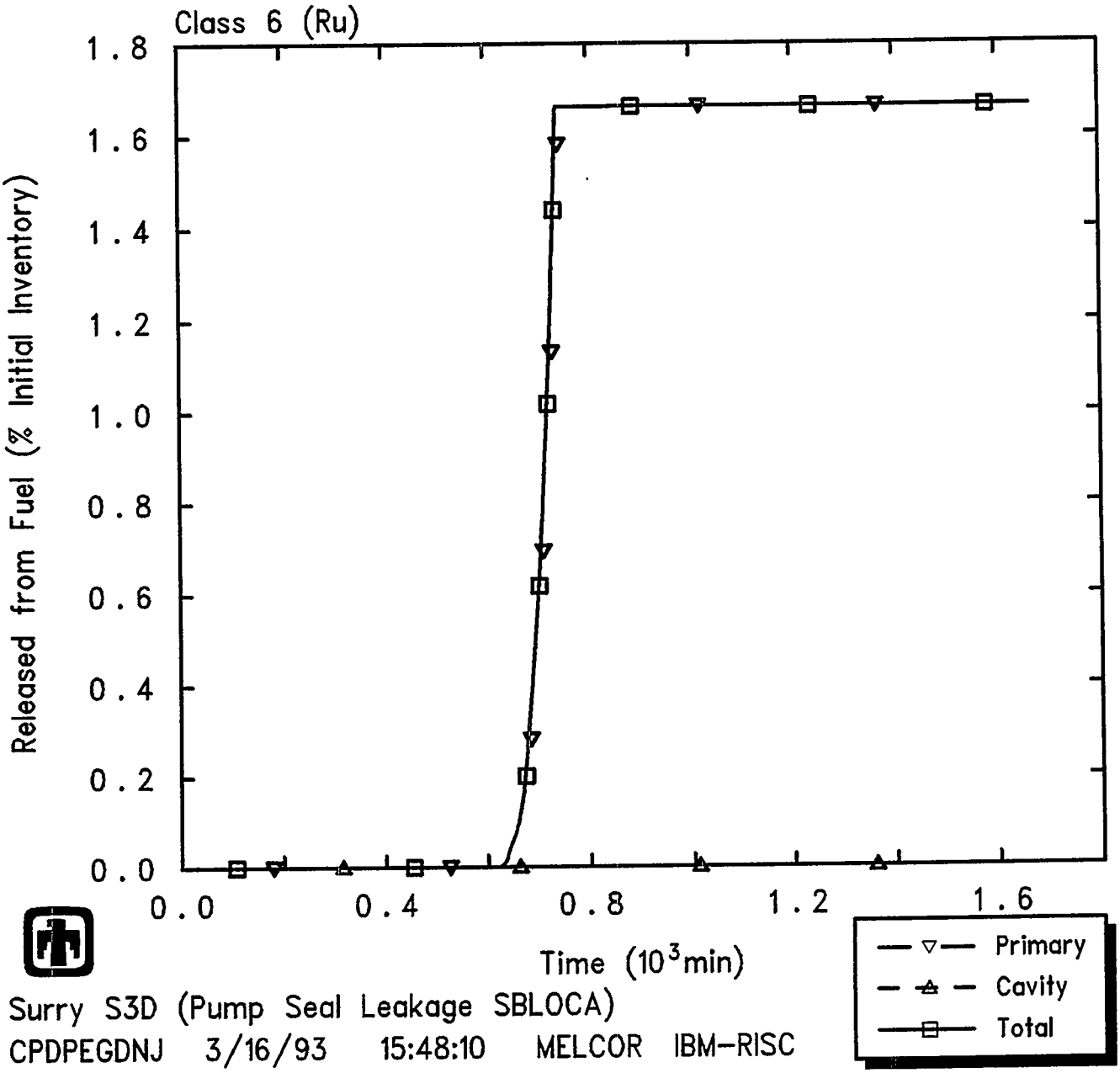

Figure 5.4.30 Release of Class 6 (Ru) Platinoid Radionuclides from Fuel in Core and in Cavity Predicted during S3D Sequence, as Percentage of Initial Inventory in Core

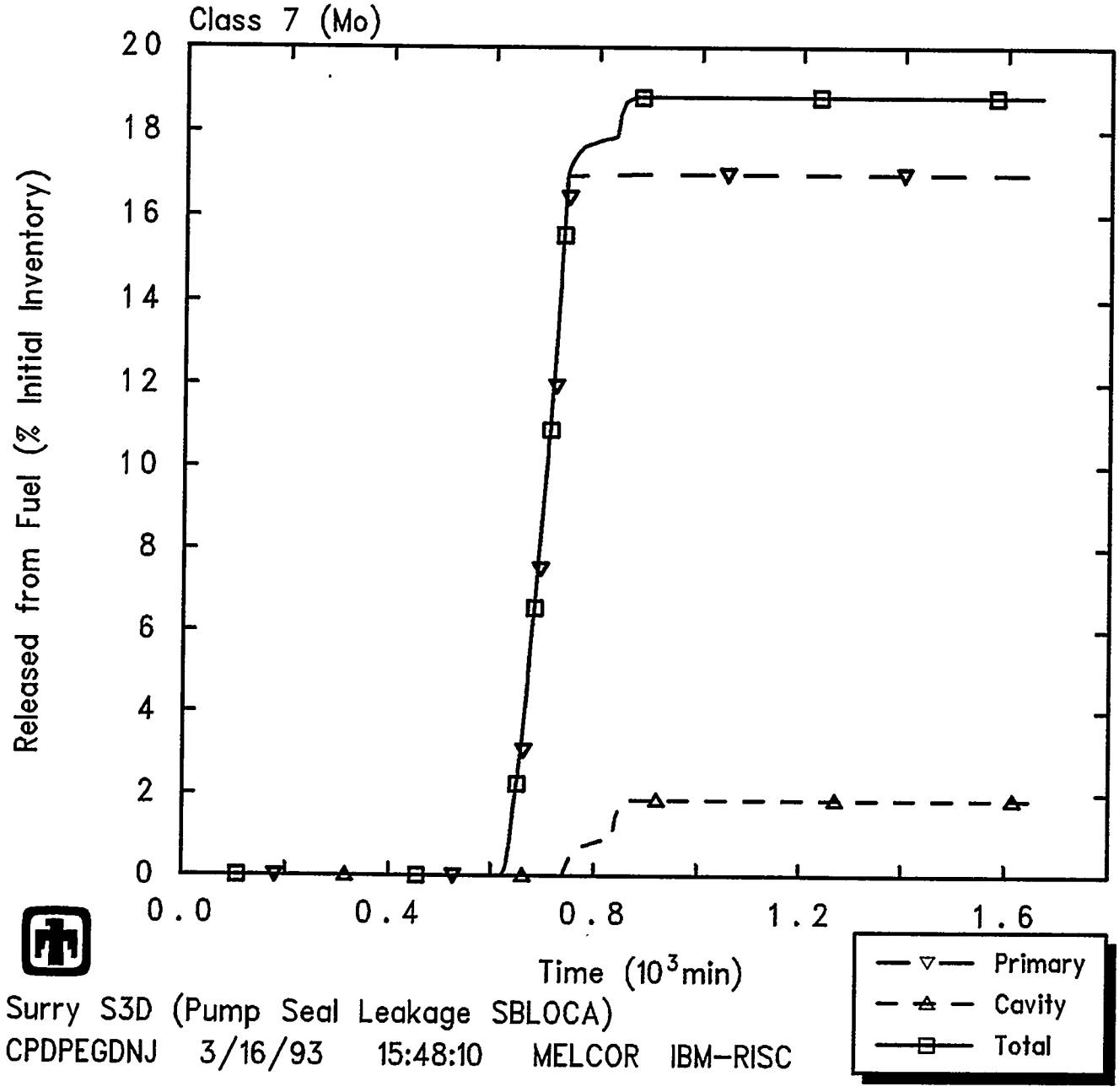

Figure 5.4.31 Release of Class 7 (Mo) Early Transition Element Radionuclides from Fuel in Core and in Cavity Predicted during S3D Sequence, as Percentage of Initial Inventory in Core

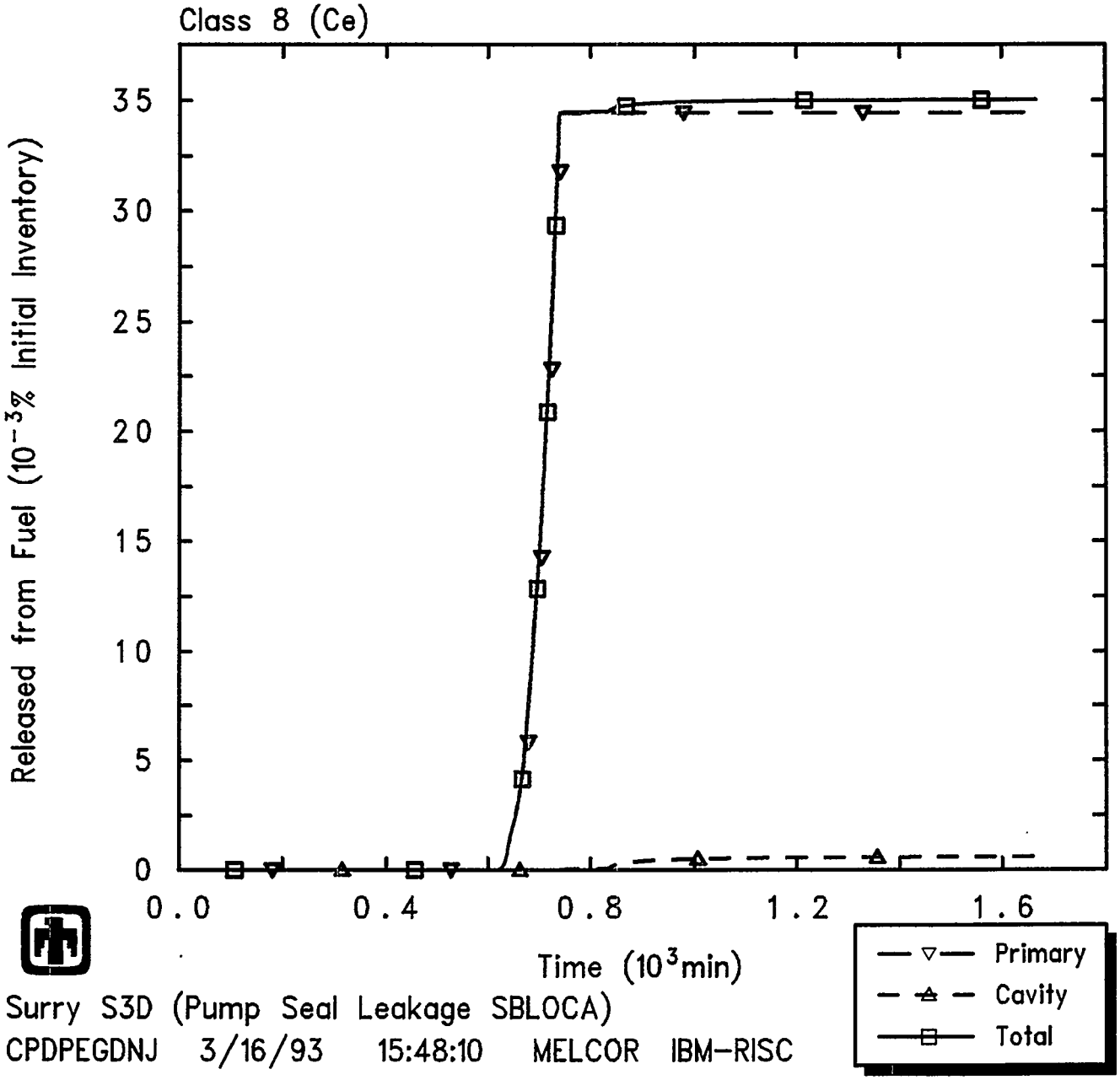

Figure 5.4.32 Release of Class 8 (Ce) Tetravalent Radionuclides from Fuel in Core and in Cavity Predicted during S3D Sequence, as Percentage of Initial Inventory in Core

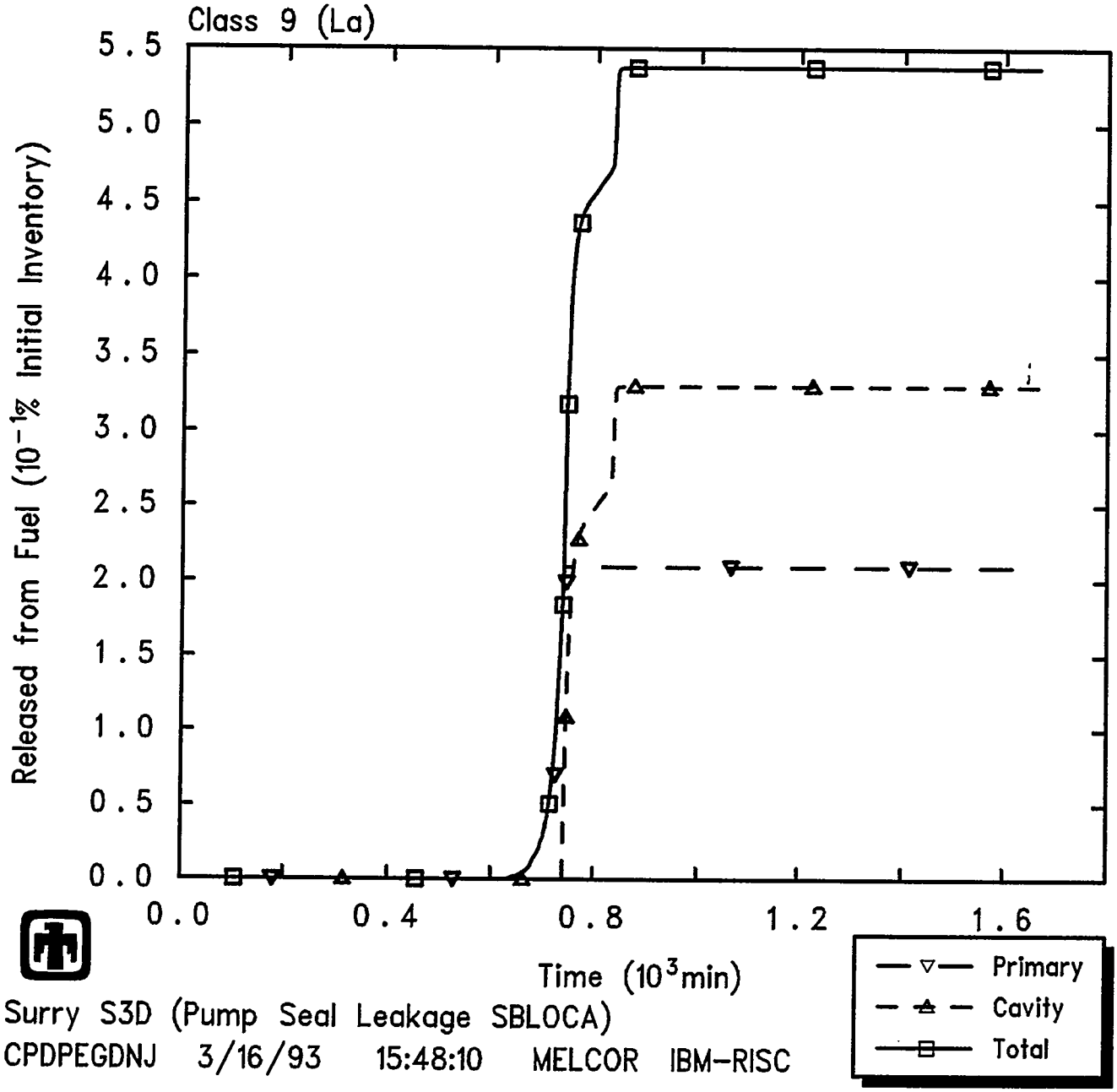

Figure 5.4.33 Release of Class 9 (La) Trivalent Radionuclides from Fuel in Core and in Cavity Predicted during S3D Sequence, as Percentage of Initial Inventory in Core

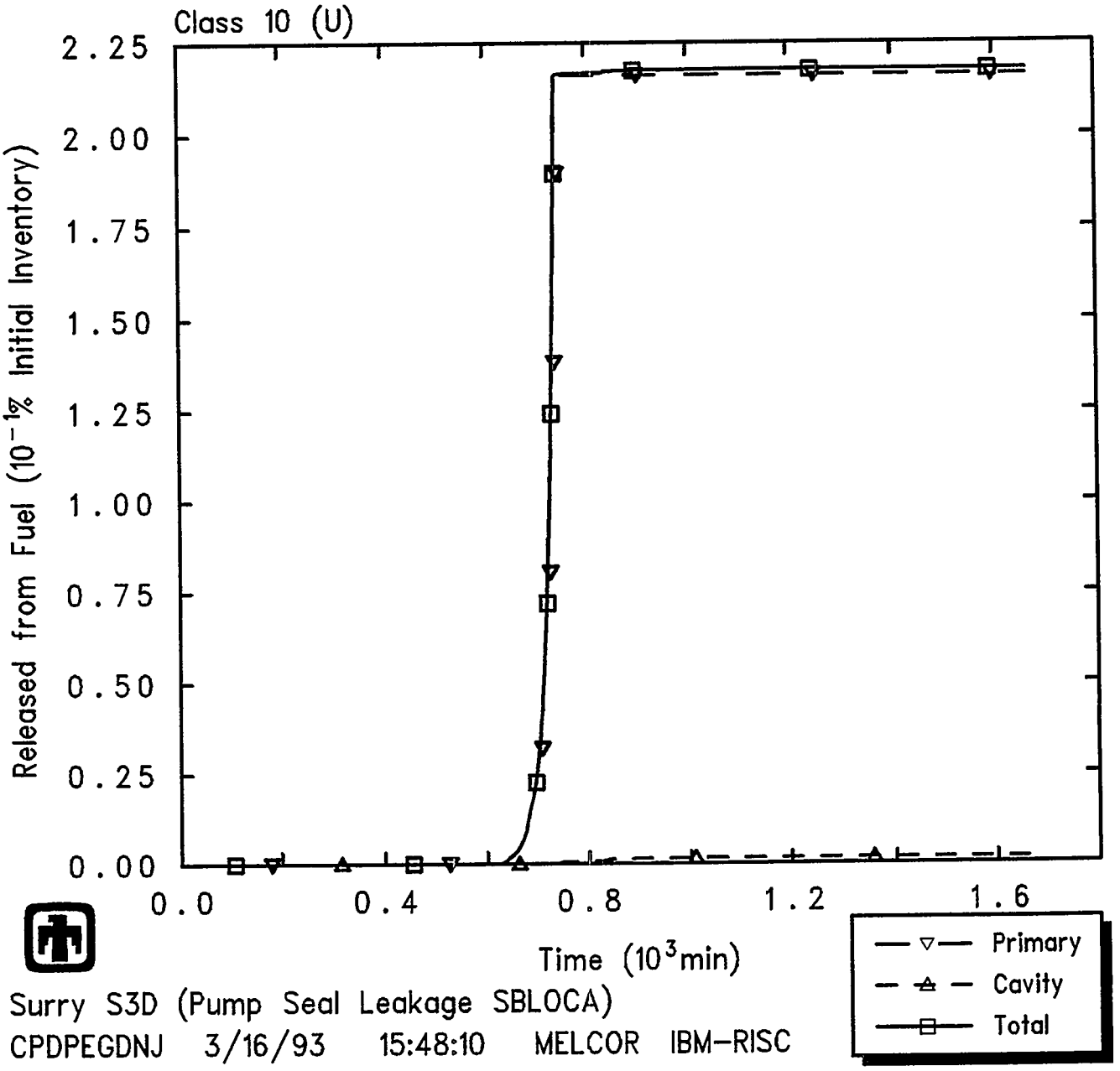

Figure 5.4.34 Release of Class 10 (U) Uranium Radionuclides from Fuel in Core and in Cavity Predicted during S3D Sequence, as Percentage of Initial Inventory in Core

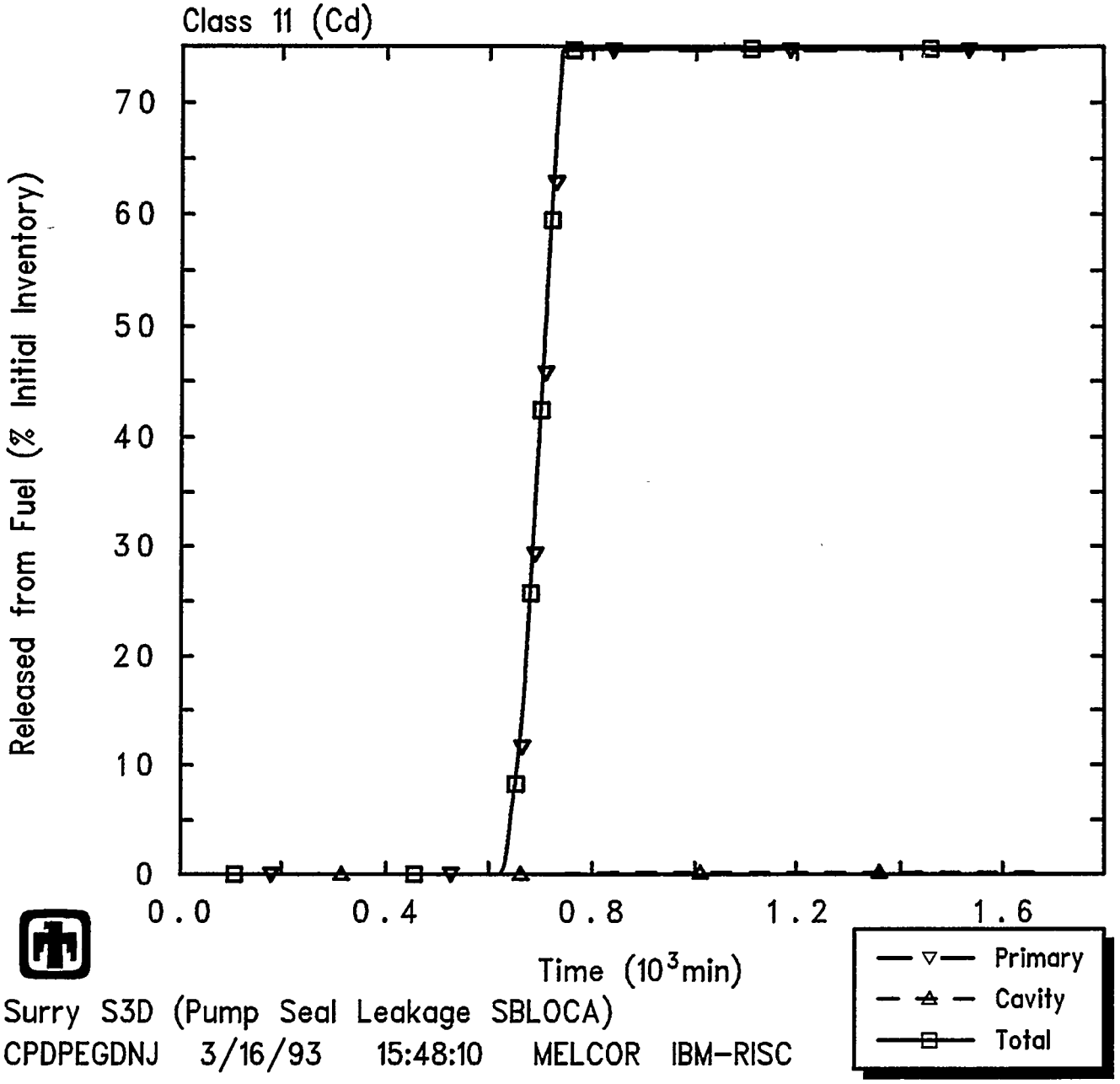

Figure 5.4.35 Release of Class 11 (Cd) More Volatile Main Group Radionuclides from Fuel in Core and in Cavity Predicted during S3D Sequence, as Percentage of Initial Inventory in Core

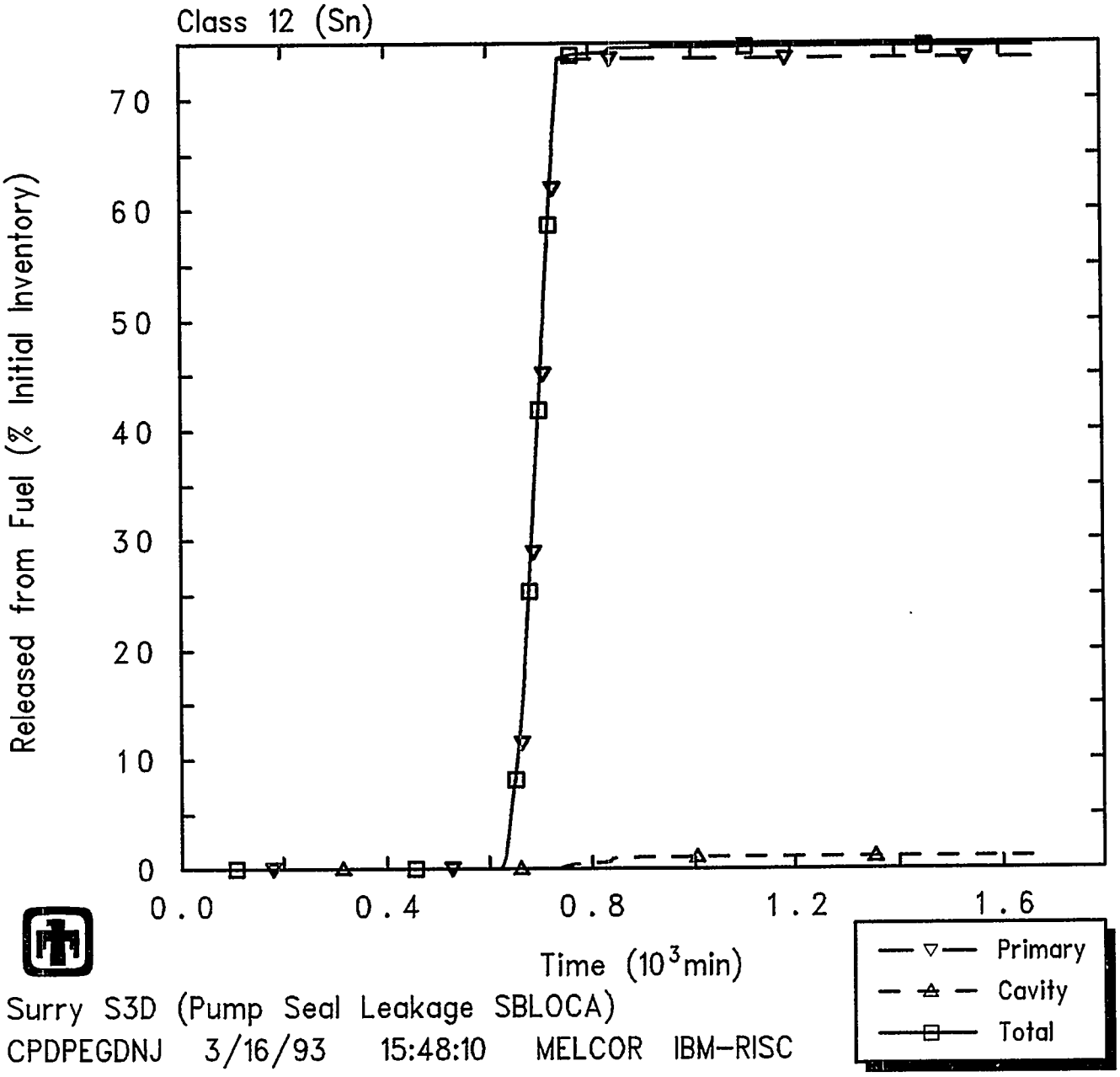

Figure 5.4.36 Release of Class 12 (Sn) Less Volatile Main Group Radionuclides from Fuel in Core and in Cavity Predicted during S3D Sequence, as Percentage of Initial Inventory in Core

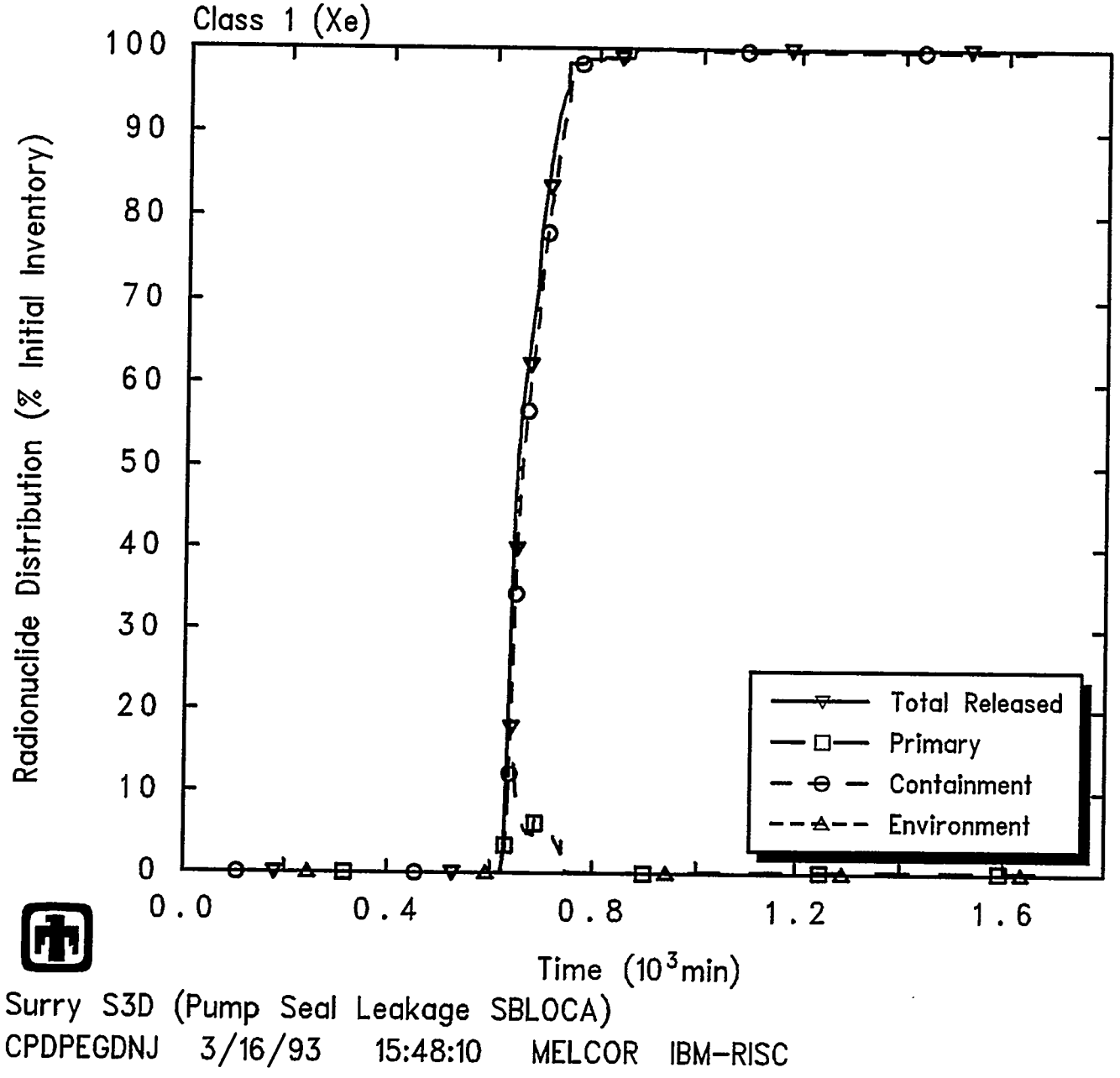

Figure 5.4.37 Distribution of Class 1 (Xe) Noble Gas Radionuclides in Primary System, Containment and Environment Predicted during S3D Sequence, as Percentage of Initial Inventory in Core

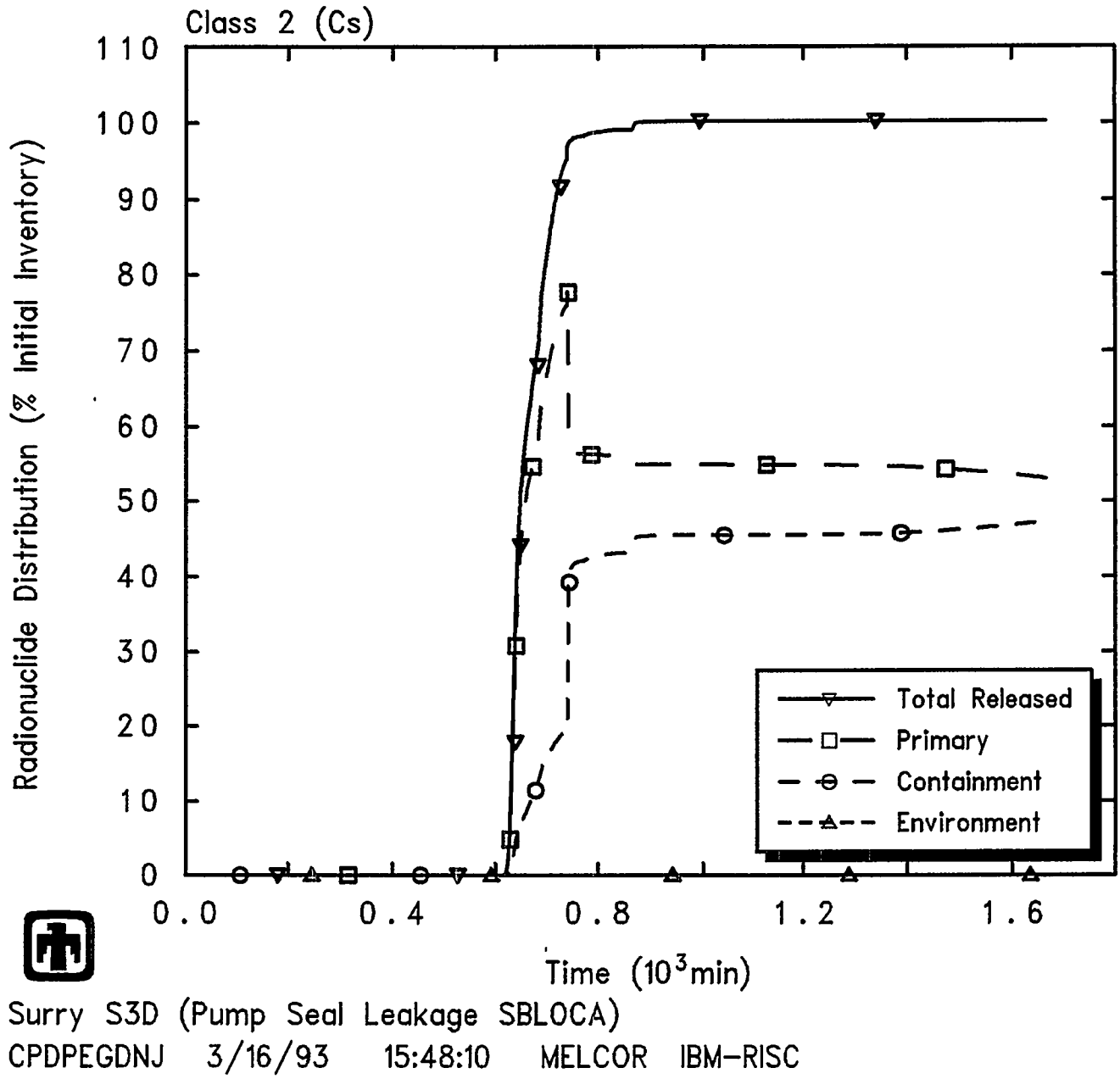

Figure 5.4.38 Distribution of Class 2 (Cs) Alkali Metal Radionuclides in Primary System, Containment and Environment Predicted during S3D Sequence, as Percentage of Initial Inventory in Core

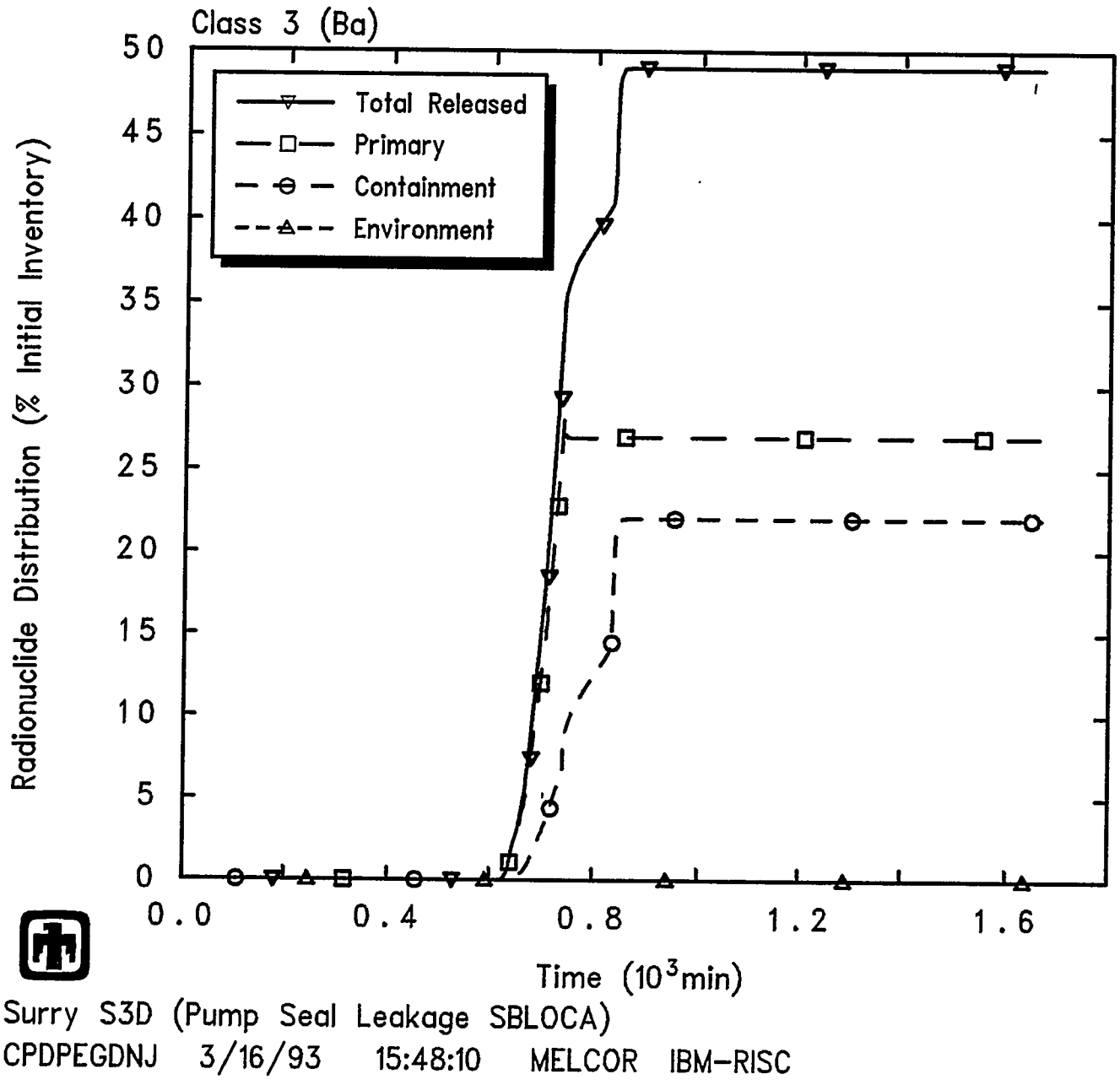

Figure 5.4.39 Distribution of Class 3 (Ba) Alkaline Earth Radionuclides in Primary System, Containment and Environment during S3D Sequence, as Percentage of Initial Inventory in Core

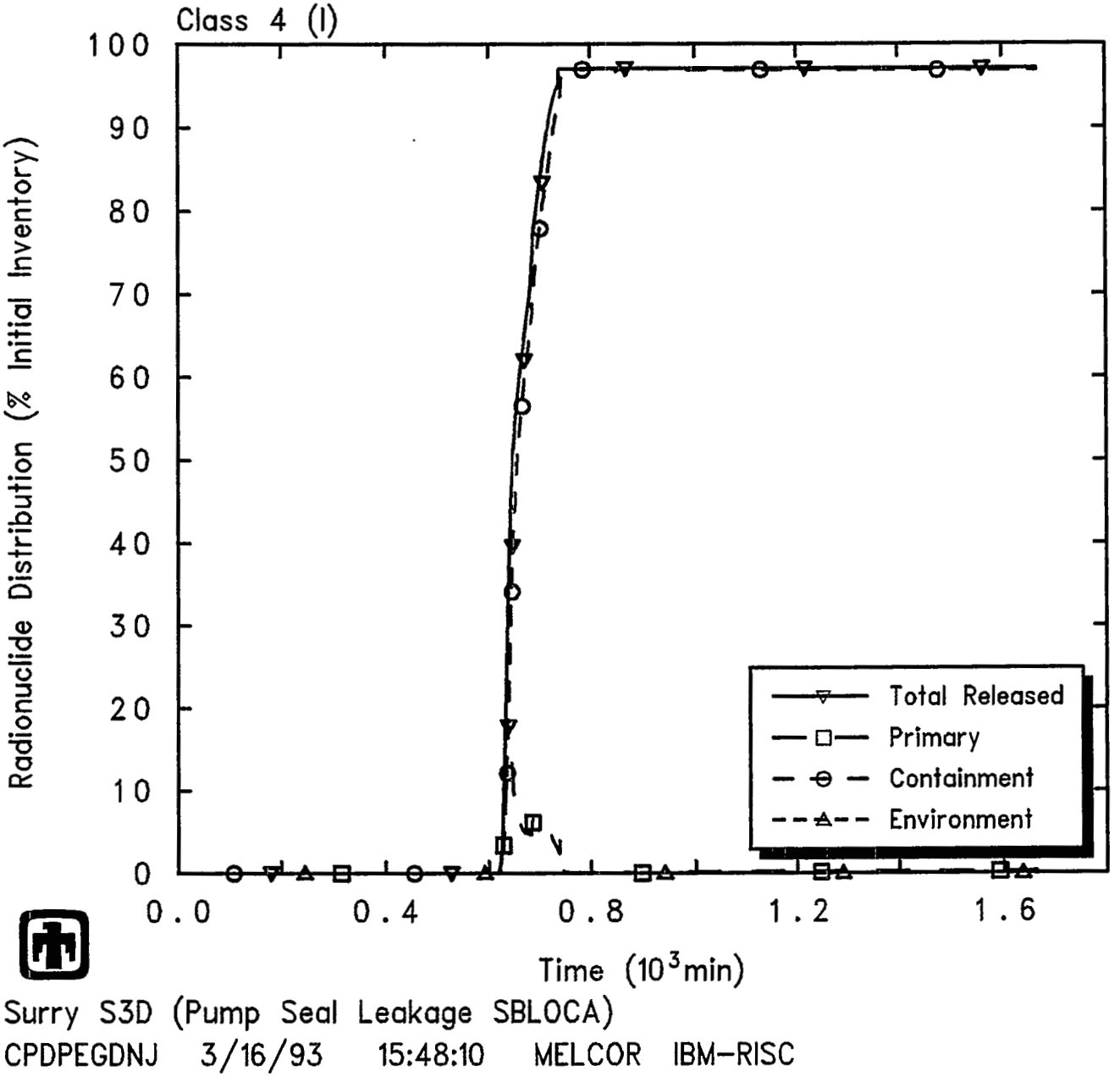

Figure 5.4.40 Distribution of Class 4 (I) Halogen Radionuclides in Primary System, Containment and Environment Predicted during S3D Sequence, as Percentage of Initial Inventory in Core

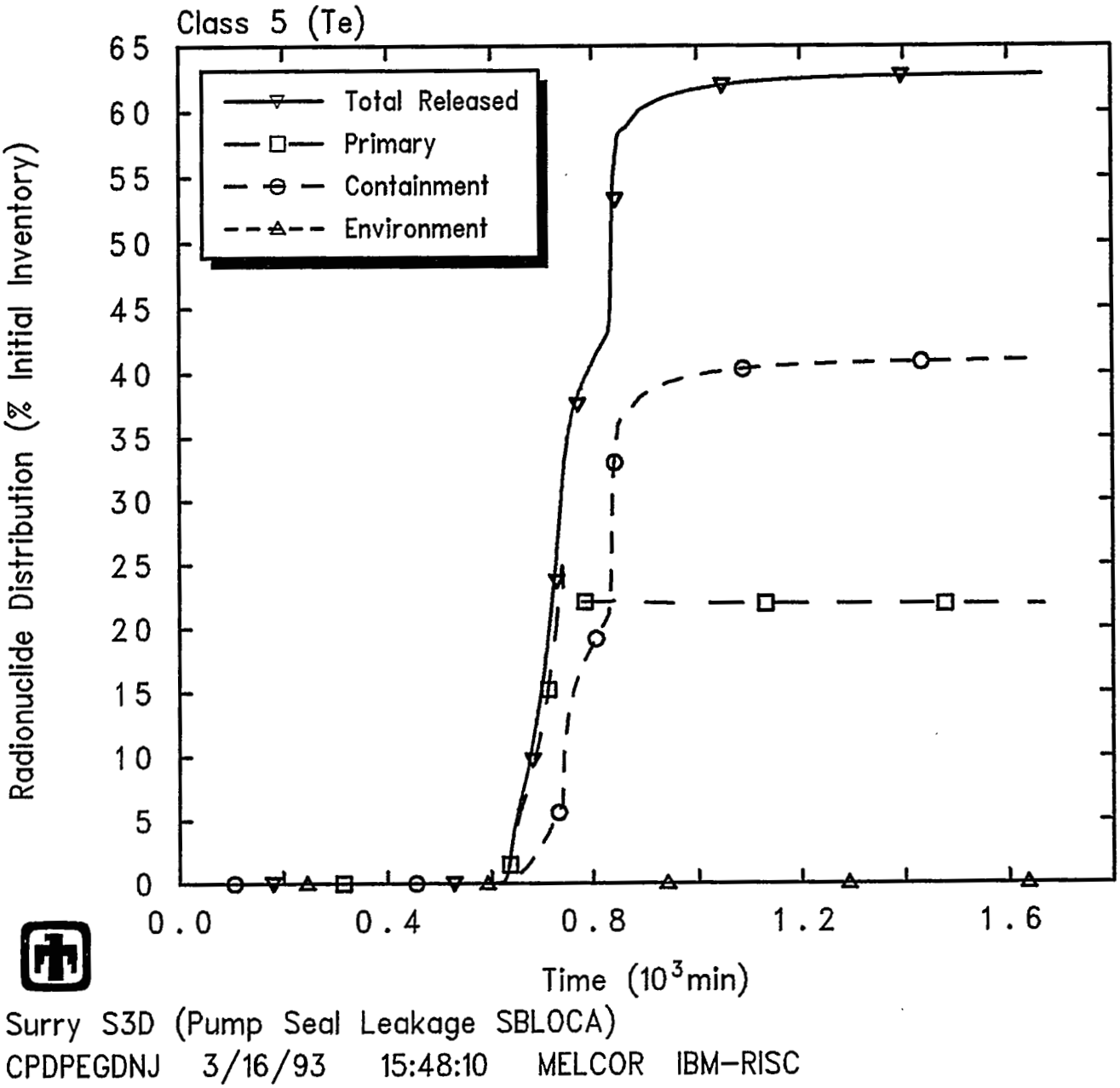

Figure 5.4.41 Distribution of Class 5 (Te) Chalcogen Radionuclides in Primary System, Containment and Environment Predicted during S3D Sequence, as Percentage of Initial Inventory in Core

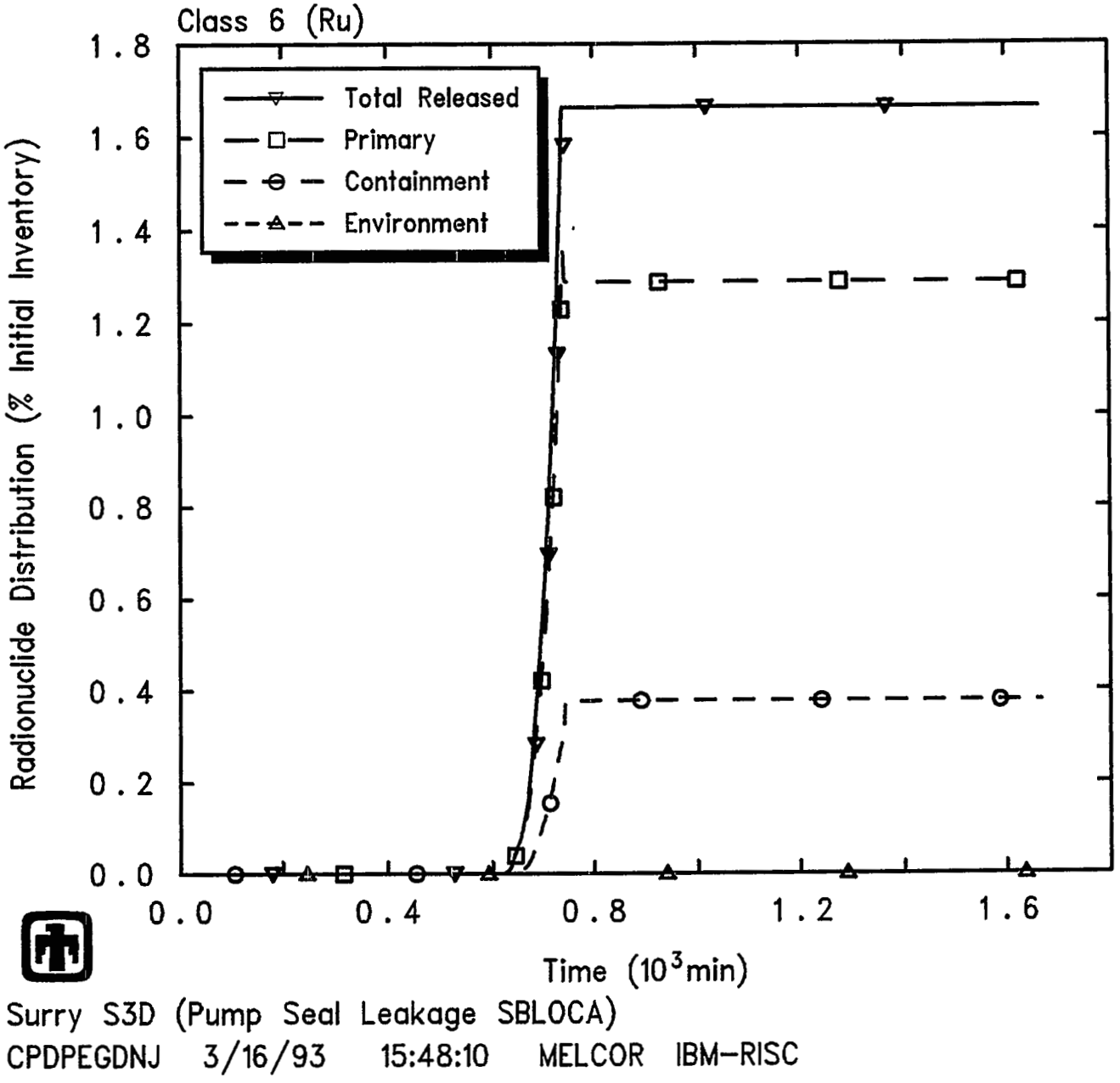

Figure 5.4.42 Distribution of Class 6 (Ru) Platinoid Radionuclides in Primary System, Containment and Environment Predicted during S3D Sequence, as Percentage of Initial Inventory in Core

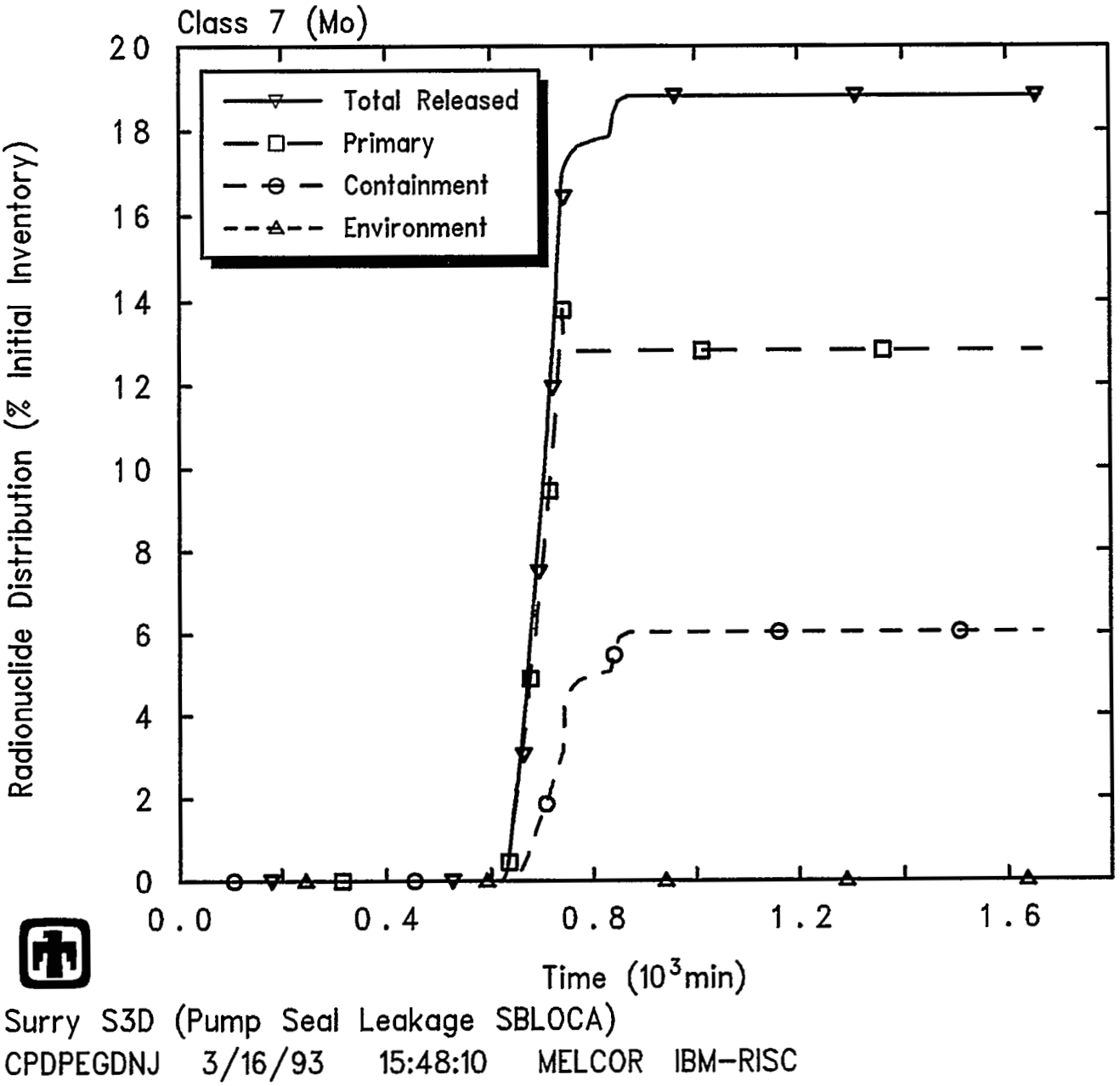

Figure 5.4.43 Distribution of Class 7 (Mo) Early Transition Element Radionuclides in Primary System, Containment and Environment Predicted during S3D Sequence, as Percentage of Initial Inventory in Core

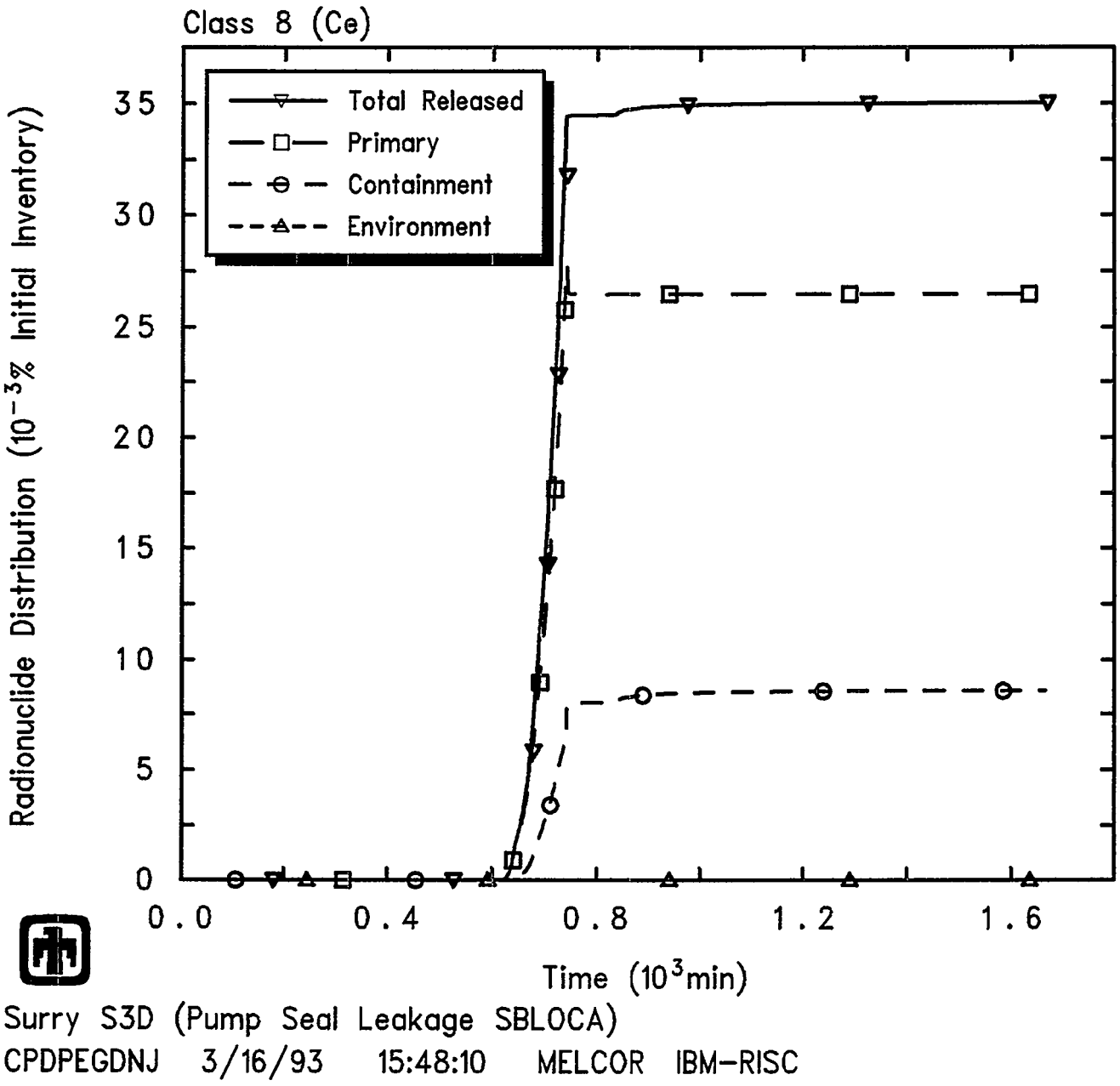

Figure 5.4.44 Distribution of Class 8 (Ce) Tetravalent Radionuclides in Primary System, Containment and Environment Predicted during S3D Sequence, as Percentage of Initial Inventory in Core

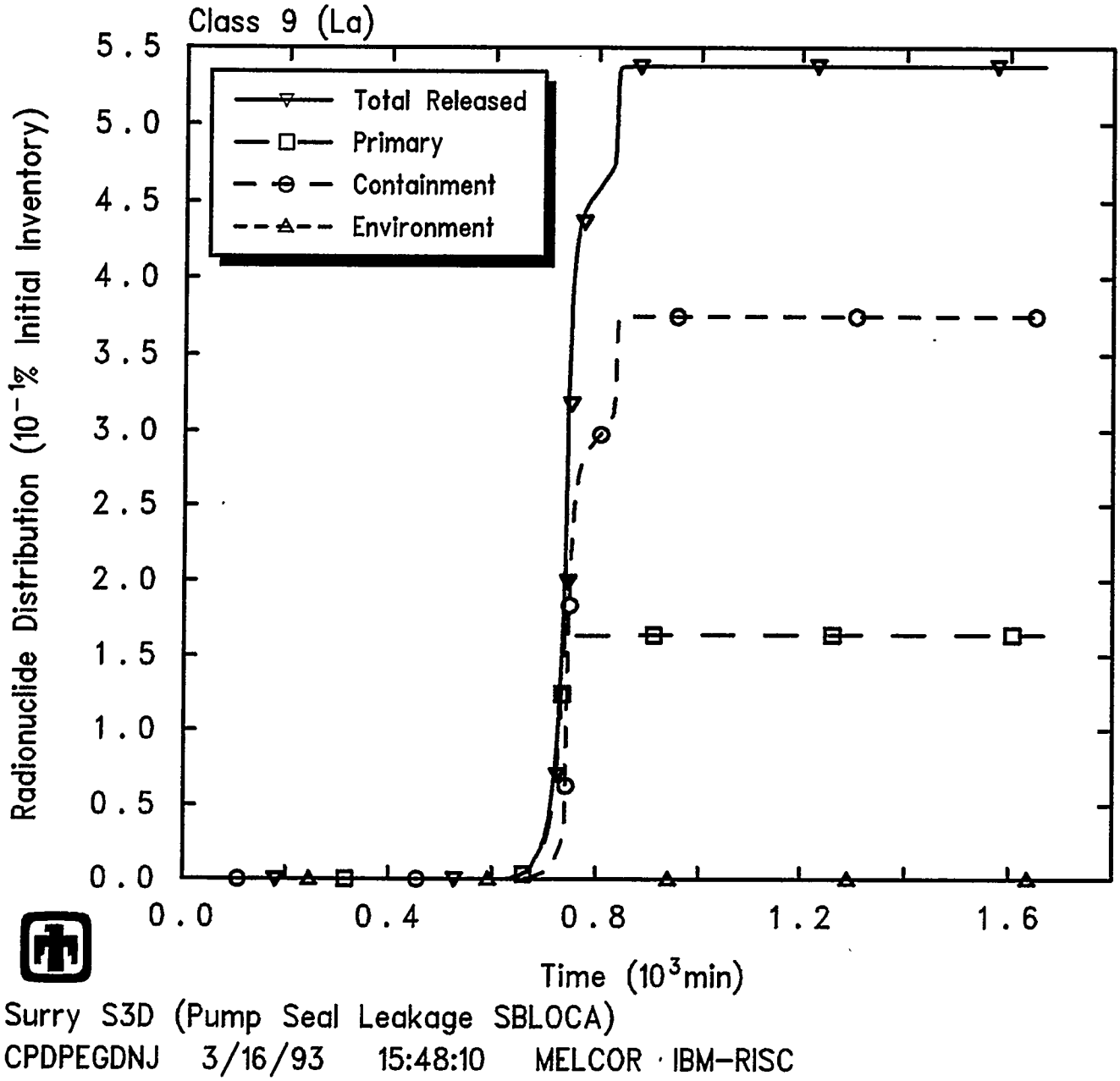

Figure 5.4.45 Distribution of Class 9 (La) Trivalent Radionuclides in Primary System, Containment and Environment Predicted during S3D Sequence, as Percentage of Initial Inventory in Core

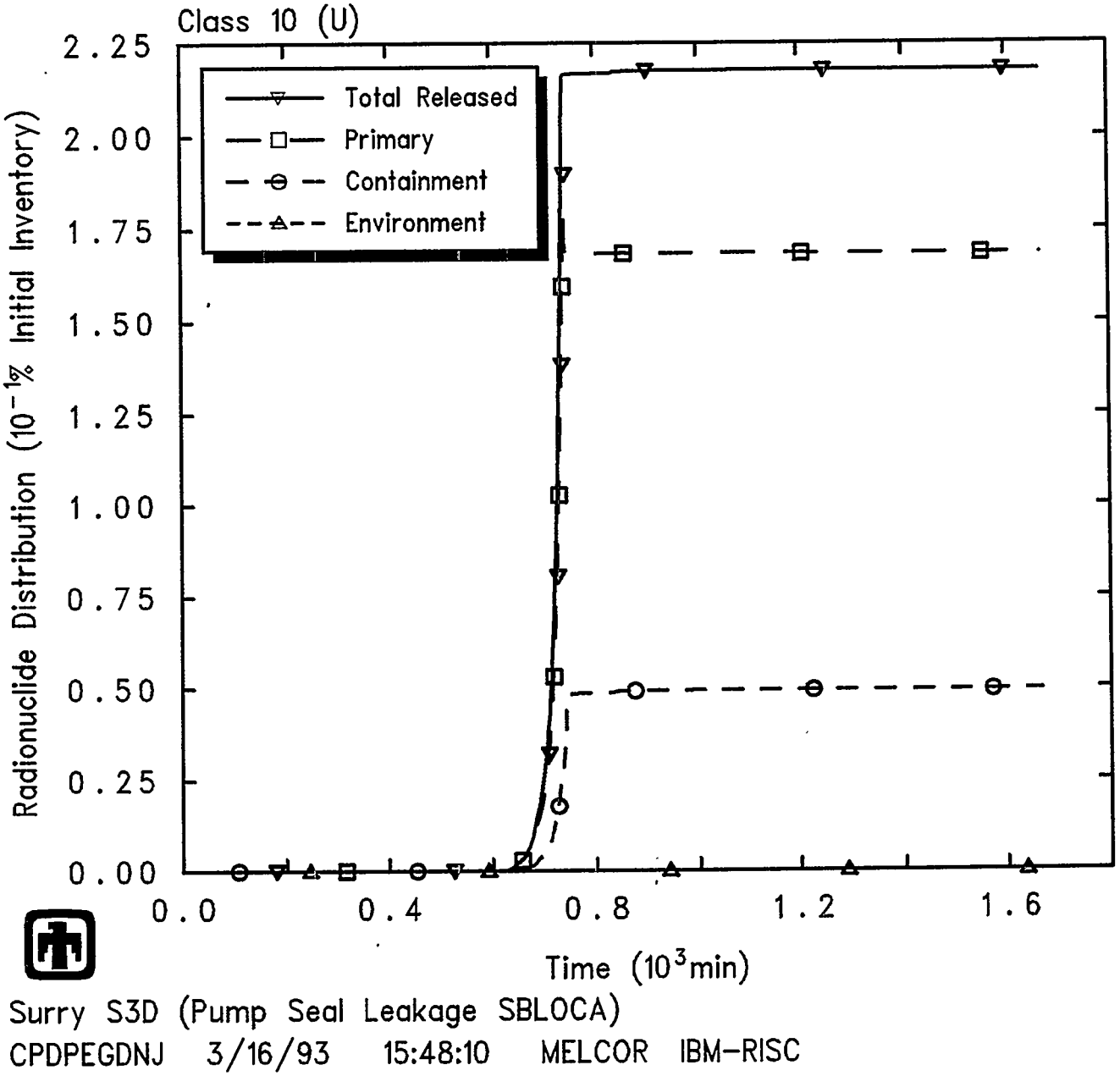

Figure 5.4.46 Distribution of Class 10 (U) Uranium Radionuclides in Primary System, Containment and Environment Predicted during S3D Sequence, as Percentage of Initial Inventory in Core

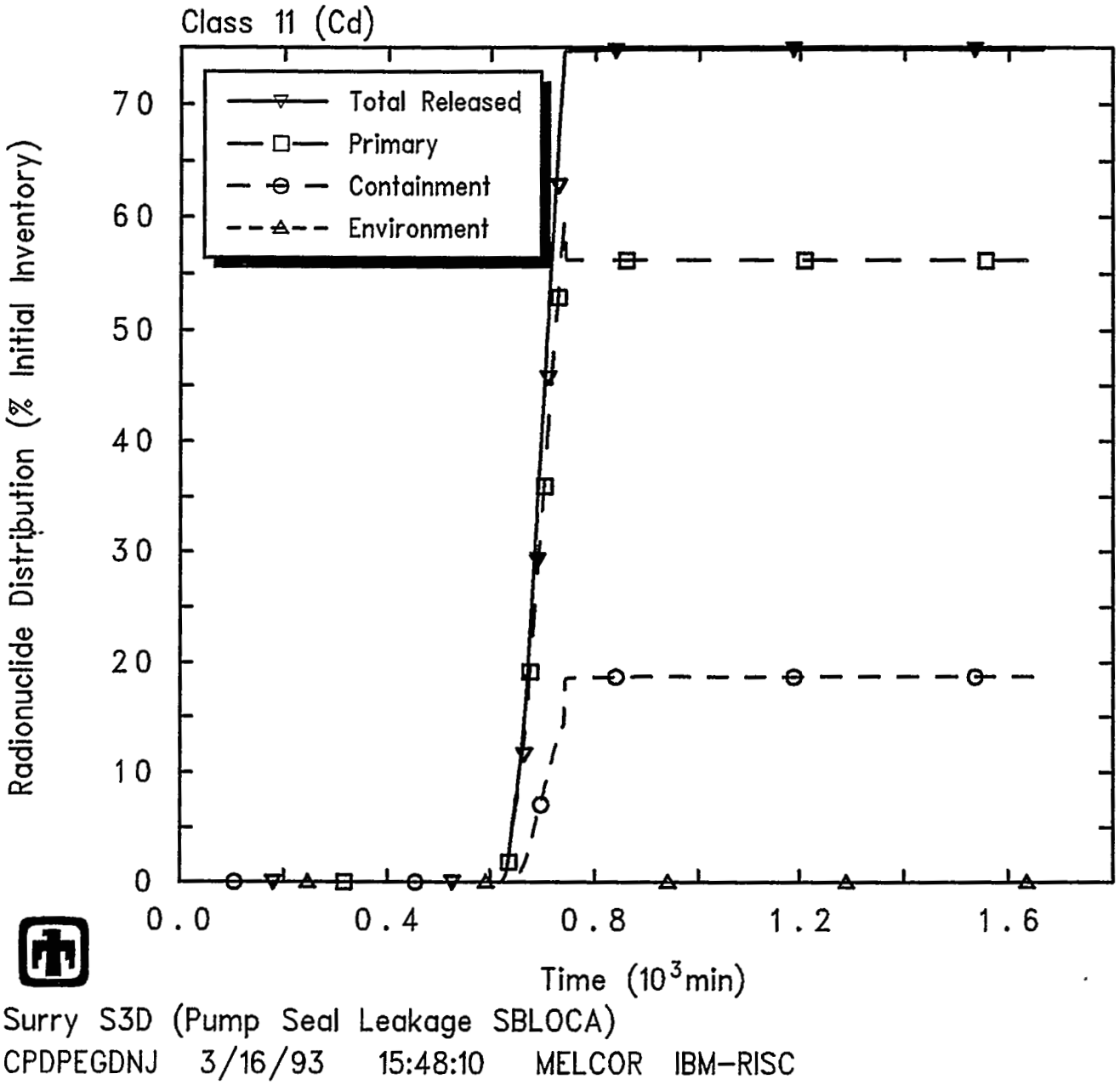

Figure 5.4.47 Distribution of Class 11 (Cd) More Volatile Main Group Radionuclides in Primary System, Containment and Environment Predicted during S3D Sequence, as Percentage of Initial Inventory in Core

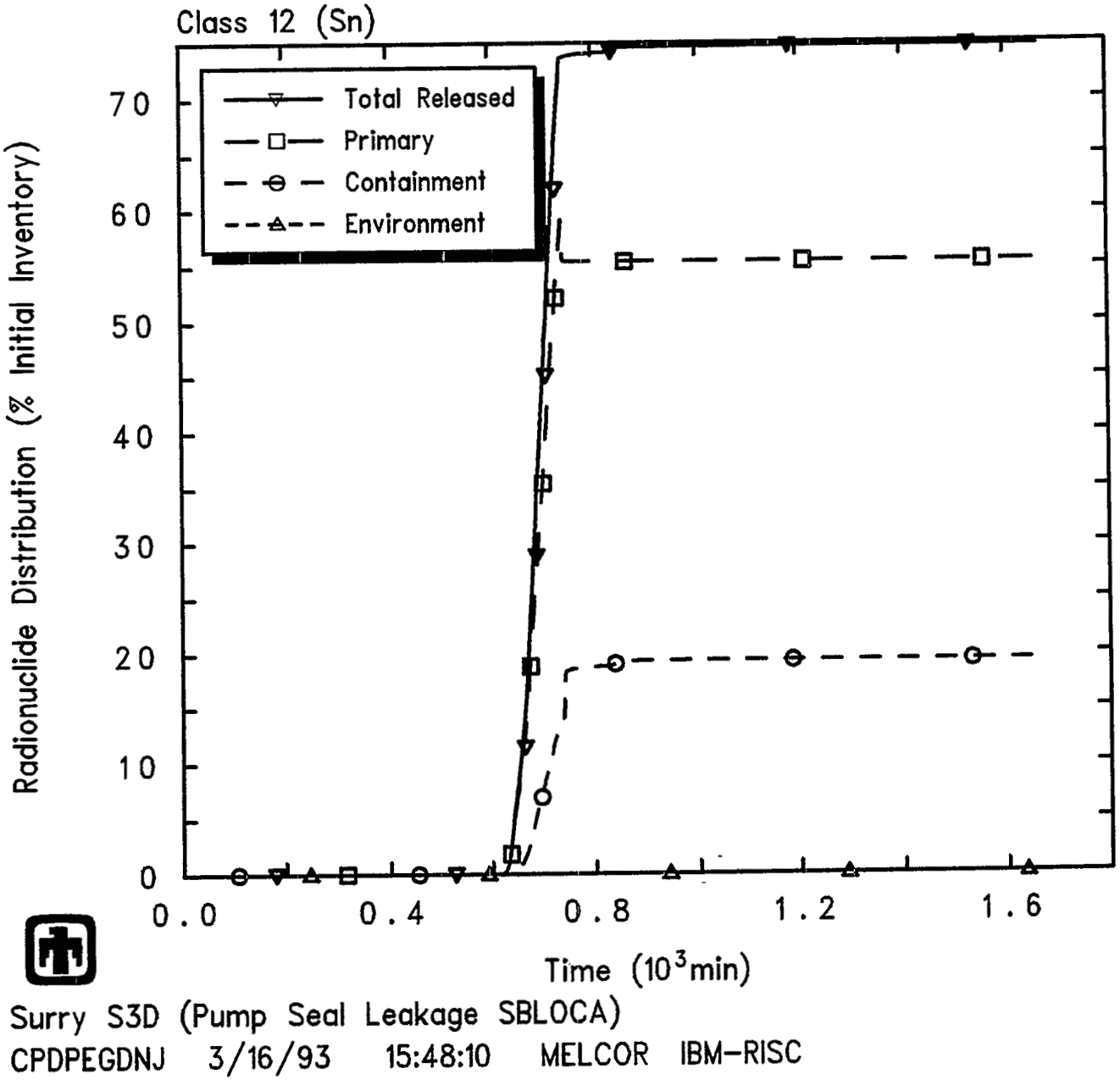

Figure 5.4.48 Distribution of Class 12 (Sn) Less Volatile Main Group Radionuclides in Primary System, Containment and Environment Predicted during S3D Sequence, as Percentage of Initial Inventory in Core

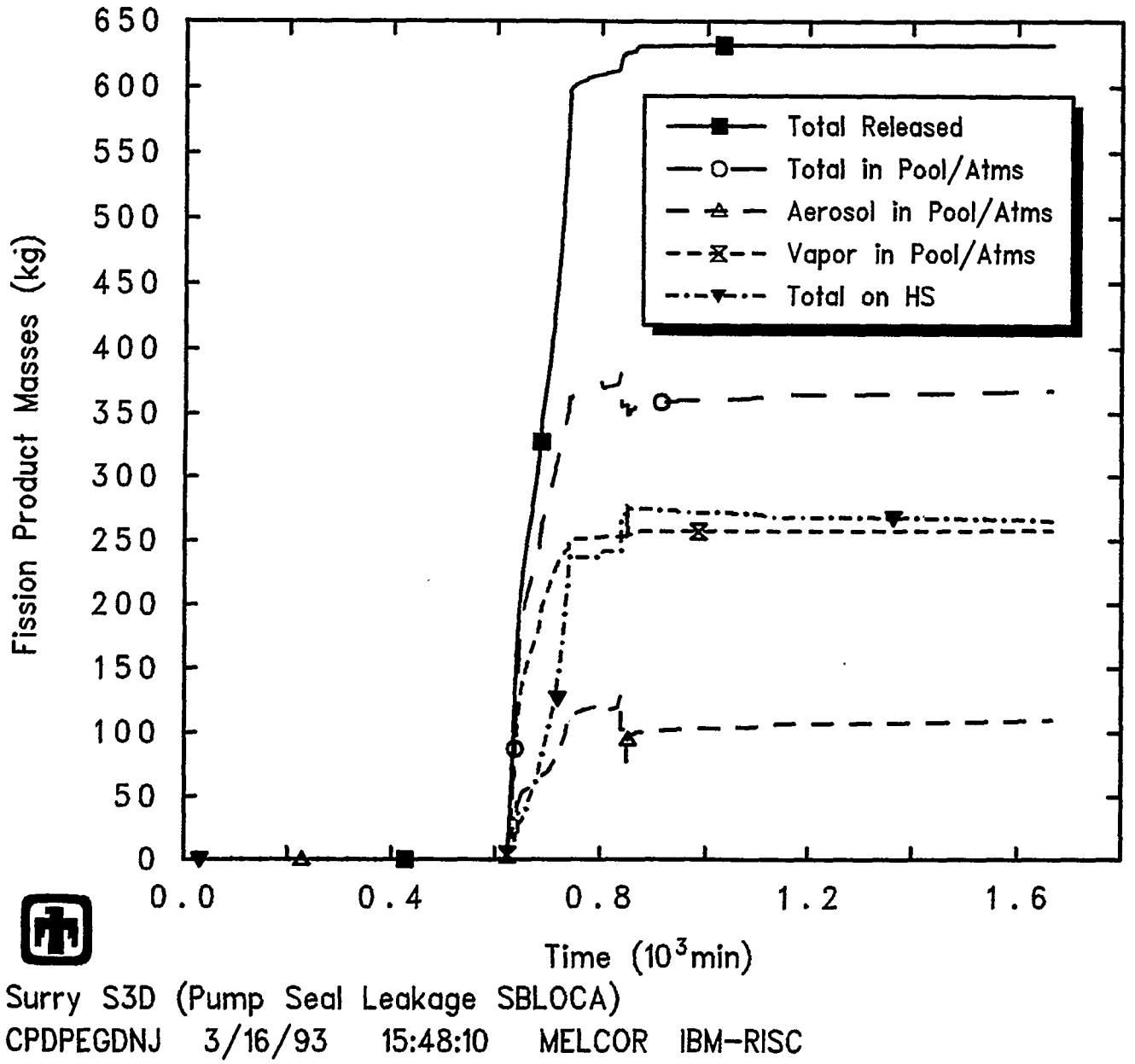

Figure 5.4.49 Total Fission Product Mass Released, and Overall Distribution, Predicted during S3D Sequence

6 Summary and Findings

This report summarizes the results from three MELCOR calculations of nuclear power plant accident sequences performed in support of the NRC's updated regulatory source term and presents comparisons with Source Term Code Package (STCP) calculations for the same sequences. The program task was to run the MELCOR program for three low-pressure sequences to identify the materials which enter containment (source terms) and are available for release to the environment, and to obtain timing of sequence events. The source terms include fission products and other materials such as those generated by core-concrete interactions. All three calculations, for both MELCOR and STCP, analyzed the Surry plant, a pressurized water reactor (PWR) with a subatmospheric containment design.

The AG sequence, a large break LOCA, assumed the availability of both passive and active Emergency Core Cooling System (ECCS) safety systems for protection of the primary system. Containment protective systems available for use included the containment fan coolers and containment sprays. Since the containment recirculation spray system coolers were inoperable, there was no capability for containment heat removal as the accident progressed. The small break LOCA sequences, S2D and S3D, assumed the ECCS systems were unavailable, with the exception of the passive accumulators. For those two accident sequences, the containment spray systems were fully operable, including the capability for containment heat removal via the containment spray recirculation system coolers. Since each of the three accident sequences progressed through core melt, core slumping, reactor vessel failure, and ex-vessel core-concrete interaction, they provided a good test of the ability of MELCOR to simulate integrated accidents that progressed to the point of radionuclide release to the containment or environment.

There were no major differences in the behavior predicted for the AG large break LOCA sequence. Both MELCOR and STCP predicted a slow pressurization of containment as the ECCS water delivered to the core is boiled off removing the decay heat. The containment was predicted to fail slightly later in time in the MELCOR calculation than in the STCP analysis, partly due to a slower pressurization rate and partly due to a higher failure pressure setpoint. After containment failure and associated loss of ECC, both codes predicted core damage, lower head failure, and debris ejection to the cavity. The core degradation process calculated by MELCOR was somewhat more gradual and extended than that predicted by STCP. Both codes predicted almost all the noble gases and alkali metal volatiles (CsOH) released, and most ofthe halogens (I). Significantly more alkali earth (Ba) release and significantly less Tellurium (Te) releases were calculated by MELCOR than by STCP. A small fraction ($\leq 5\%$) of the Mo, Cd and Sn were calculated to be released in the MELCOR analysis, with no STCP values for comparison. Both codes predicted only trace amounts of the refractories (Ru, Ce, La and U) to be released.

Fission product release results from STCP were not available for the S2D and S3D sequences for comparison to MELCOR predictions. Therefore, only timings of major events could be compared in these two cases. Neither code predicted containment failure in either case, primarily due to the continued availability for containment heat removal via the containment spray recirculation system coolers. Time to core uncovery, core damage and relocation, lower head failure and debris ejection to the cavity were not all that different. One major difference between results from from MELCOR and from STCP was the prediction of deflagrations occurring in both sequences in the MELCOR analyses, with associated containment pressure and temperature spikes; there were no deflagrations in the STCP analyses for either small break sequence.

The overall fission product source terms calculated by MELCOR for the S2D and S3D sequences, and for the AG sequence as well, showed some general similarities in predicted response. In all three cases almost all of the noble gases ($\geq 99\%$) and most (~ 85-95%) of the Cs and I volatiles were released; very little remained in the RCS and almost all were in the containment or (for the AG sequence) released to the environment. Intermediate amounts of Ba, Te, Sn, Cd and Sn (2-30%) were released, and only trace amounts ($\leq 1\%$) of the refractories Ru, Ce, La and U were predicted to be released.

References

1. Denning, R. S. et al., "Radionuclide Release Calculations for Selected Severe Accident Scenarios," NUREG/CR-4624, BMI-2139, Battelle Columbus, Vol. 3: PWR, Subatmospheric Containment Design, July 1986, and Vol. 6: Supplemental Calculations, August 1990.

2. Summers, R. M. et al., MELCOR 1.8.0: A Computer Code for Nuclear Reactor Severe Accident Source Term and Risk Assessment Analyses, NUREG/CR-5531, SAND90-0364, Sandia National Laboratories, Albuquerque, NM, January 1991.

3. Gieseke, J. A. et al., Source Term Code Package: A User's Guide, NUREG/CR-4587, BMI-2138, Battelle Columbus Laboratory, July 1986.

4. USNRC, Reactor Risk Reference Document, NUREG-1150, Office of Nuclear Regulatory Research, U. S. Nuclear Regulatory Commission, February 1987.

5. Breeding, R. J. et al., Evaluation of Severe Accident Risks: Vol. 3, Rev.1, Pt. 1: Surry Unit 1, NUREG/CR-4551, SAND86-1309, Sandia National Laboratories, Albuquerque, NM, October 1990.

6. USNRC, Reactor Safety Study -- An Assessment of Accident Risks in U. S. Commercial Nuclear Power Plants, WASH-1400 (NUREG-75/014), U. S. Nuclear Regulatory Commission, October 1975.

7. Internal Memorandum from R. J. Dallman to R. D. Copp, "MELCOR Preliminary Evaluation", RJD-50-87, Idaho National Engineering Laboratory, December 28, 1987.

8. Letter from C. A. Dobbe, INEL, to J. E. Kelly, SNL, "Transmittal of Calculational Workbooks for the MELCOR Input Decks of the Surry PWR", CAD-1-88, May 6, 1988.

9. Letter from C. A. Dobbe, INEL, to J. E. Kelly, SNL, "Transmittal of Floppy Disk Containing the MELCOR Input Decks of the Surry PWR", CAD-2-88, May 17, 1988.

10. Bayless, P. D., Analyses of Natural Circulation During a Surry Station Blackout Using SCDAP/RELAP5, NUREG/CR-5214, EGG-2547, Idaho National Engineering Laboratory, October 1988.

11. Smith, P. N. and Mason, P. L., AEA Assessment of MELCOR 1.8.1 Using Calculations for TMLB' Accident Sequences, AEA RS 5484, UK AEA Winfrith Technology Centre, March 1993.

12. L. N. Kmetyk, MELCOR 1.8.2 Assessment: Surry PWR TMLB' (with a DCH Study), SAND93-1899, Sandia National Laboratories, Albuquerque, NM, March 1994.

General Electric Company (3)
Knolls Atomic Power Laboratory
Attn: Mark Riley
Jow Semanchik
Vincent Baiamonte
P.O. Box 79
West Mifflin, PA 15122

Mohsen Khatib-Rahbar
Energy Research Inc.
P.O. Box 2034
Rockville, MD 20852

V. K. Dhir
2445 22nd Street
Santa Monica, CA 90403

R. Viskanta
Purdue University
Heat Transfer Laboratory
School of Mechnical Engineering
West Lafayette, IN 47907

Dr. Jim Gieseke
Battelle Memorial Institute
505 King Ave.
Columbus, OH 43201

M. A. Kenton
Gabor, Kenton & Associates
770 Pasquinelli Drive
Suite 426
Westmont, IL 60559

University of California (2)
Attn: W. H. Amarasooriya
T. Theofanous
ERC-CRSS
Santa Barbara, CA 93106

F. E. Haskin
University of New Mexico
Department of Chemical
and Nuclear Engineering
Albuquerque, NM 87131

J. C. Lee
University of Michigan
Dept of Nuclear Engineering
Cooley Building, North Campus
College of Engineering
Ann Arbor, MI 48109-2104
University of Wisconsin (2)

Dept. of Nuclear Engineering
Attn: M. L. Corradini
G. A. Moses
Engineering Research Building
1500 Johnson Drive
Madison, WI 53706

Ramu K. Sundaram
Manager, LOCA Analysis Group
Nuclear Engineering
Yankee Atomic Electric Company
580 Main Street
Bolton, MA 01740

John Bolin
CEGA
P.O. Box 85608
San Diego, CA 92186-9784

M. Plys
Fauske & Associates
16W070 West 83rd Street
Burr Ridge, IL 60521

Nick Trikouros
GPU Nuclear Corporation
One Upper Pond Road
Parsippany, NJ 07054

B. Raychaudhuri
Nebraska Public Power District
PRA & Engineering Review Group
P.O. Box 499
Columbus, NE 68601

Frank Elia
Stone & Webster Engineering Corp.
245 Summer Street
Boston, MA 02210

Samir S. Girgis
Atomic Energy of Canada Limited
CANDU Operations
Sheridan Park Research Community
Mississagua, Ontario
CANADA L5K1B2

Paul J. Fehrenbach
Chalk River Nuclear Laboratories
Fuel Engineering Branch, RSR Division
Chalk River, Ontario
CANADA KOJ1J0

Dr. Bohumír Kujal
Department of Reactor Technology
Nuclear Research Institute Řeˇz plc
250 68 Řež
CZECH REPUBLIC

Andrej Mitro
Institue of Radioecology and Applied
Nuclear Techniques
Barbiarska 2
P.O. Box A-41
040 61 Kosice
CHECHOSLOVAKIA

Shih-Kuei Cheng
Institute of Nuclear Energy Research
P.O. Box 3-3
Lung-Tan, Taiwan
REPUBLIC OF CHINA

Technical Research Centre of Finland (3)
Nuclear Engineering Laboratory
Attn: Lasse Mattila
Ilona Lindholm
Esko Pekkarinen
P.O. Box 208 (Tekniikantie 4)
SF-002151 Espoo
FINLAND

Jorma V. Sandberg
Finnish Center Radiation & Nucl. Safety
Dept. of Nuclear Safety
P.O. Box 268
SF-00101 Helsinki
FINLAND

Akihide Hidaka
Safety Research Department
Reactor Accident Studies and Modelling Branch
DRS-SEMAR
Cadarache Nuclear Center
13108 Sain-Paul-Lez-Durance Cedex
FRANCE

Dr. Lothar Wolf
Battelle Institute EV
AM Romerhof 35
D-6000
Frankfurt/Main 90
GERMANY

Geseelschaft fur Anlagen- und Reaktorsicherheit (3)
Attn: Ulrich Erven
Walter Erdmann
Manfred Firnhaber
Schwertnergasse 1
D-5000 Koln 1
GERMANY

Kernforschungzentrum, Karlsruhe (3)
Attn: P. Hofmann
Werner Scholtyssek
Phillip Schmuck
P.O. Box 3640
D-7500 Karlsruhe 1
GERMANY

Udo Brockmeier
University of Bochum
Energietechnik
IB-4-128
D-4630 Bochum
GERMANY

György Gyenes
Central Research Institute for Physics
Institute for Atomic Energy Research
H-1525 Budapest, P.O. Box 49
HUNGARY

Joint Research Center
Commission of European Communities
Attn: Alan Jones
Iain Shepherd
Safety Technology Institute
21020 Ispra (Va)
ITALY

Giovanni Saponaro
ENEA Natl. Comm. for R&D of Nuclear Energy
Via Vitaliano Brancati, 48
00144 Rome
ITALY

Japan Atomic Energy Research Institute (3)
Attn: Kunihisa Soda
Jun Sugimoto
Norihiro Yamano
Tokai-mura, Naka-gun, Ibaraki-ken
319-11, JAPAN

Dr. Susumi Suguri, Director General
Japan Institute of Nuclear Safety
Fujita Kankou Toranoman Bldg. 7F
3-17-1, Toranoman
Minato-Ku, Tokyo, 105
JAPAN

Masao Ogino
Mitsubishi Atomic Power Industries
4-1 Shibakoen 2-Chome
Minatoku Tokyo
JAPAN

Hidetoshi Okada
Nuclear Power Engineering Corporation
3-17-1, Toranomon Bldg. 5F
Minato-ku, Tokyo 105
JAPAN

Horohide Oikawa
Toshiba Corporation
8, Shin-Sugita, Isogo-ku
Yokoham
JAPAN

Korea Atomic Energy Research Inst. (3)
Attn: Kun-Joong Yoo
Song-Won Cho
Dong-Ha Kim
P.O. Box 7, Daeduk Danji
Taejon
SOUTH KOREA 305-353

Jae Hong Park
Safety Assessment Department
Korea Atomic Energy Research Institute
P.O. Box 16, Daeduk-Danji
Taejon
South Korea 305-353

Netherlands Energy Research Foundation (2)
Attn: Karel J. Brinkmann
E. J. Belema
P.O. Box 1
1744 ZG Petten
THE NETHERLANDS

Dr. Valery F. Strizhov
Russian Academy of Science
Institute of Nuclear Safety
Moscow, G. Tulsky, 52
113191, RUSSIA

Universidad Politecnica de Madric (2)
Attn: Augustin Alonzo Santos
Francisco Martin
E.T.S. Ingenieros Industriales
Jose Gutierrez Abascal, 2
28006 Madrid
SPAIN

Juan Bagues
Consejo de Seguridad Nuclear
Justo Dorado, 11
28040, Madrid
SPAIN

Oddbjörn Sandervåg
Statens Kärnkraftinspektion
Swedish Nuclear Power Inspectorate
Box 27106 102 52 Stockholm
SWEDEN

L. Hammar, Director
Division of Research
Swedish Nuclear Power Inspectorate
Statens Karnkraftinspektion
Sehlstedtsgatan 11
Box 27106
S-102-50 Stockholm
SWEDEN

Swiss Federal Nuclear Safety Inspectorate (4)
Attn: S. Chakraborty
Sang Lung Chan
U. Schmocker
H. P. Isaak
CH-5232 Villigen-HSK
SWITZERLAND

United Kingdom Atomic Energy Agency (3)
Winfrith Technology Center
Attn: T. Haste
S. R. Kinnersley
D. W. Sweet
Winfrith, Dorechester, Dorset
UNITED KINGDOM, DTS 8DH

United Kingdom Atomic Energy Authority (2)
Safety & Reliability Directorate
Attn: M. I. Robertson
C. Wheatley
Wigshaw Lane, Culcheth, Warrington
Cheshire, WA3 4NE
UNITED KINGDOM

Internal Distribution:

MS0736 N. R. Ortiz, 6413
MS0744 W. A. von Riesemann, 6403
MS0744 D. A. Powers, 6404
MS0747 A. L. Camp, 6412
MS0747 S. E. Dingman, 6412
MS0748 F. T. Harper, 6413
MS0742 J. E. Kelly, 6414
MS0745 S. L. Thompson (10), 6418
MS0745 R. K. Cole, 6418
MS0745 A. A. Elsbernd, 6418
MS0745 L. N. Kmetyk (10), 6418
MS0745 R. C. Smith, 6418
MS0745 R. M. Summers, 6418
MS0745 T. J. Tautges, 6418
MS0739 K. E. Washington, 6429
MS0899 Technical Library (5), 7141
MS0619 Technical Publications, 7151
MS9018 Central Technical Files, 8523-2

Distribution

Internal Distribution:

6400 N. R. Ortiz
6403 W. A. von Riesemann
6404 D. A. Powers
6412 A. L. Camp
6412 S. E. Dingman
6413 F. T. Harper
6414 J. E. Kelly
6418 S. L. Thompson (10)
6418 R. K. Cole
6418 A. A. Elsbernd
6418 L. N. Kmetyk (10)
6418 R. S. Longenbaugh
6418 R. C. Smith
6418 R. M. Summers
6418 T. J. Tautges
6429 K. E. Washington
7141 Technical Library (5)
7151 Technical Publications
8523-2 Central Technical Files

NRC FORM 335 (2-89) NRCM 1102, 3201, 3202

U.S. NUCLEAR REGULATORY COMMISSION

BIBLIOGRAPHIC DATA SHEET

(See instructions on the reverse)

1. REPORT NUMBER (Assigned by NRC Add Vol., Supp., Rev., and Addendum Numbers, If any.)

NUREG/CR-6107
SAND93-2042

2. TITLE AND SUBTITLE

Summary of MELCOR 1.8.2 Calculations for Three LOCA Sequences (AG, S2D, and S3D) at the Surry Plant

3. DATE REPORT PUBLISHED

MONTH	YEAR
March	1994

4. FIN OR GRANT NUMBER

L2486

5. AUTHOR(S)

L. Kmetyk[1]
L. Smith[2]

6. TYPE OF REPORT

Technical

7. PERIOD COVERED (Inclusive Dates)

8. PERFORMING ORGANIZATION – NAME AND ADDRESS *(If NRC, provide Division, Office or Region, U.S. Nuclear Regulatory Commission, and mailing address; if contractor, provide name and mailing address.)*

[1]Sandia National Laboratories
Albuquerque, NM 87185

[2]Geo-Centers Inc.
2201 Buena Vista, NM 87185
Albuquerque, NM 87106

9. SPONSORING ORGANIZATION – NAME AND ADDRESS *(If NRC, type "Same as above"; if contractor, provide NRC Division, Office or Region, U.S. Nuclear Regulatory Commission and mailing address.)*

Division of Safety Issue Resolution
Office of Nuclear Regulatory Research
U.S. Nuclear Regulatory Commission
Washington, DC 20555-0001

10. SUPPLEMENTARY NOTES

11. ABSTRACT *(200 words or less)*

Activities involving regulatory implementation of updated source term information were pursued. These activities include the identification of the source term, the identification of the chemical form of iodine in the source term, and the timing of the source term's entrance into containment. These activities are intended to support a more realistic source term for licensing nuclear power plants than the current TID-14844 source term and current licensing assumptions. MELCOR calculations were performed to support the technical basis for the updated source term. This report presents the results from three MELCOR calculations of nuclear power plant accident sequences and presents comparisons with Source Term Code Package (STCP) calculations for the same sequences. The three low-pressure sequences were analyzed to identify the materials which enter containment (source terms) and are available for release to the environment, and to obtain timing of sequence events. The source terms include fission products and other materials such as those generated by core-concrete interactions. All three calculations, for both MELCOR and STCP, analyzed the Surry plant, a pressurized water reactor (PWR) with a subatmospheric containment design.

12. KEY WORDS/DESCRIPTORS *(List words or phrases that will assist researchers in locating the report.)*

LOCA Analyses
MELCOR
Severe accident
Source term
Surry

13. AVAILABILITY STATEMENT

Unlimited

14. SECURITY CLASSIFICATION

(This Page)
Unclassified

(This Report)
Unclassified

15. NUMBER OF PAGES

16. PRICE